WATER WAVE SCATTERING BY A SPHERICAL STRUCTURE AND AN UNDULATING BOTTOM TOPOGRAPHY IN A TWO-LAYER FLUID

by

Smrutiranjan Mohapatra

DEPARTMENT OF MATHEMATICS

INDIAN INSTITUTE OF TECHNOLOGY GUWAHATI,

GUWAHATI-781039, INDIA

October, 2009

WATER WAVE SCATTERING BY A SPHERICAL STRUCTURE AND AN UNDULATING BOTTOM TOPOGRAPHY IN A TWO-LAYER FLUID

A Thesis submitted

in partial fulfillment of the requirements

for the degree of

DOCTOR OF PHILOSOPHY

by

Smrutiranjan Mohapatra

(Roll Number: 05612302)

to the

DEPARTMENT OF MATHEMATICS

INDIAN INSTITUTE OF TECHNOLOGY GUWAHATI

October, 2009

CERTIFICATE

It is certified that the work contained in the thesis titled **"Water wave scattering by a spherical structure and an undulating bottom topography in a two-layer fluid"** by **Smrutiranjan Mohapatra**, a student in the department of Mathematics, Indian Institute of Technology, Guwahati, for the award of the degree of Doctor of Philosophy has been carried out under my supervision and this work has not been submitted elsewhere for a degree.

October, 2009

Dr. Swaroop Nandan Bora
Associate professor
Department of Mathematics
Indian Institute of Technology, Guwahati

Dedicated

to

the Memory of My Parents

Acknowledgement

It has been a great pleasure and privilege to express my deep sense of gratitude and everlasting indebtedness to my thesis supervisor, **Dr. Swaroop Nandan Bora** who introduced me to the area of research in water wave theory and other allied branches of applied mathematics. I am immensely grateful to him for his enthusiasm, continuous encouragement and guidance which have been the main source of inspiration during the preparation of this thesis. I am also thankful to him for making me feel free in expressing my views and for sharing an excellent rapport with me. Without his help this work could not have been accomplished.

I owe my thanks to my doctoral committee members Prof. D. C. Dalal, Dr. S. Natesan and Dr. Jiten C Kalita for their valuable suggestions and meaningful comments. My sincere thanks go to Dr. Nihar Ranjan Satpathy, Dr. Sabita Sahoo and Prof. Swadheenananda Pattanayak for their constant encouragement for pursuing research.

I am very much grateful to my late parents. They were a great blessing to me while they were alive. They would have been the happiest persons in this world to see the completion of my degree. My heartiest regards go to my elder sister and her husband for their constant encouragement, patience, inspiration and immense love throughout my research period. Their devotion, not only for my research work but also for my life till date, will be treasured in my memory forever. Special thanks to my nephews Lipu, Lucky and my niece Lizi for their love and affection throughout this endeavour.

I would also like to thank my friends here at IIT Guwahati for their co-operation and pleasant company during my stay.

Finally, I would like to thank Indian Institute of Technology Guwahati (IITG) for providing me with financial assistance in the form of JRF & SRF and the necessary facilities during my research work, and Council of Scientific & Industrial Research (CSIR), Govt. of India, for providing me financial assistance through Senior Research Fellowship for completion of my thesis work.

October, 2009 **(Smrutiranjan Mohapatra)**

Abstract

This thesis studies (i) the interaction of water waves with spherical geometries in a two-layer fluid of finite depth, which is covered by either a rigid flat structure or a very thin ice shelf; (ii) the scattering of water waves by different types of unevenness on the bottom surface under such situations. To solve the ice-covered problems, the common idealization of ice as a thin elastic plate, which is static in all but its flexural response, is followed. Furthermore, the assumptions of linear and time harmonic motions are considered.

Firstly, the problem consisting of wave interaction with a spherical body submerged in either layer of the fluid is divided into two parts: one describing the scattering of waves by the fixed structure and the other describing the radiation of waves by the body into otherwise calm water. The radiation problem is further split into a number of parts, each of which corresponds to the body moving in a separate mode of motion. The physical problem involving radiation or scattering case, is reduced to a boundary value problem governed by a three-dimensional Laplace's equation for both the upper and the lower layers. The method of solution for both the fluids is based upon the multipole expansions technique. The solutions help in calculating the hydrodynamic forces acting on the spherical body for different modes of motion such as heave and sway. A number of observations are made for these motions with regard to different submersion depths. The multipole expansion method is found to be an extremely powerful method for solving radiation and scattering problems for submerged spheres. It eliminates the need to use large and cumbersome numerical packages for the solution of such problems.

Secondly, the latter part of this thesis is solely devoted to the investigation of the scattering of a train of small amplitude harmonic water waves by small bottom undulation of an ocean, which consists of a two-layer fluid, for both normal and oblique incidences. Moreover, it is assumed that both the fluids are of finite depth and the upper fluid is covered by either a rigid horizontal wall or a thin ice-cover. In this study of scattering, mixed boundary value problems are set up for the determination of two velocity potentials, corresponding to each layer, where the governing partial differential equation happens to be Laplace's equation in two-dimensions for normal incidence and Helmholtz equation in three-dimensions for oblique incidence within the fluid. The governing equation is accompanied by boundary conditions near the upper rigid boundary or the ice-cover surface, on the interface between the two fluids and on the rigid bottom boundary. As the fluid domain extends to infinity, radiation conditions or infinity conditions arise to ensure the uniqueness of the problem.

Applying a perturbation analysis, which involves a small parameter ε present in the representation of the small undulation on the channel bed or ocean-bed, directly to the boundary value problems, the original problems are reduced to two simpler boundary value problems for the first-order correction of the potentials. The mathematical tools utilized in this part of the thesis in obtaining the solution of the problem are (a) Green's function technique and application of Green's integral theorem, and (b) Fourier transform technique and application of residue theorem. From the solutions of the velocity potentials, the reflection and transmission coefficients are evaluated approximately up to the first-order of ε in terms of integrals

involving the shape function which represents the bottom undulation. Different special forms of the shape functions are considered to compute the integrals explicitly for the reflection and transmission coefficients and the results are suitably presented graphically. Out of these shape functions, the particular case of a patch of sinusoidal ripples (with the same wave number or two different wave numbers) has considerable significance due to the ability of an undulating bed to reflect incident wave energy which is important in respect of both coastal protection and of possible ripple growth if the bed is erodable. For this ripple patch, in the case of a channel bed assumed bounded above by a rigid boundary, it is observed that if the bed wave number is twice the interface wave number then there is a resonant Bragg-type interaction between the interface waves and the bed forms as observed earlier in the literature. Moreover, in case of an ocean-bed covered by an ice-cover, it is observed that when the wave is obliquely incident on the ice-cover surface we always find energy transfer to the interface, but for interfacial incident waves there are parameter ranges for which no energy transfer to the ice-cover surface is possible. Problems related to water wave scattering by different types of unevenness on the bottom of a two-layer fluid are important because of their possible applications such as in the construction of an effective reflector of the incident wave energy for protecting coastal areas from the rough ocean, and in many other areas of coastal and ocean engineering.

It is observed that the methods presented in this part of the thesis in obtaining the first-order potentials, and hence the reflection and transmission coefficients, reduce the workload to a large extent. These methods lead to a computationally more tractable form of the solutions for the scattered field. The solutions are expected to render a quantitative guidance to various types of water wave problems in a two-layer fluid.

Contents

List of Figures

Chapter 1

Introduction

1.1 Preamble

Wave scattering and its applications are encountered in many areas of physical interest, including the fields of water waves, acoustics and electromagnetic waves. A wave is a disturbance such that when it propagates through a medium, energy is transmitted to distant points without any displacement of the particle of the medium. The energy from the sun is transmitted by waves in the ether. When some musical instrument is played upon in a room, sound waves spread through the room. If we throw a stone in a pond we see waves in the pond which start from the point of striking of the stone and spread in all directions. Such water waves are also produced by pressure of wind upon the surface of water, by the relative motion of bodies like a ship moving in ocean and by obstacles in the bed of a stream. These are some easily understood examples of wave motion.

The study of different kinds of water waves is of immense importance for various applications. The practical importance of water waves is evident in areas such as hydro-acoustics, submerged navigation, hydro-biology, hydro-optics and ocean research. Particularly in ocean research, proper knowledge of water waves is required for predicting the behaviour of floating structures (immersed totally or partially) such as ships, submarines and tension-leg platforms, and for describing flows over various bottom topographies. Furthermore, the investigation of water wave patterns created by ships and other vehicles in forward motion is closely related to the calculation of the wave-making resistance and other hydrodynamics characteristics that are used in the marine design. An ocean rarely contains a fluid of constant density – it always seems to comprise of more than one fluid layer (like fresh water layer, salty water layer, mud layer etc).

A strata consists of several parallel layers with internally consistent characteristics that distinguishes it from contiguous layers, arranged one on top of another (such as different layers of tissue or cells in an organism or different layers of sedimentary rock or different layers of water), laid down by natural forces. Water stratification occurs when water of high and low salinity (halocline), as well as cold and warm water (thermocline), forms layers that act to

impede free movement to water mixing.

The present work of this thesis is concerned with a two-layer fluid only. The motions of a spherical body in a regular gravity wave in a two-layer fluid, covered by either a rigid horizontal wall or by an ice-cover, are investigated in the first half. There are plenty of practical problems where this study can be used. A simple and very useful example in the real world is the motion of a submarine of spherical shape in an ocean comprising of a two-layer fluid, each of finite depth. The motions of a spherical submarine in regular gravity waves in a two-layer fluid are analyzed by considering the submarine hull as a neutrally buoyant sphere. Another important example is that of a buoy which can be stationary or allowed to drift. This is a device used for a number of purposes including as bottom pressure sensor (for tsunami detection) or communication in emergency for submarine. A submerged sphere, which is moving either in the upper layer or in the lower layer of finite depth, is analyzed by considering linear water wave theory, which is a widely used technique for determining how a wave is diffracted by a fixed or floating structure. The underlying assumption of this theory is that the amplitudes of any waves or body motions are small compared to the other length scales in the problem. At first-order, this means that it is only necessary to consider the diffraction of a wave of a single frequency and direction. Furthermore, the velocity potential may be split into two parts: one describing the scattering of waves by a fixed structure and the other describing the radiation of waves by the body into the otherwise calm water.

Generally, water waves may be classified into two categories: in one category the wavelength is assumed to be greater than the depth of water and the corresponding study is called *shallow water wave theory*. The waves belonging to this category are tidal waves and long waves in shallow water. In the other category the wavelength is assumed to be much less than the depth of water so that the effect of the disturbance diminishes gradually as one goes downwards away from the free surface. Waves belonging to this category are termed *deep water waves*. In this case, if it is assumed that the amplitude of the wave is small compared to the wavelength, then the theory is called *linearized theory of water waves*. This theory has been derived as an approximation of the general theory on the basis of the assumption that the components of the velocities of water particles, the free surface elevation or depression and their derivatives are small quantities, *i.e.*, the motion is assumed to be very small. Though the ocean waves or surface waves are often nonlinear, the analysis in many physical problems is restricted to small amplitude waves mainly because consideration of linear theory is sufficient in offshore engineering and other related studies in handling most of the problems. Due to this reason, many scientists, researchers and ocean technologists use linearized theory of water waves to model mathematically various physical problems related to wave phenomena arising in coastal engineering. In the present thesis, all the problems are formulated and solved on the basis of linearized theory of water waves.

The other class of problems, which is investigated in the remaining part of this thesis,

studies the problem of a two-layer fluid flowing over a geometrical disturbance at the bottom of an ocean which is important for its possible application in the areas of coastal and marine engineering. The problem of reflection of incident waves by patches of small bottom undulations has received an increasing amount of attention recently, as its mechanism is important in the development of shore-parallel bars. The work presented in this part of the thesis is solely concerned with the effect of bed topography on an incident wave train.

Many physical problems arising in the areas of applied mathematics or mathematical physics can be formulated as mixed boundary value problems governed by elliptic partial differential equations. In the study of scattering or radiation of surface (or internal) harmonic water waves under the assumption of the linearized theory, the governing partial differential equation happens to be Laplace's equation in either two or three dimensions. Certain other assumptions are that the domain is unbounded, some of the boundary conditions are of mixed type and the behaviour of the velocity potential is not known completely at large distances, and the third or fourth order derivative may occur in some of the boundary conditions in certain physical problems etc. A long-standing but persistent problem in the area of wave theory is the determination of the effect of the bed topography and obstacle(s) on a given wave field. As for example, a practical problem faced by coastal engineers is to predict the amplitude of waves in harbours where both man-made breakwaters and the shape of the ocean-bed affect wave behaviour. Such problems involve scattering, diffraction and refraction of waves, and are mathematically formidable for linearized theory, even with the consideration of relatively simple bed and/or obstacle geometries. When a train of surface (or internal) waves travelling from a large distance is incident on an obstacle submerged or partially immersed in water, some parts of the wave is reflected back by the obstacle and some part is transmitted over or below it. The wave which is reflected back is known as *reflected wave* and the wave which is transmitted is known as *transmitted wave*. The reflected waves and the transmitted waves are called outgoing waves as they go away from the obstacle after striking. This process is known as *scattering*. In this scattering process the incoming or the incident wave modifies and produces scattered waves which are nothing but outgoing waves such that a combination of the incident wave and the outgoing wave occurs from which the latter can be determined. The process of determining an outgoing wave for a given incoming wave is known as the mathematical problem of scattering. In scattering theory, the reflected wave is accompanied by a constant, known as the *reflection coefficient* and the transmitted wave is accompanied by another constant, known as the *transmission coefficient*. These two physical quantities play a vital role in the mathematical study of water wave scattering problem since they provide a measure for the amount of reflected and transmitted waves. This information is useful in the construction of offshore structures or in the problem of generation of surface (or internal) waves by obstacle known as the wave-maker problem. But due to the complicacy involved, sometimes many researchers lay emphasis on the determination of these quantities directly

instead of going into details of the solution.

With this preamble we now present a brief history of various problems undertaken in some of the previous works which have relevance to this thesis.

1.2 Brief history and motivation of the present work

In linear water wave theory the radiation and diffraction problems have been fairly thoroughly studied for a homogeneous fluid and have recently been intensively investigated for a multi-layer fluid, *i.e.*, a stratified fluid. The study of surface waves in a fluid or internal waves in two fluids involves the consideration of singularities of different types in the fluids. In an unstratified fluid, the scattering and radiations problems have been solved by many researchers using different methods. The study of scattering and radiation problems involving fluids having two layers, with both layers finite or one layer infinite, has drawn reasonable attention due to various important applications.

Gourgi *et al.* [30] discussed the basic singularities in the theory of internal waves by considering a two-layer fluid when the lower fluid was of infinite or of finite depth while the upper one was of infinite height. Kassem ([36], [37]) discussed the different types of singularities that arose in one of the layers and obtained the velocity potentials describing the line and point multipoles when each layer was of finite constant depth. Linton and McIver [47] considered the interaction of waves with horizontal cylinders in a fluid consisting of a layer of finite depth bounded above by a free surface and below by an infinite layer of fluid of greater density. The motivation for this work arose due to the plan to build an underwater pipe bridge across one of the Norwegian fjords, which consist of a layer of fresh water on top of a deep layer of salt water. It was observed that time-harmonic waves propagated with two different wave numbers K and k. Multipole expansion method [73] was used to solve the radiation and scattering problems. It was found that for simple bodies, in the plane case a circular cylinder and in the three-dimensional case a sphere, solutions of the problems can be conveniently obtained. These solutions guaranteed high accuracy which made it possible to investigate the effect of various parameters in a simple manner, and provided a test for numerical methods directed at arbitrary bodies. Linton and Cadby [44] extended the work of Linton and McIver [47] to oblique scattering. Sturova [71] solved the problem of wave motions of a heavy fluid driven by the oscillations of a cylinder (radiation problem) and the scattering of an internal wave by a fixed cylinder (diffraction problem) by using multipole expansion method. The apparent mass and damping coefficients of the radiation problem and the disturbing forces and scattering coefficients of the diffraction problem were calculated. Multipole expansion technique has been used to solve three-dimensional wave-structure interaction problems involving a submerged sphere in unstratified fluids by Srokosz [69] for deep water case and by Linton [43] for finite depth case. Afterwards Cadby and Linton [9] extended this technique to the two-layer case with the consideration of one of the layers to be of infinite depth.

Ten and Kashiwagi [72] considered a two-dimensional radiation problem for a general body floating in a two-layer fluid of finite depth. A boundary integral-equation method was developed for directly computing the velocity potential on the wetted surface of a body which was immersed in both the upper and lower layers as a general case. Appropriate Green's functions were derived, and an efficient numerical method for evaluating these functions was proposed. Kashiwagi *et al.* [35] used the same boundary integral-equation method to directly obtain and solve the diffraction problem. They carried out an investigation on the effects of the fluid density ratio and the interface position on the wave exciting forces on the body and the motions of the body, including the case in which the body intersects the interface. Das and Mandal [19] investigated the wave scattering by a horizontal circular cylinder submerged in a two-layer fluid with an ice-cover for both oblique and normal incident wave trains by using the method of multipole expansions.

Problems concerning the radiation of water waves by spherical objects have received extensive attention beginning with Havelock [33] who solved the heave radiation problem for a half-immersed sphere in deep water. The method of solution adopted was to express the velocity potential as a sum of a three-dimensional wave source potentials and a linear combination of the so-called *wave-free potentials*, which are harmonic and satisfy the free surface and bottom conditions but which radiate no energy to infinity. Wang [75] used the method of Havelock [33] to examine the radiation and diffraction problems for a submerged sphere in deep water. Das and Mandal [20] formulated the problems of radiation of water waves by a submerged sphere in deep as well as in uniform finite depth water covered by an ice-cover, with the ice-cover modelled as an elastic plate of very small thickness. Using multipole expansion method, they obtained the added-mass and damping coefficients for heave and sway motions.

The scattering of linear water waves by a bed topography is governed by Laplace's equation together with appropriate boundary and radiations conditions. Such boundary value problems are, in general, somewhat difficult to solve, and explicit analytic expressions for the velocity potential are rare which occur only for certain special configurations usually involving vertical or horizontal strips as boundaries. Although the analytical solutions are rare for such boundary value problems, the quantities of physical interests, namely the reflection and transmission coefficients, can be estimated numerically by using various approximate mathematical techniques. For example, Mei and Black [55] used a variational formulation of the problem of wave scattering by a bottom-standing rectangular thick vertical barrier to obtain numerical estimates for the reflection coefficient.

Due to the great mathematical complexity of linearized free surface flow in water of variable quiescent depth, a number of approximations to the boundary value problems has been proposed by some leading researchers. In one class of approximation the vertical coordinate is removed by performing integration over the depth, thus reducing the dimension of the problem by one. Berkhoff ([5], [6]) developed a vertical integrated refraction-diffraction equation,

known as *mild-slope equation*, which was the result of such a procedure. It was based on the assumption of a mild-slope bottom. Smith and Sprinks [66] presented another derivation of the mild-slope equation, similar to that of Berkhoff but more succinct, and the mild slope approximation has since been used to produce other equations which model the effect of the bed topography on wave propagation. Booij [8] examined the accuracy of the mild-slope equation as a function of the bottom slope and has shown that acceptable results could be achieved even though the bottom slope was not moderate. Kirby [39] derived the mild-slope equation for the linear surface wave-current interaction over slowly varying topography. Copeland [17] solved the mild-slope equation in the form of a pair of first-order equations (which consists of a hyperbolic system) using a simple finite difference scheme. This offered the advantages of reduced computing time compared with the solution of a boundary value problem and also incorporated useful features. By recasting the mild-slope equation as a system of first-order differential equations, which were similar to the system of equations governing nearly horizontal flow in shallow water, a highly efficient algorithm for the latter was used iteratively by Madsen and Larsen [48] to find the stationary solution. O'Hare and Davies [60] considered the propagation of monochromatic surface waves over a region of arbitrary one-dimensional bottom topography. The smoothly varying bed topography was divided into a series of horizontal shelves and the surface wave field was calculated by successive approximation of Miles scattering matrix at each of the intervening steps [56]. Chamberlain [11] examined the scattering of a train of small amplitude harmonic waves on water by a one-dimensional topography, using the mild-slope equation. The associated boundary value problem was converted into a pair of integral equations whose solutions were approximated by variational techniques. Chamberlain [12] showed that the reflection and transmission coefficients arising from the scattering of linear water waves by a one-dimensional topography were known to possess certain symmetry properties. He showed that the same relations held in the mild-slope approximation to the full linear theory. These relations were used in the development of a decomposition method in which solutions for relatively simple depth profiles might be combined to give solutions for complicated ones. The ideas and techniques used in the study of plane wave approximation over slowly varying depth were applied by Kellin and Johnson [38] to the axi-symmetric flow.

For several bed topographies consisting of horizontal and vertical sections, numerical solutions of the integral equations arising from boundary value problems have been obtained. Staziker *et al.* [70] considered the problem of two-dimensional wave scattering by a local bed elevation of any shape on an otherwise horizontal bed (such bottom profiles are referred to as "humps") using linearized water wave theory. Green's function theory was used to convert the associated boundary value problem into an integral equation of first kind and a variational approach was then used to obtain the approximations to the amplitude of the scattered wave. Miles and Chamberlain [59] developed a systematic hierarchy of partial differential equations of linear gravity waves in water of variable depth through the expansion of the average La-

grangian in powers of depth slope. Chamberlain and Porter [14] used the mild-slope equation to examine scattering and trapping by axi-symmetric topography, mainly emphasizing on wholly submerged bed forms. Porter and Porter [63] considered the scattering and trapping of water waves, under the assumption of linearized theory, by a three-dimensional submerged topography, infinite and periodic on one horizontal co-ordinate and of finite extent in the other. The mild-slope approximation was used to reduce the governing boundary value problem to the one involving a form of the Helmholtz equation in which the coefficients depended on the topography.

Furthermore, many mixed boundary value problems corresponding to the problems of surface water waves travelling in regions of varying depth have been presented under various geometrical assumptions. Kirby [41] derived coupled equations governing the forward- and backward-scattered components of a linear wave propagating in a region of varying depth, from a second-order wave equation for linear wave motion. Evans [25] described two mechanisms for the generation of standing edge waves over a sloping beach using classical linear water wave theory. Devillard *et al.* [23] presented a theoretical study of the localization phenomenon of surface gravity waves by a rough bottom in a one-dimensional channel. They developed a renormalized-transfer-matrix approach to this problem. An elaborate description of its experimental set-up and the corresponding results can be found in Belzons *et al.* [3]. Johnson [34] presented a straight forward method that yielded explicit transmission amplitudes for Kelvin wave scattering by a topography whose isobaths were parallel, sufficiently far from the vertical, but not necessarily planner wall supporting the incident wave. Miles [58] derived the Eckart's [24] second-order, self adjoint partial differential equation for the free surface displacement of monochromatic gravity waves in water of variable depth from variational formulation by approximating the vertical variation of the velocity potential in the average Lagrangian by that for deep water waves. It was compared with the mild-slope equation, which was also of second-order and self-adjoint, and might be obtained in a similar manner for uniform finite depth. Chamberlain and Porter [13] described a method for determining those approximations to wave scattering by a bed topography which were based on second-order ordinary differential equations. The development of a decomposition method allowed the scattering matrix for an extended section of varying topography to be assembled in a piecemeal fashion.

The propagation of surface water waves in a channel with a rough bottom is, in general, a relatively difficult problem to solve analytically. A number of researchers have studied water wave propagation over an irregular bottom topography. In the classical work of Lamb [42], the free surface elevation for the two dimensional problem of steady flow over the bottom irregularities was obtained assuming irrotational motion. The problem of determining the scattering of long crested gravity wave over a bottom of arbitrary shape has received considerable attention in the literature. For a survey up to 1960, the work of Wehausen and Laitone [76] can be referred to.

O'Hare and Davies [61] made comparisons between the predictions of two models for surface wave propagation over rapidly-varying topography, one based on the extended mild- slope equation derived by Kirby [40] and the other on the successive-application matrix model described by O'Hare and Davies [60]. The models were applied to two types of undulating topography, namely sinusoidal (Davies and Heathershaw [22]) and doubly-sinusoidal beds (Guazzelli *et al.* [32]) and comparisons were made with the existing laboratory data. Using the two-dimensional linear water wave theory to the scattering of water waves by a varying bottom topography, Evans and Linton [26] adopted a new approach in which the problem was first transferred into a uniform strip resulting in a variable free surface boundary condition. This was then approximated by a finite number of sections on which the free surface boundary condition was assumed to be constant. They also developed a transition matrix theory which was used to relate the wave amplitudes at infinity.

The interaction of water waves in a two-layer fluid with an ice-cover by an obstacle or a geometrical disturbance at the bottom is considered important for its possible application in arctic and marine engineering, and as such these are being studied extensively for a long period of time. Recently there has been considerable interest in the investigation of ice-wave interaction problems due to an increase in scientific activities in polar regions. The ice-cover is modelled as a thin ice-sheet of which a smaller part is immersed in water, and is composed of materials having elastic properties. Already quite a number of researchers have considered various types of water wave problems in an ocean with an ice-cover, which is modelled as a thin elastic plate ([2], [27] and others). Fox and Squire [28] developed a precise linearized model for the reflection/transmission process due to oblique waves at the margin of a sheet of shore fast ocean-ice. Squire [67] solved the wave propagation in ocean-ice fields, modelling both the continuous ocean-ice representative of the Central Arctic Ocean and the more broken-up pack ice of the marginal ice zones. Later on, Squire and Williams [68] developed how the assimilation of ice floe submergence into theory altered the transmission of the wave trains, allowing the approximation and consequent limitations inherent in the majority of previous models that applied the under-ice boundary conditions at the mean open water surface to be assessed.

The linearized theory of small amplitude waves in a two-layer inviscid fluid, separated by a common interface, and the upper layer fluid of lower density having a free surface, is given in Lamb [42]. In such a two-layer fluid region, for a given frequency, time-harmonic gravity waves of two different modes propagate at each of the free surface and the interface. When a train of waves of a particular mode encounters an obstacle, then some of the energy from the incident wave mode is transferred to the other mode due to scattering by the obstacle. If the bed of the ocean has an undulation, the wave train is partially reflected by it, and partially transmitted over it. However, there exists a class of mostly naturally occurring bottom standing obstacles such as sand ripples, which can be assumed to be small in some sense, for which some sort of

perturbation technique can be employed in obtaining the first-order corrections to the reflection and transmission coefficients.

Chamberlain and Porter [15] examined the scattering of waves in a two-layer fluid of varying mean depth in a three-dimensional context by using linear theory. A variational technique was used to construct a particular type of approximation which had the effect of removing the vertical coordinate and reduced the problem to two coupled partial differential equations in two independent variables.

Miles [57] obtained the reflection and transmission coefficients approximately up to the first-order in terms of integrals involving a small cylindrical undulation of the bottom by using small perturbation theory for an obliquely incident wave train propagating in a single-layer fluid. Martha and Bora ([52], [53]) worked on the oblique scattering of surface wave propagation over a small undulation on the bottom of an ocean for an unstratified fluid. Employing a simplified perturbation analysis, they reduced the original boundary value problem to a first-order one and obtained the velocity potential, reflection coefficient and transmission coefficient up to the first-order by using Green's function technique and finite cosine transformation. The behavior of water waves over periodic beds was considered by Porter and Porter [64] in a two-dimensional context using linear water wave theory. Mandal and Basu [50] employed perturbation analysis while solving the problem of water wave diffraction of oblique interface waves by a bottom undulation of two laterally unbounded superposed fluids. They derived the reflection and transmission coefficients approximately up to the first-order in terms of integrals involving the shape function representing the bottom elevation. Maiti and Mandal [49] employed Green's function technique to study the reflection of oblique surface waves over small undulations in a two-layer fluid which had a free surface.

Fox and Squire [28] developed a precise linearized model for the reflection/transmission process due to oblique waves at the margin of a sheet of shore fast ocean-ice. Chakrabarti [10] solved the scattering of two-dimensional time-harmonic surface waves by a discontinuity on the surface boundary conditions, separating the clean surface and an ice-covered surface in the case of infinite depth of water. He reduced the main problem to that of solving a singular integral equation, of the Carleman type, over a semi-finite range and determined the explicit solution of the original problem. Linton and Chung [45] employed the residue calculus technique to solve the scattering of water waves by the edge of a semi-infinite ice sheet in a finite depth ocean. Using perturbation analysis, Mandal and Basu [51] investigated the diffraction of normal incident waves by a small cylindrical elevation of the bottom of a laterally unbounded ocean for an unstratified fluid covered by an ice sheet. Gayen *et al.* [29] solved the scattering of water waves by a strip of ice-cover floating on the surface of deep water. They reduced the problem to that of solving two singular integral equations of Carleman type over a semi-infinite range and solved the problem approximately by casting them into two separate Riemann-Hilbert problems with the consideration of large strip width.

Vaughan and Squire [74] solved the ocean wave scattering by natural ocean-ice transects by using Green's function technique. They focused on how the progress of wave trains affected by scattering relates to the statistical properties of the ocean-ice transects being sampled. Porter and Porter [62] investigated the three-dimensional wave scattering by an ice sheet of varying thickness floating on ocean water which had an undulating bed topography. They obtained a simplified form of the problem by deriving a variational principle equivalent to the governing equations of linear theory and invoking the mild-slope approximation in respect of the ice thickness and water depth variations. Bennetts *et al.* [4] extended the work of Porter and Porter [62] to variable quiescent depth by applying the Rayleigh-Ritz method in conjunction with a variational principle. They obtained the solution of the problem by using a multi-mode expansion to approximate the velocity potential that represented the fluid motion.

1.3 Relevant basic equations in the linear theory of water waves

In this section, we derive the basic equations associated with the linearized theory of water waves that are relevant to this thesis. In most of the books on water waves, the basic equations related to linear theory in an unstratified fluid are described in details. Here, we present the same equations which are applicable to stratified fluids. For easy understanding and from the point of view of relevance to this thesis, we present here the basic equations applicable to a two-layer fluid only. The governing equation for the fluid motions and the various boundary conditions are derived in brief.

We consider the motion under gravity in a two-layer, incompressible and inviscid fluid of densities ρ_1 and $\rho_2(< \rho_1)$ for the lower and the upper fluids, respectively, separated by a common interface. A right-handed rectangular Cartesian co-ordinate system is chosen in which the y-axis is directed vertically downwards into the lower layer fluid region and $y = 0$ is the position of the surface of separation between the two fluids at rest. The motion in each fluid is assumed to start from rest so that it is irrotational and can be described by the velocity potentials $\Phi(x, y, z, t)$ and $\Psi(x, y, z, t)$ in the lower and the upper fluids, respectively.

Since the flow under consideration is of potential kind, the fluid velocities for lower and upper layers given by, $\overrightarrow{q_1} = (u_1, v_1, w_1)$ and $\overrightarrow{q_2} = (u_2, v_2, w_2)$, respectively, can be expressed as

$$\overrightarrow{q_1} = \nabla\Phi \quad \text{and} \quad \overrightarrow{q_2} = \nabla\Psi. \tag{1.1}$$

For the lower layer fluid, the equation of continuity is

$$\nabla.\overrightarrow{q_1} = 0, \tag{1.2}$$

(for the upper layer case, equation of continuity is $\nabla.\overrightarrow{q_2} = 0$) and the corresponding Euler's equation of motion is

$$\frac{\partial\overrightarrow{q_1}}{\partial t} + (\overrightarrow{q_1}.\nabla)\overrightarrow{q_1} = g - \frac{1}{\rho_1}\nabla p_1, \tag{1.3}$$

where g is the gravitational constant and p_1 is the pressure at a point in the lower layer fluid.

After integration, Euler's equation of motion (1.3) reduces to

$$\frac{\partial \Phi}{\partial t} + \frac{1}{2}({u_1}^2 + {v_1}^2 + {w_1}^2) + \frac{p_1}{\rho_1} - gy = 0, \tag{1.4}$$

which is known as Bernoulli's equation, valid here for the lower layer. Similarly the Bernoulli's equation for the upper layer is

$$\frac{\partial \Psi}{\partial t} + \frac{1}{2}({u_2}^2 + {v_2}^2 + {w_2}^2) + \frac{p_2}{\rho_2} - gy = 0, \tag{1.5}$$

where p_2 is the pressure at a point in the upper layer fluid. Neglecting the higher order terms from the above two equations, we get the linearized Bernoulli's equations for the respective layer.

Using (1.1), the equation of continuity becomes,

$$\nabla^2 \Phi = 0 \quad \text{in the lower fluid region,} \tag{1.6}$$

$$\nabla^2 \Psi = 0 \quad \text{in the upper fluid region,} \tag{1.7}$$

both of which are Laplace's equation. Let $y = \eta(x, z, t)$ denote the depression of the interface. The linearized kinematic condition at the interface produces

$$\frac{\partial \Phi}{\partial y} = \frac{\partial \Psi}{\partial y} = \frac{\partial \eta}{\partial t} \quad \text{on} \quad y = 0, \tag{1.8}$$

where it is assumed that η and its partial derivatives are small. The condition (1.8) also gives the condition of continuity of the normal component of the velocity across the common interface.

The linearized Bernoulli's equation in the lower layer is

$$\frac{\partial \Phi}{\partial t} = gy - \frac{p_1}{\rho_1} \quad \text{in} \quad y \geq \eta. \tag{1.9}$$

Similarly, the linearized Bernoulli equation in the upper layer is

$$\frac{\partial \Psi}{\partial t} = gy - \frac{p_2}{\rho_2} \quad \text{in} \quad y \leq \eta. \tag{1.10}$$

The condition of continuity of pressure at the interface $y = \eta$ then produces

$$\frac{\partial \Phi}{\partial t} - g\eta = \rho\left(\frac{\partial \Psi}{\partial t} - g\eta\right) \quad \text{on} \quad y = \eta, \tag{1.11}$$

where $\rho = \rho_2/\rho_1$, so that $0 < \rho < 1$. Expanding $\frac{\partial \Phi}{\partial t}(x, y, z, t)$ and $\frac{\partial \Psi}{\partial t}(x, y, z, t)$ by Taylor's series about $y = 0$ and neglecting the terms of second and higher order of smallness, the above condition becomes

$$\frac{\partial \Phi}{\partial t} - g\eta = \rho\left(\frac{\partial \Psi}{\partial t} - g\eta\right) \quad \text{on} \quad y = 0. \tag{1.12}$$

Elimination of η between (1.8) and (1.12) gives one of the *linearized* conditions at the interface as

$$\frac{\partial^2 \Phi}{\partial t^2} - g\frac{\partial \Phi}{\partial y} = \rho\left(\frac{\partial^2 \Psi}{\partial t^2} - g\frac{\partial \Psi}{\partial y}\right) \quad \text{on} \quad y = 0, \tag{1.13}$$

while another linearized condition at the interface, called continuity of normal velocity, can be obtained as

$$\frac{\partial \Phi}{\partial y} = \frac{\partial \Psi}{\partial y} \quad \text{on} \quad y = 0. \tag{1.14}$$

It may be noted that in the absence of upper fluid, (1.13) reduces to the usual free surface condition for an unstratified fluid.

The condition of no motion at the bottom of the lower fluid gives

$$\nabla \Phi \to 0 \quad \text{as} \quad y \to \infty, \tag{1.15}$$

if the lower fluid extends to infinity downwards. However, if the lower fluid is of uniform finite depth H below the mean interface, then the condition (1.15) is replaced by

$$\frac{\partial \Phi}{\partial y} = 0 \quad \text{on} \quad y = H. \tag{1.16}$$

Moreover, if there is a small cylindrical deformation at the bottom of the lower layer fluid along the lateral direction which is described by $y = H + \varepsilon c(x)$, where $c(x)$ is a continuous function with compact support, and the non-dimensional parameter $\varepsilon \ll 1$ measures the smallness of the bottom deformation, then the condition (1.15) is replaced by

$$\frac{\partial \Phi}{\partial y} = 0 \quad \text{on} \quad y = H + \varepsilon c(x). \tag{1.17}$$

If the upper fluid extends to infinity upwards, then the condition of no motion at the top gives

$$\nabla \Psi \to 0 \quad \text{as} \quad y \to -\infty. \tag{1.18}$$

However, if the upper fluid is of uniform finite height h above the mean interface and is bounded by a rigid plane, then the condition (1.18) is replaced by

$$\frac{\partial \Psi}{\partial y} = 0 \quad \text{on} \quad y = -h. \tag{1.19}$$

while, if the upper fluid has a free surface, the linearized condition at this free surface of the upper fluid is

$$\frac{\partial^2 \Psi}{\partial t^2} = g \frac{\partial \Psi}{\partial y} \quad \text{on} \quad y = -h. \tag{1.20}$$

The interface depression $\eta(x, z, t)$ is given by

$$\eta(x, z, t) = \frac{1}{g(1-\rho)} \left(\frac{\partial \Phi}{\partial t} - \rho \frac{\partial \Psi}{\partial t} \right) (x, 0, z, t). \tag{1.21}$$

Derivation of ice-cover condition:

We consider that the motion in upper layer fluid is covered by a thin sheet of ice which is modelled as a thin elastic plate of uniform surface density $\delta\rho_2$ having Young's modulus E and Poisson's ratio ν; δ being a constant having dimension of length measured by $\delta = \rho_0/\rho_2$, with ρ_0 and ρ_2, respectively, being the densities of ice and the upper layer fluid. Let us choose $y = -h$ as the position of the thin ice-cover at rest.

In this case the linearized Bernoulli's equation takes the form as in (1.10), that is,

$$\frac{\partial \Psi}{\partial t} = gy - \frac{p_2}{\rho_2}. \tag{1.22}$$

Let $y = \eta(x, z, t)$ denotes the depression of the ice-covered surface below the mean horizontal level. Newton's equation of motion for a small element of the ice-covered surface produces

$$\delta\rho_2 \frac{\partial^2 \eta}{\partial t^2} = \delta\rho_2\, g + \prod - p_2 - L\nabla^4_{x,z}\,\eta \quad \text{on} \quad y = -h + \eta, \tag{1.23}$$

where $\prod$ is the atmospheric pressure and $L = Eh_0^3/[12(1-\nu^2)]$ is the flexural rigidity of the ice; h_0 being the very small thickness of ice of which a smaller part is immersed in the upper layer and $\nabla^4_{x,z}$ the two-dimensional biharmonic operator. Using (1.22) in (1.23) and after linearization, we get

$$\delta\rho_2 \frac{\partial^2 \eta}{\partial t^2} = \delta\rho_2 g + \prod - \rho_2\left(g\eta - \frac{\partial \Psi}{\partial t}\right) - L\nabla^4_{x,z}\,\eta \quad \text{on} \quad y = -h. \tag{1.24}$$

The kinematic condition is

$$\frac{\partial \eta}{\partial t} = \frac{\partial \Psi}{\partial y} \quad \text{on} \quad y = -h. \tag{1.25}$$

Eliminating η between (1.24) and (1.25) we get

$$(\Psi - \delta\Psi_y)_{tt} = (D\nabla^4_{x,z} + 1)g\Psi_y \quad \text{on} \quad y = -h, \tag{1.26}$$

where $D = L/(\rho_2 g)$.

For a time-harmonic motion with angular frequency ω, the velocity potentials $\Phi(x, y, z, t)$ and $\Psi(x, y, z, t)$ can be expressed, respectively, as

$$\Phi(x, y, z, t) = \mathrm{Re}[\phi(x, y, z, t)\mathrm{e}^{-\mathrm{i}\omega t}], \tag{1.27}$$

$$\Psi(x, y, z, t) = \mathrm{Re}[\psi(x, y, z, t)\mathrm{e}^{-\mathrm{i}\omega t}], \tag{1.28}$$

so that ϕ and ψ satisfy

$$\nabla^2\phi = 0 \quad \text{in} \quad y \geq 0, \tag{1.29}$$

$$\nabla^2\psi = 0 \quad \text{in} \quad y \leq 0, \tag{1.30}$$

$$K\phi + \frac{\partial \phi}{\partial y} = \rho\left(K\psi + \frac{\partial \psi}{\partial y}\right) \quad \text{on} \quad y = 0, \tag{1.31}$$

$$\frac{\partial \phi}{\partial y} = \frac{\partial \psi}{\partial y} = -\mathrm{i}\omega\eta \quad \text{on} \quad y = 0, \tag{1.32}$$

along with the following conditions :

(i) if the lower fluid is infinitely deep :

$$\nabla\phi \to 0 \quad \text{as} \quad y \to \infty, \tag{1.33}$$

or, (ii) if the lower fluid is of uniform finite depth H :

$$\frac{\partial \phi}{\partial y} = 0 \quad \text{on} \quad y = H, \tag{1.34}$$

or, (iii) if the lower fluid has a bottom deformation:

$$\frac{\partial \phi}{\partial y} = 0 \quad \text{on} \quad y = H + \varepsilon c(x), \tag{1.35}$$

and, (iv) if the upper fluid extends infinitely upwards :

$$\nabla\psi \to 0 \quad \text{as} \quad y \to -\infty, \tag{1.36}$$

or, (v) if the upper fluid is bounded by a rigid plane at a height h above the mean interface :

$$\frac{\partial\psi}{\partial y} = 0 \quad \text{on} \quad y = -h, \tag{1.37}$$

or, (vi) if the upper fluid has a free surface :

$$K\psi + \frac{\partial\psi}{\partial y} = 0 \quad \text{on} \quad y = -h, \tag{1.38}$$

or, (vii) if the upper fluid is bounded by a thin ice-cover :

$$K\psi + (1 - \delta K + D\nabla^2_{x,z})\psi_y = 0 \quad \text{on} \quad y = -h, \tag{1.39}$$

where $K = \omega^2/g$. For the two-dimensional case, the above ice-cover condition (1.39) is

$$K\psi + (D\partial^4_{xxxx} + 1 - \delta K)\psi_y = 0 \quad \text{on} \quad y = -h. \tag{1.40}$$

If the ice-cover is modelled as an inertial surface (*i.e.,* non-interacting floating materials having no elastic property), then $L = 0$ so that $D = 0$. Then the condition (1.40) reduces to

$$K\psi + (1 - \delta K)\psi_y = 0 \quad \text{on} \quad y = -h. \tag{1.41}$$

This condition takes the form

$$K^*\psi + \psi_y = 0 \quad \text{on} \quad y = -h, \qquad \text{if } 1 - \delta K > 0, \tag{1.42}$$

where $K^* = \frac{K}{1-\delta K} > 0$, and

$$K_0\psi - \psi_y = 0 \quad \text{on} \quad y = -h, \qquad \text{if } 1 - \delta K < 0, \tag{1.43}$$

where $K_0 = \frac{K}{\delta K - 1} > 0$. Comparing (1.42) and (1.43) with the free surface condition (1.38) on $y = -h$, it may be noted that progressive wave along an inertial surface exists only if $1 - \delta K > 0$ which means $\omega < \sqrt{\frac{g}{\delta}}$. For $1 - \delta K < 0$, that is, $\omega > \sqrt{\frac{g}{\delta}}$, the condition (1.43) does not allow existence of any progressive wave at the inertial surface.

1.4 Outline of the thesis

The work presented in this thesis is concerned with the effect of the presence of a spherical structure or a small undulating bed on an incident wave train (both normal and oblique case) in a two-layer fluid by using linearized theory. Moreover, we assume that both the fluids are of finite depth and that the upper layer of the fluid is covered by either a thin ice-cover or a rigid horizontal wall. We prescribe the incident wave train and the deviation in the still-water depth, and seek the additional waves, namely, the radiated waves, the scattered waves etc., caused by this deviation. A typical problem of this type requires the determination of velocity potentials satisfying Laplace's equation (or Helmholtz equation) within the fluids, a mixed boundary condition near the ice-cover surface or a given normal velocity near the

upper rigid boundaries, on the interface between the two fluids and a given normal velocity on the rigid bottom boundary. If the fluid domain extends to infinity in lateral direction, a radiation condition is required to ensure uniqueness. The corresponding boundary value problem is established and formally presented in the subsequent chapters. We shall refer to the problem of finding a solution of the boundary value problem as the full linear problem. Analytical solutions for the full linear problem are rare for any deviation from the constant water depth case, that is, for any deviation from a flat ocean-bed. Problems, where analytical solutions exist, are usually valid for a limited selection of straightforward geometries which include horizontal and/or vertical boundaries.

The mathematical tools utilized in this thesis are (a) Multipole expansion method, (b) Green's function technique and application of Green's integral theorem, (c) Fourier transform technique and application of residue theorem. The content of the thesis is presented in the form of eight chapters. Chapter 1 is devoted to the general introduction along with the historical background of the related work done in the scattering theory and the derivation of the basic hydrodynamic equations in the linearized theory of water waves that is utilized in the thesis. In Chapter 2, we solve the problem for the scattering of incident internal waves by a spherical structure submerged in either layer of a two-layer fluid where both the upper and the lower layers are bounded by rigid horizontal walls. Using the multipole expansion method, the governing boundary value problem arising out of the physical problem under consideration is evaluated for the coefficients related to both surge and sway motions. Chapter 3 deals with the radiation of water waves by a submerged sphere in a two-layer fluid where the upper layer has a thin ice-cover while the lower layer is bounded by a rigid horizontal bottom surface. The added mass and damping coefficients for both surge and sway motions are obtained in the same manner as was followed in Chapter 2.

Chapters 4 and 5, are devoted to the problems involving the scattering of internal water waves by small bottom undulation in a two-layer fluid for normal and oblique incidences, respectively. Using a perturbation analysis, the boundary value problems are reduced to simpler boundary value problems which involve a small parameter ε present in the representation of the small undulation of the channel-bed. Green's function technique and Fourier transform technique are applied to the simpler boundary value problems from which the reflection and transmission coefficients are determined. A patch of sinusoidal ripples having the same wave number or different wave numbers is considered as a special case of shape function, to evaluate explicitly the integrals for the reflection and transmission coefficients.

In Chapter 6, we formulate the problem for the scattering of water waves by small undulation of the ocean-bed for the normal incidence case, where the upper layer is bounded by a thin ice-cover. Then, by using the same perturbation analysis used in Chapters 4 and 5, the corresponding boundary value problem is reduced first to a simpler boundary value problem for the first-order correction of the potentials. The solutions are obtained by using two different

techniques, namely, Green's function technique and a suitable application of Green's integral theorem; and Fourier transform technique. From these solutions the quantities of physical interest, namely the reflection and transmission coefficients, are evaluated up to the first-order of ε in terms of integrals involving the shape function representing the bottom undulation. In Chapter 7, we solve the reduced boundary value problem for first-order correction of the potentials for the oblique incidence case. The solutions of the boundary value problem for the first-order corrections are obtained by using the same techniques as was applied in Chapter 6. Using these solutions the reflection and transmission coefficients are evaluated in terms of integrals involving the shape function.

In each chapter, we also present the graphical representation of the results and conclude about the behaviour of the scattering process. Each chapter contains a sizeable number of graphs validating the analytical results that we have derived.

Finally, Chapter 8 is concerned with a brief summary of results highlighting the contribution made by this thesis. It also provides information for the scope of future investigations.

Chapter 2

Radiation and scattering by a sphere in a two-layer fluid of finite depth

2.1 Introduction

In the present chapter we solve the radiation and scattering problems for a submerged sphere placed in one of the layers of a two-layer fluid with the layers bounded above and below by rigid horizontal walls, which are approximations of the free surface and the bottom surface, which form the horizontal boundaries of a channel. The corresponding heave and sway radiation problems, either in the lower or the upper layer, are solved by Thorne's multipole expansion method [73]; *i.e.*, the added-mass and damping coefficients are evaluated for both the cases. Similarly the exciting forces for these cases are evaluated after obtaining the diffraction potential for the sphere. The numerical estimates for the damping coefficients, added-mass coefficients and the exciting forces for both the motions are calculated and plotted. The earlier works were limited either to solving for the potentials only or to solving the radiation and scattering problems for the case when one of the layers was of infinite depth and a free surface was considered as the upper surface.

2.2 Mathematical formulation of the problem

We consider the irrotational motion of a two-layer inviscid and incompressible fluid of sufficiently small amplitude under the action of gravity flowing between two rigid infinite horizontal walls, which are approximations of the free surface and the bottom surface, placed at $z = -h$ and $z = H$, respectively. Each fluid is of infinite horizontal extent in x- and y-directions while the depth is considered along z-direction vertically downwards. The origin O is considered at the undisturbed interface between the upper and the lower fluids, and $z = 0$ is the mean position of the interface of the layers. We consider cylindrical polar coordinates (R, α, z) defined by $x = R\cos\alpha,\ y = R\sin\alpha,\ z = z$. We further assume that all the motions are time harmonic with angular frequency ω. Under these assumptions, the velocity potentials in the lower fluid

of density ρ_1 and in the upper fluid of density $\rho_2 < \rho_1$ can, respectively, be written as

$$\Phi(x,y,z,t) = \mathrm{Re}[\phi(x,y,z)\mathrm{e}^{-\mathrm{i}\omega t}],$$
$$\Psi(x,y,z,t) = \mathrm{Re}[\psi(x,y,z)\mathrm{e}^{-\mathrm{i}\omega t}],$$

where Re stands for the real part and the potentials ϕ and ψ satisfy Laplace's equation

$$\nabla^2\phi = \nabla^2\psi = 0, \tag{2.1}$$

in respective regions occupied by the fluids. In addition, the linearized boundary conditions at the walls (upper surface and lower surface) and on the interface are given by

$$\frac{\partial\psi}{\partial z} = 0 \qquad \text{on} \quad z = -h, \tag{2.2}$$
$$\frac{\partial\phi}{\partial z} = 0 \qquad \text{on} \quad z = H, \tag{2.3}$$
$$\frac{\partial\psi}{\partial z} = \frac{\partial\phi}{\partial z} \qquad \text{on} \quad z = 0, \tag{2.4}$$
$$K\phi + \frac{\partial\phi}{\partial z} = \rho\big(K\psi + \frac{\partial\psi}{\partial z}\big) \qquad \text{on} \quad z = 0, \tag{2.5}$$

where $K = \omega^2/g$, g is the acceleration due to gravity and $\rho = \rho_2/\rho_1 (< 1)$. The time dependence of $\mathrm{e}^{-\mathrm{i}\omega t}$ has been suppressed throughout the subsequent analysis. The boundary conditions (2.4) and (2.5) represent, respectively, the continuity of normal velocity, and the pressure at the interface.

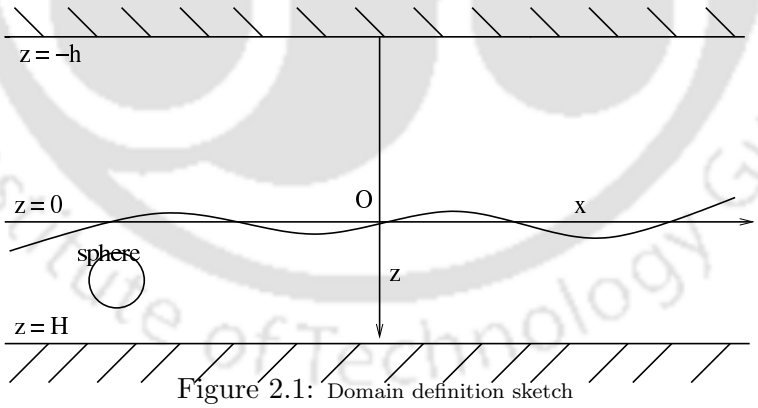

Figure 2.1: Domain definition sketch

In a two-layer fluid, with each layer finite, the progressive waves take the form

$$\psi = C_1\mathrm{e}^{\pm\mathrm{i}ux}\left[\mathrm{e}^{uz} + \mathrm{e}^{-u(z+2h)}\right],$$
$$\phi = C_1\mathrm{e}^{\pm\mathrm{i}ux}\left(\frac{1-\mathrm{e}^{-2uh}}{1-\mathrm{e}^{2uH}}\right)\left[\mathrm{e}^{uz} + \mathrm{e}^{-u(z-2H)}\right],$$

with u satisfying the dispersion relation $\Delta(u) = 0$, where

$$\begin{aligned}\Delta(u) &= (u-K\sigma)\mathrm{e}^{u(h+H)} + (u+K\sigma)\mathrm{e}^{-u(h+H)} - (u+K)\mathrm{e}^{u(h-H)} - (u-K)\mathrm{e}^{-u(h-H)},\\ &= \frac{K(\cosh uH\sinh uh + \rho\sinh uH\cosh uh)}{1-\rho} - u\sinh uh\sinh uH,\end{aligned} \tag{2.6}$$

with $\sigma = (1+\rho)/(1-\rho)$.

The above equation (2.6) has only one nonzero root, say $u = k$ (Kassem [36]). So only one non-zero wave number k can exist and the wave can propagate in either direction.

The velocity potentials take different forms in the upper and the lower regions which can be characterized by their following far-field forms, as $kR \to \infty$,

$$\psi \sim \left(\frac{2}{\pi kR}\right)^{1/2} \mathrm{e}^{\mathrm{i}kR - \mathrm{i}\pi/4} g_1(z) A(\alpha), \tag{2.7}$$

$$\phi \sim \left(\frac{2}{\pi kR}\right)^{1/2} \mathrm{e}^{\mathrm{i}kR - \mathrm{i}\pi/4} g_2(z) B(\alpha). \tag{2.8}$$

Here $A(\alpha)$ and $B(\alpha)$ are arbitrary functions of α, and the functions $g_1(z)$ and $g_2(z)$ are given by

$$g_1(z) = \mathrm{e}^{kz} + \mathrm{e}^{-k(z+2h)}, \tag{2.9}$$

$$g_2(z) = \frac{1 - \mathrm{e}^{-2kh}}{1 - \mathrm{e}^{2kH}} \left[\mathrm{e}^{kz} + \mathrm{e}^{-k(z-2H)}\right]. \tag{2.10}$$

An incident plane wave with wave number k along the positive x-axis is of the following form:

$$\psi_0 = g_1(z) \mathrm{e}^{\mathrm{i}kR\cos\alpha}, \tag{2.11}$$

$$\phi_0 = g_2(z) \mathrm{e}^{\mathrm{i}kR\cos\alpha}, \tag{2.12}$$

in the respective regions.

2.3 The radiation problem for a submerged sphere

For developing the general theory of three-dimensional wave-structure interactions in two-layer fluids we consider the problem involving a submerged sphere which is placed in either layer of the fluid. Then the radiation and scattering problems for the sphere can be calculated by using the method of multipole expansions.

Multipoles are the solutions of Laplace's equation which are singular at the center of the sphere and behave like outgoing cylindrical waves far from the singularity. We consider a neutrally buoyant sphere with the center at $(0, 0, f)$. If $f < 0$, the sphere is in the upper fluid; whereas if $f > 0$, the sphere is in the lower fluid. Having already defined cylindrical polar coordinates (R, α, z) in Section 2.2, here we define spherical polar coordinates (r, θ, α) centered on the sphere defined by the equations

$$x = r\sin\theta\cos\alpha,\ y = r\sin\theta\sin\alpha,\ z - f = r\cos\theta, \tag{2.13}$$

where $r = a$ is the surface of the sphere with $a < \mid f \mid$.

2.3.1 Sphere in the lower layer

The multipoles can be constructed using the method developed by Thorne [73]. A solution of Laplace's equation singular at $z = f$ is $r^{-(n+1)}P_n^m(\cos\theta)\cos m\alpha, n \geq m \geq 0$, and the integral representation for this case is

$$\frac{P_n^m(\cos\theta)}{r^{n+1}}\cos m\alpha = \begin{cases} \dfrac{\cos m\alpha}{(n-m)!}\displaystyle\int_0^\infty u^n\, \mathrm{e}^{-u(z-f)}J_m(uR)du, & \text{for } z > f, \\ \dfrac{(-1)^{m+n}\cos m\alpha}{(n-m)!}\displaystyle\int_0^\infty u^n\, \mathrm{e}^{u(z-f)}J_m(uR)du, & \text{for } z < f. \end{cases} \tag{2.14}$$

Now we try to solve the boundary value problem defined by (2.1)-(2.5) in the form $\psi_n^m\cos m\alpha$ and $\phi_n^m\cos m\alpha$, where

$$\psi_n^m = \frac{a^{n+1}}{(n-m)!}\int_0^\infty A(u)\cosh u(h+z)J_m(uR)du, \tag{2.15}$$

$$\phi_n^m = \left(\frac{a}{r}\right)^{n+1}P_n^m(\cos\theta) + \frac{a^{n+1}}{(n-m)!}\int_0^\infty [B(u)\cosh u(H-z) + C(u)\sinh uz]J_m(uR)du. \tag{2.16}$$

With the help of boundary conditions on the interface and near the walls we find, exactly as in [36], that

$$A(u) = \frac{K}{1-\rho}\frac{u^n[\mathrm{e}^{-u(H-f)} + (-1)^{m+n}\,\mathrm{e}^{u(H-f)}]}{\Delta(u)}, \tag{2.17}$$

$$B(u) = \frac{-u^n}{\sinh uH}\left\{\frac{K}{1-\rho}\sinh uh\left[\frac{\mathrm{e}^{-u(H-f)} + (-1)^{m+n}\mathrm{e}^{u(H-f)}}{\Delta(u)}\right] - \mathrm{e}^{-u(H-f)}\operatorname{sech} uH - (-1)^{m+n}\mathrm{e}^{-uf}\right\}, \tag{2.18}$$

$$C(u) = u^n\mathrm{e}^{-u(h-f)}\operatorname{sech} uh, \tag{2.19}$$

with $\Delta(u)$ same as dispersion relation (2.6). So the integrands in (2.15) and (2.16) have a simple pole at $u = k$. Note that $u = 0$ is not a simple pole in (2.15) and (2.16) because the numerators also vanish at $u = 0$. Since the multipoles behave like outgoing waves as $R \to \infty$, so the path of integration is indented to pass beneath the simple pole at $u = k$.

The far-field form of lower fluid potential ϕ_n^m, as $kR \to \infty$, is given by

$$\phi_n^m \sim (-\mathrm{i})^{m+1}\frac{a^{n+1}}{(n-m)!}\left(\frac{2\pi}{R}\right)^{1/2}k^{n-1/2}\mathrm{e}^{\mathrm{i}kR-\mathrm{i}\pi/4}\left(\frac{R_1}{R_2}\right), \tag{2.20}$$

where,

$$R_1 = (-1)^{m+n}[k\sinh kh + \frac{K}{1-\rho}(\sinh kh - \rho\cosh kh)]\mathrm{e}^{-kf}\cosh k(H-z) + \mathrm{e}^{-k(H-f)}\left[k\sinh kh\cosh kz - \frac{K}{1-\rho}(\sinh kh\sinh kz + \rho\cosh kh\cosh kz)\right], \tag{2.21}$$

$$R_2 = \frac{1}{4}\left\{\mathrm{e}^{-k(H-h)} + (2HK\sigma - 2Hk - 1)\mathrm{e}^{k(H+h)} + (2hK\sigma + 2hk - 1)\mathrm{e}^{-k(H+h)} + [1 + 2(H-h)(k-K)]\mathrm{e}^{k(H-h)}\right\}. \tag{2.22}$$

Expanding the velocity potential for the lower fluid, defined by (2.16), about $r = 0$ in spherical coordinate system (r, θ, α) by using the following identity [73]

$$\mathrm{e}^{\pm u(z-f)} J_m(uR) = (\pm 1)^m \sum_{s=m}^{\infty} \frac{(\pm ur)^s}{(s+m)!} P_s^m(\cos\theta), \tag{2.23}$$

ϕ_n^m can be written as

$$\phi_n^m = \left(\frac{a}{r}\right)^{n+1} P_n^m(\cos\theta) + \sum_{s=m}^{\infty} A_{ns}^m \left(\frac{r}{a}\right)^s P_s^m(\cos\theta), \tag{2.24}$$

with

$$\begin{aligned} A_{ns}^m = \frac{a}{(n-m)!(s+m)!} \int_0^{\infty} \frac{(au)^{n+s}}{\Delta(u)} \Bigg\{ (-1)^{m+n+1} \left[u \sinh uh + \frac{K}{1-\rho} (\sinh uh - \rho \cosh uh) \right] \\ \times \left[\frac{(-1)^{m+s} \mathrm{e}^{u(H-2f)} + \mathrm{e}^{-uH}}{2} \right] - \left(u \sinh uh - \frac{K\rho}{1-\rho} \cosh uh \right) \left[\frac{(-1)^{m+s} \mathrm{e}^{-uH} - \mathrm{e}^{-u(H-2f)}}{2} \right] \\ - \frac{K}{1-\rho} \sinh uh \left[\frac{(-1)^{m+s} \mathrm{e}^{-uH} - \mathrm{e}^{-u(H-2f)}}{2} \right] \Bigg\} du. \end{aligned} \tag{2.25}$$

For the computational results, the contour integral in the above expression (2.25) can be written as the sum of the principal value integral and the residual contributions corresponding to the simple pole k. However, the principal value integral can be calculated easily by using the method in [46].

The solutions of the radiation problems in the cases of heave and sway are denoted by ϕ^0 and ϕ^1, respectively. For the heave case, the body velocity is given by $U^0 = \mathrm{Re}\{U\mathrm{e}^{-\mathrm{i}\omega t}\}\hat{k}$, where $\hat{k}$ is a unit vector in the z-direction, whereas for the sway case, the body velocity is $U^1 = \mathrm{Re}\{U\mathrm{e}^{-\mathrm{i}\omega t}\}\hat{i}$, where $\hat{i}$ is a unit vector in the x-direction. Since $P_1^0(\cos\theta) = \cos\theta$ and $P_1^1(\cos\theta) = \sin\theta$, we have the following body boundary conditions for heave and sway problems:

$$\frac{\partial \phi^m}{\partial n} = U\, n_m, \qquad m = 0, 1 \qquad \text{on} \quad r = a, \tag{2.26}$$

where $n(n_0, n_1)$ is the normal vector which is defined as positive when directed into the fluid domain from the boundary of the sphere $r = a$. So for the spherical coordinate system, the components of the normal vector along the directions of the heave and sway motions are as follows:

$$n_0 = \cos\theta, \; n_1 = \sin\theta\cos\alpha.$$

Therefore the body boundary conditions (2.26) for the heave and sway problems can be reconstituted as:

$$\frac{\partial \phi^m}{\partial r} = U P_1^m(\cos\theta)\cos m\alpha \quad \text{on} \quad r = a, \quad 0 \le \theta \le \pi, \quad 0 \le \alpha < 2\pi, \quad m = 0, 1. \tag{2.27}$$

An appropriate multipole expansion for the velocity potential ϕ^m is

$$\phi^m = Ua\cos m\alpha \sum_{n=1}^{\infty} b_n^m \phi_n^m, \qquad m = 0, 1, \tag{2.28}$$

where b_n^m are unknown coefficients. Note that the $n = 0$ term has been omitted since this term corresponds to one r^{-1} singularity at the center of the sphere which is physically unacceptable, as it would imply an instantaneous flux of fluid across the surface of the sphere.

The expansion form of ϕ^m in (2.28) satisfies all the conditions of the problem except the body boundary condition (2.27). By applying this condition and using the orthogonality property of associated Legendre polynomials, we arrive at an infinite system of linear algebraic equations for the infinite number of unknowns b_n^m:

$$b_s^m - \frac{s}{s+1} \sum_{n=1}^{\infty} A_{ns}^m b_n^m = -\frac{\delta_{1s}}{2}, \qquad s \geq 1, \qquad m = 0, 1, \tag{2.29}$$

where δ_{ns} is the Kronecker delta.

For computational purpose this infinite system can be truncated to an $N \times N$ system with N number of unknowns b_s^m, $s = 1, 2, \cdots, N$. We keep increasing this N up to the value when the solution of the system converges to a required degree of accuracy. By increasing the value of N the convergence of the method can be checked, and provided the method converges, greater accuracy can be achieved at the expense of computing time by considering larger values of N. The method will converge if the values obtained for the coefficients b_s^m tend to some limiting value as $N \to \infty$. The system (2.29) is extremely well-behaved, and very good approximations can be obtained even with smaller values of N. The main advantage of the multipole expansion method for solving this particular problem is that a well-behaved system like (2.29) arises, for which the truncation parameter required to achieve accurate results is very small, and hence consideration of $N = 4$ is sufficiently appropriate to get accurate results.

The hydrodynamic forces on the sphere for heave and sway motions are given by $F^m = \mathrm{Re}\{f^m \mathrm{e}^{-\mathrm{i}\omega t}\}$ for $m = 0$ and $m = 1$, respectively. If we non-dimensionalize this time-independent part f^m with respect to the mass M of the fluid displaced by the sphere and the maximum acceleration of the sphere $U\omega$, we obtain the relation between the added-mass and damping coefficients μ^m and ν^m, respectively, for the case of lower layer fluid, which is of the following form:

$$\mu^m + \mathrm{i}\nu^m = -\frac{\rho_1}{MU} \int_0^{2\pi} \int_0^{\pi} \phi^m(a, \theta, \alpha) P_1^m(\cos\theta) \cos m\alpha \; a^2 \sin\theta \; d\theta \; d\alpha \qquad m = 0, 1. \tag{2.30}$$

With the help of (2.24) and (2.28), (2.30) reduces to

$$\mu^m + \mathrm{i}\nu^m = -[b_1^m + \sum_{n=1}^{\infty} A_{n1}^m b_n^m]. \tag{2.31}$$

Again this equation can be simplified by using (2.29) for $s = 1$:

$$\mu^m + \mathrm{i}\nu^m = -(1 + 3b_1^m) \qquad m = 0, 1. \tag{2.32}$$

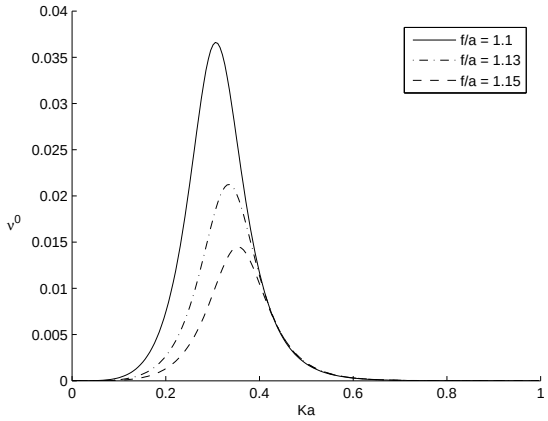

Figure 2.2: Heave damping coefficient ν^0 plotted against Ka for a submerged sphere at different depths in lower layer fluid.

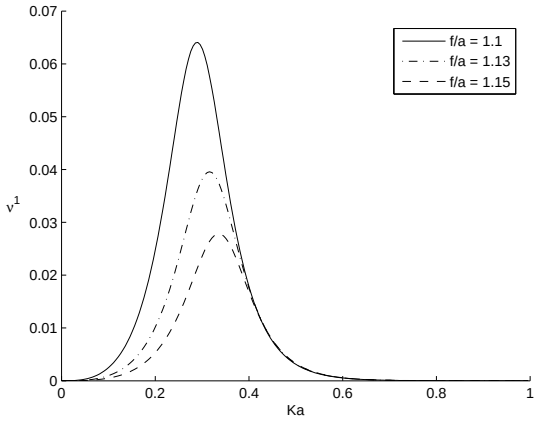

Figure 2.3: Sway damping coefficient ν^1 plotted against Ka for a submerged sphere at different depths in lower layer fluid.

Once we know the values of b_n^m from the system (2.29), we can find the values of added-mass and damping coefficients easily for heave and sway cases from (2.32). The various plots of added-mass and damping coefficient for heave and sway cases are shown in figures 2.2-2.5. For convenience, the ratio ρ $(= \rho_2/\rho_1)$ between the densities of the fluids is considered to be 0.95 (we may take the radius of the sphere to be $a = 1$) with $H = 4a$ and $h = 4a$ in all the cases. The different curves in each figure correspond to different submersion depths of the sphere in the fluid, $f/a = 1.1,\ 1.13$ and 1.15. Increasing values of f/a means that the sphere is considered away from the interface.

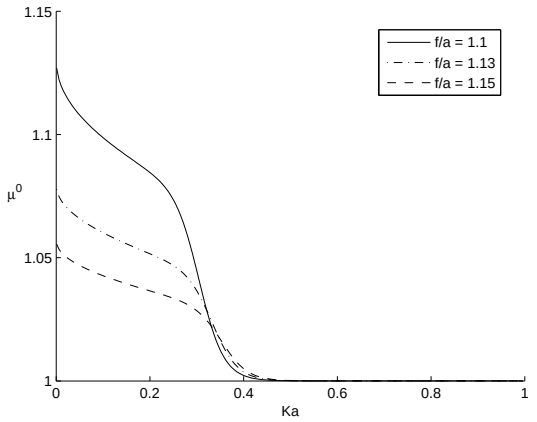

Figure 2.4: Heave added-mass μ^0 plotted against Ka for a submerged sphere at different depths in lower layer fluid.

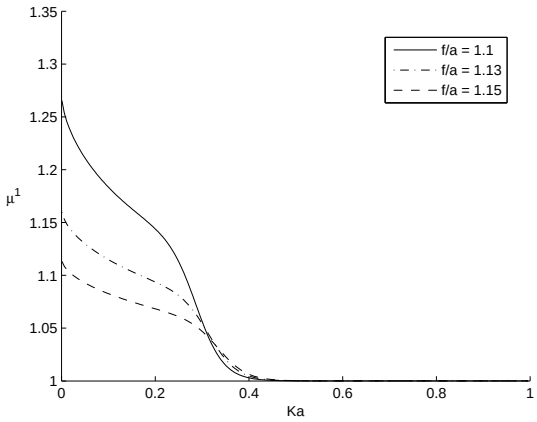

Figure 2.5: Sway added-mass μ^1 plotted against Ka for a submerged sphere at different depths in lower layer fluid.

Figures 2.2 and 2.3, respectively, show the damping coefficients of heave and sway. It can be seen that in figure 2.2 the maximum value 0.03635 occurs near $ka = 0.34254$ which corresponds to $Ka = 0.301$, and in figure 2.3 the maximum value 0.0634 occurs near $ka = 0.32578$ which corresponds to $Ka = 0.281$. It is observed that whenever the sphere is nearer to the interface

between the layers, the values of damping coefficients increase. The damping coefficient for the sway case is greater than the damping coefficient for the heave case. The values of the damping coefficients for both heave and sway are observed to be smaller than those obtained in [9] due to the absence of the free surface and the boundedness of the lower fluid in our case.

Figures 2.4 and 2.5, respectively, show the added-mass coefficients for different submersion depths for the case of heave and sway. As the immersion depth increases, the added-mass coefficients are observed to move towards the constant value of 1, which is the added-mass of a moving sphere in an infinite domain of fluid. When the sphere is closer to the interface, deviation from the value 1 is greater for the sway case than that for the heave case.

2.3.2 Sphere in the upper layer

For the problems in which the sphere is in the upper layer, we have to modify the multipoles singular at $z = f < 0$. This can be done in the same way as was done previously for the case of lower layer ($f > 0$). The suitable multipoles are:

$$\psi_n^m = \left(\frac{a}{r}\right)^{n+1} P_n^m(\cos\theta) + \frac{a^{n+1}}{(n-m)!}\int_0^\infty [A(u)\cosh u(h+z) + B(u)\sinh uz] J_m(uR)du, \quad (2.33)$$

$$\phi_n^m = \frac{a^{n+1}}{(n-m)!}\int_0^\infty C(u)\cosh u(H-z)J_m(uR)du, \quad (2.34)$$

where ϕ_n^m satisfy the condition (2.3) directly. With the help of the rest of the boundary conditions (2.2), (2.4) and (2.5), we calculate the values of the coefficients in the above equations as

$$A(u) = \frac{-u^n}{\sinh uh}\left\{\left[\frac{e^{u(h-f)} + (-1)^{m+n}e^{-u(h-f)}}{(1-\rho)\Delta(u)}\right] K\rho\sinh Hh - (-1)^{m+n}e^{-u(H-f)}\operatorname{sech} uh - e^{-uf}\right\}, \quad (2.35)$$

$$B(u) = (-1)^{m+n+1}u^n e^{-u(h-f)}\operatorname{sech} uh, \quad (2.36)$$

$$C(u) = \frac{K\rho}{1-\rho}\frac{u^n}{\Delta(u)}[e^{u(h-f)} + (-1)^{m+n}e^{-u(h-f)}], \quad (2.37)$$

where $\Delta(u)$ is same as was in the lower fluid case. After putting the values of $A(u)$ and $B(u)$, (2.33) becomes

$$\psi_n^m = \left(\frac{a}{r}\right)^{n+1} P_n^m(\cos\theta) + \frac{a^{n+1}}{(n-m)!}\int_0^\infty \frac{u^n}{\Delta(u)} Q(u) J_m(uR)du, \quad (2.38)$$

where

$$Q(u) = \left[\frac{K}{1-\rho}(\cosh uH - \rho\sinh uH) - u\sinh uH\right] e^{-uf}\cosh u(h+z) + (-1)^{m+n}e^{-u(h-f)} \times \left[\frac{K}{1-\rho}(\cosh uH\cosh uz - \rho\sinh uH\sinh uz) - u\sinh uH\cosh uz\right]. \quad (2.39)$$

For the upper layer fluid, the far-field form of the potential ψ_n^m, as $kR \to \infty$, is given by

$$\psi_n^m \sim (-\mathrm{i})^{m+1}\frac{a^{n+1}}{(n-m)!}\left(\frac{2\pi}{R}\right)^{1/2} k^{n-1/2}e^{\mathrm{i}kR - \mathrm{i}\pi/4}\left(\frac{Q_k}{R_2}\right), \quad (2.40)$$

where Q_k is the value of $Q(u)$ at $u = k$ and R_2 is same as that for the lower layer fluid case given by (2.22).

As was in the lower layer fluid case, here also the multipoles are expanded about $r = 0$ by using (2.14), that is,

$$\psi_n^m = \left(\frac{a}{r}\right)^{n+1} P_n^m(\cos\theta) + \sum_{s=m}^{\infty} B_{ns}^m \left(\frac{r}{a}\right)^s P_s^m(\cos\theta), \tag{2.41}$$

where

$$\begin{aligned} B_{ns}^m = \frac{a}{(n-m)!(s+m)!}\int_0^\infty \frac{(au)^{n+s}}{\Delta(u)}\Bigg\{\left[\frac{K}{1-\rho}(\cosh uH - \rho\sinh uH) - u\sinh uH\right] \\ \times\left[\frac{\mathrm{e}^{uh}+(-1)^{m+s}\,\mathrm{e}^{-u(h+2f)}}{2}\right] + (-1)^{m+n}\left(\frac{K}{1-\rho}\cosh uH - u\sinh uH\right) \\ \times\left[\frac{\mathrm{e}^{-u(h-2f)}+(-1)^{m+s}\,\mathrm{e}^{-uh}}{2}\right] + (-1)^{m+n}\frac{K\rho}{1-\rho}\sinh uH\left[\frac{(-1)^{m+s}\,\mathrm{e}^{-uh} - \mathrm{e}^{-u(h-2f)}}{2}\right]\Bigg\}du. \end{aligned} \tag{2.42}$$

In this case also, the velocity potential can be expanded in terms of the above multipoles as

$$\psi^m = Ua\cos m\alpha \sum_{n=1}^{\infty} b_n^m \psi_n^m \qquad m = 0, 1, \tag{2.43}$$

where b_n^m are unknown coefficients. Using the body surface condition and applying the orthogonality of associated Legendre polynomials, we get the following expression:

$$b_s^m - \frac{s}{s+1}\sum_{n=1}^{\infty} B_{ns}^m b_n^m = -\frac{\delta_{1s}}{2} \qquad s \geq 1, \qquad m = 0, 1, \tag{2.44}$$

which indicates an infinite system of linear equations. Again we solve this system of equations by truncating it to an $N \times N$ system and increasing N up to the values when the solution converges to the required degree of accuracy. The same explanation, as given in Section 2.3.1, is valid for the convergence of the method. Once the system (2.44) is solved for b_n^m, the non-dimensional added-mass and damping coefficients can be calculated exactly in the same way as was done for the coefficients μ^m and ν^m in the lower layer case.

The various graphs of added-mass and damping coefficients for heave and sway cases are shown in figures 2.6-2.9. For convenience, the ratio ρ between the densities of the fluids is taken to be 0.95 with $H = 4a$ and $h = 4a$ in all the cases. The different curves in each figure are studied for the different submersion depths of the sphere in the fluid, $f/a = -1.1, -1.13$ and -1.15. Decreasing values of f/a means that the sphere is considered away from the interface.

Figures 2.6 and 2.7, respectively, show the damping coefficients for heave and sway motions. It can be seen that in figure 2.6, the maximum value 1.38282×10^{-3} occurs near $ka = 0.46323$ which corresponds to $Ka = 0.441$ and in figure 2.7, the maximum value 3.57692×10^{-3} occurs near $ka = 0.44553$ which corresponds to $Ka = 0.421$. It is observed that whenever the sphere is nearer to the interface between the layers, the damping coefficients are greater and that

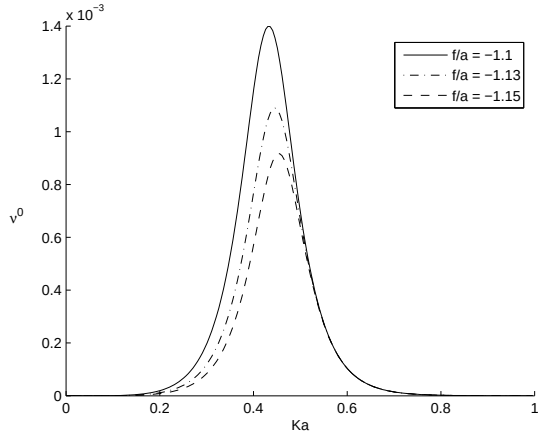

Figure 2.6: Heave damping coefficient ν^0 plotted against Ka for a submerged sphere at different depths in upper layer fluid.

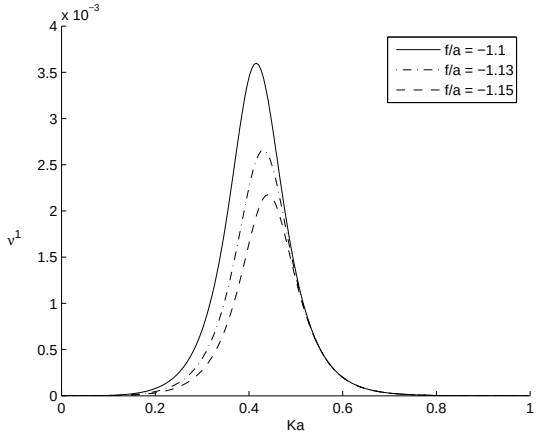

Figure 2.7: Sway damping coefficient ν^1 plotted against Ka for a submerged sphere at different depths in upper layer fluid.

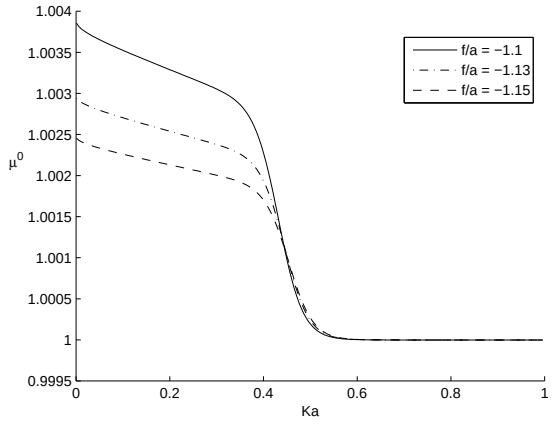

Figure 2.8: Heave added-mass μ^0 plotted against Ka for a submerged sphere at different depths in upper layer fluid.

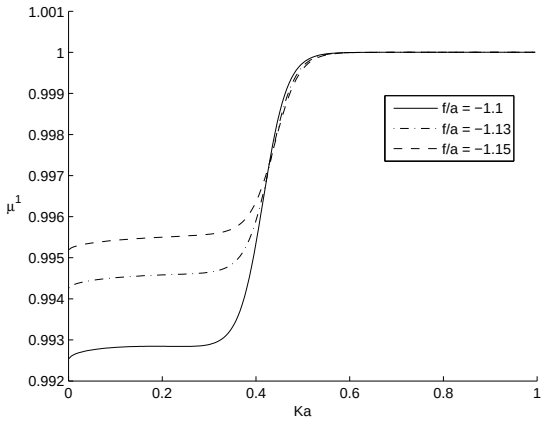

Figure 2.9: Sway added-mass μ^1 plotted against Ka for a submerged sphere at different depths in upper layer fluid.

the damping coefficients for sway motion are greater than those for the case of heave motion. Comparison of figures 2.6 and 2.7 with figures 2.2 and 2.3 shows that the values of the damping coefficients in the lower fluid is significantly greater than those in the upper fluid.

Figures 2.8 and 2.9, respectively, show the added-mass coefficients for different submersion depths for the case of heave and sway. As the immersion depth decreases the added-mass coefficients move towards to a constant value of 1. When the sphere is closer to the interface, deviation from the value 1 for the sway case is not significantly different from that for the heave case.

2.4 The scattering problem for a submerged sphere

Here we solve the problem of scattering of an incident wave of wave number k by a submerged sphere, which is placed in either of the fluid layers. In both upper and lower layer fluids, the

total potential φ (say), can be decomposed into the sum of two potentials:

$$\varphi = \varphi_I + \varphi_S, \tag{2.45}$$

where φ_I is the velocity potential due to the incident waves and φ_S due to the scattered waves. Since the potential φ satisfies (2.1)-(2.5), and the body boundary condition

$$\frac{\partial \varphi}{\partial n} = 0 \qquad \text{on the surface of the sphere, } i.e., \; r = a, \tag{2.46}$$

and also behaves like an outgoing cylindrical wave far from the sphere, therefore φ_S must satisfy (2.1)-(2.5), and the body boundary condition which is of the form

$$\frac{\partial \varphi_S}{\partial r} = -\frac{\partial \varphi_I}{\partial r} \qquad \text{on} \quad r = a. \tag{2.47}$$

2.4.1 Sphere in the lower layer

We consider an incident plane wave of wave number k and amplitude A on the interface $z = 0$ whose potential ϕ_I is of the form:

$$\begin{aligned}\phi_I &= -\frac{\mathrm{i}gA}{\omega}\left(\frac{1-\mathrm{e}^{-2kh}}{1-\mathrm{e}^{2kH}}\right)(\mathrm{e}^{kz}+\mathrm{e}^{2kH}\mathrm{e}^{-kz})\mathrm{e}^{\mathrm{i}kR\cos\alpha} \\ &= -\frac{\mathrm{i}gA}{\omega}\left(\frac{1-\mathrm{e}^{-2kh}}{1-\mathrm{e}^{2kH}}\right)(\mathrm{e}^{kz}+\mathrm{e}^{2kH}\mathrm{e}^{-kz})\sum_{m=0}^{\infty}\varepsilon_m \mathrm{i}^m J_m(kR)\cos m\alpha,\end{aligned} \tag{2.48}$$

where $\varepsilon_0 = 1, \varepsilon_m = 2$ for $m \geq 1$. Now this can be expanded, using (2.23), in spherical polar coordinates as

$$\phi_I = \frac{-\mathrm{i}gA}{\omega}\left(\frac{1-\mathrm{e}^{-2kh}}{\mathrm{e}^{-kH}-\mathrm{e}^{kH}}\right)\sum_{m=0}^{\infty}\varepsilon_m \mathrm{i}^m \cos m\alpha \sum_{s=m}^{\infty}[\mathrm{e}^{k(f-H)}+(-1)^{s+m}\,\mathrm{e}^{k(H-f)}]\frac{(kr)^s}{(s+m)!}P_s^m(\cos\theta). \tag{2.49}$$

The azimuthal angle α was known in the Section 2.3 for the radiation problem but here it is not known. So we use another more general multipole expansion which is of the form:

$$\phi_S = \frac{-\mathrm{i}gA}{\omega}\sum_{m=0}^{\infty}\sum_{n=1}^{\infty} c_n^m \phi_n^m \cos m\alpha, \tag{2.50}$$

where c_n^m are unknown coefficients which are to be determined, and ϕ_n^m the velocity potentials for the lower fluid which are given by (2.24).

Now applying the body boundary condition (2.47) and then using the orthogonality property of associated Legendre polynomials, we get an infinite system of equations for the unknown coefficients c_n^m, $n \geq 1$, which is of the form

$$c_s^m - \frac{s}{s+1}\sum_{n=1}^{\infty} c_n^m A_{ns}^m = \left(\frac{1-\mathrm{e}^{-2kh}}{\mathrm{e}^{-kH}-\mathrm{e}^{kH}}\right)[\mathrm{e}^{k(f-H)}+(-1)^{s+m}\,\mathrm{e}^{-k(f-H)}]\frac{\varepsilon_m \mathrm{i}^m s(ka)^s}{(s+1)(s+m)!}, \quad s \geq 1, \tag{2.51}$$

for each $m \geq 0$.

Here also, as in the previous case, the system can be solved by truncating it to an $N \times N$ system and increasing this N until the required degree of accuracy is acquired. The same explanation, as given in Section 2.3.1, is valid for the convergence of the method.

The time-independent part of the vertical and horizontal forces on the sphere can be calculated from the equation:

$$f^m = \rho_1 \omega \mathrm{i} \int_0^{2\pi} \int_0^{\pi} \phi(a,\theta,\alpha) P_1^m(\cos\theta) \cos m\alpha \; a^2 \sin\theta \; d\theta \; d\alpha \qquad m = 0, 1. \tag{2.52}$$

Since $\phi = \phi_I + \phi_S$, with the help of (2.49) and (2.50) and applying the orthogonality of associated Legendre polynomials, we get f^m in the form

$$f^m = \frac{4}{3}\pi a^2 \rho_1 g A \Bigg\{ \frac{1 - \mathrm{e}^{-2kh}}{\mathrm{e}^{-kh} - \mathrm{e}^{kh}} \sum_{m=0}^{\infty} \varepsilon_m \mathrm{i}^m [\mathrm{e}^{k(f-h)} + (-1)^{1+m} \, \mathrm{e}^{-k(h-f)}] \frac{ka}{(1+m)!} + \sum_{m=0}^{\infty} c_1^m + \sum_{m=0}^{\infty} \sum_{n=1}^{\infty} c_n^m A_{n1}^m \Bigg\}. \tag{2.53}$$

Using (2.51) in the above expression and then after non-dimensionalizing, we get the vertical and horizontal exciting forces $\bar{f}^0$ and $\bar{f}^1$, respectively, as:

$$\bar{f}^0 = \left| \frac{f^0}{a^2 \rho_1 g A} \right| = 4\pi |c_1^0|, \qquad \bar{f}^1 = \left| \frac{f^1}{a^2 \rho_1 g A} \right| = 4\pi |c_1^1|. \tag{2.54}$$

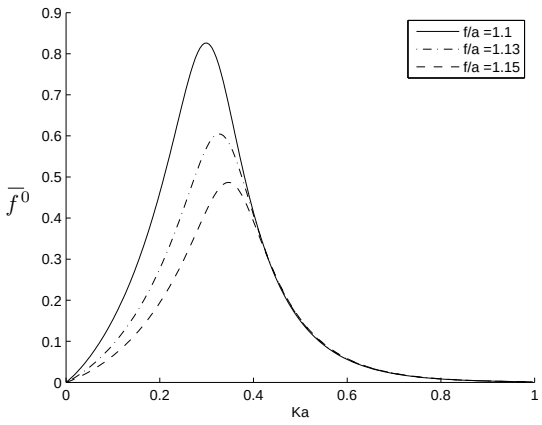

Figure 2.10: Non-dimensionalized vertical exciting force $\bar{f}^0$ plotted against Ka for a submerged sphere at different depths in lower layer fluid.

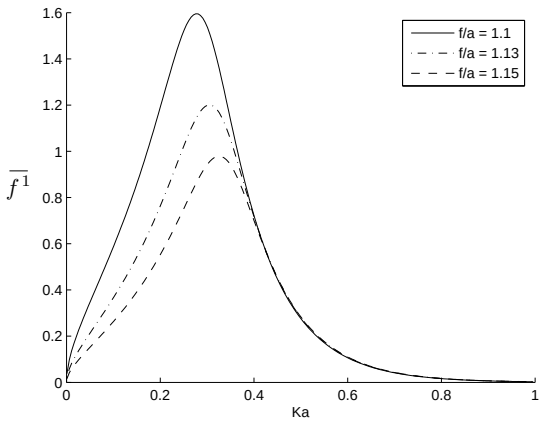

Figure 2.11: Non-dimensionalized horizontal exciting force $\bar{f}^1$ plotted against Ka for a submerged sphere at different depths in lower layer fluid.

Figures 2.10 and 2.11, respectively, show the plots of non-dimensionalized vertical and horizontal exciting forces on the sphere due to an incident wave of wave number k. In each figure the different curves correspond to different immersion depths of the sphere in the lower fluid, $f/a = 1.1,\ 1.13$ and 1.15. In all cases we consider $\rho = 0.95,\ H = 4a, h = 4a$. From these figures it can be observed that the exciting forces increase whenever the sphere is closer to the interface. Both the figures look similar but the values obtained for the vertical exciting forces $\bar{f}^1$ are greater than those for the horizontal exciting forces $\bar{f}^0$.

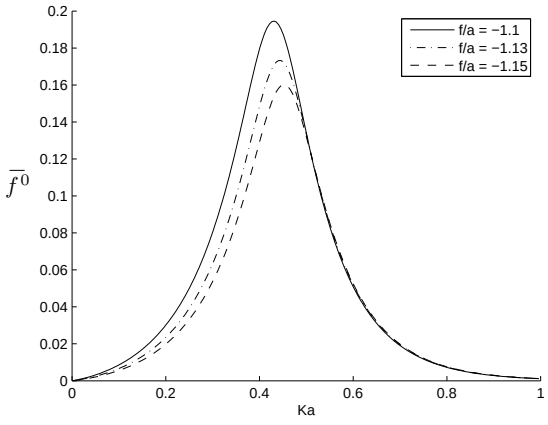

Figure 2.12: Non-dimensionalized vertical exciting force $\bar{f}^0$ plotted against Ka for a submerged sphere at different depths in upper layer fluid.

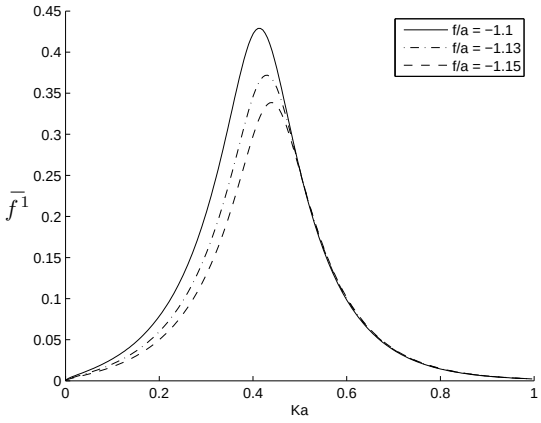

Figure 2.13: Non-dimensionalized horizontal exciting force $\bar{f}^1$ plotted against Ka for a submerged sphere at different depths in upper layer fluid.

2.4.2 Sphere in the upper layer

In the upper layer fluid the incident wave of wave number k and amplitude A on the interface $z = 0$ is of the form

$$\psi_{_I} = -\frac{\mathrm{i}gA}{\omega}\left[\mathrm{e}^{kz} + \mathrm{e}^{-k(z+2h)}\right]\mathrm{e}^{\mathrm{i}kR\cos\alpha}. \tag{2.55}$$

Now this can be expanded in spherical polar coordinates, using (2.23), as

$$\psi_{_I} = \frac{-\mathrm{i}gA}{\omega}\sum_{m=0}^{\infty}\varepsilon_m \mathrm{i}^m \cos m\alpha \sum_{s=m}^{\infty}\left[\mathrm{e}^{kf} + (-1)^{s+m}\mathrm{e}^{-k(f+2h)}\right]\frac{(kr)^s}{(s+m)!}P_s^m(\cos\theta). \tag{2.56}$$

The potential $\psi_{_S}$ can be expanded in the similar manner as in (2.50). Then applying the body boundary condition (2.47) and using the orthogonality property of associated Legendre polynomials, we get an infinite system of equations for the unknown coefficients d_n^m, $n \geq 1$, which is of the form

$$d_s^m - \frac{s}{s+1}\sum_{n=1}^{\infty} d_n^m B_{ns}^m = \left[\mathrm{e}^{kf} + (-1)^{s+m}\,\mathrm{e}^{-k(f+2h)}\right]\frac{\varepsilon_m \mathrm{i}^m\, s(ka)^s}{(s+m)!(s+1)}, \qquad s \geq 1. \tag{2.57}$$

As in the previous case, in this case also we solve the corresponding integral equation:

$$f^m = \rho_{_2}\omega\mathrm{i}\int_0^{2\pi}\int_0^{\pi}\psi(a,\theta,\alpha)P_1^m(\cos\theta)\cos m\alpha\; a^2\sin\theta\; d\theta\; d\alpha \qquad m = 0, 1. \tag{2.58}$$

After non-dimensionalizing, we get the vertical and horizontal exciting forces on the sphere which are, respectively, given by

$$\bar{f}^0 = \left|\frac{f^0}{a^2\rho_{_2}gA}\right| = 4\pi|d_1^0|, \qquad \bar{f}^1 = \left|\frac{f^1}{a^2\rho_{_2}gA}\right| = 4\pi|d_1^1|. \tag{2.59}$$

Figures 2.12 and 2.13, respectively, show the plots of non-dimensionalized vertical and horizontal exciting forces on the sphere due to an incident wave of wave number k in the upper fluid region. In each figure, the different curves correspond to different immersion depths

of the sphere in the upper fluid, $f/a = -1.1, -1.13$ and -1.15. In all cases we consider $\rho = 0.95,\ H = 4a,\ h = 4a$. From these figures it can be observed that the forces increase whenever the sphere is closer to the interface. In this case also both the figures look similar but the values obtained for the vertical exciting forces $\bar{f}^1$ are greater than those for the horizontal exciting forces $\bar{f}^0$.

All the results that are obtained throughout our work are reasonable to be compared with the work of Cadby and Linton [9] as both the problems bear similarities to a large extent. It is to be noted that there are two basic differences in the problem formulations of the present work and the work by Cadby and Linton [9]. While in [9] there was a free surface and the lower fluid was of infinite depth, which made the waves propagate with two wave numbers, our work presents a problem where the free surface has been approximated as a rigid wall and both the layers are of finite depth, which makes the wave propagate with one wave number only. Therefore it is to be expected that there must be some common features between these two works but at the same time the same values of the hydrodynamic coefficients are not to be expected. Figures 2.2–2.13 strongly illustrate the features of the work of [9], such as the comparison of the damping coefficients, added-mass coefficients and exciting forces for each of heave and sway motions, the increasing/decreasing nature of the exciting forces depending on the position of the sphere with regard to the interface, but the numerical estimates of the coefficients and the forces are not the same due to different physical considerations and formulations.

2.5 Conclusion

We have developed new expressions for multipoles, based on multipole expansion method due to Thorne [73] and Kassem [36], suitable for the solution of radiation and scattering problems concerning a submerged sphere entirely located within one of the layers of a two-layer fluid with both layers being of finite depth. The layers are bounded by upper and lower surfaces, which are approximations of the free surface and the bottom surface, respectively, in a channel. Unlike a two-layer fluid with one layer of infinite extent which has waves propagating at two different wave numbers, the waves propagate only at one wave number k in our case. By using the multipoles we solve the related radiation and scattering problems. The multipole expansion method is found to be an extremely powerful method for solving radiation and scattering problems of submerged spheres. It eliminates the need to use large and cumbersome numerical packages for the solution of such problems. The orthogonality property of associated Legendre polynomials is found to be extremely useful in evaluating various coefficients. By solving the radiation problem for heave and sway motions, the added-mass and damping coefficients are studied. The solution of the scattering problem helps us in knowing the related exciting forces associated with the submerged sphere. The values of these hydrodynamic coefficients mainly depend on the relative submersion depth with respect to the interface of the fluids. The physical

conditions under consideration and the method of solution are more powerful and physically acceptable than those used in the previous problems to solve similar type of problems. Clearly the method discussed here is applicable only to a simple and regular geometry such as sphere, but it would definitely provide an approximation to the class of problems involving bodies similar to a sphere and also could provide a check on numerical codes suitable to more elaborate structures. Furthermore, the consideration of finite depth for both the fluids makes the problem more acceptable physically. The problems formulated here have the possibility of getting extended to other forms of geometries also.

Chapter 3

Radiation by a sphere in an ice-covered two-layer fluid of finite depth

3.1 Introduction

In this chapter, we consider a two-layer fluid flow in an ocean whose upper layer is bounded above by a thin uniform ice-cover modelled as a thin elastic plate, which replaces the free surface, and the lower layer has a flat bottom surface. In this case, time-harmonic waves of a particular frequency can propagate with two different wave numbers: waves with the higher wave number propagate at the interface while waves with the lower wave number at the ice-cover. We solve the radiation problem for a submerged sphere placed in one of the layers of a two-layer fluid. The corresponding heave and sway radiation problems, either in the lower or upper layer, are solved by Thorne's multipole expansion method; *i.e.*, the added-mass and damping coefficients are evaluated for both the cases. The numerical estimates for the damping coefficients and added-mass coefficients for both the motions are evaluated and plotted. The earlier related works were limited to either solving for the potential only or solving the radiation problems for the case when one of the layers was of infinite depth with a free surface considered as the upper surface.

3.2 Mathematical formulation of the problem

We consider the irrotational motion of a two-layer inviscid incompressible fluid of relatively small amplitude under the action of gravity, neglecting any effect due to surface tension at the interface of the two fluids of which the upper layer is of finite depth and is covered by a thin uniform ice sheet modelled as a thin elastic plate, while the lower layer is bounded by a horizontal bottom surface. Each fluid is of infinite horizontal extent in x and y-directions while the depth is along z-direction which is considered vertically downwards with $z = -h$ as the mean position of the thin ice-cover. The origin O is considered at the undisturbed interface between the upper and lower fluids and $z = 0$ as the mean position of the interface of the layers. The same cylindrical coordinate system as was considered in Chapter 2 is followed here. We

further assume that all the motions are time harmonic with angular frequency ω. Under these assumptions, the velocity potentials in the lower fluid of density ρ_1 and in the upper fluid of density $\rho_2 < \rho_1$ can, respectively, be written as $\mathrm{Re}[\phi(x,y,z)\mathrm{e}^{-\mathrm{i}\omega t}]$ and $\mathrm{Re}[\psi(x,y,z)\mathrm{e}^{-\mathrm{i}\omega t}]$, where Re stands for the real part, and the potentials ϕ and ψ satisfy Laplace's equation:

$$\nabla^2\phi = \nabla^2\psi = 0 \tag{3.1}$$

in respective regions occupied by the fluids. The ratio of the densities of the two fluids ρ_2/ρ_1 (< 1) is denoted by ρ and then the linearized boundary conditions at the ice-cover, on the interface and at the bottom surface are:

$$K\psi + (D\nabla^4_{x,y} + 1 - \delta K)\frac{\partial\psi}{\partial z} = 0 \qquad \text{on} \quad z = -h, \tag{3.2}$$

$$\frac{\partial\psi}{\partial z} = \frac{\partial\phi}{\partial z} \qquad \text{on} \quad z = 0, \tag{3.3}$$

$$K\phi + \frac{\partial\phi}{\partial z} = \rho\big(K\psi + \frac{\partial\psi}{\partial z}\big) \qquad \text{on} \quad z = 0, \tag{3.4}$$

$$\frac{\partial\phi}{\partial z} = 0 \qquad \text{on} \quad z = H, \tag{3.5}$$

where $\nabla^4_{x,y} = \frac{\partial^4}{\partial x^4} + 2\frac{\partial^2}{\partial x^2}\,\frac{\partial^2}{\partial y^2} + \frac{\partial^4}{\partial y^4}$; $K = \omega^2/g$; g the acceleration due to gravity, $D = L/\rho_2 g$; L is the flexural rigidity of the elastic ice-cover, $\delta = \rho_0/(\rho_2 h_0)$; ρ_0 is the density of ice, h_0 is the very small thickness of the ice-cover.

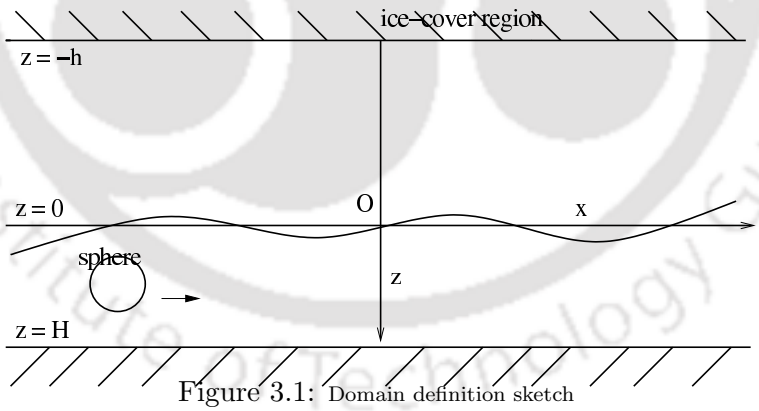

Figure 3.1: Domain definition sketch

Within this framework in a two-layer fluid, a train of progressive waves takes the form (up to an arbitrary multiplicative constant):

$$\psi = \mathrm{e}^{\pm\mathrm{i}ux}\sinh uH\left[\frac{(Du^4+1-\delta K)u\cosh u(h+z) - K\sinh u(h+z)}{K\cosh uh - (Du^4+1-\delta K)u\sinh uh}\right], \tag{3.6}$$

$$\phi = \mathrm{e}^{\pm\mathrm{i}ux}\cosh u(H-z), \tag{3.7}$$

with u satisfying the dispersion relation $\Delta(u) = 0$, where

$$\begin{aligned}\Delta(u) = {} & [u^2(1-\rho)(Du^4+1-\delta K)+K^2\rho]\sinh uh\sinh uH + K^2\cosh uh\cosh uH \\ & -uK\{(Du^4+1-\delta K)\sinh uh\cosh uH + [1+\rho(Du^4-\delta K)]\sinh uH\cosh uh\}.\end{aligned} \tag{3.8}$$

In the above dispersion equation (all the roots of the dispersion equation in a two-layer fluid, are discussed in Bhattacharjee and Sahoo [7], Chung and Fox [16]), there are two positive real roots λ_1 and λ_2 ($\lambda_1 > \lambda_2$, say) that indicate the propagating modes; a complex conjugate pair of roots corresponding to the damped propagating modes; and a countable infinity of purely imaginary roots $\mathrm{i}u_n$, $n = 1, 2, \ldots$, that relate to a set of evanescent modes, where u_n are real and positive satisfying the following equation in κ :

$$[\kappa^2(1-\rho)(D\kappa^4+1-\delta K)-K^2\rho]\sin\kappa h\sin\kappa H+K^2\cos\kappa h\cos\kappa H$$
$$+K\kappa\{(D\kappa^4+1-\delta K)\sin\kappa h\cos\kappa H+[1+\rho(D\kappa^4-\delta K)]\sin\kappa H\cos\kappa h\}=0. \qquad (3.9)$$

The negatives of all of these are also roots, being wave numbers of the waves travelling in the opposite direction. Since (3.8) has exactly two nonzero positive real roots λ_1 and λ_2, so there exist two modes of waves propagating at the interface and also just below the ice-cover along the positive x-direction.

The velocity potentials take different forms in the upper and lower regions which can be characterized by their following far-field forms, as $\lambda_j R \to \infty$ ($j = 1, 2$),

$$\psi \sim \left(\frac{2}{\pi\lambda_1 R}\right)^{1/2} \mathrm{e}^{\mathrm{i}\lambda_1 R-\mathrm{i}\pi/4}\, A(\alpha)\, g_1(z) + \left(\frac{2}{\pi\lambda_2 R}\right)^{1/2} \mathrm{e}^{\mathrm{i}\lambda_2 R-\mathrm{i}\pi/4}\, B(\alpha)\, g_2(z), \qquad (3.10)$$

$$\phi \sim \left(\frac{2}{\pi\lambda_1 R}\right)^{1/2} \mathrm{e}^{\mathrm{i}\lambda_1 R-\mathrm{i}\pi/4} A(\alpha)\cosh\lambda_1(H-z) + \left(\frac{2}{\pi\lambda_2 R}\right)^{1/2} \mathrm{e}^{\mathrm{i}\lambda_2 R-\mathrm{i}\pi/4} B(\alpha)\cosh\lambda_2(H-z), \qquad (3.11)$$

Here $A(\alpha)$ and $B(\alpha)$ are arbitrary functions of α, and the functions $g_1(z)$ and $g_2(z)$ are given by

$$g_j(z) = \frac{\sinh\lambda_j H[(D\lambda_j^4+1-\delta K)\lambda_j\cosh\lambda_j(h+z)-K\sinh\lambda_j(h+z)]}{K\cosh\lambda_j h-(D\lambda_j^4+1-\delta K)\lambda_j\sinh\lambda_j h}, \quad j = 1, 2. \qquad (3.12)$$

An incident plane wave with wavenumber λ_j along the positive x-axis is of the following form:

$$\psi_0 = g_j(z)\,\mathrm{e}^{\mathrm{i}\lambda_j R\cos\alpha}, \qquad (3.13)$$

$$\phi_0 = \cosh\lambda_j(H-z)\,\mathrm{e}^{\mathrm{i}\lambda_j R\cos\alpha}, \qquad (3.14)$$

for $j = 1, 2$ in the respective regions.

In the next section, we will consider the radiation problem for a submerged sphere in either layer of the fluid and solve the problem by multipole expansion method.

3.3 Solution by multipoles

3.3.1 Sphere submerged in the lower layer

For developing the general theory of three-dimensional wave-structure interactions in a two-layer fluid with an ice-cover, we consider the problem involving a submerged sphere which is

placed in either layer of the fluid. Then the radiation problem for a submerged sphere can be solved by using the method of multipole expansions. The same spherical coordinate system as was considered in Chapter 2 is followed here.

Hydrodynamic coefficients

The multipoles can be constructed using the method developed by Thorne [73]. A solution of Laplace's equation singular at $z = f$ is $r^{-(n+1)}P_n^m(\cos\theta)\cos m\alpha,\ n \geq m \geq 0$, and its integral representation for this case is given in Section 2.3.1.

Now we try to solve the boundary value problem defined by (3.1)-(3.5) in the form ψ_n^m and ϕ_n^m, where

$$\psi_n^m = \cos m\alpha \left[\frac{a^{n+1}}{(n-m)!}\int_0^\infty \{A(u)\ \mathrm{e}^{uz} + B(u)\ \mathrm{e}^{-uz}\}\ J_m(uR)du\right], \tag{3.15}$$

$$\phi_n^m = \cos m\alpha \left[\left(\frac{a}{r}\right)^{n+1} P_n^m(\cos\theta) + \frac{a^{n+1}}{(n-m)!}\int_0^\infty \{A_1(u)\ \mathrm{e}^{uz} + B_1(u)\ \mathrm{e}^{-uz}\}\ J_m(uR)du\right]. \tag{3.16}$$

With the help of the boundary conditions at the ice-cover, on the interface and at the bottom surface, we find $A(u),\ B(u),\ A_1(u)$ and $B_1(u)$ as

$$A(u) = \frac{[(Du^4+1-\delta K)u - K]\mathrm{e}^{uh}[(-1)^{m+n}\ \mathrm{e}^{u(H-f)} + \mathrm{e}^{-u(H-f)}]}{2[(Du^4+1-\delta K)u\sinh uh - K\cosh uh]} \times \left[\mathrm{e}^{-uH} - \frac{(Du^4+1-\delta K)uK\sinh uh - K^2\cosh uh}{\Delta(u)}\right], \tag{3.17}$$

$$B(u) = \frac{[(Du^4+1-\delta K)u + K]\mathrm{e}^{-uh}[(-1)^{m+n}\ \mathrm{e}^{u(H-f)} + \mathrm{e}^{-u(H-f)}]}{2[(Du^4+1-\delta K)u\sinh uh - K\cosh uh]} \times \left[\mathrm{e}^{-uH} - \frac{(Du^4+1-\delta K)uK\sinh uh - K^2\cosh uh}{\Delta(u)}\right], \tag{3.18}$$

$$A_1(u) = \frac{[(-1)^{m+n}\ \mathrm{e}^{-uf} + \mathrm{e}^{-u(2H-f)}][(Du^4+1-\delta K)uK\sinh uh - K^2\cosh uh]}{2\sinh uH\ \Delta(u)} + \mathrm{e}^{-u(2H-f)}, \tag{3.19}$$

$$B_1(u) = \frac{[(-1)^{m+n}\ \mathrm{e}^{u(2H-f)} + \mathrm{e}^{-uf}][(Du^4+1-\delta K)uK\sinh uh - K^2\cosh uh]}{2\sinh uH\ \Delta(u)}, \tag{3.20}$$

where $\Delta(u)$ is same as in (3.8). Now it may be noted here that $\Delta(u)$ has two simple non-zero roots at $u = \lambda_1, \lambda_2$. So the integrands in (3.15) and (3.16) have two simple poles at $u = \lambda_1, \lambda_2$. Since $u = 0$ will indicate that there is no wave in the region, hence $\sinh uH$ can never be zero, *i.e.*, the poles of the denominators of (3.19) and (3.20) will be due to $\Delta(u)$ only. Since the multipoles behave like outgoing waves as $R \to \infty$, so the path of integration is indented to pass beneath the simple poles at $u = \lambda_1$ and λ_2.

The far-field form of lower fluid potential ϕ_n^m, as $\lambda_j R \to \infty$, is given by

$$\phi_n^m \sim -\left[(-\mathrm{i})^{m+1}\frac{a^{n+1}}{(n-m)!}\left(\frac{2\pi}{R}\right)^{1/2}(\lambda_1^{n-1/2}\mathrm{e}^{\mathrm{i}\lambda_1 R - \mathrm{i}\pi/4}R_{\lambda_1} + \lambda_2^{n-1/2}\mathrm{e}^{\mathrm{i}\lambda_2 R - \mathrm{i}\pi/4}R_{\lambda_2})\right]\cos m\alpha, \tag{3.21}$$

with

$$R_{\lambda_j} = \cosh\lambda_j(H-z)\operatorname{cosech}\lambda_j H \times\frac{[(-1)^{m+n}\,\mathrm{e}^{\lambda_j(H-f)}+\mathrm{e}^{-\lambda_j(H-f)}][(D\lambda_j^4+1-\delta K)\lambda_j K\sinh\lambda_j h-K^2\cosh\lambda_j h]}{\Delta'(\lambda_j)}, \quad (3.22)$$

and $\Delta'(\lambda_j)$ denoting the derivative of $\Delta(u)$ with respect to u at $u=\lambda_j$, $j=1,2$.

Expanding the velocity potential for the lower fluid, defined by (3.16), about $r=0$ in spherical coordinate system (r,θ,α), by using the same identity (2.23) as was followed in Chapter 2, ϕ_n^m can be written as

$$\phi_n^m = \left(\frac{a}{r}\right)^{n+1} P_n^m(\cos\theta) + \sum_{s=m}^{\infty} A_{ns}^m \left(\frac{r}{a}\right)^s P_s^m(\cos\theta), \quad (3.23)$$

with

$$A_{ns}^m = \frac{a}{(n-m)!(s+m)!}\int_0^\infty \frac{(au)^{n+s}}{\Delta(u)}\,\frac{\operatorname{cosech} uH}{2}[(Du^4+1-\delta K)uK\sinh uh-K^2\cosh uh] \times[(-1)^{n+s}\,\mathrm{e}^{2u(H-f)}+(-1)^{m+s}+\mathrm{e}^{-2u(H-f)}+(-1)^{m+n}]du. \quad (3.24)$$

For the computational results, the contour integral in the above expression (3.24) can be written as the sum of the principal value integral and the residual contributions corresponding to the simple poles λ_1 and λ_2. However, the principal value integral can be calculated by using the method in [46]. The solutions of the radiation problems in case of heave and sway are denoted by ϕ^0 and ϕ^1, respectively. For the heave case, the body velocity is given by $U^0 = \mathrm{Re}\{U\mathrm{e}^{-\mathrm{i}\omega t}\}\hat{k}$ whereas for the sway case, the body velocity is $U^1 = \mathrm{Re}\{U\mathrm{e}^{-\mathrm{i}\omega t}\}\hat{i}$. We have the following body boundary conditions for heave and sway problems, respectively,

$$\frac{\partial\phi^m}{\partial r} = UP_1^m(\cos\theta)\cos m\alpha \quad \text{on} \quad r=a,\quad 0\le\theta\le\pi,\quad 0\le\alpha<2\pi,\quad m=0,1. \quad (3.25)$$

An appropriate multipole expansion for the velocity potential ϕ^m is

$$\phi^m = Ua\sum_{n=1}^{\infty} a_n^m\phi_n^m, \qquad m=0,1, \quad (3.26)$$

where a_n^m are unknown coefficients.

The expansion form of ϕ^m in (3.26) satisfies all the conditions of the problem except the body boundary condition (3.25). By applying this condition and using the orthogonality property of associated Legendre polynomials, we arrive at an infinite system of linear algebraic equations for the infinite number of unknowns a_n^m :

$$a_s^m - \frac{s}{s+1}\sum_{n=1}^{\infty} A_{ns}^m\, a_n^m = -\frac{\delta_{1s}}{2}, \qquad s\ge 1, \qquad m=0,1, \quad (3.27)$$

where δ_{ns} is the Kronecker delta.

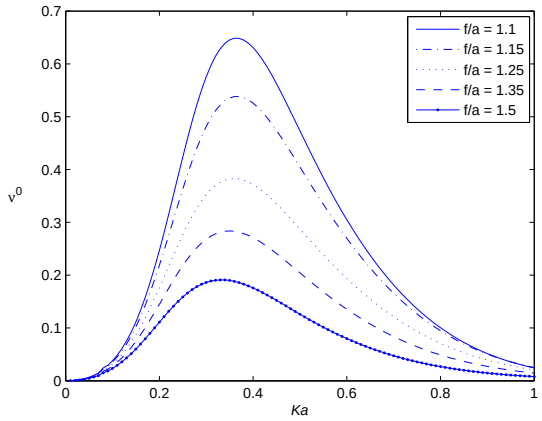

Figure 3.2: Heave damping coefficient ν^0 plotted against Ka for a submerged sphere at different depths in lower layer fluid with $D/a^4 = 1.5, \delta/a = 0.01$.

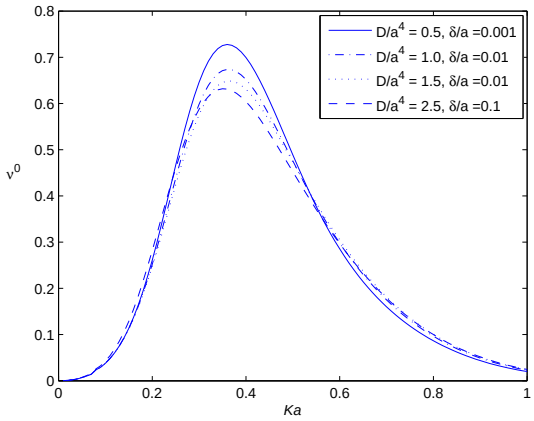

Figure 3.3: Heave damping coefficient ν^0 plotted against Ka for a submerged sphere at different ice parameters in lower layer fluid with $f/a = 1.1$.

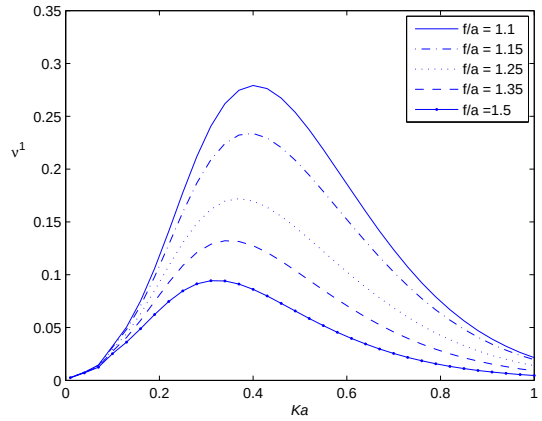

Figure 3.4: Sway damping coefficient ν^1 plotted against Ka for a submerged sphere at different depths in lower layer fluid with $D/a^4 = 1.5, \delta/a = 0.01$.

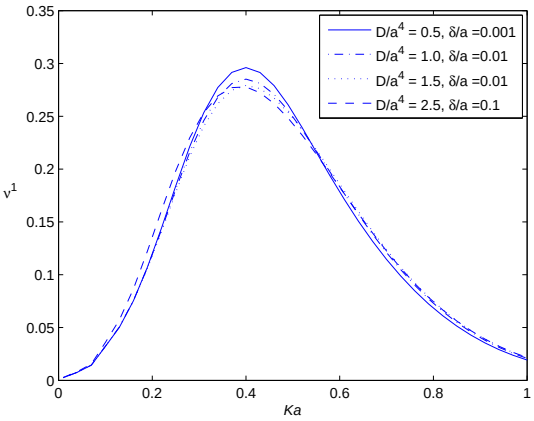

Figure 3.5: Sway damping coefficient ν^1 plotted against Ka for a submerged sphere at different ice parameters in lower layer fluid with $f/a = 1.1$.

Again we solve this system of equations by truncating it to an $N \times N$ system and increasing N up to the values when the solution converges to the required degree of accuracy. The same explanation, as in Section 2.3.1, is valid for the convergence of the method.

The hydrodynamic forces on the sphere for heave and sway motions are given by $F^m = \mathrm{Re}\{f^m \mathrm{e}^{-\mathrm{i}\omega t}\}$ for $m = 0$ and $m = 1$, respectively. If we non-dimensionalize this time-independent part f^m with respect to the mass M of the fluid displaced by the sphere and the maximum acceleration of the sphere $U\omega$, we obtain the relation between the added-mass and damping coefficients μ^m and ν^m, respectively, for the case of lower layer fluid, which is similar to equation (2.30) of Chapter 2.

With the help of (3.23) and (3.26), the relation between μ^m and ν^m, reduces to

$$\mu^m + \mathrm{i}\nu^m = -[a_1^m + \sum_{n=1}^{\infty} A_{n1}^m \, a_n^m]. \tag{3.28}$$

Again this equation can be simplified by using (3.27) for $s = 1$:

$$\mu^m + \mathrm{i}\nu^m = -(1 + 3\, a_1^m) \qquad m = 0, 1. \tag{3.29}$$

Once we know the values of a_n^m from the system (3.27), we can find the values of added-mass and damping coefficients easily from (3.29) for heave and sway cases.

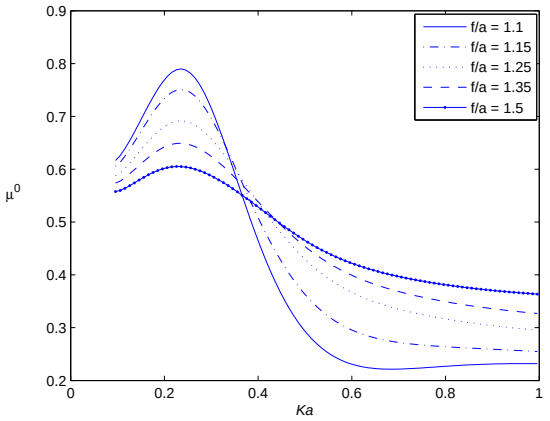

Figure 3.6: Heave added-mass coefficient μ^0 plotted against Ka for a submerged sphere at different depths in lower layer fluid with $D/a^4 = 1.5, \delta/a = 0.01$.

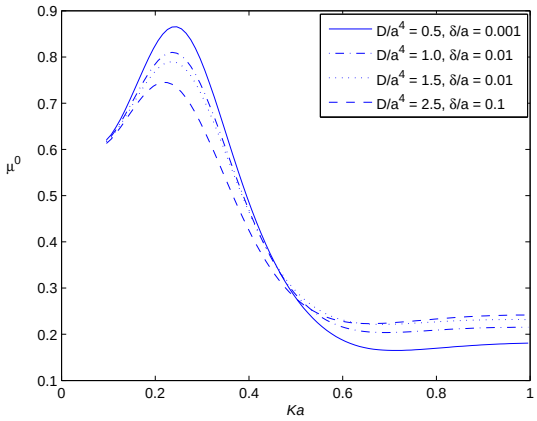

Figure 3.7: Heave added-mass coefficient μ^0 plotted against Ka for a submerged sphere at different ice parameters in lower layer fluid with $f/a = 1.1$.

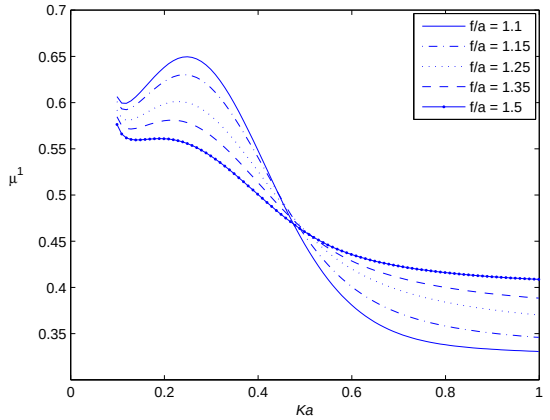

Figure 3.8: Sway added-mass coefficient μ^1 plotted against Ka for a submerged sphere at different depths in lower layer fluid with $D/a^4 = 1.5, \delta/a = 0.01$.

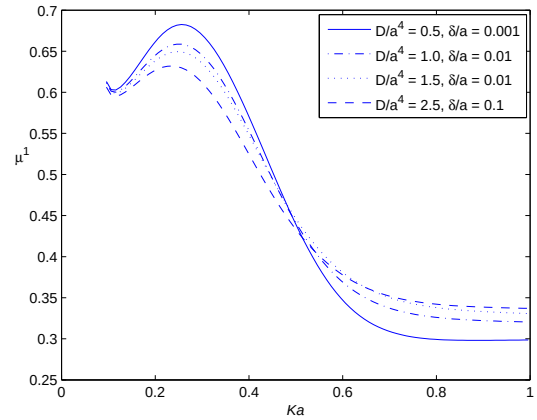

Figure 3.9: Sway added-mass coefficient μ^1 plotted against Ka for a submerged sphere at different ice parameters in lower layer fluid with $f/a = 1.1$.

Numerical results

The various plots of added-mass and damping coefficients for heave and sway cases are shown in figures 3.2-3.9. In all the cases, the depth of the lower and upper layers are taken, respectively, as $4a$ and $3a$, and the ratio ρ of the densities of the fluids as 0.5. For a two-layer fluid comprising of fresh water and salt water, the value of ρ would be ideally around 0.97. The same qualitative features are observed for such a density ratio, but the effects of the interface

are much smaller, as observed from a computational point of view. To be precise, the values of the two roots of dispersion equation approach the same value and the whole region acts like a single layer fluid of finite depth if we take the value of ρ nearer to 0.97. However, the entire analytical study for the problem consisting of a two-layer fluid of finite depth covered by ice-cover becomes inappropriate unless two wave numbers exist. For clear observation of the features, the density ratio of the fluids is chosen as 0.5. The different curves in each of the figures 3.2, 3.4, 3.6 and 3.8, are obtained by considering different submersion depths of the sphere, $f/a = 1.1,\ 1.15,\ 1.25,\ 1.35$ and 1.5, in the lower layer, while fixing the ice parameters at $D/a^4 = 1.5$ and $\delta/a = 0.01$. Increasing values of f/a means that the sphere is considered away from the interface. Figures 3.2 and 3.4, respectively, show the damping coefficients of heave and sway. It is observed that whenever the sphere is nearer to the interface between the layers, the values of damping coefficients increase so that the amplitude of the generated wave increases. The damping coefficient for heave case is greater than the damping coefficient for the sway case, similarly as was reported in [9]. Figures 3.6 and 3.8, respectively, show the added-mass coefficients for different submersion depths for the case of heave and sway. As the immersion depth increases, the added-mass for the case of heave and sway, are observed to approach a constant value greater than 0.5, which is the added-mass of a moving sphere in an infinite domain of fluid. When the sphere is closer to the interface, deviation from the value 0.5 is greater for the heave case than that for the sway case. The peak values of the added-mass for both heave and sway case, when the sphere is nearer to the interface, are observed to be similar to those obtained in [9] due to the absence of free surface and the boundedness of the lower fluid in our case.

The different curves in figures 3.3, 3.5, 3.7 and 3.9 correspond to four different sets of ice parameters $(D/a^4 = 0.5;\ \delta/a = 0.001), (D/a^4 = 1.0;\ \delta/a = 0.01), (D/a^4 = 1.5;\ \delta/a = 0.01)$ and $(D/a^4 = 2.5;\ \delta/a = 0.1)$, while f/a is fixed, for these curves, at 1.1. Figures 3.3 and 3.5, respectively, show the damping coefficients for heave and sway case, whereas figures 3.7 and 3.9, respectively, show the added-mass for the heave and sway cases. It has been observed from figures 3.3 and 3.5, that the added-mass and damping coefficients decrease when the values of ice parameters D/a^4 and δ/a increase. Here, the decreasing rate of heave damping coefficient ν^0 is very negligible as compared to that for the heave case ν^1. Again it is seen from figures 3.7 and 3.9, that as the ice parameter increases, the added-mass for heave and sway case never approach a constant value greater than 0.5.

3.3.2 Sphere submerged in the upper layer

In this section, we will consider the radiation problem for the submerged sphere which is in the upper layer of the ocean and solve this problem by multipole expansion method.

Hydrodynamic coefficients

For this case of the sphere submerged in the upper layer, we have to modify the multipoles singular at $z = f < 0$. This can be done in the same way as was done previously for the lower layer case ($f > 0$). The suitable multipoles can be written as

$$\psi_n^m = \cos m\alpha \left[\left(\frac{a}{r}\right)^{n+1} P_n^m(\cos\theta) + \frac{a^{n+1}}{(n-m)!} \int_0^\infty \{A(u)\, \mathrm{e}^{uz} + B(u)\, \mathrm{e}^{-uz}\}\, J_m(uR)du \right], \tag{3.30}$$

$$\phi_n^m = \cos m\alpha \left[\frac{a^{n+1}}{(n-m)!} \int_0^\infty \{A_1(u)\, \mathrm{e}^{uz} + B_1(u)\, \mathrm{e}^{-uz}\}\, J_m(uR)du \right]. \tag{3.31}$$

With the help of boundary conditions at the ice-cover, on the interface and at the bottom surface, we find $A(u)$, $B(u)$, $A_1(u)$ and $B_1(u)$ as follows:

$$A(u) = \frac{[(Du^4+1-\delta K)u - K]\mathrm{e}^{uh}}{2\Delta(u)} \Big((-1)^{m+n}\, \mathrm{e}^{uf} \{[(1-\rho)u - \rho K]\sinh uH - K\cosh uH\} + \mathrm{e}^{-uf}\{[(1-\rho)u + \rho K]\sinh uH - K\cosh uH\} \Big) - (-1)^{m+n}\, \mathrm{e}^{uf}, \tag{3.32}$$

$$B(u) = \frac{[(Du^4+1-\delta K)u + K]\mathrm{e}^{-uh}}{2\Delta(u)} \Big((-1)^{m+n}\, \mathrm{e}^{uf} \{[(1-\rho)u - \rho K]\sinh uH - K\cosh uH\} + \mathrm{e}^{-uf}\{[(1-\rho)u + \rho K]\sinh uH - K\cosh uH\} \Big), \tag{3.33}$$

$$A_1(u) = -\frac{\rho K \mathrm{e}^{-uH}\{[(Du^4+1-\delta K)u - K]\mathrm{e}^{u(h-f)} + (-1)^{m+n}[(Du^4+1-\delta K)u + K]\mathrm{e}^{u(f-h)}\}}{2\Delta(u)}, \tag{3.34}$$

$$B_1(u) = -\frac{\rho K \mathrm{e}^{uH}\{[(Du^4+1-\delta K)u - K]\mathrm{e}^{u(h-f)} + (-1)^{m+n}[(Du^4+1-\delta K)u + K]\mathrm{e}^{u(f-h)}\}}{2\Delta(u)}, \tag{3.35}$$

where $\Delta(u)$ is same as (3.8). After putting the values of $A(u)$ and $B(u)$, (3.30) becomes

$$\psi_n^m = \cos m\alpha \left[\left(\frac{a}{r}\right)^{n+1} P_n^m(\cos\theta) + \frac{a^{n+1}}{(n-m)!} \int_0^\infty \frac{u^n}{\Delta(u)}\, Q(u) J_m(uR)du \right], \tag{3.36}$$

where

$$Q(u) = \frac{(Du^4+1-\delta K)u\cosh u(h+z) - K\sinh u(h+z)}{\Delta(u)} \times \Big((-1)^{m+n}\, \mathrm{e}^{uf} \{[(1-\rho)u - \rho K]\sinh uH - K\cosh uH\} + \mathrm{e}^{-uf}\{[(1-\rho)u + \rho K]\sinh uH - K\cosh uH\} \Big) - (-1)^{m+n}\, \mathrm{e}^{u(z+f)}. \tag{3.37}$$

For the upper layer fluid, the far-field form of the potential ψ_n^m, as $\lambda_j R \to \infty$, can be obtained as:

$$\psi_n^m \sim -\left[(-\mathrm{i})^{m+1} \frac{a^{n+1}}{(n-m)!} \left(\frac{2\pi}{R}\right)^{1/2} (\lambda_1^{n-1/2} \mathrm{e}^{\mathrm{i}\lambda_1 R - \mathrm{i}\pi/4} R_{\lambda_1} + \lambda_2^{n-1/2} \mathrm{e}^{\mathrm{i}\lambda_2 R - \mathrm{i}\pi/4} R_{\lambda_2}) \right] \cos m\alpha, \tag{3.38}$$

with

$$R_{\lambda_j} = \frac{(D\lambda_j^4+1-\delta K)\lambda_j \cosh\lambda_j(h+z)-K\sinh\lambda_j(h+z)}{\Delta'(\lambda_j)} \times \Big((-1)^{m+n}\,\mathrm{e}^{\lambda_j f}\{[(1-\rho)\lambda_j-\rho K]\sinh\lambda_j H-K\cosh\lambda_j H\} + \mathrm{e}^{-\lambda_j f}\{[(1-\rho)\lambda_j+\rho K]\sinh\lambda_j H-K\cosh\lambda_j H\}\Big), \tag{3.39}$$

with $\Delta'(\lambda_j)$ denoting the derivative of $\Delta(u)$ at $u=\lambda_j$. As in the lower layer case, here also the multipoles are expanded about $r=0$ by using (2.23) as was followed in Chapter 2, that is,

$$\psi_n^m = \cos m\alpha\left[\left(\frac{a}{r}\right)^{n+1} P_n^m(\cos\theta) + \sum_{s=m}^{\infty} B_{ns}^m \left(\frac{r}{a}\right)^s P_s^m(\cos\theta)\right], \tag{3.40}$$

where

$$B_{ns}^m = \frac{a}{(n-m)!(s+m)!}\int_0^\infty \frac{(au)^{n+s}}{2\Delta(u)}\Big[[(1-\rho)u\sinh uH-K\cosh uH] \times\Big\{[(Du^4+1-\delta K)u-K][(-1)^{m+n}\,\mathrm{e}^{u(h+2f)}+\mathrm{e}^{uh}] +[(Du^4+1-\delta K)u+K][(-1)^{n+s}\,\mathrm{e}^{-uh}+(-1)^{m+s}\,\mathrm{e}^{-u(h+2f)}]\Big\} -\rho K\sinh uH\Big\{[(Du^4+1-\delta K)u-K][(-1)^{m+n}\,\mathrm{e}^{u(h+2f)}-\mathrm{e}^{uh}] +[(Du^4+1-\delta K)u+K][(-1)^{n+s}\,\mathrm{e}^{-uh}-(-1)^{m+s}\,\mathrm{e}^{-u(h+2f)}]\Big\}\Big]du. \tag{3.41}$$

In this case also, the velocity potential can be expanded in terms of the above multipoles as

$$\psi^m = Ua\sum_{n=1}^{\infty} b_n^m\,\psi_n^m \qquad m=0,1, \tag{3.42}$$

where b_n^m are unknown coefficients. Using the body surface condition and applying the orthogonality of associated Legendre polynomials, we get the following expression:

$$b_s^m - \frac{s}{s+1}\sum_{n=1}^{\infty} B_{ns}^m\, b_n^m = -\frac{\delta_{1s}}{2} \qquad s\geq 1, \qquad m=0,1, \tag{3.43}$$

which indicates an infinite system of linear equations. We solve this system of equations by truncating it to an $N\times N$ system and increasing N up to the values when the solution converges to the required degree of accuracy. The same explanation, as given in Section 2.3.1, is valid for the convergence of the method. Once the system (3.43) is solved for b_n^m, the non-dimensional added-mass and damping coefficients can be calculated exactly in the same way as was done for the coefficients μ^m and ν^m in the lower layer case.

Numerical results

The various graphs of added-mass and damping coefficients for heave and sway cases are shown in figures 3.10-3.17. For convenience, in all the cases, the ratio ρ between the densities of the

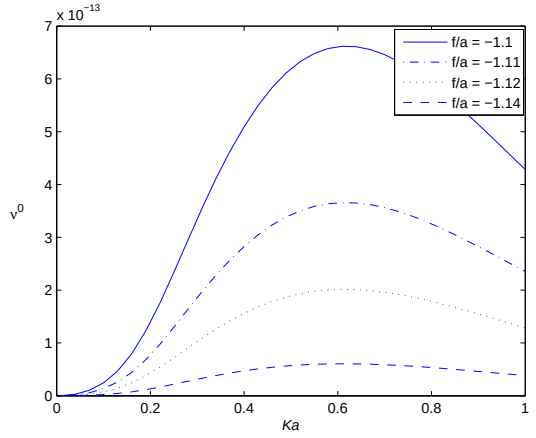

Figure 3.10: Heave damping coefficient ν^0 plotted against Ka for a submerged sphere at different depths in upper layer fluid with $D/a^4 = 1.5, \delta/a = 0.01$.

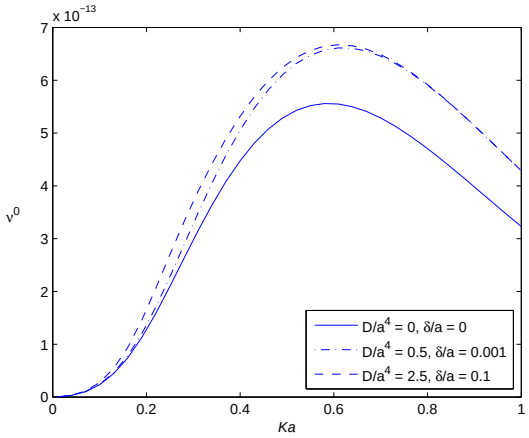

Figure 3.11: Heave damping coefficient ν^0 plotted against Ka for a submerged sphere at different ice parameters in upper layer fluid with $f/a = -1.1$.

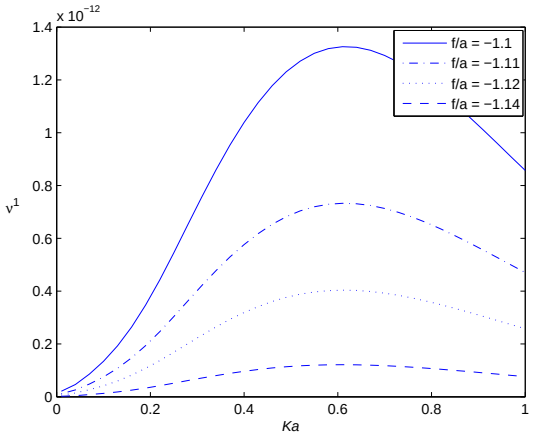

Figure 3.12: Sway damping coefficient ν^1 plotted against Ka for a submerged sphere at different depths in upper layer fluid with $D/a^4 = 1.5, \delta/a = 0.01$.

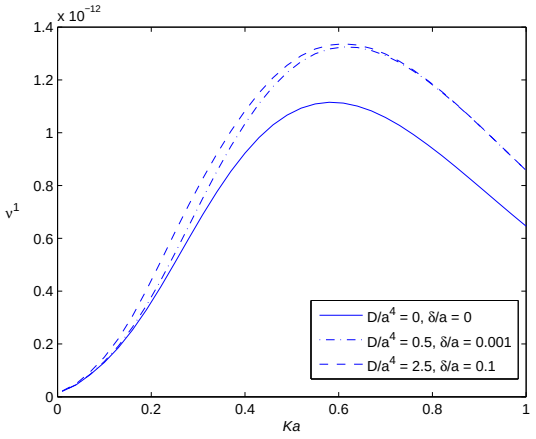

Figure 3.13: Sway damping coefficient ν^1 plotted against Ka for a submerged sphere at different ice parameters in upper layer fluid with $f/a = -1.1$.

fluids is taken to be 0.5 and the depth of the lower and upper layers, respectively, as $4a$ and $3a$. The different curves in each of the figures 3.10, 3.12, 3.14 and 3.16, are obtained by considering different submersion depths of the sphere in the upper layer fluid, $f/a = -1.1, -1.11, -1.12$ and -1.14, while fixing the ice parameters at $D/a^4 = 1.5$ and $\delta/a = 0.01$. Decreasing values of f/a means that the sphere is considered away from the interface. Figures 3.10 and 3.12, respectively, show the damping coefficients for heave and sway motions. It is observed that whenever the sphere is nearer to the interface between the layers, the damping coefficients are greater. And also the damping coefficients for sway motion are greater than those for the case of heave motion. Comparison of these figures with figures 3.2 and 3.4 shows that the values of the damping coefficients in the lower layer fluid are significantly greater than those in the upper layer fluid. Figures 3.14 and 3.16, respectively, show the added-mass coefficients for different submersion depths for the case of heave and sway. As the immersion depth decreases the added-mass coefficients move towards a constant value of 1. When the sphere is closer to

the interface, deviation from the value 1 for the sway case is not significantly different from that for the heave case.

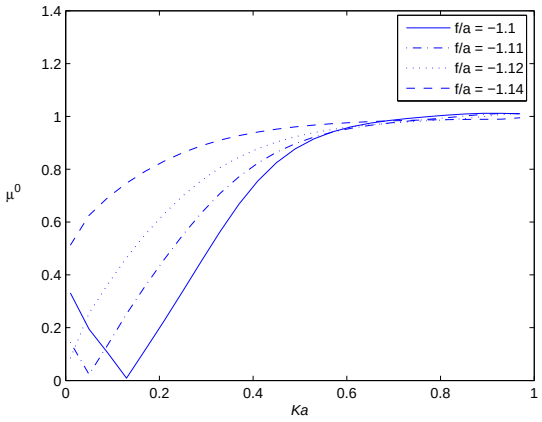

Figure 3.14: Heave added-mass coefficient μ^0 plotted against Ka for a submerged sphere at different depths in upper layer fluid with $D/a^4 = 1.5, \delta/a = 0.01$.

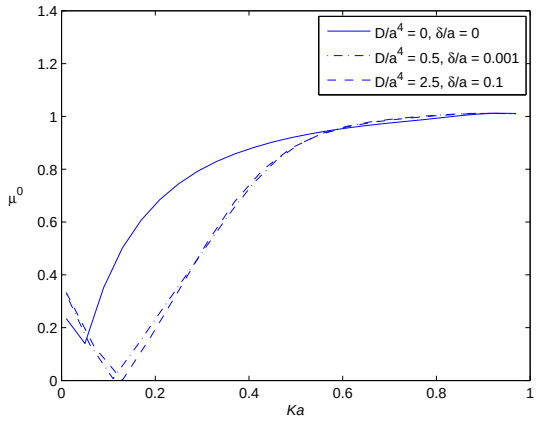

Figure 3.15: Heave added-mass coefficient μ^0 plotted against Ka for a submerged sphere at different ice parameters in upper layer fluid with $f/a = -1.1$.

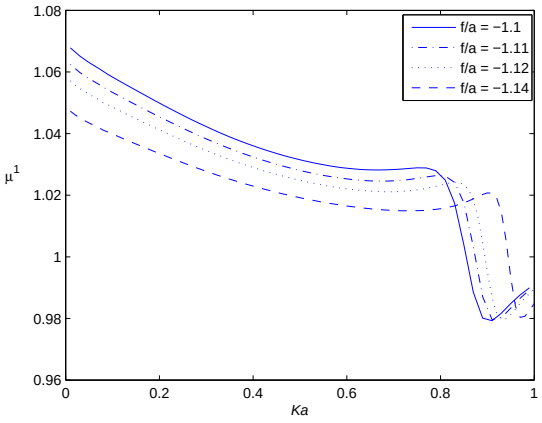

Figure 3.16: Sway added-mass coefficient μ^1 plotted against Ka for a submerged sphere at different depths in lower upper fluid with $D/a^4 = 1.5, \delta/a = 0.01$.

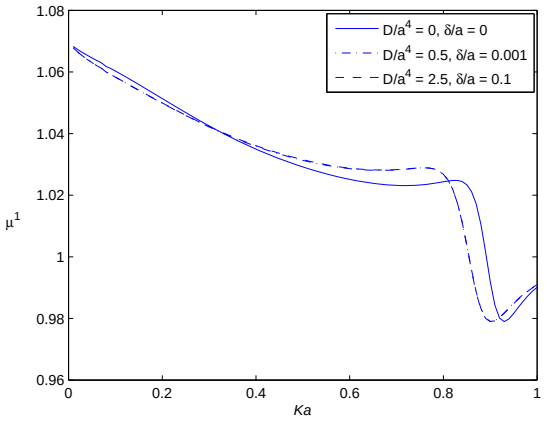

Figure 3.17: Sway added-mass coefficient μ^1 plotted against Ka for a submerged sphere at different ice parameters in upper layer fluid with $f/a = -1.1$.

The different curves in figures 3.11, 3.13, 3.15 and 3.17 correspond to three different sets of ice parameters $(D/a^4 = 0;\ \delta/a = 0), (D/a^4 = 0.5;\ \delta/a = 0.001)$ and $(D/a^4 = 2.5;\ \delta/a = 0.1)$, while f/a is fixed, for these curves, at -1.1. Figures 3.11 and 3.13, respectively, show the damping coefficients for heave and sway case, whereas figures 3.15 and 3.17, respectively, show the added-mass for the heave and sway cases. It has been observed from figures 3.11 and 3.13, that the damping coefficients for both heave and sway cases increase when the value of ice parameters D/a^4 and δ/a increase. It is also observed from these two figures that when the ice parameter increases (except the free surface value $D/a^4 = 0;\ \delta/a = 0$), the rate of change of the value of damping coefficients is very negligible for both the heave and sway case. This happens due to the presence of ice cover only. The same observation can be made for the case

of added-mass coefficients for the heave and sway cases (figures 3.15 and 3.17). As the value of ice parameter increases, the added-mass coefficients for the heave and sway case, never move towards a constant value of 1.

3.4 Conclusion

In the present chapter, based upon a multipole expansion method due to Cadby [9], Kassem [36] and Thorne [73], we have developed new expressions for multipoles, suitable for the solution of radiation problems concerning a submerged sphere entirely located within one of the layers of a two-layer fluid with both layers being of finite depth. The upper fluid is bounded above by a thin ice-cover modelled as a thin elastic plate, which replaces the free surface and the lower fluid is bounded by a horizontal bottom surface. In such a situation propagating waves can exist at two different wave numbers for any given frequency: the one with smaller wave number corresponds to an ice-surface disturbance and the other to an interfacial wave motion. By using the multipoles we solve the related radiation problem for heave and sway motions (in lower and upper layer) and study the added-mass and damping coefficients. Furthermore, the consideration of finite depth for both the fluids with ice cover makes the problem more acceptable physically.

Chapter 4

Scattering of normal internal waves in a channel with small undulations

4.1 Introduction

In the present chapter, the scattering problem discussed in Chapter 2 is taken up in which the upper fluid is bounded by a fixed wall and the lower fluid is bounded by a bottom surface which has small undulations. The scattering takes place due to a train of progressive waves propagating from negative infinity being normally incident on the channel bed having small undulations. Using a perturbation analysis involving a small non-dimensional parameter $\varepsilon(\ll 1)$, which measures the smallness of the undulation, directly to the governing boundary value problem (BVP), the original problem is reduced to a simpler BVP for the first-order correction of the potentials. The solution of this BVP is then obtained by an appropriate application of Green's integral theorem and also by Fourier transform technique applied to the potential functions describing the BVP. The reflection and transmission coefficients are subsequently evaluated approximately up to the first-order of ε in terms of integrals involving the shape function which describes the small undulation. We present two different special forms of bottom undulations, namely, a patch of sinusoidal ripples having the same wave number and a patch of sinusoidal ripples having different wave numbers. For the case of a patch of sinusoidal ripple bed, when the ripple wave number is approximately twice the wave number of the incident interface wave field, the first-order reflection coefficient is found to be increasing with the number of undulations.

4.2 Mathematical formulation

We consider the irrotational motion of a two-layer inviscid incompressible fluid under the action of gravity flowing under a rigid infinite horizontal wall which is placed at $y = -h$. There is a small cylindrical deformation described by $y = H + \varepsilon c(x)$ at the bottom of the lower layer fluid along the lateral direction, where $c(x)$ is a continuous function with compact support, H the uniform finite depth of the lower layer fluid far to either side of the undulation of the bottom.

The rigid infinite wall at $y = -h$ can be considered to be an approximation to the free surface. We neglect any effect due to surface tension at the surface separating the two fluids. Each fluid is of infinite horizontal extent in x-direction, while the depth is along y-direction which is considered vertically downwards. The origin O is considered at the undisturbed interface between the upper and the lower fluids, and $y = 0$ is the mean position of the interface of the layers. The lower fluid of density ρ_1 occupying the region $0 \leq y \leq H + \varepsilon c(x)$ is bounded by the bottom surface and the upper fluid of density $\rho_2 < \rho_1$ occupying the region $-h \leq y \leq 0$ is bounded by the fixed wall at $y = -h$. The motion is simple harmonic with a small amplitude and an angular frequency ω. For convenience let us denote the potential in the lower fluid by $\phi e^{-i\omega t}$ and that in the upper fluid by $\psi e^{-i\omega t}$, of which the actual velocity potentials are the real parts.

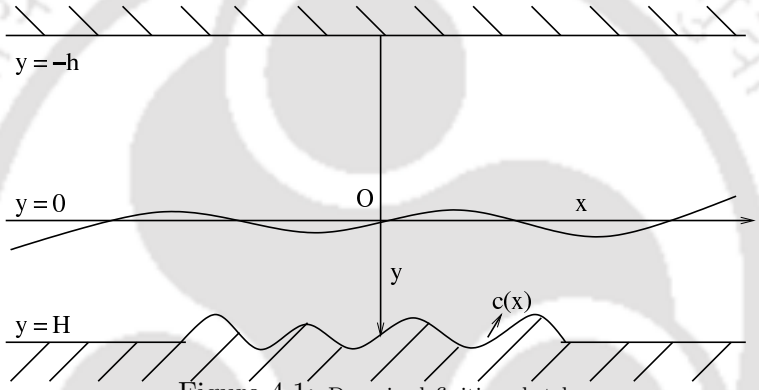

Figure 4.1: Domain definition sketch

The governing equation for each of these potentials ϕ and ψ is the Laplace's equation:

$$\nabla^2\phi = \nabla^2\psi = 0, \tag{4.1}$$

in respective regions occupied by the fluids. In addition the linearized boundary conditions on the bottom surface, near the wall and on the interface are

$$\frac{\partial\phi}{\partial n} = 0 \quad \text{on} \quad y = H + \varepsilon c(x), \tag{4.2}$$

$$\frac{\partial\psi}{\partial y} = 0 \quad \text{on} \quad y = -h, \tag{4.3}$$

$$\frac{\partial\phi}{\partial y} = \frac{\partial\psi}{\partial y} \quad \text{on} \quad y = 0, \tag{4.4}$$

$$K\phi + \frac{\partial\phi}{\partial y} = \rho(K\psi + \frac{\partial\psi}{\partial y}) \quad \text{on} \quad y = 0, \tag{4.5}$$

with $\partial/\partial n$ as the normal derivative at a point (x, y) on the bottom and $\rho = \rho_2/\rho_1 (< 1)$. As usual, the time dependence of $e^{-i\omega t}$ has been suppressed in subsequent analysis. The boundary conditions (4.4) and (4.5) represent, respectively, the continuity of normal velocity, and the pressure at the interface.

It is assumed that a train of progressive interface waves in the lower and upper fluids can

be represented by the velocity potentials

$$\phi_0(x,y) = \frac{\cosh u(H-y)}{\sinh uH}\, \mathrm{e}^{\mathrm{i}ux}, \tag{4.6}$$

$$\psi_0(x,y) = -\frac{\cosh u(h+y)}{\sinh uh}\, \mathrm{e}^{\mathrm{i}ux}, \tag{4.7}$$

with u satisfying the dispersion relation $\Delta(u) = 0$, where $\Delta(u)$ is same as in (2.6).

In the dispersion equation, there is a positive real root k, that indicates the propagating modes of the fluid at the interface and a countable infinity of purely imaginary roots $\mathrm{i}u_n$, $n = 1, 2, \cdots$, (Appendix A) that relate to a set of evanescent modes, where u_n are real and positive satisfying the following equation in κ :

$$\frac{K}{1-\rho}(\cos\kappa H \sin\kappa h + \rho \sin\kappa H \cos\kappa h) + \kappa \sin\kappa h \sin\kappa H = 0.$$

The intensity of evanescent mode of waves decays exponentially with distance from the interface at which they are formed. Due to this evanescent mode of waves appearing in the fluid region, a part of the incident interfacial wave becomes trapped and leads to a standing wave pattern over the bottom irregularities at the time when the incident wave is scattered by the bottom undulation. This phenomenon is known as *Anderson localization*. More precisely, this implies that a periodic plane wave of finite wavelength coming on to the part of the channel with a random bottom will eventually be totally reflected, *i.e.*, the amplitude of the disturbance created by the wave will die off exponentially with distance, with a typical length which is called the *localization length*. Detailed investigations related to Anderson localization can be found in Guazzelli *et al.* [31], Devillard *et al.* [23], and An and Ye [1]. But these waves do not affect the asymptotic behaviour of the resultant reflected and transmitted waves. In that sense, any sort of localization is not considered while formulating and solving the present problem.

The dispersion equation has one nonzero positive simple zero at $u = k$, on the real axis of u. So only one nonzero wave number k can exist and the wave can propagate in either direction. Note that if $k = 0$, then there is no wave in the respective regions.

The above wave train, given by (4.6) and (4.7), is partially reflected by, and partially transmitted over the bottom undulation so that ϕ and ψ have asymptotic behaviours given by

$$\phi(x,y) \sim \begin{cases} T\,\phi_0(x,y) & \text{as } x \to \infty, \\ \phi_0(x,y) + R\,\phi_0(-x,y) & \text{as } x \to -\infty, \end{cases} \tag{4.8}$$

$$\psi(x,y) \sim \begin{cases} T\,\psi_0(x,y) & \text{as } x \to \infty, \\ \psi_0(x,y) + R\,\psi_0(-x,y) & \text{as } x \to -\infty, \end{cases} \tag{4.9}$$

where R and T represent, respectively, the usual reflection and transmission coefficients in water wave problems, defined to be the ratios of the amplitude of the incident wave to that of the reflected wave and to that of the transmitted wave, respectively, and are to be determined.

Since ε is assumed to be very small, hence neglecting $\mathrm{O}(\varepsilon^2)$ terms, the boundary condition $\partial\phi/\partial n = 0$ on the bottom surface $y = H + \varepsilon c(x)$ can be expressed in an appropriate form

(Appendix B) as

$$\frac{\partial \phi}{\partial y} - \varepsilon \frac{\partial}{\partial x}\left[c(x)\frac{\partial \phi}{\partial x}\right] + \mathrm{O}(\varepsilon^2) = 0 \quad \text{on} \quad y = H. \tag{4.10}$$

It is to be noted that the conditions (4.3)-(4.5) on the wall and the interface are linear conditions satisfied on horizontal planes, and consequently perturbation technique can be applied to them without any modification whereas the linear condition (4.2) on the bottom undulations needs to get converted to (4.10) as we seek to transform it to a bottom condition on a finite depth $y = H$ instead of $y = H + \varepsilon c(x)$.

4.3 Perturbation technique

The form of the boundary condition (4.10) and the fact that an interface wave train propagating in the two-layer fluid of uniform finite depth experiences no reflection together suggest that ϕ, ψ, R and T can be expressed in terms of the perturbation parameter ε as

$$\left.\begin{array}{ll} \phi &= \phi_0 + \varepsilon\phi_1 + \mathrm{O}(\varepsilon^2), \\ \psi &= \psi_0 + \varepsilon\psi_1 + \mathrm{O}(\varepsilon^2), \\ T &= 1 + \varepsilon T_1 + \mathrm{O}(\varepsilon^2), \\ R &= \varepsilon R_1 + \mathrm{O}(\varepsilon^2), \end{array}\right\} \tag{4.11}$$

where ϕ_0, ψ_0 are given by (4.6) and (4.7) respectively.

It must be noted that such a perturbation expansion ceases to be valid at Bragg resonance when the reflection coefficient becomes much larger than the undulation parameter ε, as pointed out by Mei [54]. Also this theory is valid only for infinitesimal reflection and away from resonance. For large reflection, the perturbation series, as defined in (4.11), needs to be refined so that it can deal with the resonant case, which is reported in [54].

Using (4.11) in (4.1), (4.3),(4.4), (4.5), (4.10), (4.8) and (4.9), we find that $\phi_1(x, y)$ and $\psi_1(x, y)$ satisfy the BVP described by

$$\nabla^2\phi_1 = 0 \quad \text{on} \quad 0 \le y \le H, \tag{4.12}$$

$$\nabla^2\psi_1 = 0 \quad \text{on} \quad -h \le y \le 0, \tag{4.13}$$

$$\frac{\partial \psi_1}{\partial y} = 0 \quad \text{on} \quad y = -h, \tag{4.14}$$

$$\frac{\partial \phi_1}{\partial y} = \frac{\partial \psi_1}{\partial y} \quad \text{on} \quad y = 0, \tag{4.15}$$

$$K\phi_1 + \frac{\partial \phi_1}{\partial y} = \rho(K\psi_1 + \frac{\partial \psi_1}{\partial y}) \quad \text{on} \quad y = 0, \tag{4.16}$$

$$\frac{\partial \phi_1}{\partial y} = \frac{\mathrm{i}u}{\sinh uH}\,\frac{d}{dx}[c(x)\mathrm{e}^{\mathrm{i}ux}] \equiv p(x) \text{ on } y = H, \tag{4.17}$$

and they have the following asymptotic behaviours given by

$$\phi_1(x, y) \sim \begin{cases} T_1\ \phi_0(x, y) & \text{as } x \to \infty, \\ R_1\ \phi_0(-x, y) & \text{as } x \to -\infty, \end{cases} \tag{4.18}$$

$$\psi_1(x, y) \sim \begin{cases} T_1\ \psi_0(x, y) & \text{as } x \to \infty, \\ R_1\ \psi_0(-x, y) & \text{as } x \to -\infty. \end{cases} \tag{4.19}$$

These equations (4.12)-(4.17) are derived from the previous set of equations (4.1), (4.3)-(4.5) and (4.10) by considering the coefficients of the perturbation parameter ε.

As R_1 and T_1 appearing in (4.18) and (4.19) arise from the original equations (4.8) and (4.9), and since the total reflection coefficient R and total transmission coefficient T are same throughout the whole region (*i.e.*, both upper and lower layers), those first-order corrections R_1 and T_1 are also necessarily the same for both the layers.

4.4 Solution by Green's function technique

4.4.1 Introduction of Green's functions

To solve the above boundary value problem, we need two-dimensional source potentials for Laplace's equation due to a line source submerged in either of the two finite layers of the fluid. When the source is submerged in the lower fluid at (ξ, η), where $0 < \eta < H$, then we take $G_1(x, y; \xi, \eta)$ and $G_2(x, y; \xi, \eta)$ as the source potentials in terms of Green's function for the lower and the upper layers respectively. Similarly when the source is submerged in the upper layer fluid at (ξ, η), where $-h < \eta < 0$, then we take $G_3(x, y; \xi, \eta)$ and $G_4(x, y; \xi, \eta)$ as the source potentials in terms of Green's function for the lower and the upper fluids respectively.

Suppose the source is submerged in the lower layer fluid. Then the source potentials $G_1(x, y; \xi, \eta)$ and $G_2(x, y; \xi, \eta)$ satisfy the following BVP:

$$\nabla^2 G_1 = 0 \quad \text{on} \quad 0 < y < H, \quad \text{except at } (\xi, \eta), \tag{4.20}$$

$$\nabla^2 G_2 = 0 \quad \text{on} \quad -h < y < 0, \tag{4.21}$$

$$\frac{\partial G_2}{\partial y} = 0 \quad \text{on} \quad y = -h, \tag{4.22}$$

$$\frac{\partial G_1}{\partial y} = 0 \quad \text{on} \quad y = H, \tag{4.23}$$

$$\frac{\partial G_1}{\partial y} = \frac{\partial G_2}{\partial y} \quad \text{on} \quad y = 0, \tag{4.24}$$

$$KG_1 + \frac{\partial G_1}{\partial y} = \rho(KG_2 + \frac{\partial G_2}{\partial y}) \quad \text{on} \quad y = 0, \tag{4.25}$$

$$G_1 \sim \log R \quad \text{as} \quad R = [(x-\xi)^2 + (y-\eta)^2]^{1/2} \to 0.$$

Here G_1 and G_2 represent outgoing waves as $|x - \xi| \to \infty$.

Velocity potentials due to various types of singularities in water are generally termed as *source potentials* and have wide applications in the linearized theory of water waves. If a body in water undergoes some sort of oscillations, the resulting motion in the fluid can be described by a series of singularities placed in the body. These singularities are characterized by their giving rise to velocity potentials which are typical singular solutions of the Laplace's equation in the neighbourhood of the singularity. For the two-dimensional case these singularities are logarithmic, and for the three-dimensional case these are point sources or point multipoles.

The solutions $G_1(x,y;\xi,\eta)$ and $G_2(x,y;\xi,\eta)$, as $|x-\xi|\to\infty$, are given by

$$G_1(x,y;\xi,\eta)=\frac{2\pi \mathrm{i}K\sinh kh\cosh k(H-\eta)\cosh k(H-y)}{(1-\rho)\,\Delta'(k)\,k\sinh kH}\,\mathrm{e}^{\mathrm{i}k|x-\xi|}, \tag{4.26}$$

$$G_2(x,y;\xi,\eta)=-\frac{2\pi \mathrm{i}K\cosh k(H-\eta)\cosh k(h+y)}{(1-\rho)\,k\,\Delta'(k)}\,\mathrm{e}^{\mathrm{i}k|x-\xi|}, \tag{4.27}$$

where $\Delta(k)$ is given by (2.6) with Δ' denoting the derivative of Δ with respect to u.

In (4.26) and (4.27), the presence of the common factor

$$\frac{2\pi \mathrm{i}K\cosh k(H-\eta)}{(1-\rho)\,k\,\Delta'(k)}\,\mathrm{e}^{\mathrm{i}k|x-\xi|},$$

is due to the interface conditions (4.24) and (4.25). Physically, the normal velocity and the pressure at the interface would be the same for both the Green's potentials G_1 and G_2.

Similarly, when the source at (ξ,η), where $\eta<0$, is submerged in the upper layer fluid, then the source potentials $G_3(x,y;\xi,\eta)$ and $G_4(x,y;\xi,\eta)$ satisfy the same BVP defined by (4.20)-(4.25), and in addition, G_4 satisfies

$$G_4\sim\log R' \quad \text{as } R'=[(x-\xi)^2+(y+\eta)^2]^{1/2}\to 0, \tag{4.28}$$

and G_3, G_4 represent outgoing waves as $|x-\xi|\to\infty$. The source potentials $G_3(x,y;\xi,\eta)$ and $G_4(x,y;\xi,\eta)$, as $|x-\xi|\to\infty$, in this case, are given by

$$G_3(x,y;\xi,\eta)=-\frac{2\pi \mathrm{i}\,\rho K\cosh k(h-\eta)\,\cosh k(H-y)}{(1-\rho)\,k\,\Delta'(k)}\,\mathrm{e}^{\mathrm{i}k|x-\xi|}, \tag{4.29}$$

$$G_4(x,y;\xi,\eta)=\frac{2\pi \mathrm{i}\,\rho K\sinh kH\cosh k(h-\eta)\,\cosh k(h+y)}{(1-\rho)\,\Delta'(k)\,k\sinh kh}\,\mathrm{e}^{\mathrm{i}k|x-\xi|}. \tag{4.30}$$

Since $\nabla^2\phi_1=0$, and $\nabla^2 G_1=0$ (in the neighbourhood of the singularity) so we have $\int_V(\phi_1\nabla^2 G_1-G_1\nabla^2\phi_1)dv=0$. Hence Green's integral theorem can be applied over an appropriately curtailed volume V. Therefore in order to obtain $\phi_1(\xi,\eta)$, when (ξ,η) is submerged in the lower layer fluid, we first apply the Green's integral theorem to $\phi_1(x,y)$ and $G_1(x,y;\xi,\eta)$ to obtain

$$\int_C\left(\phi_1\frac{\partial G_1}{\partial n}-G_1\frac{\partial\phi_1}{\partial n}\right)ds=0, \tag{4.31}$$

where C is a closed contour in the xy-plane consisting of the lines $y=0,\ -X\le x\le X;\ y=H,\ -X\le x\le X;\ x=\pm X,\ 0\le y\le H$ and a small circle of radius α_1 with center at (ξ,η) and ultimately letting $X\to\infty,\ \alpha_1\to 0$, the resultant of the integral equation (4.31) becomes

$$2\pi\phi_1(\xi,\eta)-\int_{-\infty}^{\infty}p(x)G_1(x,H;\xi,\eta)dx-\int_{-\infty}^{\infty}\left(\phi_1\frac{\partial G_1}{\partial y}-G_1\frac{\partial\phi_1}{\partial y}\right)_{y=0}dx=0. \tag{4.32}$$

Then again we apply the Green's integral theorem to $\psi_1(x,y)$ and $G_2(x,y;\xi,\eta)$ with respect to the closed curve consisting of the lines $y=0,\ -X\le x\le X;\ y=-h,\ -X\le x\le X;\ x=\pm X,\ -h\le y\le 0$ and ultimately letting $X\to\infty$, the integral equation (4.31) becomes

$$\int_{-\infty}^{\infty}\left(\psi_1\frac{\partial G_2}{\partial y}-G_2\frac{\partial\psi_1}{\partial y}\right)_{y=0}dx=0. \tag{4.33}$$

Now solving (4.32) and (4.33) with the help of interface conditions at $y = 0$ we get

$$\phi_1(\xi,\eta) = \frac{1}{2\pi}\int_{-\infty}^{\infty} G_1(x,H;\xi,\eta)\; p(x)dx \tag{4.34}$$

which solves the boundary value problem for $\phi_1(x,y)$.

Similarly, to obtain $\psi_1(\xi,\eta)$, when the source at (ξ,η) is submerged in the upper layer fluid, we apply the same method as was followed for the case of lower layer. The final expression for $\psi_1(\xi,\eta)$ is found to be

$$\psi_1(\xi,\eta) = \frac{1}{2\pi\rho}\int_{-\infty}^{\infty} G_3(x,H;\xi,\eta)\; p(x)dx \tag{4.35}$$

which solves the boundary value problem for $\psi_1(x,y)$.

4.4.2 Reflection and transmission coefficients

The first-order reflection and transmission coefficients, R_1 and T_1, respectively, are now obtained by letting $\xi \to \mp\infty$ respectively, in (4.34) or (4.35) and using the corresponding infinity condition (4.18) or (4.19) with the replacement of (x,y) by (ξ,η).

To find R_1, we note from (4.18) and (4.26), respectively, that

$$\phi_1(\xi,\eta) = R_1\;\phi_0(-\xi,\eta) \quad \text{as} \quad \xi \to -\infty, \tag{4.36}$$

$$G_1(x,H;\xi,\eta) = \frac{2\pi \mathrm{i}\; K\sinh kh\cosh k(H-\eta)}{(1-\rho)\;\Delta'(k)\;k\sinh kH}\;\mathrm{e}^{\mathrm{i}k(x-\xi)} \quad \text{as} \quad \xi \to -\infty. \tag{4.37}$$

Substituting (4.36) and (4.37) in (4.34) we obtain R_1 as

$$\begin{aligned} R_1 &= \frac{\mathrm{i}K\sinh kh}{(1-\rho)\;k\;\Delta'(k)}\int_{-\infty}^{\infty}\mathrm{e}^{\mathrm{i}kx}\;p(x)dx \\ &= \frac{\mathrm{i}Kk\;\sinh kh}{(1-\rho)\;\Delta'(k)\;\sinh kH}\int_{-\infty}^{\infty}\mathrm{e}^{2\mathrm{i}kx}c(x)dx. \end{aligned} \tag{4.38}$$

Similarly to find T_1, we also note from (4.18) and (4.26), respectively, that

$$\phi_1(\xi,\eta) = T_1\;\phi_0(\xi,\eta) \qquad \text{as} \quad \xi \to \infty, \tag{4.39}$$

$$G_1(x,H;\xi,\eta) = \frac{2\pi \mathrm{i}\; K\sinh kh\cosh k(H-\eta)}{(1-\rho)\;\Delta'(k)\;k\sinh kH}\;\mathrm{e}^{-\mathrm{i}k(x-\xi)} \quad \text{as} \quad \xi \to \infty. \tag{4.40}$$

Substituting (4.39) and (4.40) in (4.34) we obtain T_1 as

$$\begin{aligned} T_1 &= \frac{\mathrm{i}K\sinh kh}{(1-\rho)\;k\;\Delta'(k)}\int_{-\infty}^{\infty}\mathrm{e}^{-\mathrm{i}kx}\;p(x)dx \\ &= -\frac{\mathrm{i}Kk\;\sinh kh}{(1-\rho)\;\Delta'(k)\;\sinh kH}\int_{-\infty}^{\infty}c(x)dx. \end{aligned} \tag{4.41}$$

Also, this is verified that the same expressions for R_1 and T_1 are obtained by letting $\xi \to \mp\infty$ in (4.19) and (4.29), respectively and solving for (4.35). So the first-order reflection and transmission coefficients can be evaluated from (4.38) and (4.41), respectively, once the shape function $c(x)$ is known.

4.5 Solution by Fourier transform technique

4.5.1 Splitting of boundary value problem

Now the boundary value problem for ϕ_1 and ψ_1, described by (4.12) to (4.19), can be split into two independent boundary value problems for ϕ_1 and ψ_1 as follows:

Boundary Value Problem-I, corresponding to ψ_1, is

$$\nabla^2\psi_1 = 0 \qquad \text{in} \qquad -h \le y \le 0, \tag{4.42}$$

$$\frac{\partial\psi_1}{\partial y} = \eta(x) \qquad \text{on} \quad y = 0, \tag{4.43}$$

$$\frac{\partial\psi_1}{\partial y} = 0 \qquad \text{on} \quad y = -h, \tag{4.44}$$

where $\eta(x)$ is assumed to be known on $y = 0$ and ψ_1 has the asymptotic behaviour

$$\psi_1(x,y) \sim \begin{cases} T_1\,\psi_0(x,y) & \text{as } x \to \infty, \\ R_1\,\psi_0(-x,y) & \text{as } x \to -\infty. \end{cases} \tag{4.45}$$

Boundary Value Problem-II, corresponding to ϕ_1, is

$$\nabla^2\phi_1 = 0 \qquad \text{in} \qquad 0 \le y \le H, \tag{4.46}$$

$$\frac{\partial\phi_1}{\partial y} = \eta(x) \qquad \text{on} \quad y = 0, \tag{4.47}$$

$$\frac{\partial\phi_1}{\partial y} = p(x) \qquad \text{on} \quad y = H \tag{4.48}$$

Here, $\eta(x)$ is same as in the Boundary Value Problem-I and ϕ_1 has the asymptotic behaviour

$$\phi_1(x,y) \sim \begin{cases} T_1\,\phi_0(x,y) & \text{as } x \to \infty, \\ R_1\,\phi_0(-x,y) & \text{as } x \to -\infty. \end{cases} \tag{4.49}$$

Now with the help of (4.43) and (4.47), (4.16) can be written in the following form:

$$K(\phi_1 - \rho\psi_1) = (\rho - 1)\eta(x) \qquad \text{on} \quad y = 0. \tag{4.50}$$

4.5.2 Fourier transform technique

To solve BVP-I and BVP-II, we now assume that ψ_1 and ϕ_1 are such that their Fourier transforms with respect to x, denoted by $\overline{\psi}_1$ and $\overline{\phi}_1$, respectively, exist and are defined by

$$\overline{\psi}_1(\xi,y) = \int_{-\infty}^{\infty} \psi_1(x,y)\mathrm{e}^{-\mathrm{i}\xi x}dx, \tag{4.51}$$

$$\overline{\phi}_1(\xi,y) = \int_{-\infty}^{\infty} \phi_1(x,y)\mathrm{e}^{-\mathrm{i}\xi x}dx. \tag{4.52}$$

Applying Fourier transform to (4.42), (4.43) and (4.44), we get the following boundary value problem for $\overline{\psi}_1(\xi,y)$:

$$\overline{\psi}_{1yy} - \xi^2\overline{\psi}_1 = 0 \qquad \text{on} \qquad -h \le y \le 0, \tag{4.53}$$

$$\overline{\psi}_{1y} = \overline{\eta}(\xi) \qquad \text{on} \quad y = 0, \tag{4.54}$$

$$\overline{\psi}_{1y} = 0 \qquad \text{on} \quad y = -h, \tag{4.55}$$

where $\overline{\eta}(\xi)$ is the Fourier transform of $\eta(x)$. The solution $\overline{\psi}_1(\xi, y)$ of the above boundary value problem is obtained as

$$\overline{\psi}_1(\xi, y) = \frac{\overline{\eta}(\xi)}{\xi \sinh \xi h} \cosh \xi(h+y). \tag{4.56}$$

Similarly, applying Fourier transform to (4.46), (4.47) and (4.48), we get the following boundary value problem for $\overline{\phi}_1(\xi, y)$:

$$\overline{\phi}_{1yy} - \xi^2 \overline{\phi}_1 = 0 \qquad \text{on} \quad 0 \le y \le H, \tag{4.57}$$

$$\overline{\phi}_{1y} = \overline{\eta}(\xi) \qquad \text{on} \quad y = 0, \tag{4.58}$$

$$\overline{\phi}_{1y} = \overline{p}(\xi) \qquad \text{on} \quad y = H, \tag{4.59}$$

where $\overline{p}(\xi)$ is the Fourier transform of $p(x)$. The solution $\overline{\phi}_1(\xi, y)$ of the above boundary value problem is obtained as

$$\overline{\phi}_1(\xi, y) = \frac{\overline{p}(\xi) \cosh \xi y - \overline{\eta}(\xi) \cosh \xi(H-y)}{\xi \sinh \xi H}. \tag{4.60}$$

In order to calculate the value of $\overline{\eta}(\xi)$, we apply Fourier transform to (4.50) and obtain

$$K(\overline{\phi}_1 - \rho \overline{\psi}_1) = (\rho - 1)\overline{\eta}(\xi) \qquad \text{on} \quad y = 0. \tag{4.61}$$

Now substituting (4.56) and (4.60) in (4.61), we obtain $\overline{\eta}(\xi)$ as

$$\overline{\eta}(\xi) = \frac{K\, \overline{p}(\xi) \sinh \xi h}{(1-\rho)\, \Delta(\xi)}, \tag{4.62}$$

where

$$\Delta(\xi) = \frac{K}{1-\rho}(\cosh \xi H \sinh \xi h + \rho \sinh \xi H \cosh \xi h) - \xi \sinh \xi h \sinh \xi H. \tag{4.63}$$

Here, $\Delta(\xi)$ has only two non-zero roots $\pm k$ on the real axis. Substituting the value of $\overline{\eta}(\xi)$ in (4.56) and (4.60), $\overline{\psi}_1(\xi, y)$ and $\overline{\phi}_1(\xi, y)$ are obtained, respectively, as follows:

$$\overline{\psi}_1(\xi, y) = \frac{K\, \overline{p}(\xi)}{(1-\rho)\, \xi\, \Delta(\xi)} \cosh \xi(h+y), \tag{4.64}$$

$$\overline{\phi}_1(\xi, y) = \frac{\overline{p}(\xi)}{\xi \sinh \xi H} \left[\cosh \xi y - \frac{K \sinh \xi h}{(1-\rho)\Delta(\xi)} \cosh \xi(H-y) \right]. \tag{4.65}$$

Now we can write the respective inverse transforms as:

$$\psi_1(x, y) = \frac{1}{2\pi} \int_{-\infty}^{\infty} \overline{\psi}_1(\xi, y)\, \mathrm{e}^{\mathrm{i}\xi x} d\xi, \tag{4.66}$$

$$\phi_1(x, y) = \frac{1}{2\pi} \int_{-\infty}^{\infty} \overline{\phi}_1(\xi, y)\, \mathrm{e}^{\mathrm{i}\xi x} d\xi. \tag{4.67}$$

Now using (4.66) and (4.67) in (4.64) and (4.65), respectively, we get $\psi_1(x, y)$ and $\phi_1(x, y)$, as follows:

$$\psi_1(x, y) = \frac{K}{2\pi(1-\rho)} \int_0^{\infty} \frac{\cosh \xi(h+y)}{\xi \Delta(\xi)} \left[\overline{p}(\xi) \mathrm{e}^{\mathrm{i}\xi x} + \overline{p}(-\xi) \mathrm{e}^{-\mathrm{i}\xi x} \right] d\xi, \tag{4.68}$$

$$\phi_1(x, y) = \frac{1}{2\pi} \int_0^{\infty} \left[\cosh \xi y - \frac{K \sinh \xi h \cosh \xi(H-y)}{(1-\rho)\Delta(\xi)} \right] \left[\frac{\overline{p}(\xi) \mathrm{e}^{\mathrm{i}\xi x} + \overline{p}(-\xi) \mathrm{e}^{-\mathrm{i}\xi x}}{\xi \sinh \xi H} \right] d\xi. \tag{4.69}$$

Here $\xi = 0$ is not a singularity of (4.68) and (4.69), because $\overline{p}(0) = 0$ only due to the condition $c(x) \to 0$ as $|x| \to \infty$. Since $\Delta(\xi)$ has a non-zero zero at $\xi = k$ on the positive real axis, so the above integral in both cases contains a pole at $\xi = k$. Therefore we make the path for each integral in both cases indented below the pole at $\xi = k$.

4.5.3 Reflection and transmission coefficients

The first-order reflection and transmission coefficients, R_1 and T_1, due to normally incident wave of mode k, are now obtained by letting $\xi \to \mp\infty$ in (4.68) or (4.69), respectively, and comparing with (4.45) or (4.49). To calculate the first-order reflection coefficient, we let $\xi \to -\infty$ in either (4.68) or (4.69). As $\xi \to -\infty$, the behaviour of $\psi_1(x, y)$ or $\phi_1(x, y)$ can be obtained by rotating the path of the integral, involving the term $\overline{p}(-\xi)$, into a contour in the first quadrant, so that we must include the residue term at the pole $\xi = k$. The path of the integral involving the term $\overline{p}(\xi)$ in (4.68) or (4.69) is rotated into a contour in the fourth quadrant so that the integral involving the term $\overline{p}(\xi)$ does not contribute as $\xi \to -\infty$. Then comparing the resultant integral value with (4.45) or (4.49) we obtain R_1 as

$$\begin{aligned} R_1 &= -\frac{\mathrm{i}K \sinh kh}{(1-\rho)\ k\ \Delta'(k)}\ \overline{p}(-k) \\ &= -\frac{\mathrm{i}Kk\ \sinh kh}{(1-\rho)\ \Delta'(k)\ \sinh kH} \int_{-\infty}^{\infty} \mathrm{e}^{2\mathrm{i}kx}\ c(x)dx. \end{aligned} \tag{4.70}$$

Similarly to find the first-order transmission coefficient, we let $\xi \to \infty$ in either (4.68) or (4.69). As $\xi \to \infty$, the behaviour of $\psi_1(x, y)$ or $\phi_1(x, y)$ can be obtained by rotating the path of the integral involving term $\overline{p}(\xi)$ into a contour in the first quadrant so that we must include the residue term at the pole $\xi = k$. The path of the integral involving the term $\overline{p}(-\xi)$ in (4.68) or (4.69) is rotated into a contour in the fourth quadrant, so that the integral involving the term $\overline{p}(-\xi)$ does not contribute as $\xi \to \infty$. Then comparing the resultant integral value with (4.45) or (4.49), we obtain T_1 as

$$\begin{aligned} T_1 &= -\frac{\mathrm{i}K \sinh kh}{(1-\rho)\ k\ \Delta'(k)}\ \overline{p}(k) \\ &= \frac{\mathrm{i}Kk\ \sinh kh}{(1-\rho)\ \Delta'(k)\ \sinh kH} \int_{-\infty}^{\infty} c(x)dx. \end{aligned} \tag{4.71}$$

Therefore, the first-order reflection and transmission coefficients can be evaluated from (4.70) and (4.71), once the shape function $c(x)$ is known. In the following section we proceed to examine the effects of reflection and transmission for two special forms of the shape function $c(x)$.

4.6 Special forms of bottom surfaces

We now consider different special forms of shape functions $c(x)$ representing the uneven bottom surface. As mentioned earlier, these functional forms of the bottom disturbance closely

resemble some naturally occurring obstacles formed at the bottom due to sedimentation and ripple growth of sands.

4.6.1 Example-I

Here we consider a special form of the shape function $c(x)$ in the form of patch of sinusoidal bottom ripples on an otherwise flat bottom:

$$c(x) = \begin{cases} a_1 \sin(lx + \delta'), & L_1 \le x \le L_2, \\ 0, & \text{otherwise .} \end{cases} \tag{4.72}$$

For continuity of the bed elevation we can take

$$L_1 = \frac{-n\pi - \delta'}{l}, \quad L_2 = \frac{m\pi - \delta'}{l},$$

where m and n are positive integers and δ' is a constant phase angle. This patch of sinusoidal ripples on the bottom surface with amplitude a_1 consists of $(n+m)/2$ ripples having the same wave number l. The corresponding reflection and transmission coefficients R_1 and T_1, respectively, are obtained as

$$R_1 = \frac{\mathrm{i}a_1 Kk \ \sinh kh}{(1-\rho)\Delta'(k) \ \sinh kH} \ \frac{l}{l^2 - (2k)^2}[(-1)^n \mathrm{e}^{2\mathrm{i}kL_1} - (-1)^m \mathrm{e}^{2\mathrm{i}kL_2}], \tag{4.73}$$

$$T_1 = -\frac{\mathrm{i}a_1 Kk \ \sinh kh}{(1-\rho)\Delta'(k) \ \sinh kH} \left[\frac{(-1)^n - (-1)^m}{l}\right]. \tag{4.74}$$

For the specific case when there is an integer number of ripple wavelengths in the patch $L_1 \le x \le L_2$ such that $m = n$ and $\delta' = 0$, we can find the reflection and transmission coefficients, respectively, as

$$R_1 = \frac{a_1 K \ \sinh kh}{(1-\rho)\Delta'(k) \ \sinh kH} \ \frac{(-1)^m \ \beta}{1-\beta^2} \ \sin(m\pi\beta), \tag{4.75}$$

$$T_1 = 0, \tag{4.76}$$

where $\beta = 2k/l$.

Equation (4.75) illustrates that for a given number of m ripples, the first-order reflection coefficient is an oscillatory function of β which is the ratio of twice the interface wave number k and the ripple wave number l. Furthermore, when the bed wave number is approximately twice the interface wave number ($2k/l \approx 1$), the theory points towards the possibility of a resonant interaction taking place between the bed and the interface. Hence, we find from (4.75) that near resonance, *i.e.*, for $2k/l \approx 1$, the limiting value of the reflection coefficient becomes

$$R_1 = -\frac{a_1 K \sinh kh}{2(1-\rho) \ \Delta'(k) \ \sinh kH} \ m\pi. \tag{4.77}$$

Note that when $2k/l$ approaches 1 and m becomes large, the reflection coefficient becomes unbounded contrary to our assumption that R_1 is a small quantity, being the first-order correction of the infinitesimal reflection. Consequently, we consider only the cases excluding these two conditions in order to avoid the contradiction arising out of resonant cases.

Thus, the reflection coefficient R_1, in this case, becomes a constant multiple of m, the number of ripples in the patch and it increases linearly with m. Although the theory breaks down when $\beta = 1$, that is when $l = 2k$, a large amount of reflection of the incident wave energy by this special form of bed surface will be generated in the neighborhood of the singularity at $\beta = 1$.

As this is a non-dissipative system and since $T_1 = 0$ and R_1 may be large, it is likely to witness a violation in the conservation of energy in the solution for the potentials. Actually the solution is required to satisfy a condition with respect to wave energy flux, *i.e.*, the incident component of wave energy flux on the undulating part is to be balanced approximately by the sum of the reflected and transmitted components. This requirement may not be fulfilled by the expressions for the reflection and transmission coefficients derived here. Here the reason for the imbalance is that the linearized analysis does not permit any attenuation of the incident interface waves as it travels over the region $L_1 \leq x \leq L_2$, which causes the predicted reflected wave in the perturbation solution to be overestimated and the transmitted wave to be very small or zero. In practice, if the reflection wave is non-zero, there must be a progressive attenuation of the incident interface waves over the region $L_1 \leq x \leq L_2$. Davies [21] has suggested a correction procedure to establish a proper energy balance in the solution.

4.6.2 Example-II

Now, we consider another special form of the shape function $c(x)$ in the form of a different type of patch of sinusoidal ripples on the bottom surface given by

$$c(x) = \begin{cases} a_1 \sin(l_1 x), & L_3 \leq x \leq 0, \\ a_1 \sin(l_2 x), & 0 \leq x \leq L_4, \\ 0, & \text{otherwise}\ . \end{cases} \tag{4.78}$$

Here also, for continuity of the bed elevation we can take

$$L_3 = \frac{-n\pi}{l_1}, \quad L_4 = \frac{m\pi}{l_2},$$

where m and n are positive even integers. This is a patch of sinusoidal ripples on the bottom surface with amplitude a_1 on an otherwise flat bottom. The patch in the region $L_3 \leq x \leq 0$ consists of $n/2$ number of ripples having the wave number l_1 and the patch in the region $0 \leq x \leq L_4$ consists of $m/2$ number of ripples having the wave number l_2.

Substituting the value of $c(x)$ from (4.78) into (4.38) and (4.41), we obtain the reflection coefficient R_1 and transmission coefficient T_1, respectively, as follows:

$$R_1 = \frac{\mathrm{i}a_1 K k \sinh kh}{(1-\rho)\Delta'(k)\sinh kH} \left\{ \frac{l_1}{l_1^2-(2k)^2}[(-1)^n\, \mathrm{e}^{2\mathrm{i}kL_3} - 1] + \frac{l_2}{l_2^2-(2k)^2}[1-(-1)^m\, \mathrm{e}^{2\mathrm{i}kL_4}] \right\}, \tag{4.79}$$

$$T_1 = -\frac{\mathrm{i}a_1 K k\ \sinh kh}{(1-\rho)\Delta'(k)\sinh kH} \left[\frac{(-1)^n - 1}{l_1} + \frac{1-(-1)^m}{l_2} \right]. \tag{4.80}$$

In this case, if we take $m = n$ and $l_1 = l_2 = l$, in (4.79) and (4.80) respectively, then they reduce to (4.75) and (4.76) of Example-I, where all the ripples have the same wave number l.

As in Example-I, when the bed wave number is approximately twice the interface wave number, *i.e.*, $l_1 \approx 2k$ and $l_2 \approx 2k$, here also the theory predicts a possible resonant interaction between the bed and the interface. Hence, under this condition, we can find the limiting value of the reflection coefficient R_1 from (4.79) as

$$R_1 = -\frac{a_1 K \sinh kh}{4(1-\rho)\,\Delta'(k)\,\sinh kH}\,(m+n)\pi. \tag{4.81}$$

As was observed in Example-I, here also R_1 is a constant multiple of $(m+n)/2$, the total number of ripples in the patch of the undulation. Hence, the reflection coefficient increases linearly with m and n. Although the theory breaks down when either $l_1 = 2k$ or $l_2 = 2k$, a large amount of reflection of the incident wave energy by this special form of bed surface will be generated in the neighborhood of the singularities at $l_1 = 2k$ or $l_2 = 2k$.

4.7 Numerical results

We considered two special forms of bottom surfaces in the previous section. In this section, we present the results for the first-order reflection coefficient in graphical form.

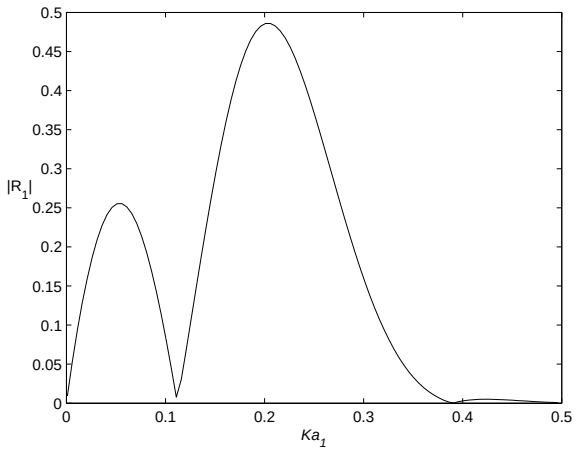

Figure 4.2: Reflection coefficient $|R_1|$ plotted against Ka_1 for $la_1 = 0.52$; $m = 2$.

In Example-I, a patch of sinusoidal bottom undulations on the channel bed is considered because of its considerable physical significance like the ability of an undulating bed to reflect incident wave energy which is important for a channel flow consisting of a two-layer fluid. We consider the graphical representations, followed from (4.75), for the non-dimensionalized first-order reflection coefficient $|R_1|$ due to an incident interface wave of wave number k and a ripple bed with wave number l having m number of ripple wavelengths in the patch of the bottom. In figure 4.2, $|R_1|$ is plotted against Ka_1 for $la_1 = 0.52, m = 2$. This is most evident in the curve that the maximum value of $|R_1|$ is 0.48577 which is attained at $ka_1 = 0.21202$ (when $Ka_1 = 0.206$). In figure 4.3, different curves correspond to different number of ripples $m = 1, 3, 5$ in the patch of the undulation. For all curves, we consider $\rho = 0.95, a_1 = 1, H =$

$10a_1, h = 10a_1, la_1 = 0.52$. The curve which corresponds to $m = 1$, the maximum value of $|R_1|$ is 0.38698 which is attained at $ka_1 = 0.15019$ (when $Ka_1 = 0.136$). Similarly the curve corresponding to $m = 3$ shows the maximum value of $|R_1|$ as 0.61218 which is attained at $ka_1 = 0.23522$ (when $Ka_1 = 0.231$) and the curve corresponding to $m = 5$ shows the maximum value of $|R_1|$ as 0.91414 which is attained at $ka_1 = 0.24938$ (when $Ka_1 = 0.246$). From figure 4.3 it is clear that the peak value of $|R_1|$ is attained when the ripple wave number la_1 of the bottom undulation becomes approximately twice as large as the interface wave number ka_1. As m, the number of ripples, increases, the value of ka_1 converges to a number in the neighborhood of 0.26 (*i.e.*, of $la_1/2$) and also the peak value of the non-dimensionalized reflection coefficient $|R_1|$ increases. Its oscillatory nature against Ka_1 is more noticeable with the number of zeros of $|R_1|$ increased but the general feature of $|R_1|$ remains the same.

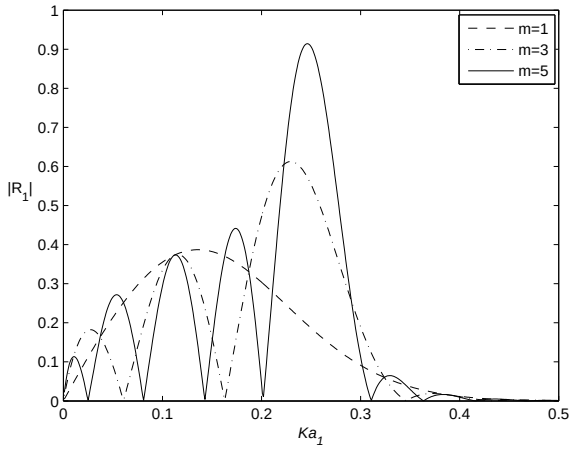

Figure 4.3: Reflection coefficient $|R_1|$ plotted against Ka_1 for $la_1 = 0.52$; $m = 1, 3$ and 5.

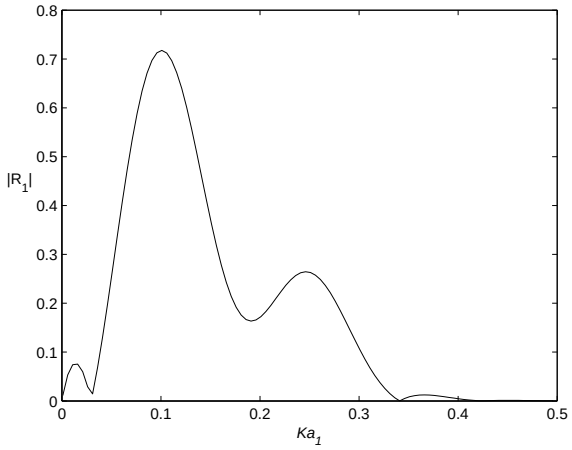

Figure 4.4: Reflection coefficient $|R_1|$ plotted against Ka_1 for $l_1a_1 = 0.52$; $l_2a = 0.26$; $n = 3$; $m = 2$.

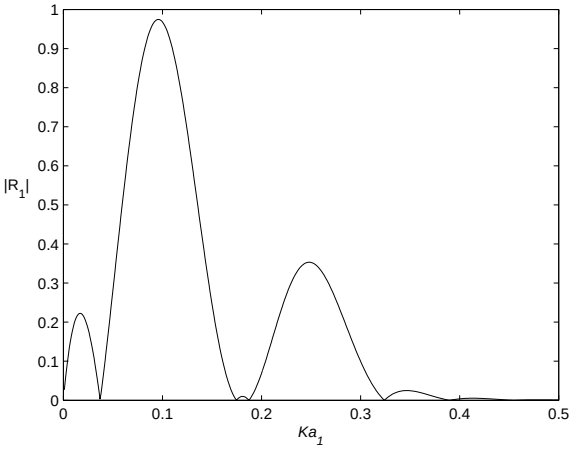

Figure 4.5: Reflection coefficient $|R_1|$ plotted against Ka_1 for $l_1a_1 = 0.52$; $l_2a_1 = 0.26$; $n = 4$; $m = 2$.

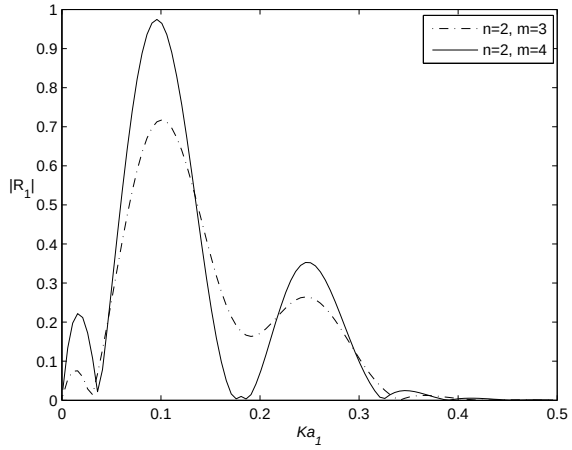

Figure 4.6: Reflection coefficient $|R_1|$ plotted against Ka_1 for $l_1a_1 = 0.26$; $l_2a_1 = 0.52$; $n = 2$; $m = 3$ and $n = 2$; $m = 4$.

In Example-II, another special patch of sinusoidal bottom undulations with ripples having two different wave numbers l_1 and l_2 is considered instead of a single ripple wave number. For this we consider the numerical computations, calculated from (4.79), for the non-dimensionalized first-order reflection coefficient $|R_1|$, due to an incident interface wave of wave number k, with two different ripple wave numbers l_1 and l_2, respectively, having m and n number of ripple wavelengths in the patch of the bottom. In this case, we again consider $\rho = 0.95, a_1 = 1, H = 10a_1, h = 10a_1$. In figure 4.4, $|R_1|$ is plotted against Ka_1 for $l_1a_1 = 0.52, l_2a_1 = 0.26, n = 3, m = 2$. This is most evident in the curve that the first maximum value of $|R_1|$ is 0.71758 which is attained at $ka_1 = 0.1208$ (when $Ka_1 = 0.101$). The second maximum value of $|R_1|$ is 0.2644, attained at $ka_1 = 0.24938$ (when $Ka_1 = 0.246$). In figure 4.5, $|R_1|$ is plotted against Ka_1 for $l_1a_1 = 0.52, l_2a_1 = 0.26, n = 4, m = 2$. For this case, the number of ripples increases from $n = 3, m = 2$ to $n = 4, m = 2$. The first maximum value of $|R_1|$ is 0.97456 which is attained at $ka_1 = 0.11663$ (when $Ka_1 = 0.096$) and second maximum value of $|R_1|$ is 0.35262, attained at $ka_1 = 0.24938$ (when $Ka_1 = 0.246$). Therefore, we observe from figure 4.5 that $|R_1|$ has two peak values which are attained when the ripple wave numbers l_1a_1 and l_2a_1 of the bottom undulation become approximately twice as large as interface wave number ka_1. Again, as the numbers of ripple n and m increase, the peak value of non-dimensionalized reflection coefficient $|R_1|$ increases, and its oscillatory nature against Ka is more noticeable with the number of zeros of $|R_1|$ increased but the general feature of $|R_1|$ remains the same as was observed in figure 4.3.

It may be noted that the relatively larger values of $|R_1|$ appear for near-resonant cases and also for the consideration of more number of ripples, *i.e.*, for increasing values of m in Example-I and for increasing values of both m and n in Example-II.

In figure 4.6, $|R_1|$ is plotted against Ka_1 for $l_1a_1 = 0.26, l_2a_1 = 0.52, n = 2, m = 3$. In the second curve, the numbers of ripple increase from $n = 2, m = 3$ to $n = 2, m = 4$. From the figure it is observed that even if the roles of l_1a_1 and l_2a_1 are reversed, the same conclusion can be observed as shown by figures 4.4 and 4.5.

4.8 Conclusion

A perturbation analysis has been developed to study the interaction of a given first-order motion of a two-layer fluid with an uneven bed topography and thereby finding new expressions for the first-order corrections to the reflection and transmission coefficients for the problem of internal wave propagation over bottom undulations in a two-layer fluid with both layers finite. It enables us to reduce the given boundary value problem to a simpler form and to easily handle it though the theory breaks down at resonance. The determination of the first-order potentials and hence the reflection and transmission coefficients, becomes easier while employing Green's integral theorem and introducing Green's functions. The main advantage of this method, demonstrated through the example of a patch of sinusoidal ripples, is that a very few

ripples may be needed to produce a substantial amount of reflected energy. Again by using Fourier transform technique, we obtain the same values as was by Green's function technique. Another main result that follows is that for the ripples having two different wave numbers, the interaction between the bed and the interface near resonance attains in the neighborhood of the singularity when the ripple wave numbers of the bottom undulation become approximately twice as large as interface wave number. The solutions to problems related to water wave scattering in a two-layer fluid, with both layers of finite depth, over an uneven bottom topography have not been investigated by anyone earlier. It is hoped that the results obtained here can be used quantitatively for this kind of problems.

Chapter 5

Scattering of oblique internal waves in a channel with small undulations

5.1 Introduction

The work presented in this chapter deals with the scattering problem of Chapter 4 but here we consider a train of progressive (internal) waves propagating from negative infinity which is obliquely incident on the channel bed having small undulations. Using a perturbation analysis, involving a small parameter ε, directly to the governing boundary value problem (BVP), we reduce the original problem to a simpler BVP for the first-order correction of the potentials. The solution of this BVP is then obtained by an appropriate use of Green's integral theorem to the potential functions describing the BVP. The reflection and transmission coefficients are evaluated approximately up to the first-order of ε in terms of integrals involving the shape function. For validation of our analytical results, we consider the same two examples as was considered in Chapter 4.

5.2 Mathematical formulation of the problem

We consider the flow of a two-layer fluid through a channel, the upper layer of which is bounded by a fixed wall and the lower layer by a bottom surface with small cylindrical undulation. A right-handed Cartesian coordinate system is used in which xz-plane coincides with the undisturbed surface between the two fluids. The y-axis points vertically downwards with $y = 0$ as the interface and $y = -h$ as the position of the fixed wall. Here, the bottom of the lower layer with small undulation is described by $y = H + \varepsilon c(x)$, where H and $c(x)$ are same as in Chapter 4. We follow the same procedure, as was followed in Chapter 4, to formulate and solve this scattering problem. Under usual assumptions of linear water wave theory and in view of the geometry of the problem, *i.e.*, because of the uniformity in z-direction, the time harmonic velocity potential in the lower fluid of density ρ_1 can be described by $\mathrm{Re}[\phi(x,y)\mathrm{e}^{\mathrm{i}\nu z}\mathrm{e}^{-\mathrm{i}\omega t}]$ and that in the upper layer fluid of density $\rho_2 < \rho_1$ by $\mathrm{Re}[\psi(x,y)\mathrm{e}^{\mathrm{i}\nu z}\mathrm{e}^{-\mathrm{i}\omega t}]$, where the complex-

valued potentials ϕ and ψ, respectively, must satisfy the modified Helmholtz equation:

$$(\nabla^2_{x,y} - \nu^2)\phi = 0 \qquad \text{in lower fluid,} \tag{5.1}$$

$$(\nabla^2_{x,y} - \nu^2)\psi = 0 \qquad \text{in upper fluid.} \tag{5.2}$$

The linearized boundary conditions at the bottom of the channel, on the interface and at the wall are:

$$\frac{\partial \phi}{\partial n} = 0 \qquad \text{on} \quad y = H + \varepsilon c(x), \tag{5.3}$$

$$\frac{\partial \phi}{\partial y} = \frac{\partial \psi}{\partial y} \qquad \text{on} \quad y = 0, \tag{5.4}$$

$$K\phi + \frac{\partial \phi}{\partial y} = \rho(K\psi + \frac{\partial \psi}{\partial y}) \qquad \text{on} \quad y = 0, \tag{5.5}$$

$$\frac{\partial \psi}{\partial y} = 0 \qquad \text{on} \quad y = -h, \tag{5.6}$$

Within this framework in a two-layer fluid, a train of progressive interface waves, which takes the form (up to an arbitrary multiplicative constant) $\phi_0(x,y)\mathrm{e}^{\mathrm{i}\nu z}$ and $\psi_0(x,y)\mathrm{e}^{\mathrm{i}\nu z}$ in the lower layer and the upper layer, respectively, where

$$\phi_0(x,y) = \frac{\cosh u(H-y)}{\sinh uH}\, \mathrm{e}^{\mathrm{i}\mu x}, \tag{5.7}$$

$$\psi_0(x,y) = -\frac{\cosh u(h+y)}{\sinh uh}\, \mathrm{e}^{\mathrm{i}\mu x}, \tag{5.8}$$

is obliquely incident upon the bottom undulation from negative infinity. Here $\mu = u\cos\theta$, $\nu = u\sin\theta$, with θ as the angle of oblique incidence of progressive interface waves ($\theta = 0$ corresponds to normal incidence), and u satisfying the dispersion relation $\Delta(u) = 0$, where $\Delta(u)$ is same as in (2.6). Since the dispersion equation has one non-zero simple zero at $u = k$, say, on the real axis of u, so only one non-zero wave mode k can exist and the wave can propagate in either direction.

The wave trains, given by $\phi_0(x,y)\mathrm{e}^{\mathrm{i}\nu z}$ and $\psi_0(x,y)\mathrm{e}^{\mathrm{i}\nu z}$, are partially reflected by and partially transmitted over the bottom undulation so that the far-field behaviours of ϕ and ψ are given by

$$\phi(x,y) \sim \begin{cases} T\ \phi_0(x,y) & \text{as } x \to \infty, \\ \phi_0(x,y) + R\ \phi_0(-x,y) & \text{as } x \to -\infty, \end{cases} \tag{5.9}$$

$$\psi(x,y) \sim \begin{cases} T\ \psi_0(x,y) & \text{as } x \to \infty, \\ \psi_0(x,y) + R\ \psi_0(-x,y) & \text{as } x \to -\infty, \end{cases} \tag{5.10}$$

where R and T, respectively, represent the usual reflection and transmission coefficient due to an oblique incident wave, and are to be determined.

Assuming, for small bottom undulation, ε to be very small and neglecting the second order terms, here the boundary condition $\partial\phi/\partial n = 0$ on the bottom surface $y = H + \varepsilon c(x)$ can be expressed in the same appropriate form (4.10).

5.3 Perturbation technique

Let us consider a train of progressive interface waves to be obliquely incident at an angle θ, $0 \leq \theta \leq \pi/2$, on the bottom undulation. If there is no bottom undulation, then the incident wave train will propagate without any hindrance and there will be only transmission. The same perturbation expansion (4.11) as was considered in Chapter 4 is followed here.

Using (4.11) in (5.1), (5.2), (4.10), (5.4), (5.5), (5.6), (5.9), (5.10) and equating the first-order terms of ε in both sides of the equations, we find that the first-order potentials ϕ_1 and ψ_1 satisfy a coupled boundary value problem described by

$$(\nabla^2_{x,y} - \nu^2)\phi_1 = 0 \quad \text{in} \;\; 0 \leq y \leq H, \tag{5.11}$$

$$(\nabla^2_{x,y} - \nu^2)\psi_1 = 0 \quad \text{in} \;\; -h \leq y \leq 0, \tag{5.12}$$

$$\frac{\partial \phi_1}{\partial y} = \frac{1}{\sinh kH}\left\{ \mathrm{i}\mu \frac{d}{dx}[c(x)\mathrm{e}^{\mathrm{i}\mu x}] - \nu^2 c(x)\mathrm{e}^{\mathrm{i}\mu x} \right\} \equiv p(x) \quad \text{on } y = H, \tag{5.13}$$

$$\frac{\partial \phi_1}{\partial y} = \frac{\partial \psi_1}{\partial y} \quad \text{on} \quad y = 0, \tag{5.14}$$

$$K\phi_1 + \frac{\partial \phi_1}{\partial y} = \rho(K\psi_1 + \frac{\partial \psi_1}{\partial y}) \quad \text{on} \quad y = 0, \tag{5.15}$$

$$\frac{\partial \psi_1}{\partial y} = 0 \quad \text{on} \quad y = -h, \tag{5.16}$$

$$\phi_1(x,y) \sim \begin{cases} T_1\, \phi_0(x,y) & \text{as } x \to \infty, \\ R_1\, \phi_0(-x,y) & \text{as } \; x \to -\infty. \end{cases} \tag{5.17}$$

$$\psi_1(x,y) \sim \begin{cases} T_1\, \psi_0(x,y) & \text{as } x \to \infty, \\ R_1\, \psi_0(-x,y) & \text{as } \; x \to -\infty. \end{cases} \tag{5.18}$$

To solve the above coupled boundary value problem, we need two-dimensional source potentials (in terms of Green's function) for the modified Helmholtz equation due to a source submerged in either layer of the two-layer fluids, each of finite depth. When the source is submerged in the lower fluid at (ξ, η), where $0 < \eta < H$, then we consider $G_1(x, y; \xi, \eta)$ and $G_2(x, y; \xi, \eta)$ to be the source potentials in terms of Green's function for the lower and the upper layers, respectively. Similarly when the source is submerged in the upper layer fluid at (ξ, η), where $-h < \eta < 0$, then we consider $G_3(x, y; \xi, \eta)$ and $G_4(x, y; \xi, \eta)$ to be the source potentials in terms of Green's function for the lower and the upper layers, respectively.

5.4 Solution by Green's function technique

5.4.1 Introduction of Green's functions

Suppose the source is submerged in the lower layer fluid. Then the source potentials in terms of Green's functions $G_1(x, y; \xi, \eta)$ and $G_2(x, y; \xi, \eta)$ satisfy the following boundary value problem

$$(\nabla^2_{x,y} - \nu^2)G_1 = 0 \quad \text{on} \quad 0 < y < H, \quad \text{except at } (\xi, \eta), \tag{5.19}$$

$$(\nabla^2_{x,y} - \nu^2)G_2 = 0 \quad \text{on} \quad -h \le y \le 0, \tag{5.20}$$

$$\frac{\partial G_1}{\partial y} = 0 \quad \text{on} \quad y = H, \tag{5.21}$$

$$\frac{\partial G_1}{\partial y} = \frac{\partial G_2}{\partial y} \quad \text{on} \quad y = 0, \tag{5.22}$$

$$KG_1 + \frac{\partial G_1}{\partial y} = \rho(KG_2 + \frac{\partial G_2}{\partial y}) \quad \text{on} \quad y = 0, \tag{5.23}$$

$$\frac{\partial G_2}{\partial y} = 0 \quad \text{on} \quad y = -h, \tag{5.24}$$

$$G_1 \sim K_0(\nu r) \quad \text{as} \quad r = \{(x-\xi)^2+(y-\eta)^2\}^{1/2} \to 0, \tag{5.25}$$

where $K_0(\nu r)$ denotes the modified Bessel function of second kind. G_1 and G_2 represent outgoing waves as $|x - \xi| \to \infty$.

The solutions $G_1(x, y; \xi,\eta)$ and $G_2(x, y; \xi,\eta)$, as $|x - \xi| \to \infty$, are given by

$$G_1(x, y; \xi, \eta) = -\frac{2\pi \mathrm{i} K \sinh kh \cosh k(H-\eta) \cosh k(H-y)}{(1-\rho)\ \Delta'(k)\ \mu \sinh kH}\ \mathrm{e}^{\mathrm{i}\mu|x-\xi|}, \tag{5.26}$$

$$G_2(x, y; \xi, \eta) = \frac{2\pi \mathrm{i} K \cosh k(H-\eta) \cosh k(h+y)}{(1-\rho)\ \Delta'(k)\ \mu}\ \mathrm{e}^{\mathrm{i}\mu|x-\xi|}, \tag{5.27}$$

where k is the real positive root of the dispersion relation $\Delta(u) = 0$, where $\Delta(u)$ is given by (2.6). Similarly, when the source term (ξ, η), where $\eta < 0$, is submerged in the upper layer fluid, then the source potentials $G_3(x, y; \xi, \eta)$ and $G_4(x, y; \xi, \eta)$ satisfy the same boundary value problem (5.19)-(5.24) and in addition, G_4 satisfies

$$G_4 \sim K_0(\nu r_1) \qquad \text{as} \quad r_1 = \{(x-\xi)^2+(y+\eta)^2\}^{1/2} \to 0,$$

and G_3, G_4 also represent outgoing waves as $|x - \xi| \to \infty$.

The source potentials $G_3(x, y; \xi, \eta)$ and $G_4(x, y; \xi, \eta)$ as $|x-\xi| \to \infty$, in this case are given by

$$G_3(x, y; \xi, \eta) = \frac{2\pi \mathrm{i} \rho K \cosh k(h-\eta) \cosh k(H-y)}{(1-\rho)\ \Delta'(k)\ \mu}\ \mathrm{e}^{\mathrm{i}\mu|x-\xi|}, \tag{5.28}$$

$$G_4(x, y; \xi, \eta) = -\frac{2\pi \mathrm{i} \rho K \sinh kH \cosh k(h-\eta)\ \cosh k(h+y)}{(1-\rho)\ \Delta'(k)\ \mu\ \sinh kh}\ \mathrm{e}^{\mathrm{i}\mu|x-\xi|}. \tag{5.29}$$

To calculate $\phi_1(\xi, \eta)$, when (ξ, η), $0 < \eta < h$, is submerged in the lower layer fluid, we first apply the Green's integral theorem to $\phi_1(x, y)$ and $G_1(x, y; \xi, \eta)$ in the form

$$\int_C \left(\phi_1 \frac{\partial G_1}{\partial n} - G_1 \frac{\partial \phi_1}{\partial n}\right) ds = 0, \tag{5.30}$$

where C is a closed contour in the xy-plane consisting of the lines $y = 0$ $(-X \le x \le X)$, $y = H$ $(-X \le x \le X)$, $x = \pm X$ $(0 \le y \le H)$ and a small circle of radius α_1 with center at (ξ, η)

and ultimately letting $X \to \infty,\ \alpha_1 \to 0$. Then there will be no contribution to the integral from the line $x = \pm X$, as ϕ_1 and $G_1 \to 0$ when $X \to \pm\infty$. Thus the resultant form of the integral equation (5.30) will be

$$-2\pi\phi_1(\xi,\eta) + \int_{-\infty}^{\infty} p(x) G_1(x,H;\xi,\eta)dx + \int_{-\infty}^{\infty} \left(\phi_1 \frac{\partial G_1}{\partial y} - G_1 \frac{\partial \phi_1}{\partial y}\right)_{y=0} dx = 0. \tag{5.31}$$

We again apply the Green's integral theorem to $\psi_1(x,y)$ and $G_2(x,y;\xi,\eta)$ in the form

$$\int_{C'} \left(\psi_1 \frac{\partial G_2}{\partial n} - G_2 \frac{\partial \psi_1}{\partial n}\right) ds = 0. \tag{5.32}$$

where C' is a closed counter consisting of the lines $y = -h\ (-X \le x \le X),\ y = 0\ (-X \le x \le X),\ x = \pm X\ (-h \le y \le 0)$ and ultimately letting $X \to \infty$. Here, we note that $G_2(x,y;\xi,\eta)$ has no singularity in the upper region. Again there will be no contribution to the integral from the line $y = -h$ due to the same boundary condition satisfied by ψ_1 and G_2 there. Thus the resultant integral equation (5.32) will be

$$\int_{-\infty}^{\infty} \left(\psi_1 \frac{\partial G_2}{\partial y} - G_2 \frac{\partial \psi_1}{\partial y}\right)_{y=0} dx = 0. \tag{5.33}$$

Now solving (5.32) and (5.33) with the help of interface conditions at $y = 0$ we will get

$$\phi_1(\xi,\eta) = \frac{1}{2\pi} \int_{-\infty}^{\infty} G_1(x,H;\xi,\eta)\ p(x)\ dx, \qquad 0 < \eta < H, \tag{5.34}$$

which solves the boundary value problem for $\phi_1(x,y)$.

Similarly, to calculate $\psi_1(\xi,\eta)$, when the source term $(\xi,\eta),\ -h < \eta < 0$, is submerged in the upper layer fluid, we apply the same procedure as was followed previously for the case of lower layer fluid. The final expression for $\psi_1(\xi,\eta)$ will be

$$\psi_1(\xi,\eta) = \frac{1}{2\pi\rho} \int_{-\infty}^{\infty} G_3(x,H;\xi,\eta)\ p(x)\ dx \qquad -h < \eta < 0, \tag{5.35}$$

which solves the boundary value problem for $\psi_1(x,y)$.

5.5 Reflection and transmission coefficients

The first-order reflection and transmission coefficients R_1 and T_1 are now obtained by letting $\xi \to -\infty$ and $\xi \to \infty$ respectively, in (5.34) or (5.35) and comparing with (5.17) or (5.18) with the replacement of (x,y) by (ξ,η).

To find R_1, we note from (5.17) and (5.26), respectively, that

$$\phi_1(\xi,\eta) = R_1\ \phi_0(-\xi,\eta) \quad \text{as} \quad \xi \to -\infty, \tag{5.36}$$

$$G_1(x,H;\xi,\eta) = -\frac{2\pi \mathrm{i}\ K \sinh kh \cosh k(H-\eta)}{(1-\rho)\ \Delta'(k)\ \mu\ \sinh kH}\ \mathrm{e}^{\mathrm{i}\mu(x-\xi)} \quad \text{as } \xi \to -\infty. \tag{5.37}$$

Substituting (5.36) and (5.37) in (5.34) we obtain R_1 as

$$\begin{aligned} R_1 &= -\frac{\mathrm{i}K \sinh kh}{(1-\rho)\ \mu\ \Delta'(k)} \int_{-\infty}^{\infty} \mathrm{e}^{\mathrm{i}\mu x}\ p(x)\ dx \\ &= -\frac{\mathrm{i}Kk\ \sinh kh\ \cos 2\theta \sec\theta}{(1-\rho)\ \Delta'(k)\ \sinh kH} \int_{-\infty}^{\infty} \mathrm{e}^{2\mathrm{i}kx\cos\theta} c(x)\ dx \quad (\text{using}\ \ \mu = k\cos\theta). \end{aligned} \tag{5.38}$$

Similarly to find T_1, we also note from (5.17) and (5.26), respectively, that

$$\phi_1(\xi,\eta) = T_1\ \phi_0(\xi,\eta) \quad \text{as} \quad \xi \to \infty, \tag{5.39}$$

$$G_1(x,H;\xi,\eta) = -\frac{2\pi \mathrm{i}\ K \sinh kh \cosh k(H-\eta)}{(1-\rho)\ \Delta'(k)\ \mu\ \sinh kH}\ \mathrm{e}^{-\mathrm{i}\mu(x-\xi)} \quad \text{as} \quad \xi \to \infty. \tag{5.40}$$

Substituting (5.39) and (5.40) in (5.34) we obtain T_1 as

$$\begin{aligned} T_1 &= -\frac{\mathrm{i}K \sinh kh}{(1-\rho)\ \mu\ \Delta'(k)} \int_{-\infty}^{\infty} \mathrm{e}^{-\mathrm{i}\mu x}\ p(x)\ dx \\ &= \frac{\mathrm{i}Kk\ \sinh kh\ \sec\theta}{(1-\rho)\ \Delta'(k)\ \sinh kH} \int_{-\infty}^{\infty} c(x)\ dx. \end{aligned} \tag{5.41}$$

This is also verified that the same expression for R_1 and T_1 are obtained by letting $\xi \to -\infty$ and $\xi \to \infty$ respectively, in (5.18) and (5.28), and solve for (5.35). So the first-order reflection and transmission coefficient can be evaluated from (5.38) and (5.41) respectively, once the shape function $c(x)$ is known.

In the following section we proceed to examine the effects of reflection and transmission for some special forms of the shape function $c(x)$.

5.6 Special forms of bottom surfaces

Here, we consider the same special sinusoidal forms of the shape function $c(x)$ as was considered in Chapter 4 to represent the uneven bottom surface.

5.6.1 Example-I

In this case, we consider the same special form of the shape function $c(x)$ as was considered in Section 4.6.1. For this case, the reflection and transmission coefficients can be calculated, by substituting the value of $c(x)$ from (4.72) into (5.38) and (5.41), respectively. The value of R_1 and T_1, respectively, are obtained as

$$R_1 = -\frac{\mathrm{i}a_1Kk\ \sinh kh\ \cos 2\theta \sec\theta}{(1-\rho)\Delta'(k)\ \sinh kH}\ \frac{l}{l^2-(2\mu)^2}\ [(-1)^n\ \mathrm{e}^{2\mathrm{i}\mu L_1} - (-1)^m\ \mathrm{e}^{2\mathrm{i}\mu L_2}], \tag{5.42}$$

$$T_1 = \frac{\mathrm{i}a_1Kk\ \sinh kh\ \sec\theta}{(1-\rho)\Delta'(k)\ \sinh kH} \left[\frac{(-1)^n-(-1)^m}{l}\right]. \tag{5.43}$$

In the situation when there is an integer number of ripples wavelengths in the patch $L_1 \le x \le L_2$ such that $m = n$ and $\delta' = 0$, we can find the reflection and transmission coefficients, respectively, as

$$R_1 = -\frac{a_1K\ \sinh kh\ \cos 2\theta \sec\theta}{(1-\rho)\Delta'(k)\ \sinh kH}\ \frac{(-1)^m\ (2k/l)}{1-\beta^2}\ \sin(m\pi\beta), \tag{5.44}$$

$$T_1 = 0, \tag{5.45}$$

where $\beta = 2\mu/l$.

Equation (5.44) illustrates that for a given number of m ripples, the first-order reflection coefficient is an oscillatory function of β which is the ratio of twice the component of the

interface wave number along x-axis and the ripple wave number. Furthermore, when the bed wave number is twice the component of the interface wave number along x-axis, that is, $2\mu/l = 1$, the theory points towards the possibility of a resonant interaction between the bed and the interface. Hence, we find from (5.44) that

$$R_1 = \frac{a_1 K \sinh kh \ \cos 2\theta \sec^2\theta}{2(1-\rho)\,\Delta'(k)\ \sinh kH}\, m\pi. \tag{5.46}$$

Thus, the reflection coefficient R_1, in this case, becomes a constant multiple of m, the number of ripples in the patch. Hence, the reflection coefficient R_1 increases linearly with m. Although the theory breaks down when $\beta = 1$, that is, $2\mu = l$, a large amount of reflection of the incident wave energy by this special form of bed surface will be generated in the neighborhood of the singularity at $\beta = 1$.

The remarks made in Section 4.6.1 about the violation in the conservation of energy in the solution of the potentials for the normal incidence hold good for the oblique incidence also.

5.6.2 Example-II

We consider the same special form of the shape function $c(x)$ of Section 4.6.2.

Substituting the value of $c(x)$ from (4.78) into (5.38) and (5.41), we obtain the reflection coefficient R_1 and transmission coefficient T_1, respectively, as follows:

$$R_1 = -\frac{\mathrm{i}a_1 Kk \sinh kh \cos 2\theta \sec\theta}{(1-\rho)\Delta'(k)\ \sinh kH}\left\{\frac{l_1}{l_1^2-(2\mu)^2}[(-1)^n\ \mathrm{e}^{2\mathrm{i}\mu L_3}-1] + \frac{l_2}{l_2^2-(2\mu)^2}[1-(-1)^m\ \mathrm{e}^{2\mathrm{i}\mu L_4}]\right\}, \tag{5.47}$$

$$T_1 = \frac{\mathrm{i}a_1 Kk\ \sinh kh\ \sec\theta}{(1-\rho)\Delta'(k)\ \sinh kH}\left[\frac{(-1)^n-1}{l_1} + \frac{1-(-1)^m}{l_2}\right]. \tag{5.48}$$

In this case, if we take $m = n$ and $l_1 = l_2 = l$, in (5.47) and (5.48) respectively, then they reduce to (5.44) and (5.45) of the previous example, where all the ripples have the same wave number l.

As in Example-I, when the bed wave number is twice the component of the interface wave number along x-axis, that is, $l_1 = 2\mu$ and $l_2 = 2\mu$, here also the theory predicts a resonant interaction between the bed and the interface. Hence, under this condition, we can find the reflection coefficient R_1 from (5.47) as

$$R_1 = \frac{a_1 K \sinh kh \ \cos 2\theta \sec^2\theta}{4(1-\rho)\,\Delta'(k)\ \sinh kH}\,(m+n)\pi. \tag{5.49}$$

As in Example-I, it is observed here also that R_1 is a constant multiple of $(m+n)/2$, the total number of ripples in the patch of the undulation. Hence, the reflection coefficient R_1 increases linearly with m and n. Although the theory breaks down when either $l_1 = 2\mu$ or $l_2 = 2\mu$, a large amount of reflection of the incident wave energy by this special form of bed surface will be generated in the neighborhood of the singularities at $l_1 = 2\mu$ or $l_2 = 2\mu$.

5.7 Numerical results

In this section, the numerical computation related to the two special forms of bottom surfaces mentioned in the previous section is shown for the first-order reflection and transmission coefficients.

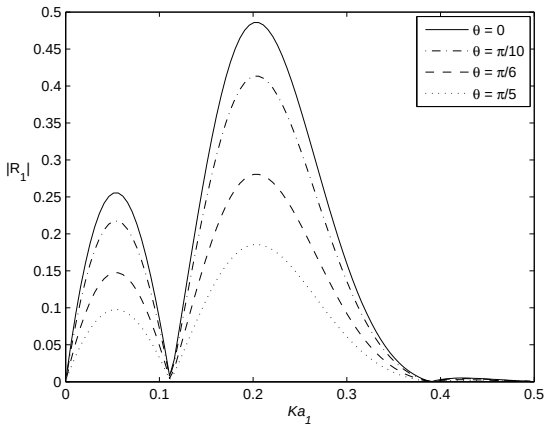

Figure 5.1: Reflection coefficient $|R_1|$ plotted against Ka_1 for $la_1 = 0.52$ and $m = 2$.

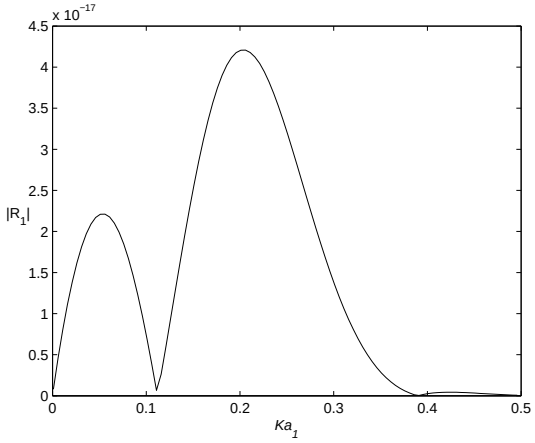

Figure 5.2: Reflection coefficient $|R_1|$ plotted against Ka_1 for $la_1 = 0.52$; $m = 2$; $\theta = \pi/4$.

In Example-I, a patch of sinusoidal bottom undulations on the channel bed is considered because of its considerable physical significance in the ability of an undulating bed to reflect incident wave energy which is important for a channel flow consisting of a two-layer fluid. We consider the numerical computations for the non-dimensionalized first-order reflection coefficient $|R_1|$, which is calculated from (5.44), due to an obliquely incident wave on the undulating bed in the lower layer at an angle θ to the positive x-axis with the undulation having ripple wave number l and m number of ripple wavelengths in the patch. In figure 5.1, different curves of $|R_1|$ are shown against Ka_1 for $\rho = 0.95$; $H = 10a_1$; $h = 10a_1$; $la_1 = 0.52$; $m = 2$; $\theta = 0$; $\pi/10$; $\pi/6$; and $\pi/5$. It may be noted that for $\theta = 0$ (the case of normal incidence), the maximum value of $|R_1|$ is 0.48577, attained at $\mu a_1 = 0.21202$ (when $Ka_1 = 0.206$), that is, when the ripple wave number la_1 of the bottom undulation becomes approximately twice as large as the interface wave number μa_1. The same conclusion can be observed when the value of θ is non-zero (the case of oblique incidence). Another common feature in figure 5.1 is the oscillating nature of the absolute values of the first-order coefficients as functions of the wave number Ka_1. In figure 5.2, $|R_1|$ is plotted against Ka_1 for $la_1 = 0.52$, $m = 2$, and $\theta = \pi/4$. For this value of θ, the reflection coefficient $|R_1|$ is much less (almost negligible) compared to the other angles of oblique incidence, *e.g.*, $\theta = \pi/6, \pi/5$. As the angle of incidence θ increases, the peak value of $|R_1|$ decreases. For the case of normal incidence, the peak value of $|R_1|$ is the largest.

In figure 5.3, different curves correspond to different number of ripples $m = 1,\ 3,\ 5$ in the patch of the undulation. In this figure, for all curves, we consider $\theta = 0$, $\rho = 0.95$, $H =$

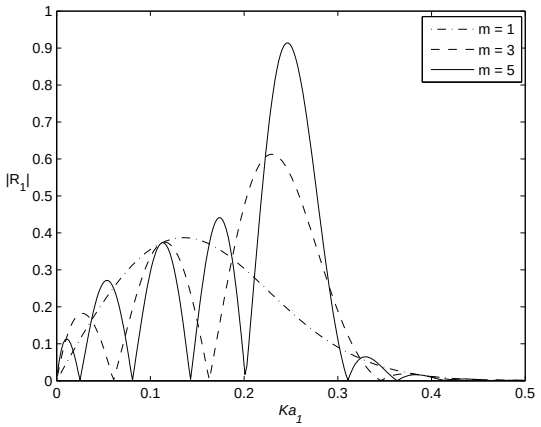

Figure 5.3: Reflection coefficient $|R_1|$ plotted against Ka_1 for $\theta = 0$ and $la_1 = 0.52$.

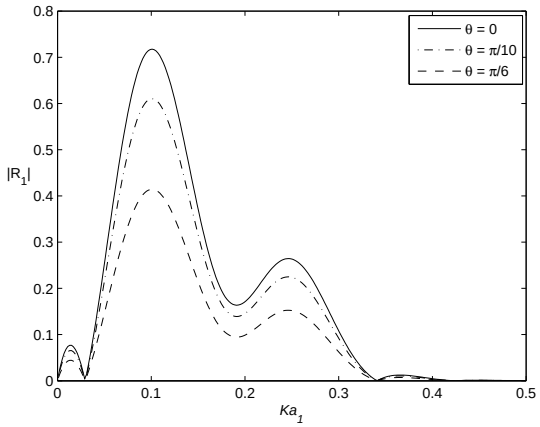

Figure 5.4: Reflection coefficient $|R_1|$ plotted against Ka_1 for $l_1a_1 = 0.52$; $l_2a_1 = 0.26$; $n = 3$ and $m = 2$.

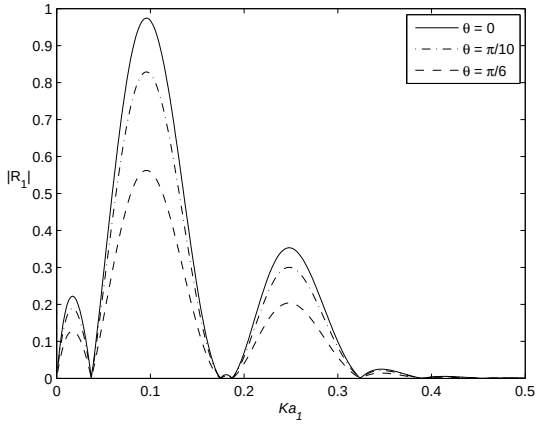

Figure 5.5: Reflection coefficient $|R_1|$ plotted against Ka_1 for $l_1a_1 = 0.52$; $l_2a_1 = 0.26$; $n = 4$ and $m = 2$.

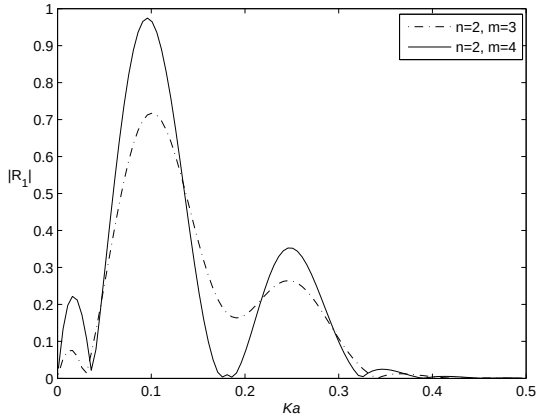

Figure 5.6: Reflection coefficient $|R_1|$ plotted against Ka_1 for $\theta = 0$; $l_1a_1 = 0.26$ and $l_2a_1 = 0.52$.

$10a_1$, $h = 10a_1$, $la_1 = 0.52$. The curve which corresponds to $m = 1$, the maximum value of $|R_1|$ is 0.38698, attained at $\mu a_1 = 0.15019$ (when $Ka_1 = 0.136$). Similarly for the curve corresponding to $m = 3$, the maximum value of $|R_1|$ is 0.61218, attained at $\mu a_1 = 0.23522$ (when $Ka_1 = 0.231$) and for the curve corresponding to $m = 5$, the maximum value of $|R_1|$ is 0.91414, attained at $\mu a_1 = 0.24938$ (when $Ka_1 = 0.246$). From figure 5.3, it is clear that the peak value of $|R_1|$ is attained when the ripple wave number la_1 of the bottom undulation becomes approximately twice as large as the interface wave number μa_1. As m, the number of ripples, increases, the value of μa_1 converges to a number in the neighborhood of 0.26, *i.e.*, for $la_1/2$, where $|R_1|$ attains its maximum, and also the peak value of non-dimensionalized reflection coefficient $|R_1|$ increases. Its oscillatory nature against Ka_1 is more noticeable with the number of zeros of $|R_1|$ increased but the general feature of $|R_1|$ remains the same.

In Example-II, another special patch of sinusoidal bottom undulations with ripples having two different wave numbers l_1 and l_2 are considered instead of a single ripple wave number

of the previous example. For this example, we consider the numerical computations for the non-dimensionalized first-order reflection coefficient $|R_1|$, which is calculated from (5.47), due to an obliquely incident wave on the undulating bed in the lower layer at an angle θ to the positive x-axis with the undulation having two different ripple wave numbers l_1 and l_2, respectively, and m and n number of ripple wavelengths in the patch. Here we again consider $\rho = 0.95,\ H = 10a_1$ and $h = 10a_1$. In figure 5.4, $|R_1|$ is plotted against Ka_1 for $l_1a_1 = 0.52,\ l_2a_1 = 0.26,\ n = 3,\ m = 2,$ and $\theta = 0,\ \pi/10,\ \pi/6$. It may be noted that for $\theta = 0$ (the case of normal incidence), the first maximum value of $|R_1|$ is 0.71758, attained at $\mu a_1 = 0.1208$ (when $Ka_1 = 0.101$). The second maximum value of $|R_1|$ that corresponds to the same ($\theta = 0$) curve is 0.2644, attained at $\mu a_1 = 0.24938$ (when $Ka_1 = 0.246$). The same general feature can be observed for other non-zero values of θ (the case of oblique incidence). Again, as the angle of incidence θ increases, the peak value of $|R_1|$ decreases. For the case of normal incidence, the peak value of $|R_1|$ is the largest. In figure 5.5, $|R_1|$ is plotted against Ka_1 for $l_1a_1 = 0.52,\ l_2a_1 = 0.26,\ n = 4,\ m = 2,$ and $\theta = 0,\ \pi/10,\ \pi/6$. In this case the number of ripples increases from $n = 3,\ m = 2$ to $n = 4,\ m = 2$. In the figure, for $\theta = 0$, the first maximum value of $|R_1|$ is 0.97456, attained at $\mu a_1 = 0.11663$ (when $Ka_1 = 0.096$) and second maximum value of $|R_1|$ is 0.35262, attained at $\mu a_1 = 0.24938$ (when $Ka_1 = 0.246$). Therefore, we observe from this figure that for any angle $\theta,\ 0 \leq \theta < \pi/2,\ |R_1|$ has two peak values which are attained when the ripple wave numbers l_1a_1 and l_2a_1 of the bottom undulation become approximately twice as large as oblique interface wave number μa_1, and if the angle of incidence increases, the value of $|R_1|$ decreases. Again, as the numbers of ripples, n and m, increase, the peak value of non-dimensionalized reflection coefficient $|R_1|$ increases, and its oscillatory nature against Ka_1 is more noticeable with the number of zeros of $|R_1|$ increased but the general feature of $|R_1|$ remains the same.

In figure 5.6, $|R_1|$ is plotted against Ka_1 for $\theta = 0,\ l_1a_1 = 0.26,\ l_2a_1 = 0.52,\ n = 2,\ m = 3$. In the second curve, the number of ripples increase from $n = 2,\ m = 3$ to $n = 2,\ m = 4$. From the figure it is observed that even if the roles of l_1a_1 and l_2a_1 are reversed, the same conclusion can be drawn as was previously with figures 5.4 and 5.5.

5.8 Conclusion

The work described in this chapter is the extended work of the classical problem of oblique water wave scattering by a bottom undulation in a two-layer fluid, when a rigid horizontal wall, which forms the horizontal boundary of a channel, replaces the free surface. In such a situation propagating waves can exist at only one wave number for any given frequency. Using a simplified perturbation analysis, the problem is reduced up to first-order to a coupled boundary value problem and that boundary value problem is solved by a method based Green's integral theorem with the introduction of appropriate Green's functions. First-order approximations to the reflection and transmission coefficients are obtained in terms of computable integrals

and depicted graphically through a number of figures. The main advantage of this method, demonstrated through the example of a patch of sinusoidal ripples, is that a very few ripples may be needed to produce a substantial amount of reflected energy. Also it is observed that for small angles of incidence, the reflected energy is more as compared to other angles of incidence up to $\pi/4$. Another main result that follows is that, for the ripples having two different wave numbers, the resonant interaction between the bed and the interface attains in the neighborhood of the singularity when the ripple wave numbers of the bottom undulation become twice the interface wave number. The problem and solution method described here are different from the previous works in the sense that the free surface has been approximated by a horizontal wall and the bottom surface contains undulation. The solution developed here is expected to be helpful in considering two-layer fluid problems in a channel with uneven bottom surface.

Chapter 6

Normal wave propagation over bottom undulation in an ice-covered two-layer fluid

6.1 Introduction

It appears that there is a considerable interest in the study of various types of water wave problems with bottom undulation in the presence of a thin ice-sheet floating on water, with the ice-sheet being modelled as a thin elastic plate. Investigations of such water wave problems have gained reasonable importance due to various reasons. One of these is to understand the mechanism and effects of internal wave propagation through the marginal ice zone in the polar regions. Furthermore, another important reason for considering this kind of problems stems from the need to construct an effective reflector of the incident wave energy for protecting coastal areas from the rough ocean in the polar regions. In this chapter, we consider a two-layer fluid whose upper layer is bounded above by a thin uniform ice-cover and the lower layer has a bottom undulation. The scattering takes place due to a train of progressive waves propagating from negative infinity which is normally incident on the undulating ocean bed. In this case, time-harmonic waves of a particular frequency can propagate with two different wave numbers: the waves with the higher wave number propagate at the interface while the waves with lower wave number at the ice-cover. Applying perturbation analysis, we reduce the original problem to a simpler boundary value problem (BVP) for the first-order correction of the potentials. The solution of this BVP is then obtained by an appropriate use of Green's integral theorem to the potential functions describing the BVP. In addition, Fourier transform technique is also used to find the respective potentials. The reflection and transmission coefficients are evaluated approximately up to the first-order of ε in terms of integrals involving the shape function. We present a special form of bottom undulation: a patch of sinusoidal ripples having two different wave numbers for two consecutive stretches.

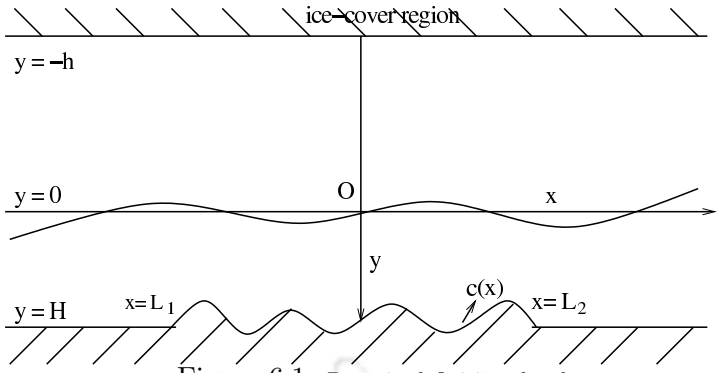

Figure 6.1: Domain definition sketch

6.2 Mathematical formulation of the problem

We consider the irrotational motion of a two-layer inviscid incompressible fluid of relatively small amplitude under the action of gravity, neglecting any effect due to surface tension at the interface of the two fluids of which the upper layer is of finite depth h and is covered by a thin uniform ice sheet modelled as a thin elastic plate, while the lower layer is bounded by a bottom surface with small cylindrical undulation. Each fluid is of infinite horizontal extent in x-direction while the depth is along y-direction which is considered vertically downwards with $y = -h$ as the mean position of the thin ice-cover. The origin O is considered at the undisturbed interface between the upper and lower fluids, and $y = 0$ as the mean position of the interface of the layers. Here, the bottom of the lower layer with small undulation is described by $y = H + \varepsilon c(x)$. Under the usual assumptions of linear water wave theory, velocity potentials in the lower and upper layer, respectively, can be defined for normal waves in the form:

$$\left.\begin{aligned} \Phi(x,y,t) &= \mathrm{Re}[\phi(x,y)\mathrm{e}^{-\mathrm{i}\omega t}] \\ \Psi(x,y,t) &= \mathrm{Re}[\psi(x,y)\mathrm{e}^{-\mathrm{i}\omega t}] \end{aligned}\right\}, \tag{6.1}$$

where $\phi(x,y)$ and $\psi(x,y)$, respectively, are complex-valued potential functions for the lower layer fluid $(0 < y < H)$ of density ρ_1 and the upper layer fluid $(-h < y < 0)$ of density $\rho_2 < \rho_1$.

The governing equation for the boundary value problems involving these potentials ϕ and ψ is the Laplace's equation:

$$\nabla^2\phi = 0 \qquad \text{in the lower fluid,} \tag{6.2}$$

$$\nabla^2\psi = 0 \qquad \text{in the upper fluid.} \tag{6.3}$$

The ratio of the densities of the two fluids ρ_2/ρ_1 (< 1) is denoted by ρ and the linearized boundary conditions at the bottom surface, on the interface and at the ice-cover are:

$$\frac{\partial \phi}{\partial n} = 0 \qquad \text{on} \quad y = H + \varepsilon c(x), \tag{6.4}$$

$$\frac{\partial \phi}{\partial y} = \frac{\partial \psi}{\partial y} \qquad \text{on} \quad y = 0, \tag{6.5}$$

$$K\phi + \frac{\partial \phi}{\partial y} = \rho(K\psi + \frac{\partial \psi}{\partial y}) \qquad \text{on} \quad y = 0, \tag{6.6}$$

$$K\psi + \left(D\frac{\partial^4}{\partial x^4} + 1 - \delta K\right)\frac{\partial \psi}{\partial y} = 0 \qquad \text{on} \quad y = -h, \tag{6.7}$$

where $D = L/(\rho_2 g)$, L the flexural rigidity of the elastic ice-cover; $\delta = (\rho_0/\rho_2)h_0$, ρ_0 is the density of the ice; h_0 is the very small thickness of the ice-cover and $\partial/\partial n$ the derivative normal to the bottom at a point (x, y).

Within this framework in a two-layer fluid, a train of progressive waves take the form (up to an arbitrary multiplicative constant)

$$\phi = \mathrm{e}^{\pm \mathrm{i}kx} \cosh k(H - y) \qquad \text{in} \quad 0 \le y \le H, \tag{6.8}$$

$$\psi = \mathrm{e}^{\pm \mathrm{i}kx} f(k, y) \qquad \text{in} \quad -h \le y \le 0, \tag{6.9}$$

$$\text{where} \quad f(k, y) = \frac{\sinh kH \left[(Dk^4+1-\delta K)k \cosh k(h+y) - K \sinh k(h+y)\right]}{K \cosh kh - (Dk^4+1-\delta K)k \sinh kh}, \tag{6.10}$$

with k satisfying the dispersion relation $\Delta(k) = 0$, where

$$\begin{aligned}\Delta(k) = {} & [k^2(1-\rho)(Dk^4+1-\delta K) + K^2\rho] \sinh kh \sinh kH + K^2 \cosh kh \cosh kH \\ & - Kk\{(Dk^4+1-\delta K) \sinh kh \cosh kH + [1+\rho(Dk^4-\delta K)] \sinh kH \cosh kh\},\end{aligned} \tag{6.11}$$

which is similar as (3.8).

In the above equation, there are two positive real roots m and M, say, that indicate the propagating modes, a complex conjugate pair of roots corresponding to the damped propagating modes, and a countable infinity of purely imaginary roots k_n, $n = 1, 2, \cdots$, that relate to a set of evanescent modes. The negatives of all of these are also roots, being wave numbers of the waves travelling in the opposite direction (discussed in [7]). Since (6.11) has exactly two nonzero positive real roots m and M ($m < M$, say), so there exist two modes of waves propagating at the interface and also just below the ice-cover along the positive x-direction.

A train of progressive waves of mode m propagating along x-axis is of the form

$$\phi_0(x, y) = \mathrm{e}^{\pm \mathrm{i}mx} \cosh m(H - y) \qquad \text{in} \quad 0 \le y \le H, \tag{6.12}$$

$$\psi_0(x, y) = \mathrm{e}^{\pm \mathrm{i}mx} f(m, y) \qquad \text{in} \quad -h \le y \le 0. \tag{6.13}$$

Similarly, a train of progressive waves of mode M propagating along x-axis is of the form

$$\phi_0(x, y) = \mathrm{e}^{\pm \mathrm{i}Mx} \cosh M(H - y) \qquad \text{in} \quad 0 \le y \le H, \tag{6.14}$$

$$\psi_0(x, y) = \mathrm{e}^{\pm \mathrm{i}Mx} f(M, y) \qquad \text{in} \quad -h \le y \le 0. \tag{6.15}$$

Therefore, if a wave train of mode m is normally incident on the positive x-axis on the cylindrical undulation at the bottom of a two-layer fluid, then the reflected and transmitted waves of both the modes m and M occur. Since the wave train is partially reflected by, and partially transmitted over the bottom undulation, the far-field behaviours of ϕ and ψ, respectively, are given by

$$\phi(x,y) \sim \begin{cases} \cosh m(H-y)(\mathrm{e}^{\mathrm{i}mx} + r^{(m)}\mathrm{e}^{-\mathrm{i}mx}) + R^{(m)} \cosh M(H-y)\mathrm{e}^{-\mathrm{i}Mx} & \text{as } x \to -\infty, \\ t^{(m)} \cosh m(H-y)\mathrm{e}^{\mathrm{i}mx} + T^{(m)} \cosh M(H-y)\mathrm{e}^{\mathrm{i}Mx} & \text{as } x \to \infty, \end{cases} \tag{6.16}$$

$$\psi(x,y) \sim \begin{cases} f(m,y)(\mathrm{e}^{\mathrm{i}mx} + r^{(m)}\mathrm{e}^{-\mathrm{i}mx}) + R^{(m)} f(M,y)\mathrm{e}^{-\mathrm{i}Mx} & \text{as } x \to -\infty, \\ t^{(m)} f(m,y)\mathrm{e}^{\mathrm{i}mx} + T^{(m)} f(M,y)\mathrm{e}^{\mathrm{i}Mx} & \text{as } x \to \infty. \end{cases} \tag{6.17}$$

The unknown coefficients $r^{(m)}$ and $R^{(m)}$ are the reflection coefficients associated with reflected wave modes m and M, respectively, due to the normally incident wave of mode m and are to be determined. Similarly, $t^{(m)}$ and $T^{(m)}$ are the transmission coefficients associated with transmitted wave modes m and M, respectively, due to the normally incident wave of mode m and are to be determined.

Assuming, for small bottom undulation, ε to be very small and neglecting the second order terms, the boundary condition $\partial\phi/\partial n = 0$ on the bottom surface $y = H + \varepsilon c(x)$ can be expressed in an appropriate form as

$$\frac{\partial \phi}{\partial y} - \varepsilon \frac{\partial}{\partial x}\left[c(x)\frac{\partial \phi}{\partial x}\right] + \mathrm{O}(\varepsilon^2) = 0 \qquad \text{on} \quad y = H. \tag{6.18}$$

Similarly, for a wave train of mode M normally incident on the bottom undulation of a two-layer fluid and propagating along the positive x-axis, the far-field behaviour of ϕ and ψ, respectively, are given by

$$\phi(x,y) \sim \begin{cases} \cosh M(H-y)(\mathrm{e}^{\mathrm{i}Mx} + R^{(M)}\mathrm{e}^{-\mathrm{i}Mx}) + r^{(M)} \cosh m(H-y)\mathrm{e}^{-\mathrm{i}mx} & \text{as } x \to -\infty, \\ T^{(M)} \cosh M(H-y)\mathrm{e}^{\mathrm{i}Mx} + t^{(M)} \cosh m(H-y)\mathrm{e}^{\mathrm{i}mx} & \text{as } x \to \infty, \end{cases} \tag{6.19}$$

$$\psi(x,y) \sim \begin{cases} f(M,y)(\mathrm{e}^{\mathrm{i}Mx} + R^{(M)}\mathrm{e}^{-\mathrm{i}Mx}) + r^{(M)} f(m,y)\mathrm{e}^{-\mathrm{i}mx} & \text{as } x \to -\infty, \\ T^{(M)} f(M,y)\mathrm{e}^{\mathrm{i}Mx} + t^{(M)} f(m,y)\mathrm{e}^{\mathrm{i}mx} & \text{as } x \to \infty, \end{cases} \tag{6.20}$$

where the unknown coefficients $r^{(M)}$ and $R^{(M)}$ denote the reflection coefficients of modes m and M, respectively, due to an normally incident wave of mode M and are to be determined. Similarly, $t^{(M)}$ and $T^{(M)}$ denote the transmission coefficients of modes m and M, respectively, due to the normally incident wave of mode M and are to be determined. Thus, if the incident wave has mode M, then it satisfies the respective Laplace's equation, the ice-surface condition, interface condition and the bottom condition (6.18). Moreover, ϕ and ψ also satisfy the far-field conditions (6.19) and (6.20) involving the unknown coefficients $r^{(M)}$, $R^{(M)}$, $t^{(M)}$ and $T^{(M)}$.

Determination of these coefficients $r^{(M)}$, $R^{(M)}$, $t^{(M)}$ and $T^{(M)}$ (correspondingly $r^{(m)}$, $R^{(m)}$, $t^{(m)}$ and $T^{(m)}$ for mode m) for a general type of bottom undulation is quite a difficult task. However, assuming small bottom undulation, perturbation method can be employed

here to obtain these coefficients up to first-order. Using the perturbation technique, the lower layer $0 < y < H + \varepsilon c(x),\ -\infty < x < \infty$, is reduced to the uniform finite strip $0 < y < H,\ -\infty < x < \infty$, in the following mathematical analysis.

6.3 Perturbation technique

Since there are two modes of wave propagating at the interface and also just below the ice-cover along the positive x-direction, for each potential mode the first-order reflection and transmission coefficients associated with respective mode of waves can be calculated by the following procedure.

Let us first consider a train of progressive waves of mode m to be normally incident on the bottom undulation. If there is no bottom undulation, then the normally incident wave train will propagate without any hindrance and there will be only transmission. This, along with the appropriate form of the boundary condition (6.18), suggest that ϕ, ψ, $r^{(m)}$, $R^{(m)}$, $t^{(m)}$ and $T^{(m)}$ which were introduced (for wave mode m) in the last section, can be expressed in terms of the small parameter ε as:

$$\left.\begin{aligned} \phi &= \phi_0 + \varepsilon\,\phi_1 + \mathrm{O}(\varepsilon^2), \\ \psi &= \psi_0 + \varepsilon\,\psi_1 + \mathrm{O}(\varepsilon^2), \\ r^{(m)} &= \varepsilon\, {r_1}^{(m)} + \mathrm{O}(\varepsilon^2), \\ R^{(m)} &= \varepsilon\, {R_1}^{(m)} + \mathrm{O}(\varepsilon^2), \\ t^{(m)} &= 1 + \varepsilon\, {t_1}^{(m)} + \mathrm{O}(\varepsilon^2), \\ T^{(m)} &= \varepsilon\, {T_1}^{(m)} + \mathrm{O}(\varepsilon^2), \end{aligned}\right\} \tag{6.21}$$

where ϕ_0 and ψ_0 are given by (6.12) and (6.13), respectively.

It must be noted that such a perturbation expansion ceases to be valid at Bragg resonance when the reflection coefficient becomes much larger than the undulation parameter ε, as pointed out by Mei [54]. It may be recalled that Bragg resonance occurs when the ripple wave number of the bottom undulation is twice the interface wave number. However, to overcome this Bragg resonance situation, Mei [54] developed wave evolution and reflection theory at and near Bragg resonance condition for shore-parallel sinusoidal bars. Since Bragg resonance is not taken into account in our study, the perturbation expansions as given by (6.21) is valid throughout our work. Our theory is valid only for infinitesimal reflection and away from resonance.

Using (6.21) in (6.2), (6.3) and boundary conditions (6.18), (6.5)-(6.7), (6.16), (6.17) and then comparing the first-order terms of ε on both sides of the equations, we find that the first-order potentials $\phi_1(x, y)$ and $\psi_1(x, y)$ satisfy a coupled boundary value problem described by

$$\nabla^2\phi_1 = 0 \qquad \text{in} \quad 0 \le y \le H, \tag{6.22}$$

$$\nabla^2\psi_1 = 0 \qquad \text{in} \quad -h \le y \le 0, \tag{6.23}$$

$$\frac{\partial\phi_1}{\partial y} = \mathrm{i}m\frac{d}{dx}\left[c(x)\mathrm{e}^{\mathrm{i}mx}\right] \equiv p(x) \text{ on } y = H, \tag{6.24}$$

$$\frac{\partial\phi_1}{\partial y} = \frac{\partial\psi_1}{\partial y} \qquad \text{on} \quad y = 0, \tag{6.25}$$

$$K\phi_1 + \frac{\partial\phi_1}{\partial y} = \rho(K\psi_1 + \frac{\partial\psi_1}{\partial y}) \qquad \text{on} \quad y = 0, \tag{6.26}$$

$$K\psi_1 + \left(D\frac{\partial^4}{\partial x^4} + 1 - \delta K\right)\frac{\partial\psi_1}{\partial y} = 0 \qquad \text{on} \quad y = -h, \tag{6.27}$$

$$\phi_1(x,y) \sim \begin{cases} r_1^{(m)}\cosh m(H-y)\mathrm{e}^{-\mathrm{i}mx} + R_1^{(m)}\cosh M(H-y)\mathrm{e}^{-\mathrm{i}Mx} & \text{as } x \to -\infty, \\ t_1^{(m)}\cosh m(H-y)\mathrm{e}^{\mathrm{i}mx} + T_1^{(m)}\cosh M(H-y)\mathrm{e}^{\mathrm{i}Mx} & \text{as } x \to \infty, \end{cases} \tag{6.28}$$

$$\psi_1(x,y) \sim \begin{cases} r_1^{(m)}f(m,y)\mathrm{e}^{-\mathrm{i}mx} + R_1^{(m)}f(M,y)\mathrm{e}^{-\mathrm{i}Mx} & \text{as } x \to -\infty, \\ t_1^{(m)}f(m,y)\mathrm{e}^{\mathrm{i}mx} + T_1^{(m)}f(M,y)\mathrm{e}^{\mathrm{i}Mx} & \text{as } x \to \infty. \end{cases} \tag{6.29}$$

To solve the above coupled boundary value problem described by (6.22)-(6.27), we need two-dimensional source potentials (in terms of Green's function) for Laplace's equation due to a source submerged in either of the two layers. Then Green's integral theorem will be employed and the first-order coefficients $r_1^{(m)}$, $R_1^{(m)}$, $t_1^{(m)}$ and $T_1^{(m)}$ will be obtained in terms of integrals involving the shape function $c(x)$. When the source is submerged in the lower fluid at (ξ,η), $0 < \eta < H$, then we consider $G_1(x,y;\xi,\eta)$ and $G_2(x,y;\xi,\eta)$ to be the source potentials in terms of Green's function for the lower and upper layer fluids, respectively. Similarly when the source is submerged in the upper layer fluid at (ξ,η), $-h < \eta < 0$, then we consider $G_3(x,y;\xi,\eta)$ and $G_4(x,y;\xi,\eta)$ to be the source potentials in terms of Green's function for the lower and upper layer fluids, respectively.

6.4 Solution by Green's function technique

6.4.1 Introduction of Green's functions

Suppose the source is submerged in the lower layer fluid. Then, for $0 < \eta < H$, the source potentials in terms of Green's functions $G_1(x,y;\xi,\eta)$ and $G_2(x,y;\xi,\eta)$ satisfy the following boundary value problem:

$$\nabla^2 G_1 = 0 \qquad \text{in} \quad 0 < y < H, \quad \text{except at } (\xi,\eta), \tag{6.30}$$

$$\nabla^2 G_2 = 0 \qquad \text{in} \quad -h \le y \le 0, \tag{6.31}$$

$$\frac{\partial G_1}{\partial y} = 0 \qquad \text{on} \quad y = H, \tag{6.32}$$

$$\frac{\partial G_1}{\partial y} = \frac{\partial G_2}{\partial y} \qquad \text{on} \quad y = 0, \tag{6.33}$$

$$KG_1 + \frac{\partial G_1}{\partial y} = \rho(KG_2 + \frac{\partial G_2}{\partial y}) \qquad \text{on} \quad y = 0, \tag{6.34}$$

$$KG_2 + \left(D\frac{\partial^4}{\partial x^4} + 1 - \delta K\right)\frac{\partial G_2}{\partial y} = 0 \qquad \text{on} \quad y = -h, \tag{6.35}$$

$$G_1 \sim \log r \qquad \text{as} \quad r = \sqrt{(x-\xi)^2 + (y-\eta)^2} \to 0. \tag{6.36}$$

If a body in water undergoes some sort of oscillations, the resulting motion in the fluid can be described by a series of singularities placed in the body. These singularities are characterized by their giving rise to velocity potentials which are typical singular solutions of the Laplace's equation in the neighbourhood of the singularity. For the two-dimensional case these singularities are either logarithmic type or multipole type, and for the three-dimensional case these are point sources or point multipoles.

Both G_1 and G_2 represent outgoing waves as $|x-\xi| \to \infty$. We look for solutions to the above boundary value problem in the following form

$$G_1(x,y;\xi,\eta) = \log\frac{r}{r_1} + \int_0^\infty [A(k)\cosh k(H-y) + B(k)\sinh k(H-y)]\cos k(x-\xi)dk, \tag{6.37}$$

$$G_2(x,y;\xi,\eta) = \frac{1}{\rho}\log\frac{r}{r_1} + \int_0^\infty [A_1(k)\cosh k(h+y) + B_1(k)\sinh k(h+y)]\cos k(x-\xi)dk, \tag{6.38}$$

where $r_1 = \sqrt{(x-\xi)^2 + (y+2h+\eta)^2}$.
In order that the boundary conditions (6.30)-(6.36) are satisfied, the values of $A(k), B(k), A_1(k)$ and $B_1(k)$ in the solutions $G_1(x,y;\xi,\eta)$ and $G_2(x,y;\xi,\eta)$ are obtained as follows:

$$\begin{aligned} A(k) = \frac{1}{\Delta(k)}\Big[& -2\mathrm{e}^{-k(h+\eta)}\Big([K^2 - k^2(Dk^4+1-\delta K)](1-\rho)\sinh kh\cosh kh \\ & + Kk\{[1+\rho(Dk^4-\delta K)]\cosh^2 kh - (Dk^4+1-\delta K)\sinh^2 kh\}\Big) \\ & - 2\mathrm{e}^{-k(h+H)}\sinh k(h+\eta)\Big\{(K\sinh kH - k\cosh kH)[(Dk^4+1-\delta K)k\sinh kh - K\cosh kh] \\ & + \rho\cosh kH[(K\cosh kh + k\sinh kh)k(Dk^4+1-\delta K) - K(K\sinh kh + k\cosh kh)]\Big\}\Big], \end{aligned} \tag{6.39}$$

$$B(k) = -2\mathrm{e}^{-k(h+H)}\sinh k(h+\eta), \tag{6.40}$$

$$\begin{aligned} A_1(k) = & \frac{-2Kk(Dk^4+1-\delta K)}{\Delta(k)} \\ & \times\left[\mathrm{e}^{-k(h+\eta)}(\sinh kh\sinh kH + \cosh kh\cosh kH) + \mathrm{e}^{-k(h+H)}\sinh k(h+\eta)\right], \end{aligned} \tag{6.41}$$

$$B_1(k) = 2K^2\left[\frac{\mathrm{e}^{-k(h+\eta)}(\sinh kh\sinh kH + \cosh kh\cosh kH) + \mathrm{e}^{-k(h+H)}\sinh k(h+\eta)}{\Delta(k)}\right] - \frac{2}{\rho}\mathrm{e}^{-k(h+\eta)}, \tag{6.42}$$

where $\Delta(k)$ is same as given by (6.11), and the path of the integration in the integrals in (6.37)-(6.38) are indented below the poles at $k = m$ and $k = M$ on the real axis so as to ensure the outgoing natures of G_1 and G_2 far away from the source. As $|x-\xi| \to \infty$, the above

Green's functions assume the following form:

$$G_1(x,y;\xi,\eta) = -2\pi \mathrm{i}K\left[\frac{S(m)\cosh m(H-\eta)\cosh m(H-y)}{m\ \sinh mH\ \Delta'(m)}\ \mathrm{e}^{\mathrm{i}m\,|x-\xi|} + \frac{S(M)\cosh M(H-\eta)\cosh M(H-y)}{M\ \sinh MH\ \Delta'(M)}\ \mathrm{e}^{\mathrm{i}M|x-\xi|}\right], \tag{6.43}$$

$$G_2(x,y;\xi,\eta) = -2\pi \mathrm{i}K\left[\frac{Q_1(m)\cosh m(H-\eta)}{m\ \Delta'(m)}\ \mathrm{e}^{\mathrm{i}m\,|x-\xi|} + \frac{Q_1(M)\cosh M(H-\eta)}{M\ \Delta'(M)}\ \mathrm{e}^{\mathrm{i}M|x-\xi|}\right], \tag{6.44}$$

where

$$S(k) = K\cosh kh - (Dk^4+1-\delta K)k\sinh kh, \tag{6.45}$$

$$Q_1(k) = (Dk^4+1-\delta K)k\cosh k(h+y) - K\sinh k(h+y), \qquad k = m, M. \tag{6.46}$$

Similarly, when the source term (ξ,η), $-h < \eta < 0$, is submerged in the upper layer, then the source potentials $G_3(x,y;\xi,\eta)$ and $G_4(x,y;\xi,\eta)$ satisfy the same type of boundary value problem, as given by (6.30)-(6.35), with G_1 replaced by G_3 and G_2 by G_4, and additionally G_4 satisfying

$$G_4 \sim \log r \qquad \text{as} \quad r = \sqrt{(x-\xi)^2+(y-\eta)^2}\ \to 0.$$

G_3 and G_4 also represent outgoing waves as $|x-\xi| \to \infty$. Here also, we look for solutions G_3 and G_4 satisfying the boundary value problem under consideration in the following form:

$$G_3(x,y;\xi,\eta) = \rho\log\frac{r}{r_1} + \int_0^\infty [E(k)\cosh k(H-y) + F(k)\sinh k(H-y)]\cos k(x-\xi)dk, \tag{6.47}$$

$$G_4(x,y;\xi,\eta) = \log\frac{r}{r_1} + \int_0^\infty [E_1(k)\cosh k(h+y) + F_1(k)\sinh k(h+y)]\cos k(x-\xi)dk. \tag{6.48}$$

In order to satisfy the respective boundary conditions, the values of $E(k)$, $F(k)$, $E_1(k)$ and $F_1(k)$, which are present in the source potentials in terms of Green's functions $G_3(x,y;\xi,\eta)$ and $G_4(x,y;\xi,\eta)$, are obtained in the following form:

$$\begin{aligned} E(k) = -\frac{2\rho}{\Delta(k)}\Big[&\mathrm{e}^{-k(h+H)}\sinh k(h+\eta) \\ &\times\Big((k\cosh kH - K\sinh kH)[K\cosh kh - (Dk^4+1-\delta K)k\sinh kh] \\ &-\rho\{[K^2-k^2(Dk^4+1-\delta K)]\sinh kh\cosh kH - Kk(Dk^4-\delta K)\cosh kh\cosh kH\} \\ &+(1-\rho)\mathrm{e}^{kH}\{Kk(Dk^4-\delta K)\cosh kh - [K^2-k^2(Dk^4+1-\delta K)]\sinh kh\}\Big) \\ &+Kk(Dk^4+1-\delta K)\mathrm{e}^{-k(h+\eta)}\Big], \end{aligned} \tag{6.49}$$

$$F(k) = -2\rho\mathrm{e}^{-k(h+H)}\sinh k(h+\eta), \tag{6.50}$$

$$\begin{aligned} E_1(k) = \frac{k(Dk^4+1-\delta K)}{(Dk^4+1-\delta K)k\sinh kh - K\cosh kh}\Big[&-E(k)\sinh kH + 2(1-\rho)\mathrm{e}^{-kh}\sinh k(h+\eta) \\ &+2\mathrm{e}^{-k(h+\eta)}\cosh kh + 2\rho\,\mathrm{e}^{-k(h+H)}\sinh k(h+\eta)\cosh kH\Big], \end{aligned} \tag{6.51}$$

$$F_1(k) = -\frac{K\ E_1(k)}{k(Dk^4+1-\delta K)} - 2\mathrm{e}^{-k(h+\eta)}, \tag{6.52}$$

where $\Delta(k)$ is same as given by (6.11) and the path of the integration in the integrals in (6.47)-(6.48) are indented below the poles at $k = m$ and $k = M$ on the real axis so as to ensure the outgoing natures of G_3 and G_4 far away from the source. As $|x-\xi| \to \infty$, the above Green's functions assume the following form:

$$G_3(x,y;\xi,\eta) = 2\pi \mathrm{i}\rho K\left[\frac{Q_2(m)\cosh m(H-y)}{m\,\Delta'(m)}\,\mathrm{e}^{\mathrm{i}m\,|x-\xi|} + \frac{Q_2(M)\cosh M(H-y)}{M\,\Delta'(M)}\,\mathrm{e}^{\mathrm{i}M|x-\xi|}\right], \quad (6.53)$$

$$G_4(x,y;\xi,\eta) = 2\pi \mathrm{i}\rho K\left[\frac{Q_2(m)\sinh mH}{m\,\Delta'(m)}\frac{Q_1(m)}{S(m)}\,\mathrm{e}^{\mathrm{i}m\,|x-\xi|} + \frac{Q_2(M)\sinh MH}{M\,\Delta'(M)}\frac{Q_1(M)}{S(M)}\,\mathrm{e}^{\mathrm{i}M|x-\xi|}\right], \quad (6.54)$$

where

$$Q_2(k) = K\sinh k(h+\eta) - (Dk^4+1-\delta K)k\cosh k(h+\eta), \qquad k = m, M. \quad (6.55)$$

If the flexural rigidity of the elastic ice-cover is assumed to be zero along with absence of the ice-cover (implying $D = 0$ and $\delta = 0$), the representation of the Green's functions as $|x-\xi| \to \infty$, given by (6.43), (6.44), (6.53) and (6.54), coincide with the corresponding source potentials obtained earlier in Maiti and Mandal [49] for the normal case where the two-layer fluid had a free surface and a bottom undulation.

Since $\nabla^2\phi_1 = 0$ and $\nabla^2 G_1 = 0$ (in the neighbourhood of the singularity), so we have $\int_V(\phi_1\nabla^2 G_1 - G_1\nabla^2\phi_1)dv = 0$. Hence Green's integral theorem can be applied over an appropriately curtailed volume V. Therefore in order to obtain $\phi_1(\xi,\eta)$, when (ξ,η) is submerged in the lower layer fluid, we first apply the Green's integral theorem to $\phi_1(x,y)$ and $G_1(x,y;\xi,\eta)$ to obtain

$$\int_C \left(\phi_1\frac{\partial G_1}{\partial n} - G_1\frac{\partial\phi_1}{\partial n}\right)ds = 0, \quad (6.56)$$

where C is a closed contour in the xy-plane consisting of the lines $y = 0,\ -X \le x \le X;\ y = H,\ -X \le x \le X,\ x = \pm X,\ 0 \le y \le H$ and a small circle of radius α_1 with center at (ξ,η) and ultimately let $X \to \infty$ and $\alpha_1 \to 0$. Then there will be no contribution to the integral from the line $x = \pm X$, as both ϕ_1 and G_1 approach zero when $X \to \pm\infty$. Thus the resultant form of the integral equation (6.56) is

$$-2\pi\phi_1(\xi,\eta) + \int_{-\infty}^{\infty} p(x)G_1(x,H;\xi,\eta)dx + \int_{-\infty}^{\infty}\left(\phi_1\frac{\partial G_1}{\partial y} - G_1\frac{\partial\phi_1}{\partial y}\right)_{y=0}dx = 0. \quad (6.57)$$

Then again, we apply the Green's integral theorem to $\psi_1(x,y)$ and $G_2(x,y;\xi,\eta)$ in the form

$$\int_{C'}\left(\psi_1\frac{\partial G_2}{\partial n} - G_2\frac{\partial\psi_1}{\partial n}\right)ds = 0, \quad (6.58)$$

where C' is a closed counter consisting of the lines $y = -h,\ -X \le x \le X;\ y = 0,\ -X \le x \le X;\ x = \pm X,\ -h \le y \le 0$ and ultimately let $X \to \infty$. Here, we note that $G_2(x,y;\xi,\eta)$ has no singularity in the upper region. Now (6.58) can be rewritten as

$$-\int_{-\infty}^{\infty}\left(\psi_1\frac{\partial G_2}{\partial y} - G_2\frac{\partial\psi_1}{\partial y}\right)_{y=-h}dx - \int_{-h}^{0}\left(\psi_1\frac{\partial G_2}{\partial y} - G_2\frac{\partial\psi_1}{\partial y}\right)_{x=-\infty}dy$$
$$+\int_{-\infty}^{\infty}\left(\psi_1\frac{\partial G_2}{\partial y} - G_2\frac{\partial\psi_1}{\partial y}\right)_{y=0}dx + \int_{-h}^{0}\left(\psi_1\frac{\partial G_2}{\partial y} - G_2\frac{\partial\psi_1}{\partial y}\right)_{x=\infty}dy = 0. \quad (6.59)$$

Use of the ice-cover condition on $y = -h$ and the asymptotic results for ψ_1 and G_2, make the first integral equal to zero for any large value of X (see Mandal and Basu [51]). The second and fourth integrals will not contribute when $X \to \infty$, due to the outgoing nature of both ψ_1 and G_2 as $x \to \pm\infty$. Thus the resultant integral of (6.59) is

$$\int_{-\infty}^{\infty} \left(\psi_1 \frac{\partial G_2}{\partial y} - G_2 \frac{\partial \psi_1}{\partial y} \right)_{y=0} dx = 0. \tag{6.60}$$

Now solving (6.57) and (6.60) with the help of the interface conditions at $y = 0$, we get

$$\phi_1(\xi, \eta) = \frac{1}{2\pi} \int_{-\infty}^{\infty} G_1(x, H; \xi, \eta)\, p(x) dx \qquad 0 < \eta < H, \tag{6.61}$$

which solves the boundary value problem for $\phi_1(x, y)$.

Similarly, to calculate $\psi_1(\xi, \eta)$, when the source term (ξ, η), $-h < \eta < 0$, is submerged in the upper layer fluid, we apply the same procedure as was followed previously for the case of the lower layer fluid. The final expression for $\psi_1(\xi, \eta)$ is

$$\psi_1(\xi, \eta) = \frac{1}{2\pi\rho} \int_{-\infty}^{\infty} G_3(x, H; \xi, \eta)\, p(x) dx \qquad -h < \eta < 0, \tag{6.62}$$

which solves the boundary value problem for $\psi_1(x, y)$.

6.4.2 Reflection and transmission coefficients

The first-order reflection and transmission coefficients $r_1^{(m)}$, $t_1^{(m)}$ and $R_1^{(m)}$, $T_1^{(m)}$ with respect to the modes m and M, respectively, due to the normally incident wave of mode m, are now obtained by letting $\xi \to \mp\infty$, in (6.61) or (6.62) and comparing with (6.28) or (6.29) with (x, y) replaced by (ξ, η). Thus we obtain the values of $r_1^{(m)}$ and $R_1^{(m)}$ as

$$r_1^{(m)} = -\frac{\mathrm{i}Km\, S(m)}{\sinh mH\ \Delta'(m)} \int_{-\infty}^{\infty} \mathrm{e}^{2\mathrm{i}mx}\, c(x) dx, \tag{6.63}$$

$$R_1^{(m)} = -\frac{\mathrm{i}Km\, S(M)}{\sinh MH\ \Delta'(M)} \int_{-\infty}^{\infty} \mathrm{e}^{\mathrm{i}(m+M)x}\, c(x) dx. \tag{6.64}$$

Similarly to find $t_1^{(m)}$ and $T_1^{(m)}$, we consider $\phi_1(x, y)$ from (6.28) with (x, y) replaced by (ξ, η) and $G_1(x, y; \xi, \eta)$ from (6.43) with $\xi \to \infty$, and use them in (6.61) to get

$$t_1^{(m)} = \frac{\mathrm{i}Km\, S(m)}{\sinh mH\ \Delta'(m)} \int_{-\infty}^{\infty} c(x) dx, \tag{6.65}$$

$$T_1^{(m)} = \frac{\mathrm{i}Km\, S(M)}{\sinh MH\ \Delta'(M)} \int_{-\infty}^{\infty} \mathrm{e}^{\mathrm{i}(m-M)x}\, c(x) dx. \tag{6.66}$$

This is also verified that the same expressions for $r_1^{(m)}$, $R_1^{(m)}$, $t_1^{(m)}$ and $T_1^{(m)}$ are obtained by letting $\xi \to -\infty$ and $\xi \to \infty$, respectively, in (6.29) and (6.53), and solving for (6.62). Therefore, the two first-order reflection coefficients and the two first-order transmission coefficients can be evaluated from (6.63)-(6.66), once the shape function $c(x)$ is known.

When we consider a train of progressive waves of mode M to be normally incident on the bottom undulation, the same mathematical procedure described above for the case of mode m is followed to obtain the first-order reflection and transmission coefficients $r_1^{(M)}$, $R_1^{(M)}$, $t_1^{(M)}$ and $T_1^{(M)}$. The final expressions for this case are as follows:

$$r_1^{(M)} = -\frac{\mathrm{i}KM\ S(m)}{\sinh mH\ \Delta'(m)} \int_{-\infty}^{\infty} \mathrm{e}^{\mathrm{i}(M+m)x}\ c(x)dx, \tag{6.67}$$

$$R_1^{(M)} = -\frac{\mathrm{i}KM\ S(M)}{\sinh MH\ \Delta'(M)} \int_{-\infty}^{\infty} \mathrm{e}^{2\mathrm{i}Mx}\ c(x)dx, \tag{6.68}$$

$$t_1^{(M)} = \frac{\mathrm{i}KM\ S(m)}{\sinh mH\ \Delta'(m)} \int_{-\infty}^{\infty} \mathrm{e}^{\mathrm{i}(M-m)x}\ \ c(x)dx, \tag{6.69}$$

$$T_1^{(M)} = \frac{\mathrm{i}KM\ S(M)}{\sinh MH\ \Delta'(M)} \int_{-\infty}^{\infty} c(x)dx. \tag{6.70}$$

Here, if we take $D = 0$ and $\delta = 0$ (*i.e.*, the flexural rigidity of elastic ice-cover is assumed to be zero and the ice-cover is absent), then all the above results from (6.63)-(6.70) coincide with the corresponding results in Maiti and Mandal [49].

6.5 Solution by Fourier transform technique

Now the above boundary value problem for ϕ_1 and ψ_1, described by (6.22) to (6.29), can be decomposed into two independent boundary value problems for ϕ_1 and ψ_1 as follows:

Boundary Value Problem-I, corresponding to ϕ_1, is

$$\nabla^2\phi_1 = 0 \qquad \text{in} \quad 0 \le y \le H, \tag{6.71}$$

$$\frac{\partial\phi_1}{\partial y} = \eta(x) \qquad \text{on} \quad y = 0, \tag{6.72}$$

$$\frac{\partial\phi_1}{\partial y} = p(x) \qquad \text{on} \quad y = H, \tag{6.73}$$

where $\eta(x)$ is assumed to be known on $y = 0$ and ϕ_1 has the asymptotic behaviour

$$\phi_1(x,y) \sim \begin{cases} r_1^{(m)}\ \cosh m(H-y)\mathrm{e}^{-\mathrm{i}mx} + R_1^{(m)} \cosh M(H-y)\mathrm{e}^{-\mathrm{i}Mx} & \text{as } x \to -\infty, \\ t_1^{(m)} \cosh m(H-y)\mathrm{e}^{\mathrm{i}mx} + T_1^{(m)} \cosh M(H-y)\mathrm{e}^{\mathrm{i}Mx} & \text{as } \ x \to \infty, \end{cases} \tag{6.74}$$

Boundary Value Problem-II, corresponding to ψ_1, is

$$\nabla^2\psi_1 = 0 \quad \text{in} \quad -h \le y \le 0, \tag{6.75}$$

$$\frac{\partial\psi_1}{\partial y} = \eta(x) \quad \text{on} \quad y = 0, \tag{6.76}$$

$$K\psi_1 + \left(D\frac{\partial^4}{\partial x^4} + 1 - \delta K\right)\frac{\partial\psi_1}{\partial y} = 0 \quad \text{on} \quad y = -h, \tag{6.77}$$

Here, the value of $\eta(x)$ is same as in Boundary Value Problem-I, and ψ_1 has the asymptotic behaviour

$$\psi_1(x,y) \sim \begin{cases} r_1^{(m)}\ f(m,y)\mathrm{e}^{-\mathrm{i}mx} + R_1^{(m)} f(M,y)\mathrm{e}^{-\mathrm{i}Mx} & \text{as } x \to -\infty, \\ t_1^{(m)} f(m,y)\mathrm{e}^{\mathrm{i}mx} + T_1^{(m)} f(M,y)\mathrm{e}^{\mathrm{i}Mx} \text{ as } x \to \infty. \end{cases} \tag{6.78}$$

Now using (6.72) and (6.76), (6.26) can be written in the following form:

$$K(\phi_1 - \rho\psi_1) = (\rho - 1)\eta(x) \qquad \text{on} \quad y = 0. \tag{6.79}$$

6.5.1 Fourier transform technique

Applying Fourier transform, as defined in Chapter 4, to (6.71), (6.72) and (6.73), we get the following boundary value problem for $\overline{\phi}_1(\xi, y)$:

$$\overline{\phi}_{1yy} - \xi^2\overline{\phi}_1 = 0 \quad \text{on} \quad 0 \le y \le H, \tag{6.80}$$

$$\overline{\phi}_{1y} = \overline{\eta}(\xi) \quad \text{on} \quad y = 0, \tag{6.81}$$

$$\overline{\phi}_{1y} = \overline{p}(\xi) \quad \text{on} \quad y = H, \tag{6.82}$$

where $\overline{\eta}(\xi)$ and $\overline{p}(\xi)$ are the Fourier transforms of $\eta(x)$ and $p(x)$, respectively. The solution $\overline{\phi}_1(\xi, y)$ of the above boundary value problem is obtained as

$$\overline{\phi}_1(\xi, y) = \frac{\overline{p}(\xi)\cosh\xi y - \overline{\eta}(\xi)\cosh\xi(H-y)}{\xi\sinh\xi H}. \tag{6.83}$$

Similarly, applying Fourier transform to (6.75), (6.76) and (6.77), we get the following boundary value problem for $\overline{\psi}_1(\xi, y)$:

$$\overline{\psi}_{1yy} - \xi^2\overline{\psi}_1 = 0 \quad \text{on} \quad -h \le y \le 0, \tag{6.84}$$

$$\overline{\psi}_{1y} = \overline{\eta}(\xi) \quad \text{on} \quad y = 0, \tag{6.85}$$

$$K\overline{\psi}_1 + (D\xi^4 + 1 - \delta K)\overline{\psi}_{1y} = 0 \quad \text{on} \quad y = -h, \tag{6.86}$$

The solution $\overline{\psi}_1(\xi, y)$ of the above boundary value problem is obtained as

$$\overline{\psi}_1(\xi, y) = \frac{K\sinh\xi(h+y) - (D\xi^4 + 1 - \delta K)\xi\cosh\xi(h+y)}{K\cosh\xi h - (D\xi^4 + 1 - \delta K)\xi\sinh\xi h}\ \frac{\overline{\eta}(\xi)}{\xi}. \tag{6.87}$$

In order to calculate $\overline{\eta}(\xi)$, by applying Fourier transform to (6.79), we obtain

$$K(\overline{\phi}_1 - \rho\overline{\psi}_1) = (\rho - 1)\overline{\eta}(\xi) \quad \text{on} \quad y = 0. \tag{6.88}$$

Now substituting (6.83) and (6.87) in (6.88), we obtain $\overline{\eta}(\xi)$ as

$$\overline{\eta}(\xi) = \frac{K\ \overline{p}(\xi)\ \{K\cosh\xi h - (D\xi^4 + 1 - \delta K)\xi\sinh\xi h\}}{\Delta(\xi)}, \tag{6.89}$$

where $\Delta(\xi)$ is same as given by (6.11). Substituting the value of $\overline{\eta}(\xi)$ in (6.83) and (6.87), the values of $\overline{\phi}_1(\xi, y)$ and $\overline{\psi}_1(\xi, y)$, respectively, are obtained as follows:

$$\overline{\phi}_1(\xi, y) = \frac{\overline{p}(\xi)}{\xi\sinh\xi H}\left\{\cosh\xi y - \frac{K[K\cosh\xi h - (D\xi^4 + 1 - \delta K)\xi\sinh\xi h]\cosh\xi(H-y)}{\Delta(\xi)}\right\}, \tag{6.90}$$

$$\overline{\psi}_1(\xi, y) = \frac{K\ \overline{p}(\xi)\ [K\sinh\xi(h+y) - (D\xi^4 + 1 - \delta K)\xi\cosh\xi(h+y)]}{\xi\ \Delta(\xi)}. \tag{6.91}$$

By using the inverse Fourier transform technique, as defined in Chapter 4, we obtain the solution of BVP-I and BVP-II, for ϕ_1 and ψ_1 respectively, given by

$$\phi_1(x,y) = \frac{1}{2\pi}\int_{-\infty}^{\infty}\left\{\cosh\xi y - \frac{K[K\cosh\xi h-(D\xi^4+1-\delta K)\xi\sinh\xi h]\cosh\xi(H-y)}{\Delta(\xi)}\right\} \times\frac{\overline{p}(\xi)\ \mathrm{e}^{i\xi x}}{\xi\sinh\xi H}\ d\xi, \tag{6.92}$$

$$\psi_1(x,y) = \frac{K}{2\pi}\int_{-\infty}^{\infty}\frac{K\sinh\xi(h+y)-(D\xi^4+1-\delta K)\xi\cosh\xi(h+y)}{\xi\ \Delta(\xi)}\ \overline{p}(\xi)\mathrm{e}^{\mathrm{i}\xi x}\ d\xi. \tag{6.93}$$

Here $\xi = 0$ is not a singularity of (6.92) and (6.93), because $\overline{p}(0) = 0$ due to $c(x) \to 0$ as $|x| \to \infty$. Since $\Delta(\xi)$ has non-zero zeros at $\xi = \pm m$ and $\xi = \pm M$, on the real axis of ξ, so the above integral on both cases contains poles at $\xi = \pm m$ and $\xi = \pm M$.

6.5.2 Reflection and transmission coefficients

The first-order reflection and transmission coefficients $r_1^{(m)}, t_1^{(m)}$ and $R_1^{(m)}, T_1^{(m)}$ with respect to the modes m and M, respectively, due to normally incident wave of mode m, are now obtained by letting $\xi \to \mp\infty$ in (6.92) or (6.93) and comparing with (6.74) or (6.78). To calculate the first-order reflection coefficients, we let $\xi \to -\infty$ in either (6.92) or (6.93). As $\xi \to -\infty$, the behaviour of $\phi_1(x,y)$ or $\psi_1(x,y)$ can be obtained by rotating the path of the integral, involving the term $\overline{p}(-\xi)$ into a contour in the first quadrant, so that we must include the residue terms at the poles $\xi = m$ and $\xi = M$. The path of the integral involving the term $\overline{p}(\xi)$ in (6.92) or (6.93) is rotated into a contour in the fourth quadrant so that the integral involving the term $\overline{p}(\xi)$ does not contribute as $\xi \to -\infty$. Then comparing the resultant integral value with (6.74) or (6.78) (on replacing x by ξ), we obtain $r_1^{(m)}$ and $R_1^{(m)}$ as

$$\begin{aligned} r_1^{(m)} &= -\frac{\mathrm{i}K\ S(m)}{m\sinh mH\ \Delta'(m)}\overline{p}(-m) \\ &= -\frac{\mathrm{i}Km\ S(m)}{\sinh mH\ \Delta'(m)}\int_{-\infty}^{\infty}\mathrm{e}^{2\mathrm{i}mx}\ c(x)dx, \end{aligned} \tag{6.94}$$

$$\begin{aligned} R_1^{(m)} &= -\frac{\mathrm{i}K\ S(M)}{M\sinh MH\ \Delta'(M)}\overline{p}(-M) \\ &= -\frac{\mathrm{i}Km\ S(M)}{\sinh MH\ \Delta'(M)}\int_{-\infty}^{\infty}\mathrm{e}^{\mathrm{i}(m+M)x}\ \ c(x)dx, \end{aligned} \tag{6.95}$$

where $S(k)$, for $k = m, M$, is already defined in the previous section.

Similarly to find the first-order transmission coefficients, we let $\xi \to \infty$ in either (6.92) or (6.93). As $\xi \to \infty$, the behaviour of $\phi_1(x,y)$ or $\psi_1(x,y)$ can be obtained by rotating the path of the integral involving the term $\overline{p}(\xi)$ into a contour in the first quadrant so that we must include the residue terms at the poles $\xi = m$ and $\xi = M$. The path of the integral involving the term $\overline{p}(-\xi)$ in (6.92) or (6.93) is rotated into a contour in the fourth quadrant, so that the integral involving the term $\overline{p}(-\xi)$ does not contribute as $\xi \to \infty$. Then comparing the resultant integral value with the (6.74) or (6.78) (on replacing x by ξ), we obtain $t_1^{(m)}$ and $T_1^{(m)}$

as follows:

$$t_1^{(m)} = \frac{\mathrm{i}Km\ S(m)}{\sinh mH\ \Delta'(m)} \int_{-\infty}^{\infty} c(x)dx, \tag{6.96}$$

$$T_1^{(m)} = \frac{\mathrm{i}Km\ S(M)}{\sinh MH\ \Delta'(M)} \int_{-\infty}^{\infty} \mathrm{e}^{\mathrm{i}(m-M)x}\ c(x)dx. \tag{6.97}$$

Therefore, the two first-order reflection coefficients and the two first-order transmission coefficients can be evaluated from (6.94)-(6.97), once the shape function $c(x)$ is known.

When we consider a train of progressive waves of mode M to be normally incident on the bottom undulation, the same mathematical procedure described above for the case of mode m is followed to obtain the first-order reflection and transmission coefficients $r_1^{(M)}, R_1^{(M)}, t_1^{(M)}$ and $T_1^{(M)}$. The final expressions for these coefficients are as follows:

$$r_1^{(M)} = -\frac{\mathrm{i}KM\ S(m)}{\sinh mH\ \Delta'(m)} \int_{-\infty}^{\infty} \mathrm{e}^{\mathrm{i}(M+m)x}\ c(x)dx, \tag{6.98}$$

$$R_1^{(M)} = -\frac{\mathrm{i}KM\ S(M)}{\sinh MH\ \Delta'(M)} \int_{-\infty}^{\infty} \mathrm{e}^{2\mathrm{i}Mx}\ c(x)dx, \tag{6.99}$$

$$t_1^{(M)} = \frac{\mathrm{i}KM\ S(m)}{\sinh mH\ \Delta'(m)} \int_{-\infty}^{\infty} \mathrm{e}^{\mathrm{i}(M-m)x}\ c(x)dx, \tag{6.100}$$

$$T_1^{(M)} = \frac{\mathrm{i}KM\ S(M)}{\sinh MH\ \ \Delta'(M)} \int_{-\infty}^{\infty} c(x)dx. \tag{6.101}$$

Both the solution methods, *i.e.*, Green's function technique and Fourier transform technique, discussed in this chapter, agree to the same values of the reflection and transmission coefficients.

6.6 Special form of bottom surface

Here, we consider the familiar special sinusoidal form of the shape function $c(x)$ for the uneven bottom surface – Example-II in Chapter 4. As mentioned earlier, these functional forms of the bottom disturbance closely resemble some naturally occurring obstacles formed at the bottom due to sedimentation and ripple growth of sands. Davies [21] studied sinusoidal form of undulations in an ocean bed for a single-layer fluid by using Fourier transform technique and found that an undulating bed has the ability to reflect incident wave energy which has important implications in respect of coastal protection as well as possible ripple growth if the bed is erodible. Because of the importance of the bed topographies with sinusoidal ripples from the application point of view, significant emphasis is laid upon them and subsequently consideration of the following example is deemed appropriate.

The shape function $c(x)$ in the form of patch of sinusoidal bottom ripples on the bottom surface with amplitude a_1 on an otherwise flat bottom has the form

$$c(x) = \begin{cases} a_1 \sin(l_1 x), & L_1 \le x \le 0, \\ a_1 \sin(l_2 x), & 0 \le x \le L_2, \\ 0, & \text{otherwise}\ , \end{cases} \tag{6.102}$$

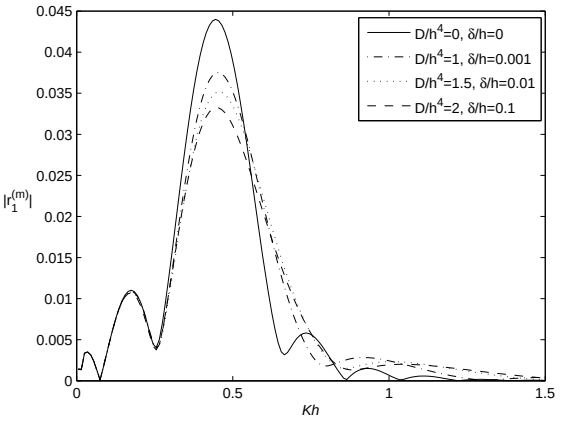

Figure 6.2: Reflection coefficient $|r_1^{(m)}|$ due to an incident wave of wave number m for $\rho = 0.5$, $H/h = 2$, $a_1/h = 0.1$, $n = 3$, $l_1h = 1$ and $l_2h = 1.1$.

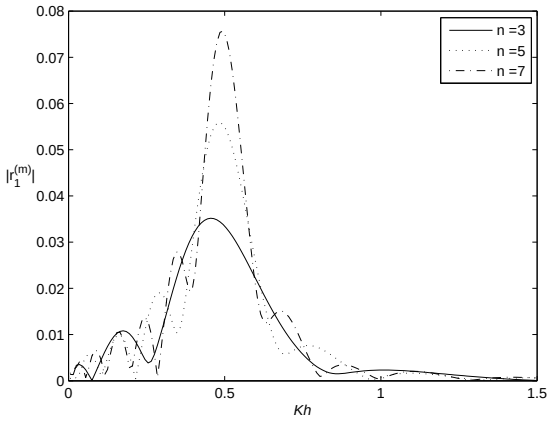

Figure 6.3: Reflection coefficient $|r_1^{(m)}|$ due to an incident wave of wave number m for $D/h^4 = 1.5$, $\delta/h = 0.01$, $\rho = 0.5$, $H/h = 2$, $a_1/h = 0.1$, $l_1h = 1$ and $l_2h = 1.1$.

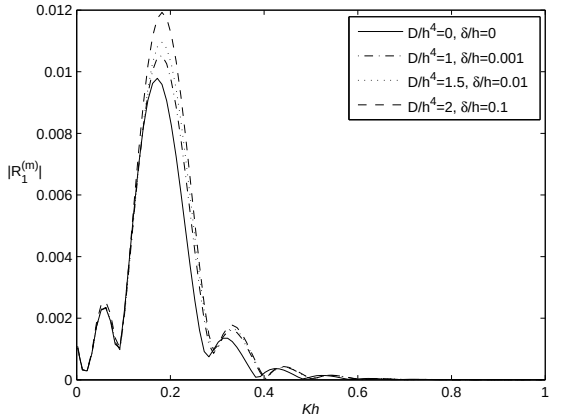

Figure 6.4: Reflection coefficient $|R_1^{(m)}|$ due to an incident wave of wave number m for $\rho = 0.5$, $H/h = 2$, $a_1/h = 0.1$, $n = 3$, $l_1h = 1$ and $l_2h = 1.1$.

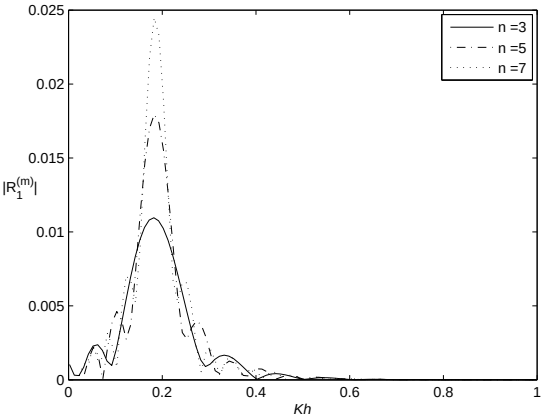

Figure 6.5: Reflection coefficient $|R_1^{(m)}|$ due to an incident wave of wave number m for $D/h^4 = 1.5$, $\delta/h = 0.01$, $\rho = 0.5$, $H/h = 2$, $a_1/h = 0.1$, $l_1h = 1$ and $l_2h = 1.1$.

where l_1 and l_2, respectively, are the wave numbers of the patches in the regions $L_1 \le x \le 0$ and $0 \le x \le L_2$. For continuity of the bed elevation we can take

$$L_1 = \frac{-n\pi}{l_1}, \quad L_2 = \frac{n\pi}{l_2},$$

where n is a positive integer. The patch in each of the regions $L_1 \le x \le 0$ and $0 \le x \le L_2$ consists of $n/2$ number of ripples. Note that instead of taking the same number of ripples in each patch, one can also take different number of ripples in each of the two patches of the bottom undulation. By taking $l_1 = l_2$, the above example reduces to the simple and common example of a single patch of sinusoidal ripple bed.

The first-order reflection and transmission coefficients $r_1^{(m)}$, $R_1^{(m)}, t_1^{(m)}$ and $T_1^{(m)}$ with respect to the modes m and M, respectively, due to the normally incident wave of mode m, are now obtained by substituting $c(x)$ from (6.102) into (6.63)-(6.66). These coefficients are found

as

$$r_1^{(m)}=-\frac{\mathrm{i}a_1KmS(m)}{\sinh mH\Delta'(m)}\left(\frac{l_1\{(-1)^n\exp[-(2\mathrm{i}mn\pi)/l_1]-1\}}{l_1^2-4m^2}+\frac{l_2[1-(-1)^n\exp(2\mathrm{i}mn\pi/l_2)]}{l_2^2-4m^2}\right), \tag{6.103}$$

$$R_1^{(m)}=-\frac{\mathrm{i}a_1KmS(M)}{\sinh MH\Delta'(M)}\left(\frac{l_1\{(-1)^n\exp[-\mathrm{i}n\pi(m+M)/l_1]-1\}}{l_1^2-(m+M)^2}+\frac{l_2\{1-(-1)^n\exp[\mathrm{i}n\pi(m+M)/l_2]\}}{l_2^2-(m+M)^2}\right), \tag{6.104}$$

$$t_1^{(m)}=\frac{\mathrm{i}a_1KmS(m)}{\sinh mH\Delta'(m)}\left[\frac{(-1)^n-1}{l_1}+\frac{1-(-1)^n}{l_2}\right], \tag{6.105}$$

$$T_1^{(m)}=\frac{\mathrm{i}a_1KmS(M)}{\sinh MH\Delta'(M)}\left(\frac{l_1\{(-1)^n\exp[-\mathrm{i}n\pi(m-M)/l_1]-1\}}{l_1^2-(m-M)^2}+\frac{l_2\{1-(-1)^n\exp[\mathrm{i}n\pi(m-M)/l_2]\}}{l_2^2-(m-M)^2}\right). \tag{6.106}$$

Similarly, the reflection and transmission coefficients $r_1^{(M)}$, $R_1^{(M)}$, $t_1^{(M)}$ and $T_1^{(M)}$ with respect to the modes m and M, respectively, due to the normally incident wave of mode M, are now obtained by substituting $c(x)$ from (6.102) into (6.67)-(6.70). These coefficients are found as

$$r_1^{(M)}=-\frac{\mathrm{i}a_1KMS(m)}{\sinh mH\Delta'(m)}\left(\frac{l_1\{(-1)^n\exp[-\mathrm{i}n\pi(M+m)/l_1]-1\}}{l_1^2-(M+m)^2}+\frac{l_2\{1-(-1)^n\exp[\mathrm{i}n\pi(M+m)/l_2]\}}{l_2^2-(M+m)^2}\right), \tag{6.107}$$

$$R_1^{(M)}=-\frac{\mathrm{i}a_1KMS(M)}{\sinh MH\Delta'(M)}\left(\frac{l_1\{(-1)^n\exp[-(2\mathrm{i}Mn\pi)/l_1]-1\}}{l_1^2-4M^2}+\frac{l_2[1-(-1)^n\exp(2\mathrm{i}Mn\pi/l_2)]}{l_2^2-4M^2}\right), \tag{6.108}$$

$$t_1^{(M)}=\frac{\mathrm{i}a_1KMS(m)}{\sinh mH\Delta'(m)}\left(\frac{l_1\{(-1)^n\exp[-\mathrm{i}n\pi(M-m)/l_1]-1\}}{l_1^2-(M-m)^2}+\frac{l_2\{1-(-1)^n\exp[\mathrm{i}n\pi(M-m)/l_2]\}}{l_2^2-(M-m)^2}\right), \tag{6.109}$$

$$T_1^{(M)}=\frac{\mathrm{i}a_1KMS(M)}{\sinh MH\Delta'(M)}\left[\frac{(-1)^n-1}{l_1}+\frac{1-(-1)^n}{l_2}\right]. \tag{6.110}$$

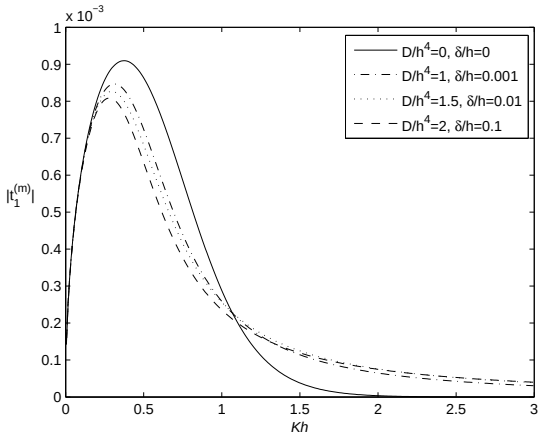

Figure 6.6: Transmission coefficient $|t_1^{(m)}|$ due to an incident wave of wave number m for $\rho=0.5$, $H/h=2$, $a_1/h=0.1$, $n=3$, $l_1h=1$ and $l_2h=1.1$.

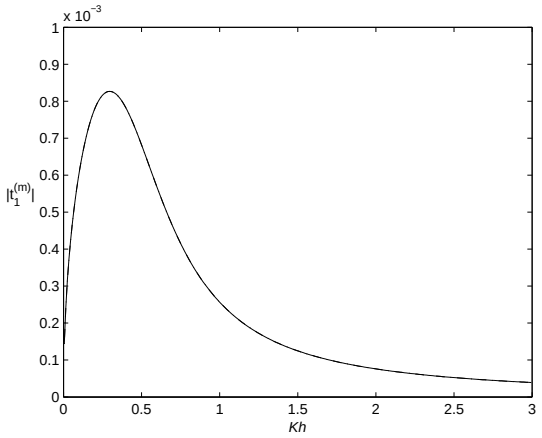

Figure 6.7: Transmission coefficient $|t_1^{(m)}|$ due to an incident wave of wave number m for $D/h^4=1.5$, $\delta/h=0.01$, $\rho=0.5$, $H/h=2$, $a_1/h=0.1$, $l_1h=1$ and $l_2h=1.1$.

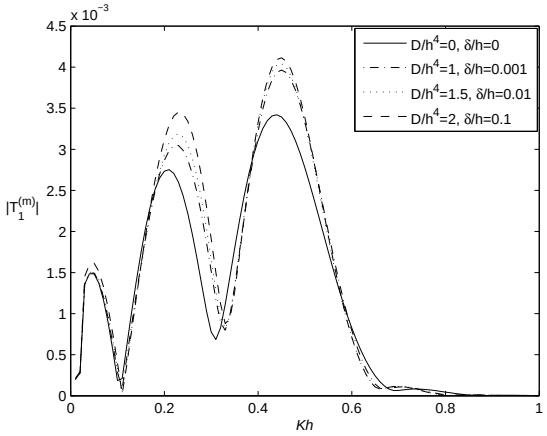

Figure 6.8: Transmission coefficient $|T_1^{(m)}|$ due to an incident wave of wave number m for $\rho = 0.5,\ H/h = 2,\ a_1/h = 0.1,\ n = 3,\ l_1h = 1$ and $l_2h = 1.1$.

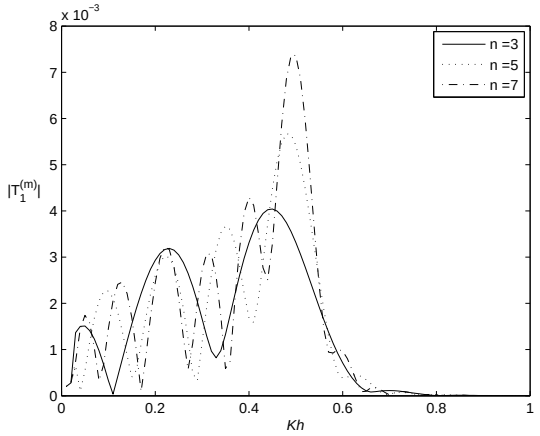

Figure 6.9: Transmission coefficient $|T_1^{(m)}|$ due to an incident wave of wave number m for $D/h^4 = 1.5,\ \delta/h = 0.01,\ \rho = 0.5,\ H/h = 2,\ a_1/h = 0.1,\ l_1h = 1$ and $l_2h = 1.1$.

6.7 Numerical results

In figures 6.2-6.9, the first-order reflection and transmission coefficients are shown for the case of a normally incident wave train of wave number m (an ice-cover mode) propagating along the positive x-axis over the small bottom undulation. In all the figures, the density ratio ρ is taken as 0.5, the depth ratio H/h as 2, the amplitude of the sinusoidal ripples a_1/h as 0.1 and the ripple wave numbers as $l_1h = 1$ and $l_2h = 1.1$. These choices of l_1h and l_2h makes it easier to observe the reflection coefficient than against some more varied values of l_1h and l_2h in which case the oscillation is difficult to observe. That is, if the strip width increases, the tendency for oscillation decreases. In other words, there is no qualitative changes for the varied values of l_1h and l_2h. The different curves in figures 6.2, 6.4, 6.6 and 6.8 correspond to four different sets of ice parameters $(D/h^4 = 0,\ \delta/h = 0)$, $(D/h^4 = 1,\ \delta/h = 0.001)$, $(D/h^4 = 1.5,\ \delta/h = 0.01)$ and $(D/h^4 = 2,\ \delta/h = 0.1)$, while n is fixed, for these curves, at 3. The peak values of the reflection coefficient $|r_1^{(m)}|$ and the transmission coefficient $|t_1^{(m)}|$ of waves of wave number m for the normally incident wave of wave number m, shown in figures 6.2 and 6.6, respectively, decrease as the values of the ice parameters D/h^4 and δ/h increase. Figures 6.4 and 6.8, respectively, show the first-order reflection and transmission coefficients of the wave number M due to the normally incident wave of wave number m and it is observed that as the values of the ice parameters increase, the peak values of the $|R_1^{(m)}|$ and $|T_1^{(m)}|$ increase but their nonzero values show that some conversion of energy from one wave number to the other is always possible. Observing all the figures, it can be concluded that the reflection coefficient of the waves with wave number M is found to be smaller in comparison to those for the waves with wave number m and the transmission coefficient of the waves of wave number m is much smaller than that in the case of the waves with wave number M.

The different curves in figures 6.3, 6.5, 6.7 and 6.9 correspond to different number of ripples

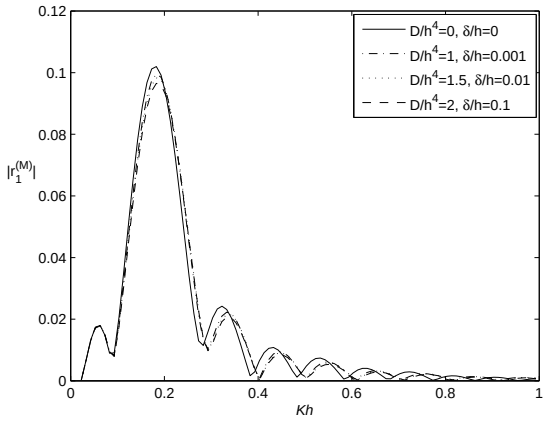

Figure 6.10: Reflection coefficient $|r_1^{(M)}|$ due to an incident wave of wave number M for $\rho = 0.5,\ H/h = 2,\ a_1/h = 0.1,\ n = 3,\ l_1h = 1$ and $l_2h = 1.1$.

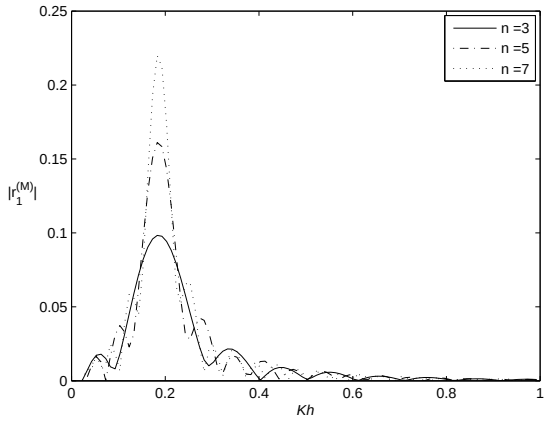

Figure 6.11: Reflection coefficient $|r_1^{(M)}|$ due to an incident wave of wave number M for $D/h^4 = 1.5,\ \delta/h = 0.01,\ \rho = 0.5,\ H/h = 2,\ a_1/h = 0.1,\ l_1h = 1$ and $l_2h = 1.1$.

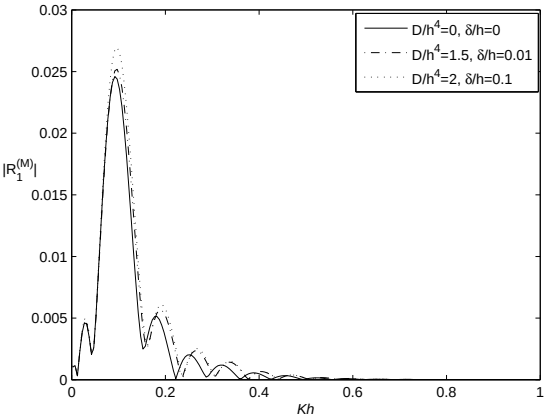

Figure 6.12: Reflection coefficient $|R_1^{(M)}|$ due to an incident wave of wave number M for $\rho = 0.5,\ H/h = 2,\ a_1/h = 0.1,\ n = 3,\ l_1h = 1$ and $l_2h = 1.1$.

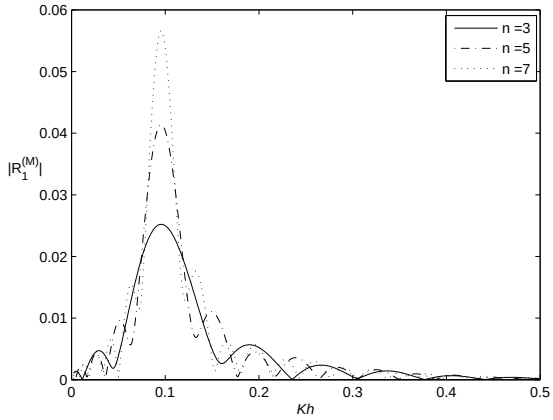

Figure 6.13: Reflection coefficient $|R_1^{(M)}|$ due to an incident wave of wave number M for $D/h^4 = 1.5,\ \delta/h = 0.01,\ \rho = 0.5,\ H/h = 2,\ a_1/h = 0.1,\ l_1h = 1$ and $l_2h = 1.1$.

in the bottom surface, when the ice parameters are fixed at $D/h^4 = 1.5,\ \delta/h = 0.01$ for all these curves. It is clear from these figures (except figure 6.7) that the peak values of reflection and transmission coefficients of the waves of wave number m and M, for the normally incident wave of wave number m, increase when the number of ripples increases. But when the number of ripples becomes very large, the reflection and transmission coefficients become unbounded. That means the perturbation expansion which is discussed in Section 6.3, ceases to be valid when the reflection coefficient becomes much larger than the undulation parameter, as pointed out by Mei [54]. Figure 6.7 shows that the first-order transmission coefficient $|t_1^{(m)}|$ is fixed for all odd values of n, and there is no transmission for even values of n (since the expressions of $t_1^{(m)}$ and $T_1^{(M)}$, given by (6.65) and (6.70), contain integrals whose integrand is $c(x)$ only, and hence for the example under consideration, the integral value would be either 0 or 1 with respect to even or odd value of n, respectively). From a physical point of view, when we consider the

propagation of waves over bottom undulation, destructive interference of waves occurs. Since the values of $t_1^{(m)}$ and $T_1^{(M)}$ depend on shape function $c(x)$ only, which is a sinusoidal wave, so the resulting displacement of wave for these cases would be zero for even value of n and some constant value for odd value of n. From the figures 6.2-6.9, it is also clear that the number of zeros of reflection and transmission coefficients (except for $|t_1^{(m)}|$) is very less in comparison to that of the example of Maiti and Mandal [49] in the case of normal incident wave. This happens due to the presence of the ice-cover and the different ripple wave numbers in the patch of the undulation. Another common feature in these figures is the oscillating nature of the absolute values of the first-order coefficients as functions of the wave number Kh.

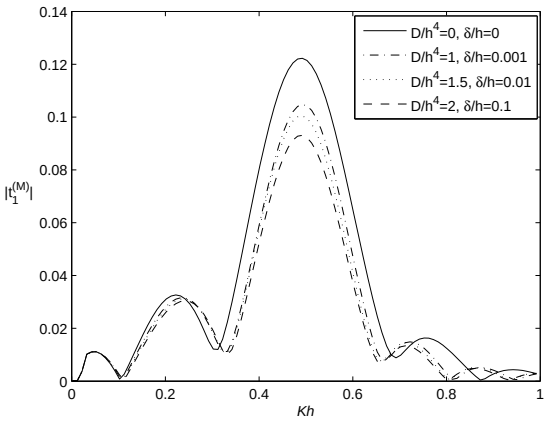

Figure 6.14: Transmission coefficient $|t_1^{(M)}|$ due to an incident wave of wave number M for $\rho = 0.5,\ H/h = 2,\ a_1/h = 0.1,\ n = 3,\ l_1h = 1$ and $l_2h = 1.1$.

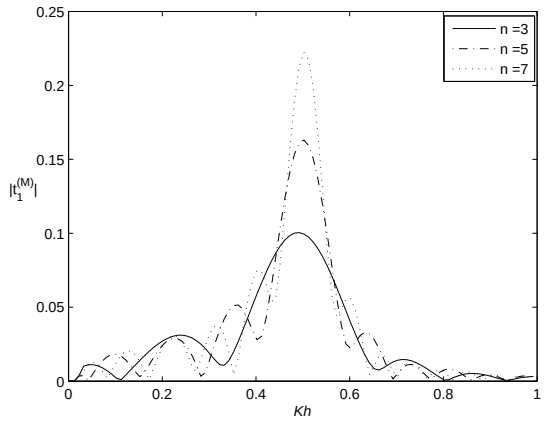

Figure 6.15: Transmission coefficient $|t_1^{(M)}|$ due to an incident wave of wave number M for $D/h^4 = 1.5,\ \delta/h = 0.01,\ \rho = 0.5,\ H/h = 2,\ a_1/h = 0.1,\ l_1h = 1$ and $l_2h = 1.1$.

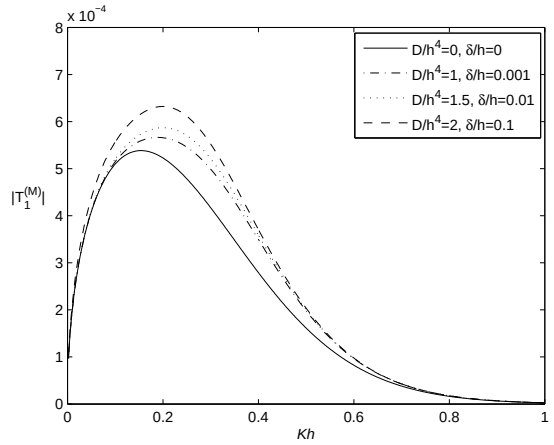

Figure 6.16: Transmission coefficient $|T_1^{(M)}|$ due to an incident wave of wave number M for $\rho = 0.5,\ H/h = 2,\ a_1/h = 0.1,\ n = 3,\ l_1h = 1$ and $l_2h = 1.1$.

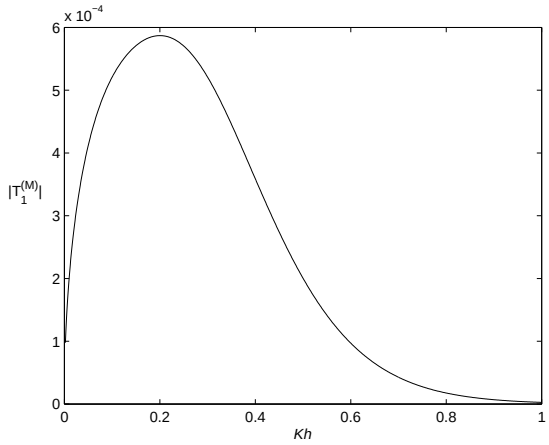

Figure 6.17: Transmission coefficient $|T_1^{(M)}|$ due to an incident wave of wave number M for $D/h^4 = 1.5,\ \delta/h = 0.01,\ \rho = 0.5,\ H/h = 2,\ a_1/h = 0.1,\ l_1h = 1$ and $l_2h = 1.1$.

Similarly the case of normally incident wave of wave number M (an interfacial mode) is interesting due to the presence of the ice-cover where some energy is always possible to be

converted from one wave mode to the other (like the normally incident wave of wave number m). For this case, figures 6.10-6.17 show the first-order reflection coefficients $|r_1^{(M)}|$, $|R_1^{(M)}|$ and transmission coefficients $|t_1^{(M)}|$, $|T_1^{(M)}|$ against Kh for $\rho = 0.5$, $H/h = 2$, $a_1/h = 0.1$ and the ripple wave numbers $l_1 h = 1$ and $l_2 h = 1.1$. The different curves in figures 6.10 and 6.14, representing $|r_1^{(M)}|$ and $|t_1^{(M)}|$, correspond to four different sets of ice parameters $(D/h^4 = 0,\ \delta/h = 0)$, $(D/h^4 = 1,\ \delta/h = 0.001)$, $(D/h^4 = 1.5,\ \delta/h = 0.01)$ and $(D/h^4 = 2,\ \delta/h = 0.1)$, while n is fixed, for all these curves, at 3. These two figures show that as the values of the ice parameters increase, the peak values of the reflection and transmission coefficient $|r_1^{(M)}|$ and $|t_1^{(M)}|$, respectively, decrease. Here, the decreasing rate of $|r_1^{(M)}|$ is very negligible as compared to $|t_1^{(M)}|$. Figures 6.12 and 6.16 show the reflection coefficient $|R_1^{(M)}|$ and transmission coefficient $|T_1^{(M)}|$ corresponding to different ice parameters, while the number of ripples is fixed, for all these curves, at 3. It is clear from these two figures that as the values of the ice parameters D/h^4 and δ/h increase, the peak values of reflection coefficient $|R_1^{(M)}|$ and the transmission coefficient $|T_1^{(M)}|$ also increase. Also the nonzero values of the reflection and transmission coefficient (from figures 6.10, 6.12, 6.14, 6.16) due to the normal incident wave of wave mode M show that there is always a possibility of some conversion of energy from one wave number to the other.

For the different curves in figures 6.11, 6.13 and 6.15 showing the reflection and transmission coefficient corresponding to different numbers of ripples on the bottom surface, the ice parameters are fixed at $D/h^4 = 1.5$, $\delta/h = 0.01$. In these figures, as the number of ripples increases from 3 to 7, the reflection coefficient $|r_1^{(M)}|$ (for waves with wave number m), $|R_1^{(M)}|$ (for waves with wave number M) and transmission coefficient $t_1^{(M)}$ (for waves with wave number m) due to the normally incident wave of wave mode M always exist and their peak values increase accordingly. But when the number of ripples becomes very large, the reflection and transmission coefficient will become unbounded. Therefore in this mode M also, it must be noted that such a perturbation expansion which is discussed in Section 6.3 ceases to be valid at Bragg resonance when the reflection coefficient becomes much larger than the undulation parameter. Figure 6.17 shows that the first-order transmission coefficient $|T_1^{(M)}|$, due to an incident wave of wave number M, is fixed for all odd values of n, and there is no transmission for even values of n. All the above numerical values of the reflection and transmission coefficients have been checked for their correctness from the energy identities. If the incident angle is taken to be zero in the work of Maiti and Mandal [49] for their oblique problem with a free surface, then our above results are comparable to theirs when $D/h^4 \to 0$, $\delta/h \to 0$ and if the ripple wave numbers in the patches are same, as suggested by the computations.

6.8 Conclusion

The work described in this chapter is the classical problem of normal water wave scattering by a small bottom undulation in a two-layer fluid flowing in an ocean, where the upper layer

is of finite height and is bounded above by a thin ice-cover modelled as a thin elastic plate, which replaces the free surface. In such a situation propagating waves can exist at two different wave number for any given frequency, the one with smaller wave number corresponds to an ice-surface disturbance and the other to an interfacial wave motion. Using a perturbation analysis, the problem is reduced up to first-order to a coupled boundary value problem which is solved by a method based on Green's integral theorem with the introduction of appropriate Green's functions. The particular case of a patch of sinusoidal ripples on the ocean-bed is of considerable significance due to the ability of an undulating bed to reflect incident wave energy, which is important in respect of both coastal protection, and possible ripple growth if the bed can be eroded. As an instance, erosion sand-ripple bottoms exist on shores and banks of several islands near the polar regions and our work discussed in this chapter can be observed as an analysis of how waves interact with these kinds of bottoms. For this particular example of a patch of sinusoidal ripples having two different wave numbers over two consecutive stretches, first-order approximations to the reflection and transmission coefficients are obtained in terms of computable integrals and depicted graphically through a number of figures. The main advantage of this method, demonstrated through this example, is that a very few ripples may be needed to produce a substantial amount of reflected energy. This method may be useful in the construction of an effective reflector of the incident wave energy for protecting coastal areas from the rough ocean in the polar regions. But in real sense, it will be too costly to do so. This kind of wave erosion related problems are evident for parts of Arctic region on the South Beaufort Ocean. However, the solution developed here is expected to be helpful for a wide class of two-layer fluid problems with ice-cover in these regions with uneven bottom surface.

Chapter 7

Oblique wave propagation over bottom undulation in ice-covered fluid

7.1 Introduction

The work presented in this chapter deals with the scattering problem of Chapter 6 but here we consider a train of progressive waves propagating from negative infinity which is obliquely incident on the undulating ocean bed having small undulations. Applying perturbation analysis, involving a small parameter $\varepsilon \ll 1$, we reduce the original problem to a simpler boundary value problem (BVP) for the first-order correction of the potentials. The solution of this BVP is then obtained by an appropriate use of Green's integral theorem to the potential functions describing the BVP. Fourier transform technique is also used to obtain the respective potentials. The reflection and transmission coefficients are evaluated approximately up to the first-order of ε in terms of integrals involving the shape function. We present a special form of bottom undulation: a patch of sinusoidal ripples having two different wave numbers for two consecutive stretches.

7.2 Mathematical formulation of the problem

We consider the irrotational motion of a two-layer inviscid incompressible fluid of relatively small amplitude under the action of gravity, neglecting any effect due to surface tension at the interface of the two fluids of which the upper layer is of finite depth h and is covered by a thin uniform ice sheet modelled as a thin elastic plate, while the lower layer is bounded by a bottom surface with small cylindrical undulation. Each fluid is of infinite horizontal extent in x and z-directions while the depth is along y-direction which is considered vertically downwards with $y = -h$ as the mean position of the thin ice-cover. The origin O is considered at the undisturbed interface between the upper and lower fluids, and $y = 0$ as the mean position of the interface of the layers. Here, the bottom of the lower layer with small undulation is described by $y = H + \varepsilon c(x)$. Under the usual assumptions of linear water wave theory and in view of the geometry of the problem, *i.e.*, because of the uniformity in z- direction, velocity

potentials in the lower and the upper layer, respectively, can be defined for oblique waves in the form

$$\Phi(x,y,z,t) = \mathrm{Re}[\phi(x,y)\mathrm{e}^{\mathrm{i}\nu z}\mathrm{e}^{-\mathrm{i}\omega t}] \quad \text{and} \quad \Psi(x,y,z,t) = \mathrm{Re}[\psi(x,y)\mathrm{e}^{\mathrm{i}\nu z}\mathrm{e}^{-\mathrm{i}\omega t}], \tag{7.1}$$

where $\phi(x,y)$ and $\psi(x,y)$, respectively, are complex-valued potential functions for the lower layer fluid $(0 < y < H)$ of density ρ_1 and the upper layer fluid $(-h < y < 0)$ of density $\rho_2 < \rho_1$, ν the z-component of the wave number.

The governing equation for the boundary value problems involving these potentials ϕ and ψ is the modified Helmholtz equation:

$$(\nabla^2_{x,y} - \nu^2)\phi = 0 \qquad \text{in the lower fluid,} \tag{7.2}$$

$$(\nabla^2_{x,y} - \nu^2)\psi = 0 \qquad \text{in the upper fluid.} \tag{7.3}$$

The ratio of the densities of the two fluids ρ_2/ρ_1 (< 1) is denoted by ρ and the linearized boundary conditions at the bottom surface, on the interface and at the ice-cover are (Das and Mandal [19])

$$\frac{\partial \phi}{\partial n} = 0 \qquad \text{on} \quad y = H + \varepsilon c(x), \tag{7.4}$$

$$\frac{\partial \phi}{\partial y} = \frac{\partial \psi}{\partial y} \qquad \text{on} \quad y = 0, \tag{7.5}$$

$$K\phi + \frac{\partial \phi}{\partial y} = \rho(K\psi + \frac{\partial \psi}{\partial y}) \quad \text{on} \quad y = 0, \tag{7.6}$$

$$K\psi + \left[D\Big(\frac{\partial^2}{\partial x^2} - \nu\Big)^2 + 1 - \delta K\right]\frac{\partial \psi}{\partial y} = 0 \quad \text{on} \quad y = -h, \tag{7.7}$$

where $D = L/(\rho_2 g)$; where L is the flexural rigidity of the elastic ice-cover given by $L = Eh_0^3/[12(1-\gamma^2)]$; E and γ, respectively, are the Young's modulus and Poisson's ratio for ice, h_0 is the very small thickness of the ice-cover, $\delta = (\rho_0/\rho_2)h_0$; ρ_0 is the density of ice.

Within this framework in a two-layer fluid, a train of progressive waves take the form (up to an arbitrary multiplicative constant)

$$\phi = \exp(\pm \mathrm{i}x\sqrt{k^2 - \nu^2})\, \cosh k(H-y) \qquad \text{in} \quad 0 \le y \le H, \tag{7.8}$$

$$\psi = \exp(\pm \mathrm{i}x\sqrt{k^2 - \nu^2})\, f(k,y) \qquad \text{in} \quad -h \le y \le 0, \tag{7.9}$$

$$\text{where} \quad f(k,y) = \frac{\sinh kH\left[(Dk^4 + 1 - \delta K)k\cosh k(h+y) - K\sinh k(h+y)\right]}{K\cosh kh - (Dk^4 + 1 - \delta K)k\sinh kh}, \tag{7.10}$$

with k satisfying the dispersion relation $\Delta(k) = 0$, where $\Delta(k)$ is same as (6.11) which was followed in Chapter 6.

A train of progressive waves of mode m is of the form

$$\phi(x,y) = \exp(\pm \mathrm{i}x\sqrt{m^2 - \nu^2})\, \cosh m(H-y) \qquad \text{in} \quad 0 \le y \le H, \tag{7.11}$$

$$\psi(x,y) = \exp(\pm \mathrm{i}x\sqrt{m^2 - \nu^2})\, f(m,y) \qquad \text{in} \quad -h \le y \le 0, \tag{7.12}$$

where we must have $\nu < m$ in order that these progressive waves exist. Similarly, a train of progressive waves of mode M is of the form

$$\phi(x,y) = \exp(\pm \mathrm{i}x\sqrt{M^2-\nu^2})\ \cosh M(H-y) \qquad \text{in} \quad 0 \le y \le H, \tag{7.13}$$

$$\psi(x,y) = \exp(\pm \mathrm{i}x\sqrt{M^2-\nu^2})\ f(M,y) \qquad \text{in} \quad -h \le y \le 0. \tag{7.14}$$

Here also we must have $\nu < M$ for these progressive waves to exist.

An incident plane wave of mode m making an angle θ, $0 \le \theta < \pi/2$, with the positive x-axis is of the form:

$$\phi_0(x,y) = \exp(\mathrm{i}mx\cos\theta)\ \cosh m(H-y) \qquad \text{in} \quad 0 \le y \le H, \tag{7.15}$$

$$\psi_0(x,y) = \exp(\mathrm{i}mx\cos\theta)\ f(m,y) \qquad \text{in} \quad -h \le y \le 0, \tag{7.16}$$

where $\nu = m\sin\theta$.

We know that $\sqrt{M^2-\nu^2}$ is real since $M > m$ and so the scattered waves of mode M will exist for all values of m, *i.e.*, for all values of K (since for different values of K, we get different m and M) and for all incident angles θ. The angle $\theta_{_M}$ of the scattered waves of wave number M is given by

$$\tan\theta_{_M} = \frac{m\sin\theta}{\beta_1}, \tag{7.17}$$

where $\beta_1 = \sqrt{M^2 - m^2\sin^2\theta}$. Since $\beta_1 > m\cos\theta$, we know that $\tan\theta_M < \tan\theta$ and hence $|\theta_{_M}| < \theta$.

Therefore, if a wave train of mode m is obliquely incident at an angle θ, $0 \le \theta < \pi/2$, on the positive x-axis on the cylindrical undulation at the bottom of a two-layer fluid, then the reflected and transmitted waves of both the modes m and M occur for any angle of incidence θ. Since the wave train is partially reflected by, and partially transmitted over the bottom undulation, the far-field behaviours of ϕ and ψ, respectively, are given by

$$\phi(x,y) \sim \begin{cases} \cosh m(H-y)[\exp(\mathrm{i}mx\cos\theta) + r^{(m)}\exp(-\mathrm{i}mx\cos\theta)] \\ \qquad\qquad +R^{(m)}\cosh M(H-y)\exp(-\mathrm{i}\beta_1 x) & \text{as } x \to -\infty, \\ t^{(m)}\cosh m(H-y)\exp(\mathrm{i}mx\cos\theta) + T^{(m)}\cosh M(H-y)\exp(\mathrm{i}\beta_1 x) & \text{as } x \to \infty, \end{cases} \tag{7.18}$$

$$\psi(x,y) \sim \begin{cases} f(m,y)[\exp(\mathrm{i}mx\cos\theta) + r^{(m)}\exp(-\mathrm{i}mx\cos\theta)] \\ \qquad\qquad +R^{(m)}f(M,y)\exp(-\mathrm{i}\beta_1 x) & \text{as } x \to -\infty, \\ t^{(m)}f(m,y)\exp(\mathrm{i}mx\cos\theta) + T^{(m)}f(M,y)\exp(\mathrm{i}\beta_1 x) & \text{as } x \to \infty. \end{cases} \tag{7.19}$$

The unknown coefficients $r^{(m)}$ and $R^{(m)}$ are the reflection coefficients associated with the reflected wave modes m and M, respectively, due to an obliquely incident wave of mode m and are to be determined. Similarly, $t^{(m)}$ and $T^{(m)}$ are the transmission coefficients associated with the transmitted wave modes m and M, respectively, due to an obliquely incident wave of mode m and are to be determined.

Assuming, for small bottom undulation, ε to be very small and neglecting the second order terms, the boundary condition $\partial\phi/\partial n = 0$ on the bottom surface $y = H + \varepsilon c(x)$ can be expressed in the same form as in (6.18).

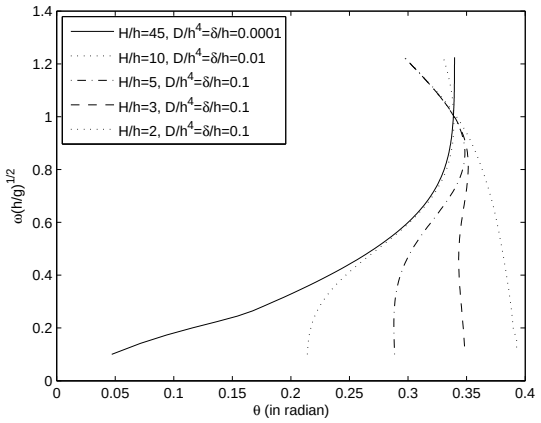

Figure 7.1: Non-dimensionalized cut-off frequency $\omega_c(h/g)^{1/2}$ due to an incident wave of wave number M with an ice-cover; $\rho = 0.5$.

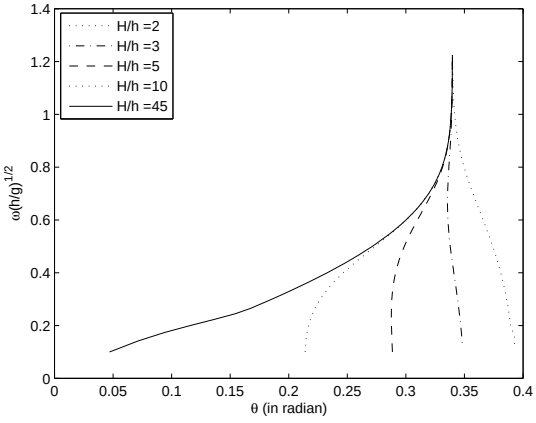

Figure 7.2: Non-dimensionalized cut-off frequency $\omega_c(h/g)^{1/2}$ due to an incident wave of wave number M with an ice-cover; $D/h^4 = 0.0001$, $\delta/h = 0.0001$, and $\rho = 0.5$.

Now, we consider the case of an incident plane wave of mode M making an angle θ, $0 \leq \theta < \pi/2$, with the positive x-axis, which is given by

$$\phi_0(x,y) = \exp(\mathrm{i}Mx\cos\theta)\ \cosh M(H-y) \qquad \text{in} \quad 0 \leq y \leq H, \tag{7.20}$$

$$\psi_0(x,y) = \exp(\mathrm{i}Mx\cos\theta)\ f(M,y) \qquad \text{in} \quad -h \leq y \leq 0, \tag{7.21}$$

where $\nu = M\sin\theta$. Therefore, $\sqrt{m^2-\nu^2} = \sqrt{m^2 - M^2\sin^2\theta} \equiv \beta_2$ (say).

Since $K = \omega^2/g$, which depends on frequency ω, so by (6.11), for every distinct non-zero ω (*i.e.*, for non-zero K), we get two positive wave numbers m and M. However, for a given angle θ, there may be a value of ω for which $m = M\sin\theta$ and thus $\beta_2 = 0$. We call this value as the cut-off frequency and denote it by ω_c . For $\omega > \omega_c$, that is, for $m > M\sin\theta$ (for fixed θ), we have real values of β_2 and so reflected and transmitted waves of mode m will exist and propagate in the fluid. However, for $\omega < \omega_c$, that is, for $m < M\sin\theta$ (for fixed θ), β_2 will be imaginary which corresponds to an evanescent mode and hence there do not exist any reflected and transmitted waves of mode m. This means that in this case we have no propagating waves of wave number m.

Figure 7.1 shows the non-dimensionalized cut-off frequency $\omega_c(h/g)^{1/2}$ plotted against the incident wave angle $\theta = \sin^{-1}(m/M)$, for $H/h = 2, 3, 5, 10, 45$ and density ratio $\rho = 0.5$. The different curves (from right to left) in figure 7.1 correspond to $D/h^4 = 0.1$ and $\delta/h = 0.1$ (except for the two curves in the left, for one of which $D/h^4 = 0.01$, $\delta/h = 0.01$ and for the other $D/h^4 = 0.0001$, $\delta/h = 0.0001$). It is observed from this figure that for an incident wave of mode M making an angle θ with the positive x-axis, for which the point $(\theta, \omega(h/g)^{1/2})$ is situated on the right side of the curve, there are no propagating waves of wave number m for this value of $\omega(h/g)^{1/2}$. It may be noted that for very small value of D/h^4, *e.g.*, 0.0001 with small $\delta/h = 0.0001$ and $H/h = 45$, the curve for $\omega_c(h/g)^{1/2}$ almost coincides with the curve given in figure 1 of Das and Mandal [19] where the lower layer was taken to be infinitely deep and the

upper layer contained ice-cover. Moreover, in the case of oblique incidence for a two-layer fluid with a free surface, there exists a critical angle θ_c which was also observed by Linton and Cadby [44]. Due to the presence of the ice-cover, we observe that for some values of incident angle θ less than this critical angle θ_c, there exist now one or two or three cut-off frequencies. For the frequencies either less than the cut-off frequency or lying in between the two appropriate cut-off frequencies, there will be a transfer of energy from the waves of higher wave number to the waves of lower wave number during the scattering process. The higher cut-off frequency increases rapidly as the value of the ice-cover parameter decreases, and becomes very large as the ice-cover parameter value becomes very small since the cut-off frequency curve becomes almost asymptotically parallel to the $\omega(h/g)^{1/2}$-axis in the $(\theta, \omega(h/g)^{1/2})$-plane. Figure 7.2 shows the non-dimensionalized cut-off frequency $\omega_c(h/g)^{1/2}$ plotted against the wave angles θ for $\rho = 0.5,\ D/h^4 = 0.0001,\ \delta/h = 0.0001$ and $H/h = 2, 3, 5, 10, 45$, due to an incident wave of wave number M. The curves in this figure almost coincide with those for the two-layer fluid problem with bottom undulation where the upper fluid was bounded by a free surface (figure 1 of Maiti and Mandal [49]). This happens due to the presence of the very thin ice-cover which replaces approximately the free surface of two-layer fluid flow.

For $\theta > \theta_c$, there are no propagating waves of wave number m for any frequency. When they do exist, the angle θ_m of the scattered waves of wave number m is given by

$$\tan\theta_m = \frac{M\sin\theta}{\beta_2}\ , \tag{7.22}$$

and $|\theta_m| > \theta$.

Therefore, for a wave train of mode M obliquely incident on the bottom undulation of a two-layer fluid and making an angle $\theta < \sin^{-1}(m/M)$ with the positive x-axis, the far-field behaviours of ϕ and ψ, respectively, are given by

$$\phi(x,y) \sim \begin{cases} \cosh M(H-y)[\exp(\mathrm{i}Mx\cos\theta) + R^{(M)}\exp(-\mathrm{i}Mx\cos\theta)] \\ \qquad\qquad + r^{(M)}\cosh m(H-y)\exp(-\mathrm{i}\beta_2 x) \quad \text{as } x\to-\infty, \\ T^{(M)}\cosh M(H-y)\exp(\mathrm{i}Mx\cos\theta) + t^{(M)}\cosh m(H-y)\exp(\mathrm{i}\beta_2 x) \quad \text{as } x\to\infty, \end{cases} \tag{7.23}$$

$$\psi(x,y) \sim \begin{cases} f(M,y)[\exp(\mathrm{i}Mx\cos\theta) + R^{(M)}\exp(-\mathrm{i}Mx\cos\theta)] \\ \qquad\qquad + r^{(M)} f(m,y)\exp(-\mathrm{i}\beta_2 x) \quad \text{as } x\to-\infty, \\ T^{(M)} f(M,y)\exp(\mathrm{i}Mx\cos\theta) + t^{(M)} f(m,y)\exp(\mathrm{i}\beta_2 x) \quad \text{as } x\to\infty, \end{cases} \tag{7.24}$$

where the unknown coefficients $r^{(M)}$ and $R^{(M)}$ denote the reflection coefficients of modes m and M, respectively, due to an obliquely incident wave of mode M and are to be determined. Similarly, $t^{(M)}$ and $T^{(M)}$ denote the transmission coefficients of modes m and M, respectively, due to the obliquely incident wave of mode M and are to be determined. In order that the coefficients $r^{(M)}$ and $T^{(M)}$ exist, the angle of incidence θ must satisfy the relation $\theta < \sin^{-1}(m/M)$. Thus, if the incident wave has mode M, then it satisfies the respective Helmholtz equation with $\nu = M\sin\theta,\ 0 \le \theta < \sin^{-1}(m/M)$, the ice-surface condition, interface condition and the bottom condition (6.18). Also ϕ and ψ satisfy the far-field conditions (7.23) and (7.24) involving the unknown coefficients $r^{(M)}, R^{(M)}, t^{(M)}$ and $T^{(M)}$.

Determination of these coefficients $r^{(M)}, R^{(M)}, t^{(M)}$ and $T^{(M)}$ (correspondingly $r^{(m)}, R^{(m)}$, $t^{(m)}$ and $T^{(m)}$ for mode m) for a general type of bottom undulation is quite a difficult task. However, assuming small bottom undulation, perturbation method can be employed here to obtain these coefficients up to first-order. Using the perturbation technique, the lower layer $0 < y < H+\varepsilon c(x),\ -\infty < x < \infty$, is reduced to the uniform finite strip $0 < y < H,\ -\infty < x < \infty$, in the following mathematical analysis.

7.3 Perturbation technique

Since there are two modes of wave propagating at the interface and also just below the ice-cover along the positive x-direction, for each potential mode the first-order reflection and transmission coefficients associated with respective mode of waves can be calculated by the following procedure.

Let us first consider a train of progressive waves of mode m to be obliquely incident at an angle $\theta,\ 0 \le \theta < \pi/2$, on the bottom undulation. If there is no bottom undulation, then the obliquely incident wave train will propagate without any hindrance and there will be transmission only. This, along with the appropriate form of the boundary condition (6.18), suggest that $\phi,\ \psi,\ r^{(m)},\ R^{(m)},\ t^{(m)}$ and $T^{(m)}$ which were introduced (for wave mode m) in the last section, can be expressed in terms of small parameter ε with the help of same perturbation expansions (6.21) as was followed in Chapter 6.

Using (6.21) in (7.2), (7.3) and boundary conditions (6.18), (7.5)-(7.7), (7.18), (7.19) with $\nu = m\sin\theta$ and then comparing the first-order terms of ε on both sides of the equations, we find that the first-order potentials $\phi_1(x,y)$ and $\psi_1(x,y)$ satisfy a coupled boundary value problem described by

$$(\nabla^2_{x,y} - \nu^2)\phi_1 = 0 \qquad \text{in} \quad 0 \le y \le H, \tag{7.25}$$

$$(\nabla^2_{x,y} - \nu^2)\psi_1 = 0 \qquad \text{in} \quad -h \le y \le 0, \tag{7.26}$$

$$\frac{\partial \phi_1}{\partial y} = \mathrm{i}m\cos\theta \frac{\mathrm{d}}{\mathrm{d}x}\Big[c(x)\exp(\mathrm{i}mx\cos\theta)\Big] - m^2\sin^2\theta\, c(x)\exp(\mathrm{i}mx\cos\theta) \equiv p(x) \text{ on } y = H, \tag{7.27}$$

$$\frac{\partial \phi_1}{\partial y} = \frac{\partial \psi_1}{\partial y} \qquad \text{on} \quad y = 0, \tag{7.28}$$

$$K\phi_1 + \frac{\partial \phi_1}{\partial y} = \rho\Big(K\psi_1 + \frac{\partial \psi_1}{\partial y}\Big) \qquad \text{on} \quad y = 0, \tag{7.29}$$

$$K\psi_1 + \left[D\Big(\frac{\partial^2}{\partial x^2} - \nu\Big)^2 + 1 - \delta K\right]\frac{\partial \psi_1}{\partial y} = 0 \qquad \text{on} \quad y = -h, \tag{7.30}$$

$$\phi_1(x,y) \sim \begin{cases} r_1^{(m)}\cosh m(H-y)\exp(-\mathrm{i}mx\cos\theta) \\ \qquad\qquad + R_1^{(m)}\cosh M(H-y)\exp(-\mathrm{i}\beta_1 x) \ \text{ as } x \to -\infty, \\ t_1^{(m)}\cosh m(H-y)\exp(\mathrm{i}mx\cos\theta) + T_1^{(m)}\cosh M(H-y)\exp(\mathrm{i}\beta_1 x) \quad \text{as } x \to \infty, \end{cases} \tag{7.31}$$

$$\psi_1(x,y) \sim \begin{cases} r_1^{(m)} f(m,y)\exp(-\mathrm{i}mx\cos\theta) + R_1^{(m)} f(M,y)\exp(-\mathrm{i}\beta_1 x) \quad \text{as } x \to -\infty, \\ t_1^{(m)} f(m,y)\exp(\mathrm{i}mx\cos\theta) + T_1^{(m)} f(M,y)\exp(\mathrm{i}\beta_1 x) \quad \text{as } x \to \infty. \end{cases} \tag{7.32}$$

To solve the above coupled boundary value problem described by (7.25)-(7.30), we need two-dimensional source potentials (in terms of Green's function) for the modified Helmholtz equation due to a source submerged in either of the two layers. Then Green's integral theorem will be employed and the first-order coefficients $r_1^{(m)}, R_1^{(m)}, t_1^{(m)}$ and $T_1^{(m)}$ will be obtained in terms of integrals involving the shape function $c(x)$. When the source is submerged in the lower fluid at $(\xi,\eta),\ 0<\eta<H$, then we consider $G_1(x,y;\xi,\eta)$ and $G_2(x,y;\xi,\eta)$, respectively, to be the source potentials in terms of Green's function for the lower and upper layer fluids. Similarly when the source is submerged in the upper layer fluid at $(\xi,\eta),\ -h<\eta<0$, then we consider $G_3(x,y;\xi,\eta)$ and $G_4(x,y;\xi,\eta)$, respectively, to be the source potentials in terms of Green's function for the lower and upper layer fluids.

7.4 Solution by Green's function technique

7.4.1 Introduction of Green's functions

Suppose the source is submerged in the lower layer fluid. Then the source potentials in terms of Green's functions $G_1(x,y;\xi,\eta)$ and $G_2(x,y;\xi,\eta)$ satisfy the following boundary value problem

$$(\nabla^2_{x,y}-\nu^2)G_1=0 \qquad \text{in} \quad 0<y<H, \quad \text{except at } (\xi,\eta), \tag{7.33}$$

$$(\nabla^2_{x,y}-\nu^2)G_2=0 \qquad \text{in} \quad -h\le y\le 0, \tag{7.34}$$

$$\frac{\partial G_1}{\partial y}=0 \quad \text{on} \quad y=H, \tag{7.35}$$

$$\frac{\partial G_1}{\partial y}=\frac{\partial G_2}{\partial y} \qquad \text{on} \quad y=0, \tag{7.36}$$

$$KG_1+\frac{\partial G_1}{\partial y}=\rho(KG_2+\frac{\partial G_2}{\partial y}) \qquad \text{on} \quad y=0, \tag{7.37}$$

$$KG_2+\left[D\big(\frac{\partial^2}{\partial x^2}-\nu\big)^2+1-\delta K\right]\frac{\partial G_2}{\partial y}=0 \qquad \text{on} \quad y=-h, \tag{7.38}$$

$$G_1\sim K_0(\nu r) \qquad \text{as} \quad r=\sqrt{(x-\xi)^2+(y-\eta)^2}\to 0, \tag{7.39}$$

where $K_0(\nu r)$ is the modified Bessel function of second kind. Also both G_1 and G_2 represent outgoing waves as $|x-\xi|\to\infty$. We look for solutions to the above boundary value problem in the following form:

$$G_1(x,y;\xi,\eta)=K_0(\nu r)-K_0(\nu r_1)+\frac{1}{\mu}\int_\nu^\infty [A(k)\cosh k(H-y)+B(k)\sinh k(H-y)]\cos\mu(x-\xi)\mathrm{d}k, \tag{7.40}$$

$$G_2(x,y;\xi,\eta)=\frac{K_0(\nu r)-K_0(\nu r_1)}{\rho}+\frac{1}{\mu}\int_\nu^\infty [A_1(k)\cosh k(h+y)+B_1(k)\sinh k(h+y)]\cos\mu(x-\xi)\mathrm{d}k, \tag{7.41}$$

where $\mu=\sqrt{k^2-\nu^2}$, $r_1=\sqrt{(x-\xi)^2+(y+2h+\eta)^2}$. In order that the boundary conditions (7.33)-(7.39) are satisfied and for $|x-\xi|\to\infty$, the above Green's functions $G_1(x,y;\xi,\eta)$ and

$G_2(x,y;\xi,\eta)$ are in the following form:

$$G_1(x,y;\xi,\eta) = -2\pi \mathrm{i}K\left[\frac{S(m)\ \cosh m(H-\eta)\cosh m(H-y)}{\sinh mH\ \ \Delta'(m)\ \sqrt{m^2-\nu^2}}\exp(\mathrm{i}\sqrt{m^2-\nu^2}\ |x-\xi|)\right.$$
$$\left.+\frac{S(M)\ \cosh M(H-\eta)\cosh M(H-y)}{\sinh MH\ \ \Delta'(M)\ \sqrt{M^2-\nu^2}}\exp(\mathrm{i}\sqrt{M^2-\nu^2}\ |x-\xi|)\right], \quad (7.42)$$

$$G_2(x,y;\xi,\eta) = -2\pi \mathrm{i}K\left[\frac{Q_1(m)\ \cosh m(H-\eta)}{\Delta'(m)\ \sqrt{m^2-\nu^2}}\exp(\mathrm{i}\sqrt{m^2-\nu^2}\ |x-\xi|)\right.$$
$$\left.+\frac{Q_1(M)\ \cosh M(H-\eta)}{\Delta'(M)\ \sqrt{M^2-\nu^2}}\exp(\mathrm{i}\sqrt{M^2-\nu^2}\ |x-\xi|)\right], \quad (7.43)$$

where

$$\Delta'(k) = k\{[2(1-\rho)-KH](Dk^4+1-\delta K)+4Dk^4(1-\rho)-Kh[1+\rho(Dk^4-\delta K)]\}\sinh kh\sinh kH$$
$$+\{[k^2(1-\rho)(Dk^4+1-\delta K)+K^2\rho]h+K^2H-K[1+\rho(5Dk^4-\delta K)]\}\cosh kh\sinh kH$$
$$+\{[k^2(1-\rho)(Dk^4+1-\delta K)+K^2\rho]H+K[Kh-(5Dk^4+1-\delta K)]\}\sinh kh\cosh kH$$
$$-Kk\{h(Dk^4+1-\delta K)+H[1+\rho(Dk^4-\delta K)]\}\cosh kh\cosh kH, \quad (7.44)$$

$$S(k) = K\cosh kh-(Dk^4+1-\delta K)k\sinh kh, \quad (7.45)$$

$$Q_1(k) = (Dk^4+1-\delta K)k\cosh k(h+y)-K\sinh k(h+y), \qquad k=m,M. \quad (7.46)$$

Similarly, when the source term $(\xi,\eta),\ -h<\eta<0$, is submerged in the upper layer fluid, then the source potentials $G_3(x,y;\xi,\eta)$ and $G_4(x,y;\xi,\eta)$ satisfy the same type of boundary value problem, as given by (7.33)-(7.38), with G_1 replaced by G_3 and G_2 by G_4, and in addition, G_4 satisfies

$$G_4 \sim K_0(\nu r) \quad \text{as} \quad r=\sqrt{(x-\xi)^2+(y-\eta)^2}\ \to 0.$$

G_3 and G_4 also represent outgoing waves as $|x-\xi|\to\infty$. Here also, we look for solutions G_3 and G_4, satisfying the boundary value problem given by (7.33)-(7.38), in the following form

$$G_3(x,y;\xi,\eta) = \rho[K_0(\nu r)-K_0(\nu r_1)]+\frac{1}{\mu}\int_\nu^\infty [E(k)\cosh k(H-y)+F(k)\sinh k(H-y)]\cos\mu(x-\xi)\mathrm{d}k, \quad (7.47)$$

$$G_4(x,y;\xi,\eta) = K_0(\nu r)-K_0(\nu r_1)+\frac{1}{\mu}\int_\nu^\infty [E_1(k)\cosh k(h+y)+F_1(k)\sinh k(h+y)]\cos\mu(x-\xi)\mathrm{d}k, \quad (7.48)$$

In order to satisfy the respective boundary conditions and for $|x-\xi|\to\infty$, the source potentials in terms of Green's functions $G_3(x,y;\xi,\eta)$ and $G_4(x,y;\xi,\eta)$ in this case are obtained in the following form:

$$G_3(x,y;\xi,\eta) = 2\pi\mathrm{i}\ \rho K\left[\frac{Q_2(m)\ \cosh m(H-y)}{\Delta'(m)\ \sqrt{m^2-\nu^2}}\exp(\mathrm{i}\sqrt{m^2-\nu^2}\ |x-\xi|)\right.$$
$$\left.+\frac{Q_2(M)\ \cosh M(H-y)}{\Delta'(M)\ \sqrt{M^2-\nu^2}}\exp(\mathrm{i}\sqrt{M^2-\nu^2}\ |x-\xi|)\right], \quad (7.49)$$

$$G_4(x,y;\xi,\eta) = 2\pi\mathrm{i}\ \rho K\left[\frac{Q_2(m)\ \sinh mH}{\Delta'(m)\ \sqrt{m^2-\nu^2}}\ \frac{Q_1(m)}{S(m)}\ \exp(\mathrm{i}\sqrt{m^2-\nu^2}\ |x-\xi|)\right.$$
$$\left.+\frac{Q_2(M)\ \sinh MH}{\Delta'(M)\ \sqrt{M^2-\nu^2}}\ \frac{Q_1(M)}{S(M)}\ \exp(\mathrm{i}\sqrt{M^2-\nu^2}\ |x-\xi|)\right], \quad (7.50)$$

where

$$Q_2(k) = K\sinh k(h+\eta) - (Dk^4 + 1 - \delta K)k\cosh k(h+\eta), \qquad k = m, M. \quad (7.51)$$

If the flexural rigidity of elastic ice-cover is assumed to be zero along with consideration of absence of the ice-cover (implying $D = 0$ and $\delta = 0$), the representation of the Green's functions when $|x-\xi| \to \infty$, given by (7.42), (7.43), (7.49) and (7.50), coincide with the corresponding source potentials obtained earlier in Maiti and Mandal (2006) where the two-layer fluid had a free surface and a bottom undulation.

To evaluate $\phi_1(\xi,\eta)$, when the source term (ξ,η), $0 < \eta < H$, is submerged in the lower layer fluid, we apply the Green's integral theorem to $\phi_1(x,y)$ and $G_1(x,y;\xi,\eta)$ in the form

$$\int_C \left(\phi_1 \frac{\partial G_1}{\partial n} - G_1 \frac{\partial \phi_1}{\partial n}\right) \mathrm{d}s = 0, \quad (7.52)$$

where C is a closed contour in the xy-plane consisting of the lines $y = 0$, $-X \le x \le X$; $y = H$, $-X \le x \le X$; $x = \pm X$, $0 \le y \le H$, and a small circle of radius α_1 with center at (ξ,η) and ultimately letting $X \to \infty$ and $\alpha_1 \to 0$. Then there will be no contribution to the integral from the line $x = \pm X$, as both ϕ_1 and G_1 approach zero when $X \to \pm\infty$. Thus the resultant form of the integral equation (7.52) is

$$-2\pi\phi_1(\xi,\eta) + \int_{-\infty}^{\infty} p(x)G_1(x,H;\xi,\eta)\mathrm{d}x + \int_{-\infty}^{\infty}\left(\phi_1\frac{\partial G_1}{\partial y} - G_1\frac{\partial\phi_1}{\partial y}\right)_{y=0}\mathrm{d}x = 0. \quad (7.53)$$

Then again, we apply the Green's integral theorem to $\psi_1(x,y)$ and $G_2(x,y;\xi,\eta)$ in the form

$$\int_{C'} \left(\psi_1 \frac{\partial G_2}{\partial n} - G_2 \frac{\partial \psi_1}{\partial n}\right) \mathrm{d}s = 0, \quad (7.54)$$

where C' is a closed counter consisting of the lines $y = -h$, $-X \le x \le X$; $y = 0$, $-X \le x \le X$; $x = \pm X$, $-h \le y \le 0$, and ultimately letting $X \to \infty$. Here, we note that $G_2(x,y;\xi,\eta)$ has no singularity in the upper region. Now (7.54) can be rewritten as

$$\begin{aligned} &-\int_{-\infty}^{\infty}\left(\psi_1\frac{\partial G_2}{\partial y} - G_2\frac{\partial\psi_1}{\partial y}\right)_{y=-h}\mathrm{d}x - \int_{-h}^{0}\left(\psi_1\frac{\partial G_2}{\partial y} - G_2\frac{\partial\psi_1}{\partial y}\right)_{x=-\infty}\mathrm{d}y \\ &+\int_{-\infty}^{\infty}\left(\psi_1\frac{\partial G_2}{\partial y} - G_2\frac{\partial\psi_1}{\partial y}\right)_{y=0}\mathrm{d}x + \int_{-h}^{0}\left(\psi_1\frac{\partial G_2}{\partial y} - G_2\frac{\partial\psi_1}{\partial y}\right)_{x=\infty}\mathrm{d}y = 0. \quad (7.55) \end{aligned}$$

Use of the ice-cover condition on $y = -h$ and the asymptotic results for ψ_1 and G_2 make the first integral equal to zero for any large value of X (see Mandal and Basu [51]). The second and fourth integrals will not contribute when $X \to \infty$, due to the outgoing nature of both ψ_1 and G_2 as $x \to \pm\infty$. Thus the resultant integral of (7.55) is

$$\int_{-\infty}^{\infty}\left(\psi_1\frac{\partial G_2}{\partial y} - G_2\frac{\partial\psi_1}{\partial y}\right)_{y=0}\mathrm{d}x = 0. \quad (7.56)$$

Now solving (7.53) and (7.56) with the help of interface conditions at $y = 0$ we get

$$\phi_1(\xi,\eta) = \frac{1}{2\pi}\int_{-\infty}^{\infty} G_1(x,H;\xi,\eta)\, p(x)\mathrm{d}x \qquad 0 < \eta < H, \quad (7.57)$$

which solves the boundary value problem for $\phi_1(x, y)$.

Similarly, to evaluate $\psi_1(\xi, \eta)$, when the source term (ξ, η), $-h < \eta < 0$, is submerged in the upper layer fluid, we apply the same procedure as done previously for the case of lower layer fluid. The final expression for $\psi_1(\xi, \eta)$ is

$$\psi_1(\xi, \eta) = \frac{1}{2\pi\rho} \int_{-\infty}^{\infty} G_3(x, H; \xi, \eta)\ p(x)\mathrm{d}x \qquad -h < \eta < 0, \tag{7.58}$$

which solves the boundary value problem for $\psi_1(x, y)$.

7.4.2 Reflection and transmission coefficients

The first-order reflection and transmission coefficients $r_1^{(m)}, t_1^{(m)}$ and $R_1^{(m)}, T_1^{(m)}$ with respect to the modes m and M, respectively, due to an oblique incident wave of mode m, are now obtained by letting $\xi \to \mp\infty$, in (7.57) or (7.58) and comparing with (7.31) or (7.32) by replacing (x, y) with (ξ, η). Thus we obtain $r_1^{(m)}$ and $R_1^{(m)}$ as

$$r_1^{(m)} = -\frac{\mathrm{i}Km\ S(m)\ \cos 2\theta \sec\theta}{\sinh mH\ \ \Delta'(m)} \int_{-\infty}^{\infty} \exp(2\mathrm{i}mx\cos\theta)\ c(x)\mathrm{d}x, \tag{7.59}$$

$$R_1^{(m)} = -\frac{\mathrm{i}Km\ S(M)\ (\beta_1\cos\theta - m\sin^2\theta)}{\sinh MH\ \Delta'(M)\ \beta_1} \int_{-\infty}^{\infty} \exp[\mathrm{i}x(m\cos\theta + \beta_1)]\ c(x)\mathrm{d}x. \tag{7.60}$$

Similarly to find $t_1^{(m)}$ and $T_1^{(m)}$, we consider $\phi_1(x, y)$ from (7.31) by replacing (x, y) with (ξ, η) and $G_1(x, y; \xi, \eta)$ from (7.42) with $\xi \to \infty$, and using them in (7.57), we get

$$t_1^{(m)} = \frac{\mathrm{i}Km\ S(m)\ \sec\theta}{\sinh mH\ \ \Delta'(m)} \int_{-\infty}^{\infty} c(x)\mathrm{d}x, \tag{7.61}$$

$$T_1^{(m)} = \frac{\mathrm{i}Km\ S(M)\ (\beta_1\cos\theta + m\sin^2\theta)}{\sinh MH\ \ \Delta'(M)\ \beta_1} \int_{-\infty}^{\infty} \exp[\mathrm{i}x(m\cos\theta - \beta_1)]\ c(x)\mathrm{d}x. \tag{7.62}$$

This is also verified that the same expressions for $r_1^{(m)}, R_1^{(m)}, t_1^{(m)}$ and $T_1^{(m)}$ are obtained by letting $\xi \to -\infty$ and $\xi \to \infty$, respectively, in (7.32) and (7.49), and solving for (7.58). Therefore, the two first-order reflection coefficients and the two first-order transmission coefficients can be evaluated from (7.59)-(7.62), once the shape function $c(x)$ is known.

When we consider a train of progressive waves of mode M to be obliquely incident at an angle θ, $0 \le \theta < \sin^{-1}(m/M)$, on the bottom undulation, the same mathematical procedure, described above for the case of mode m, is followed in obtaining the first-order reflection and transmission coefficients $r_1^{(M)}, R_1^{(M)}, t_1^{(M)}$ and $T_1^{(M)}$. The final expressions for this case are as follows:

$$r_1^{(M)} = -\frac{\mathrm{i}KM\ S(m)\ (\beta_2\cos\theta - M\sin^2\theta)}{\sinh mH\ \ \Delta'(m)\ \beta_2} \int_{-\infty}^{\infty} \exp[\mathrm{i}x(M\cos\theta + \beta_2)]\ c(x)\mathrm{d}x, \tag{7.63}$$

$$R_1^{(M)} = -\frac{\mathrm{i}KM\ S(M)\ \cos 2\theta \sec\theta}{\sinh MH\ \ \Delta'(M)} \int_{-\infty}^{\infty} \exp(2\mathrm{i}Mx\cos\theta)\ c(x)\mathrm{d}x, \tag{7.64}$$

$$t_1^{(M)} = \frac{\mathrm{i}KM\ S(m)\ (\beta_2\cos\theta + M\sin^2\theta)}{\sinh mH\ \ \Delta'(m)\ \beta_2} \int_{-\infty}^{\infty} \exp[\mathrm{i}x(M\cos\theta - \beta_2)]\ c(x)\mathrm{d}x, \tag{7.65}$$

$$T_1^{(M)} = \frac{\mathrm{i}KM\ S(M)\ \sec\theta}{\sinh MH\ \ \Delta'(M)} \int_{-\infty}^{\infty} c(x)\mathrm{d}x. \tag{7.66}$$

Here, if we take $D = 0$ and $\delta = 0$ (*i.e.*, the flexural rigidity of elastic ice-cover is assumed to be zero and the ice-cover to be absent), then all the above results, (7.59)-(7.66), coincide with the corresponding results in Maiti and Mandal [49].

7.5 Solution by Fourier transform technique

Now the above BVP for ϕ_1 and ψ_1, described by (7.25) to (7.32), can be decomposed into two independent BVPs for ϕ_1 and ψ_1 as follows:

BVP-I, corresponding to ϕ_1, is

$$(\nabla^2_{x,y} - \nu^2)\phi_1 = 0 \qquad \text{in} \quad 0 \le y \le H, \tag{7.67}$$

$$\frac{\partial \phi_1}{\partial y} = \eta(x) \qquad \text{on} \quad y = 0, \tag{7.68}$$

$$\frac{\partial \phi_1}{\partial y} = p(x) \qquad \text{on} \quad y = H, \tag{7.69}$$

where $\eta(x)$ is assumed to be known on $y = 0$ and ϕ_1 has the asymptotic behaviour

$$\phi_1(x,y) \sim \begin{cases} r_1^{(m)} \cosh m(H-y)\mathrm{e}^{-\mathrm{i}mx} + R_1^{(m)} \cosh M(H-y)\mathrm{e}^{-\mathrm{i}Mx} & \text{as } x \to -\infty, \\ t_1^{(m)} \cosh m(H-y)\mathrm{e}^{\mathrm{i}mx} + T_1^{(m)} \cosh M(H-y)\mathrm{e}^{\mathrm{i}Mx} & \text{as } x \to \infty, \end{cases} \tag{7.70}$$

BVP-II, corresponding to ψ_1, is

$$(\nabla^2_{x,y} - \nu^2)\psi_1 = 0 \quad \text{in} \quad -h \le y \le 0, \tag{7.71}$$

$$\frac{\partial \psi_1}{\partial y} = \eta(x) \quad \text{on} \quad y = 0, \tag{7.72}$$

$$K\psi_1 + \left[D\Big(\frac{\partial^2}{\partial x^2} - \nu\Big)^2 + 1 - \delta K\right]\frac{\partial \psi_1}{\partial y} = 0 \qquad \text{on} \quad y = -h, \tag{7.73}$$

Here, the value of $\eta(x)$ is same as in the BVP-I and ψ_1 has the asymptotic behaviour

$$\psi_1(x,y) \sim \begin{cases} r_1^{(m)} f(m,y)\mathrm{e}^{-\mathrm{i}mx} + R_1^{(m)} f(M,y)\mathrm{e}^{-\mathrm{i}Mx} & \text{as } x \to -\infty, \\ t_1^{(m)} f(m,y)\mathrm{e}^{\mathrm{i}mx} + T_1^{(m)} f(M,y)\mathrm{e}^{\mathrm{i}Mx} & \text{as } x \to \infty. \end{cases} \tag{7.74}$$

Now using (7.68) and (7.72), (7.29) can be written in the following form:

$$K(\phi_1 - \rho\psi_1) = (\rho - 1)\eta(x) \qquad \text{on} \quad y = 0. \tag{7.75}$$

7.5.1 Fourier transform technique

Applying Fourier transform, as was defined in Chapter 4, to (7.67), (7.68) and (7.69), we get the following boundary value problem for $\overline{\phi}_1(\xi, y)$:

$$\overline{\phi}_{1yy} - \widehat{\xi}^2\overline{\phi}_1 = 0 \quad \text{on} \quad 0 \le y \le H, \tag{7.76}$$

$$\overline{\phi}_{1y} = \overline{\eta}(\xi) \quad \text{on} \quad y = 0, \tag{7.77}$$

$$\overline{\phi}_{1y} = \overline{p}(\xi) \quad \text{on} \quad y = H, \tag{7.78}$$

where $\widehat{\xi^2} = \xi^2 + \nu^2$, and $\overline{\eta}(\xi)$, $\overline{p}(\xi)$ are the Fourier transforms of $\eta(x)$ and $p(x)$, respectively. The solution $\overline{\phi}_1(\widehat{\xi}, y)$ of the above boundary value problem is obtained as

$$\overline{\phi}_1(\widehat{\xi}, y) = \frac{\overline{p}(\xi)\cosh\widehat{\xi}y - \overline{\eta}(\xi)\cosh\widehat{\xi}(H-y)}{\widehat{\xi}\sinh\widehat{\xi}H}. \tag{7.79}$$

Similarly, applying Fourier transform to (7.71), (7.72) and (7.73), we get the following boundary value problem for $\overline{\psi}_1(\widehat{\xi}, y)$:

$$\overline{\psi}_{1yy} - \widehat{\xi^2}\overline{\psi}_1 = 0 \quad \text{on} \quad -h \le y \le 0, \tag{7.80}$$

$$\overline{\psi}_{1y} = \overline{\eta}(\xi) \quad \text{on} \quad y = 0, \tag{7.81}$$

$$K\overline{\psi}_1 + (D\widehat{\xi^4} + 1 - \delta K)\overline{\psi}_{1y} = 0 \quad \text{on} \quad y = -h, \tag{7.82}$$

The solution $\overline{\psi}_1(\widehat{\xi}, y)$ of the above boundary value problem is obtained as

$$\overline{\psi}_1(\widehat{\xi}, y) = \frac{K\sinh\widehat{\xi}(h+y) - (D\widehat{\xi^4} + 1 - \delta K)\widehat{\xi}\cosh\widehat{\xi}(h+y)}{K\cosh\widehat{\xi}h - (D\widehat{\xi^4} + 1 - \delta K)\widehat{\xi}\sinh\widehat{\xi}h}\,\frac{\overline{\eta}(\xi)}{\widehat{\xi}}. \tag{7.83}$$

In order to calculate the value of $\overline{\eta}(\xi)$, by applying Fourier transform to (7.75) we obtain

$$K(\overline{\phi}_1 - \rho\overline{\psi}_1) = (\rho - 1)\overline{\eta}(\xi) \quad \text{on} \quad y = 0. \tag{7.84}$$

Now substituting (7.79) and (7.83) in (7.84), we obtain the value of $\overline{\eta}(\xi)$ as

$$\overline{\eta}(\xi) = \frac{K\,\overline{p}(\xi)[K\cosh\widehat{\xi}h - (D\widehat{\xi^4} + 1 - \delta K)\widehat{\xi}\sinh\widehat{\xi}h]}{\Delta(\widehat{\xi})}, \tag{7.85}$$

where $\Delta(\widehat{\xi})$ is same as was in (6.11).

Moreover, by (6.11) $\Delta(\widehat{\xi})$ here has only two non-zero positive roots m and M. Substituting the value of $\overline{\eta}(\xi)$ in (7.79) and (7.83), and taking the inverse Fourier transform, as was defined in Chapter 4, the solution for the velocity potential $\phi_1(x, y)$ and $\psi_1(x, y)$, respectively, are obtained as follows:

$$\phi_1(x,y) = \frac{1}{2\pi}\int_{-\infty}^{\infty}\left\{\cosh\widehat{\xi}y - \frac{K[K\cosh\widehat{\xi}h - (D\widehat{\xi^4} + 1 - \delta K)\widehat{\xi}\sinh\widehat{\xi}h]\cosh\widehat{\xi}(H-y)}{\Delta(\widehat{\xi})}\right\} \times \frac{\overline{p}(\xi)\mathrm{e}^{i\xi x}}{\widehat{\xi}\sinh\widehat{\xi}H}d\xi, \tag{7.86}$$

$$\psi_1(x,y) = \frac{K}{2\pi}\int_{-\infty}^{\infty}\frac{[K\sinh\widehat{\xi}(h+y) - (D\widehat{\xi^4} + 1 - \delta K)\widehat{\xi}\cosh\widehat{\xi}(h+y)]}{\widehat{\xi}\,\Delta(\widehat{\xi})}\,\overline{p}(\xi)\mathrm{e}^{\mathrm{i}\xi x}d\xi. \tag{7.87}$$

Since $\Delta(\widehat{\xi})$ has two non-zero zeros at $\widehat{\xi} = m$ and $\widehat{\xi} = M$, correspondingly at $\xi_1 = \sqrt{m^2 - \nu^2}$ and $\xi_2 = \sqrt{M^2 - \nu^2}$, respectively, on the positive real axis of ξ, so the above integral on both cases contains poles at ξ_1 and ξ_2. Therefore we make the path for each integral in both cases indented below the poles at ξ_1 and ξ_2.

7.5.2 Reflection and transmission coefficients

The first-order reflection and transmission coefficients $r_1^{(m)}, t_1^{(m)}$ and $R_1^{(m)}, T_1^{(m)}$ with respect to the modes m and M, respectively, due to the obliquely incident wave of mode m (here $\nu = m\sin\theta$), are now obtained by letting $\xi \to \mp\infty$ in (7.86) or (7.87) and comparing with (7.70) or (7.74). We follow the same procedures, as was followed in Section 6.5.2, to calculate the first-order reflection and transmission coefficients. The values of $r_1^{(m)}$ and $R_1^{(m)}$ are obtained as:

$$r_1^{(m)} = -\frac{\mathrm{i}K\ S(m)}{m\sinh mH\ \Delta'(m)}\overline{p}(-m\cos\theta)$$
$$= -\frac{\mathrm{i}Km\ S(m)\cos 2\theta\sec\theta}{\sinh mH\ \Delta'(m)}\int_{-\infty}^{\infty}\mathrm{e}^{2\mathrm{i}mx\cos\theta}c(x)dx, \tag{7.88}$$
$$R_1^{(m)} = -\frac{\mathrm{i}K\ S(M)}{M\sinh MH\ \Delta'(M)}\overline{p}(-\sqrt{M^2-m^2\sin^2\theta})$$
$$= -\frac{\mathrm{i}Km\ S(M)(\beta_1\cos\theta - m\sin^2\theta)}{\sinh MH\ \Delta'(M)\ \beta_1}\int_{-\infty}^{\infty}\mathrm{e}^{\mathrm{i}x(m\cos\theta+\beta_1)}c(x)dx, \tag{7.89}$$

where $S(m), S(M)$ and β_1 are already defined previously.

Similarly the values of $t_1^{(m)}$ and $T_1^{(m)}$ are obtained as follows:

$$t_1^{(m)} = \frac{\mathrm{i}Km\ S(m)\sec\theta}{\sinh mH\ \Delta'(m)}\int_{-\infty}^{\infty}c(x)dx, \tag{7.90}$$
$$T_1^{(m)} = \frac{\mathrm{i}Km\ S(M)(\beta_1\cos\theta + m\sin^2\theta)}{\sinh MH\ \Delta'(M)\ \beta_1}\int_{-\infty}^{\infty}\mathrm{e}^{\mathrm{i}x(m\cos\theta-\beta_1)}\ c(x)dx. \tag{7.91}$$

Therefore, the two first-order reflection coefficients and the two first-order transmission coefficients can be evaluated from (7.88)-(7.91), once the shape function $c(x)$ is known.

When we consider a train of progressive waves of mode M to be obliquely incident on the bottom undulation (here $\nu = M\sin\theta$), the same mathematical procedure described above for the case of mode m is followed to obtain the first-order reflection and transmission coefficients $r_1^{(M)}, R_1^{(M)}, t_1^{(M)}$ and $T_1^{(M)}$. The final expressions for this case are as follows:

$$r_1^{(M)} = -\frac{\mathrm{i}KM\ S(m)(\beta_2\cos\theta - M\sin^2\theta)}{\sinh mH\ \Delta'(m)\ \beta_2}\int_{-\infty}^{\infty}\mathrm{e}^{\mathrm{i}x(M\cos\theta+\beta_2)}\ c(x)dx, \tag{7.92}$$
$$R_1^{(M)} = -\frac{\mathrm{i}KM\ S(M)\cos 2\theta\sec\theta}{\sinh MH\ \Delta'(M)}\int_{-\infty}^{\infty}\mathrm{e}^{2\mathrm{i}Mx\cos\theta}c(x)dx, \tag{7.93}$$
$$t_1^{(M)} = \frac{\mathrm{i}KM\ S(m)(\beta_2\cos\theta + M\sin^2\theta)}{\sinh mH\ \Delta'(m)\ \beta_2}\int_{-\infty}^{\infty}\mathrm{e}^{\mathrm{i}x(M\cos\theta-\beta_2)}\ c(x)dx, \tag{7.94}$$
$$T_1^{(M)} = \frac{\mathrm{i}KM\ S(M)\sec\theta}{\sinh MH\ \Delta'(M)}\int_{-\infty}^{\infty}c(x)dx. \tag{7.95}$$

Here, if we take $D = 0$ and $\delta = 0$, *i.e.*, the flexural rigidity of elastic ice-cover is assumed to be zero and the ice-cover is absent), then all the above results from (7.88)-(7.95) coincide with the corresponding results in Maiti and Mandal [49].

Both the solution methods, *i.e.*, Green's function technique and Fourier transform technique, discussed in this chapter agree to the same values of the reflection and transmission coefficients.

In the following section we proceed to examine the effects of reflection and transmission for a special sinusoidal form of the shape function $c(x)$.

7.6 Special form of bottom surface

Here, we consider the same special sinusoidal form of the shape function $c(x)$ for the uneven bottom surface, as was considered in (6.102) in Chapter 6.

The first-order reflection and transmission coefficients $r_1^{(m)}, R_1^{(m)}, t_1^{(m)}$ and $T_1^{(m)}$ with respect to the modes m and M, respectively, due to an oblique incident wave of mode m, are now obtained by substituting $c(x)$ from (6.102) into (7.59)-(7.62). These coefficients are obtained as

$$r_1^{(m)} = -\frac{\mathrm{i}a_1 Km\ S(m)\cos 2\theta\sec\theta}{\sinh mH\ \ \Delta'(m)} \times\left(\frac{l_1\{(-1)^n\exp[-(2\mathrm{i}mn\pi\cos\theta)/l_1]-1\}}{l_1^2-4m^2\cos^2\theta}+\frac{l_2\{1-(-1)^n\exp[(2\mathrm{i}mn\pi\cos\theta)/l_2]\}}{l_2^2-4m^2\cos^2\theta}\right), \tag{7.96}$$

$$R_1^{(m)} = -\frac{\mathrm{i}a_1 Km\ S(M)\ (\beta_1\cos\theta - m\sin^2\theta)}{\sinh MH\ \ \Delta'(M)\ \beta_1} \times\left(\frac{l_1\{(-1)^n\exp[-\mathrm{i}n\pi(m\cos\theta+\beta_1)/l_1]-1\}}{l_1^2-(m\cos\theta+\beta_1)^2}+\frac{l_2\{1-(-1)^n\exp[\mathrm{i}n\pi(m\cos\theta+\beta_1)/l_2]\}}{l_2^2-(m\cos\theta+\beta_1)^2}\right), \tag{7.97}$$

$$t_1^{(m)} = \frac{\mathrm{i}a_1 Km\ S(m)\ \sec\theta}{\sinh mH\ \ \Delta'(m)}\left\{\frac{[(-1)^n-1]}{l_1}+\frac{[1-(-1)^n]}{l_2}\right\}, \tag{7.98}$$

$$T_1^{(m)} = \frac{\mathrm{i}a_1 Km\ S(M)\ (\beta_1\cos\theta + m\sin^2\theta)}{\sinh MH\ \ \Delta'(M)\ \beta_1} \times\left(\frac{l_1\{(-1)^n\exp[-\mathrm{i}n\pi(m\cos\theta-\beta_1)/l_1]-1\}}{l_1^2-(m\cos\theta-\beta_1)^2}+\frac{l_2\{1-(-1)^n\exp[\mathrm{i}n\pi(m\cos\theta-\beta_1)/l_2]\}}{l_2^2-(m\cos\theta-\beta_1)^2}\right). \tag{7.99}$$

Similarly, the reflection and transmission coefficients $r_1^{(M)}, R_1^{(M)}, t_1^{(M)}$ and $T_1^{(M)}$ with respect to the modes m and M, respectively, due to an oblique incident wave of mode M, are now obtained by substituting $c(x)$ from (6.102) into (7.63)-(7.66). These coefficients are obtained as

$$r_1^{(M)} = -\frac{\mathrm{i}a_1 KM\ S(m)\ (\beta_2\cos\theta - M\sin^2\theta)}{\sinh mH\ \ \Delta'(m)\ \beta_2} \times\left(\frac{l_1\{(-1)^n\exp[-\mathrm{i}n\pi(M\cos\theta+\beta_2)/l_1]-1\}}{l_1^2-(M\cos\theta+\beta_2)^2}+\frac{l_2\{1-(-1)^n\exp[\mathrm{i}n\pi(M\cos\theta+\beta_2)/l_2]\}}{l_2^2-(M\cos\theta+\beta_2)^2}\right), \tag{7.100}$$

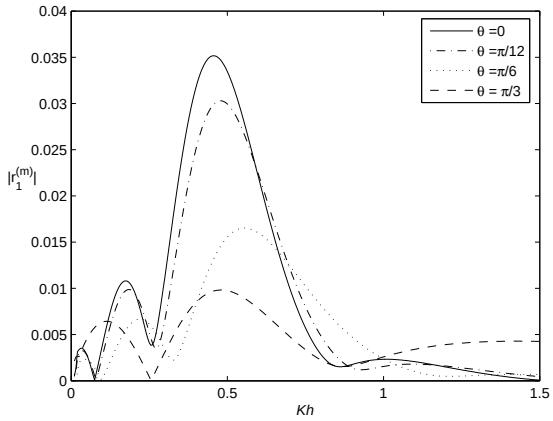

Figure 7.3: Reflection coefficient $|r_1^{(m)}|$ due to an incident wave of wave number m for $D/h^4 = 1.5$, $\delta/h = 0.01$, $\rho = 0.5$, $H/h = 2$, $a_1/h = 0.1$, $n = 3$, $l_1 h = 1$ and $l_2 h = 1.1$.

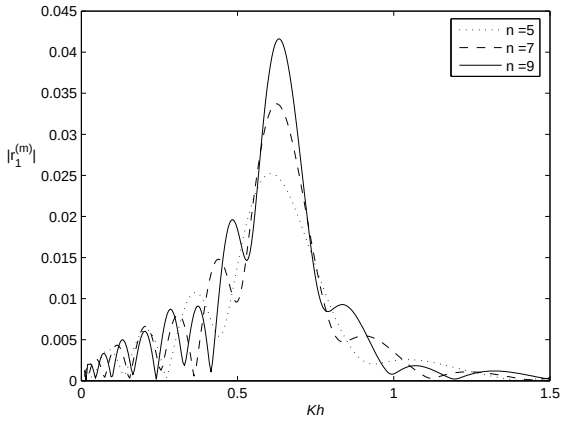

Figure 7.4: Reflection coefficient $|r_1^{(m)}|$ due to an incident wave of wave number m for $D/h^4 = 1.5$, $\delta/h = 0.01$, $\rho = 0.5$, $H/h = 2$, $a_1/h = 0.1$, $\theta = \pi/6$, $l_1 h = 1$ and $l_2 h = 1.1$.

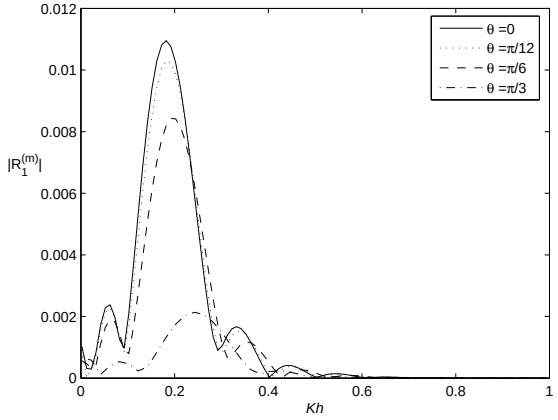

Figure 7.5: Reflection coefficient $|R_1^{(m)}|$ due to an incident wave of wave number m for $D/h^4 = 1.5$, $\delta/h = 0.01$, $\rho = 0.5$, $H/h = 2$, $a_1/h = 0.1$, $n = 3$, $l_1 h = 1$ and $l_2 h = 1.1$.

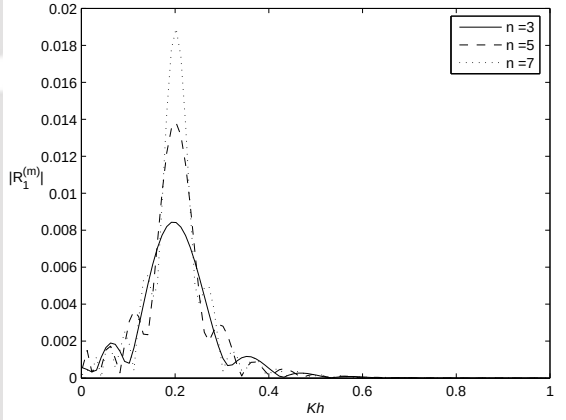

Figure 7.6: Reflection coefficient $|R_1^{(m)}|$ due to an incident wave of wave number m for $D/h^4 = 1.5$, $\delta/h = 0.01$, $\rho = 0.5$, $H/h = 2$, $a_1/h = 0.1$, $\theta = \pi/6$, $l_1 h = 1$ and $l_2 h = 1.1$.

$$R_1^{(M)} = -\frac{\mathrm{i}a_1 KM\ S(M)\ \cos 2\theta \sec\theta}{\sinh MH\ \ \Delta'(M)} \times\left(\frac{l_1\{(-1)^n \exp[-(2\mathrm{i}Mn\pi\cos\theta)/l_1] - 1\}}{l_1^2 - 4M^2\cos^2\theta} + \frac{l_2\{1-(-1)^n \exp[(2\mathrm{i}Mn\pi\cos\theta)/l_2]\}}{l_2^2 - 4M^2\cos^2\theta}\right), \quad (7.101)$$

$$t_1^{(M)} = \frac{\mathrm{i}a_1 KM\ S(m)\ (\beta_2\cos\theta + M\sin^2\theta)}{\sinh mH\ \ \Delta'(m)\ \beta_2} \times\left(\frac{l_1\{(-1)^n \exp[-\mathrm{i}n\pi(M\cos\theta-\beta_2)/l_1] - 1\}}{l_1^2 - (M\cos\theta-\beta_2)^2} + \frac{l_2\{1-(-1)^n \exp[\mathrm{i}n\pi(M\cos\theta-\beta_2)/l_2]\}}{l_2^2 - (M\cos\theta-\beta_2)^2}\right), \quad (7.102)$$

$$T_1^{(M)} = \frac{\mathrm{i}a_1 KM\ S(M)\ \sec\theta}{\sinh MH\ \ \Delta'(M)}\left\{\frac{[(-1)^n - 1]}{l_1} + \frac{[1-(-1)^n]}{l_2}\right\}. \quad (7.103)$$

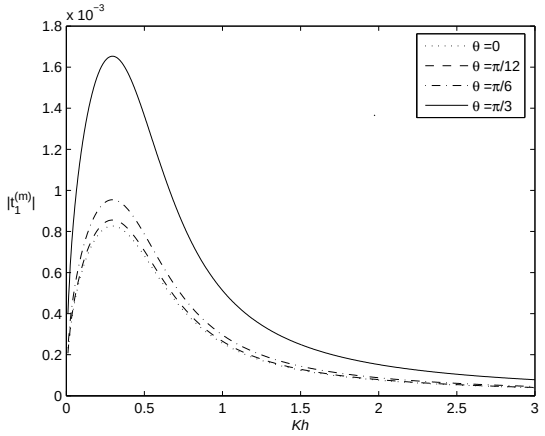

Figure 7.7: Transmission coefficient $|t_1^{(m)}|$ due to an incident wave of wave number m for $D/h^4 = 1.5$, $\delta/h = 0.01$, $\rho = 0.5$, $H/h = 2$, $a_1/h = 0.1$, $n = 3$, $l_1 h = 1$ and $l_2 h = 1.1$.

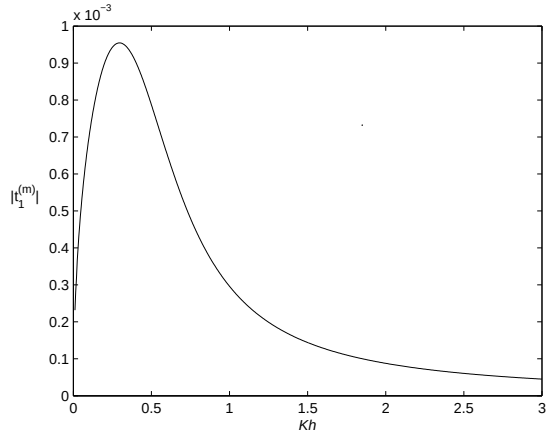

Figure 7.8: Transmission coefficient $|t_1^{(m)}|$ due to an incident wave of wave number m for $D/h^4 = 1.5$, $\delta/h = 0.01$, $\rho = 0.5$, $H/h = 2$, $a_1/h = 0.1$, $\theta = \pi/6$, $l_1 h = 1$ and $l_2 h = 1.1$.

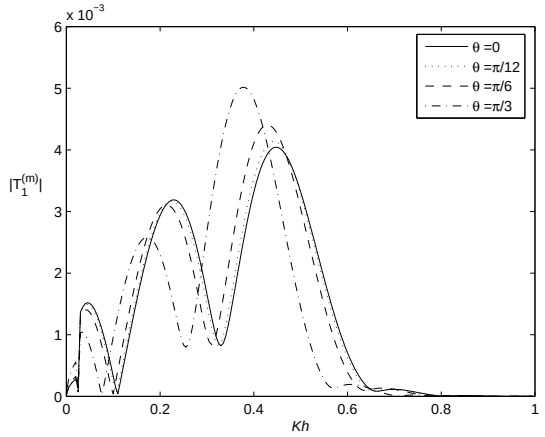

Figure 7.9: Transmission coefficient $|T_1^{(m)}|$ due to an incident wave of wave number m for $D/h^4 = 1.5$, $\delta/h = 0.01$, $\rho = 0.5$, $H/h = 2$, $a_1/h = 0.1$, $n = 3$, $l_1 h = 1$ and $l_2 h = 1.1$.

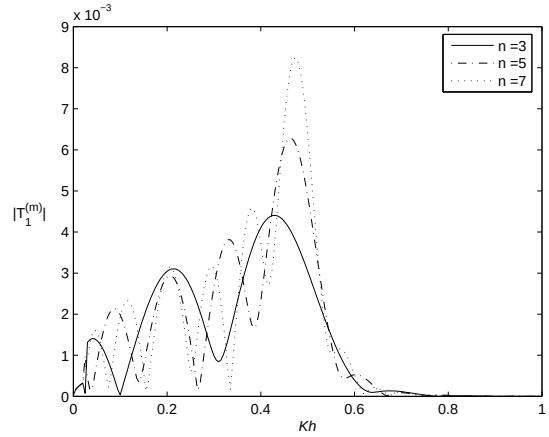

Figure 7.10: Transmission coefficient $|T_1^{(m)}|$ due to an incident wave of wave number m; $D/h^4 = 1.5$, $\delta/h = 0.01$, $\rho = 0.5$, $H/h = 2$, $a_1/h = 0.1$, $\theta = \pi/6$, $l_1 h = 1$ and $l_2 h = 1.1$.

7.7 Numerical results

In figures 7.3–7.10, the first-order reflection and transmission coefficients are shown for the case of a wave train of wave number m (an ice-cover mode) obliquely incident at an angle θ to the positive x-axis on the bottom undulation. In all the figures, the ice parameters are fixed at $D/h^4 = 1.5$, $\delta/h = 0.01$, the depth ratio H/h as 2, the amplitude of the sinusoidal ripples a_1/h as 0.1, the ripple wave numbers as $l_1 h = 1$ and $l_2 h = 1.1$ and the density ratio ρ taken as 0.5. The different curves in figures 7.3, 7.5, 7.7 and 7.9 correspond to four different angles of incidence, $\theta = 0,\ \pi/12,\ \pi/6$ and $\pi/3$, while n is fixed at 3 for these curves. The peak values of the reflection coefficient $|r_1^{(m)}|$ and the transmission coefficient $|t_1^{(m)}|$ of waves of wave number m for an obliquely incident wave of wave number m, shown in figures 7.3 and 7.7, respectively, decrease as the angle of incidence θ increases. Figures 7.5 and 7.9, respectively, show the first-

order reflection and transmission coefficients of the wave number M for an obliquely incident wave of wave number m and it is observed that as the angle of incidence increases, $|R_1^{(m)}|$ decreases while $|T_1^{(m)}|$ increases but their non-zero values show that there is some conversion of energy from one wave number to the other. This effect is also observed in the oblique scattering problem in a two-layer fluid with a free surface. From all the figures, the reflection coefficient of the waves of wave number M is found to be smaller in comparison to those for the waves with wave number m and the transmission coefficient of the waves of wave number m is much smaller than that in the case of the waves with wave number M.

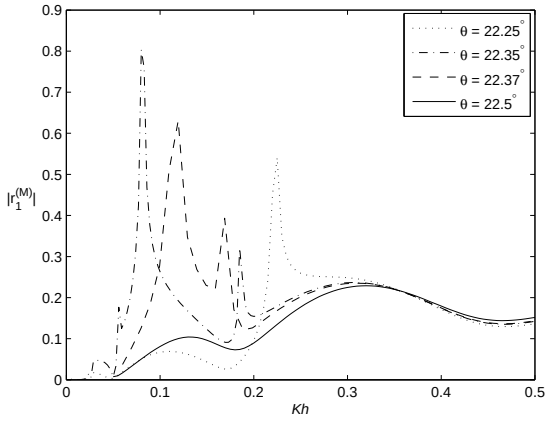

Figure 7.11: Reflection coefficient $|r_1^{(M)}|$ due to an incident wave of wave number M for $D/h^4 = 1.5$, $\delta/h = 0.01$, $\rho = 0.5$, $H/h = 2$, $a_1/h = 0.1$, $n = 3$, $l_1h = 1$ and $l_2h = 1.1$.

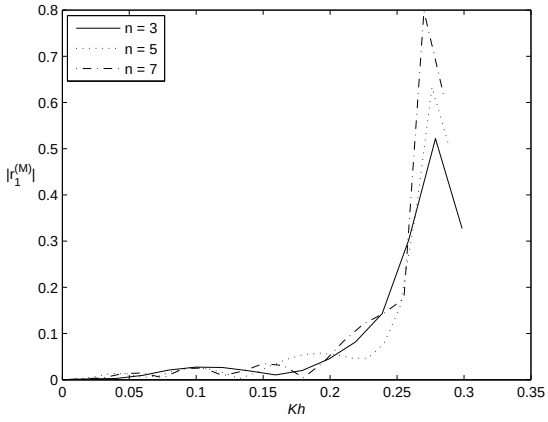

Figure 7.12: Reflection coefficient $|r_1^{(M)}|$ due to an incident wave of wave number M; $D/h^4 = 1.5$, $\delta/h = 0.01$, $\rho = 0.5$, $H/h = 2$, $a_1/h = 0.1$, $\theta = 22°$, $l_1h = 1$ and $l_2h = 1.1$.

The different curves in figures 7.4, 7.6, 7.8 and 7.10 correspond to different number of ripples in the bottom surface, when the angle of incidence is fixed at $\theta = \pi/6$ for all these curves. It is clear from these figures (except figure 7.8) that the peak values of reflection and transmission coefficients of the waves of wave number m and M, for an obliquely incident wave of wave number m, increase when the number of ripple increases. Figure 7.8 shows that the first-order transmission coefficient $|t_1^{(m)}|$ is fixed for all odd values of n, and there is no transmission for even values of n. From the figures 7.3–7.10, it is also clear that the number of zeros of reflection and transmission coefficients (except for $|t_1^{(m)}|$) is very less in comparison to that of the example of Maiti and Mandal [49]. This happens due to the presence of the ice-cover and the different ripple wave numbers in the patch of the undulation. Another common feature in these figures is the oscillating nature of the absolute values of the first-order coefficients as functions of the wave number Kh.

The case of an obliquely incident wave of wave number M (an interfacial mode) is more interesting due to the presence of the cut-off frequencies below which no energy is converted from one wave number to the other. For this case, figures 7.11–7.17 show the first-order reflection coefficients $|r_1^{(M)}|$, $|R_1^{(M)}|$ and transmission coefficients $|t_1^{(M)}|$, $|T_1^{(M)}|$ against Kh for $D/h^4 = 1.5$, $\delta/h = 0.01$, $\rho = 0.5$, $H/h = 2$, $a_1/h = 0.1$ and the ripple wave numbers $l_1h = 1$

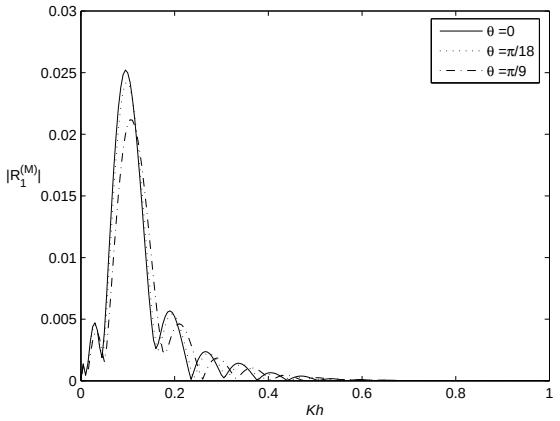

Figure 7.13: Reflection coefficient $|R_1^{(M)}|$ due to an incident wave of wave number M for $D/h^4 = 1.5$, $\delta/h = 0.01$, $\rho = 0.5$, $H/h = 2$, $a_1/h = 0.1$, $n = 3$, $l_1h = 1$ and $l_2h = 1.1$.

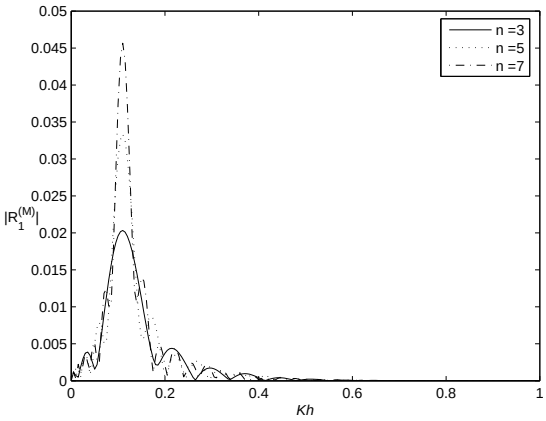

Figure 7.14: Reflection coefficient $|R_1^{(M)}|$ due to an incident wave of wave number M; $D/h^4 = 1.5$, $\delta/h = 0.01$, $\rho = 0.5$, $H/h = 2$, $a_1/h = 0.1$, $\theta = 22°$, $l_1h = 1$ and $l_2h = 1.1$.

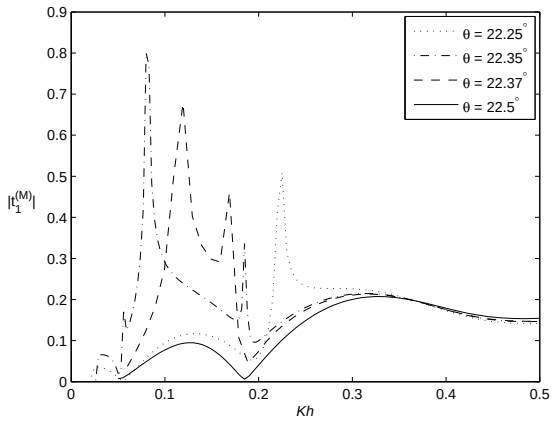

Figure 7.15: Transmission coefficient $|t_1^{(M)}|$ due to an incident wave of wave number M for $D/h^4 = 1.5$, $\delta/h = 0.01$, $\rho = 0.5$, $H/h = 2$, $a_1/h = 0.1$, $n = 3$, $l_1h = 1$ and $l_2h = 1.1$.

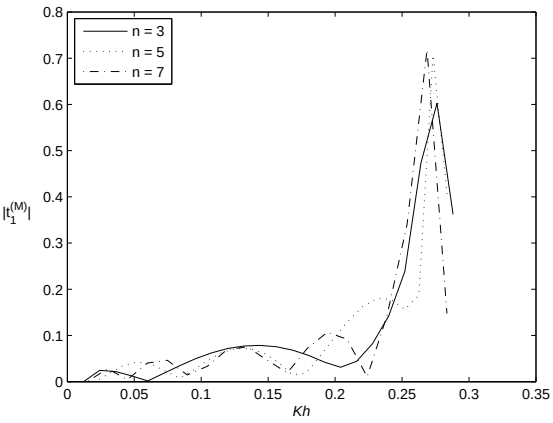

Figure 7.16: Transmission coefficient $|t_1^{(M)}|$ due to an incident wave of wave number M; $D/h^4 = 1.5$, $\delta/h = 0.01$, $\rho = 0.5$, $H/h = 2$, $a_1/h = 0.1$, $\theta = 22°$, $l_1h = 1$ and $l_2h = 1.1$.

and $l_2h = 1.1$. The different curves in figures 7.11 and 7.15, representing $|r_1^{(M)}|$ and $|t_1^{(M)}|$, correspond to different values of the incident angles $\theta = 22.25°, 22.35°, 22.37°$ and $22.5°$, while n is fixed at 3 for all these curves. When $\theta = 22.5°$, which is greater than the critical angle $\theta_c = 22.38°$ for the given values of the different parameters Kh, there is no wave of wave number m propagating in the fluid. For these two figures, we have the following cut-off frequencies: $\omega_c(h/g)^{1/2} = 0.4701; (0.4301, 0.2864, 0.2345); (0.4123, 0.3406)$ which correspond to the incident angles $22.25°, 22.35°, 22.37°$, respectively. For these angles and for frequencies either less than the cut-off frequency or lying in between the two appropriate cut-off frequencies, there will be conversion of energy from one mode to the other. For the curves which correspond to $\theta = 22.25°, 22.35°, 22.37°$ there are one, two, three spikes in the curves, respectively, because of one, two, three cut-off frequencies present in the curves. Since $\theta = 22.5°$, which is greater than the critical angle for the given parameter values Kh, there is no spike on the curve. From

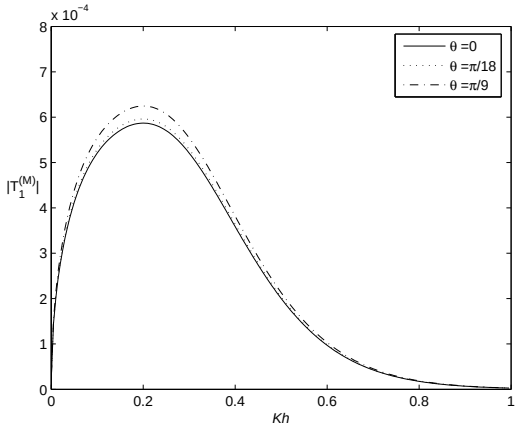

Figure 7.17: Transmission coefficient $|T_1^{(M)}|$ due to an incident wave of wave number M for $D/h^4 = 1.5$, $\delta/h = 0.01$, $\rho = 0.5$, $H/h = 2$, $a_1/h = 0.1$, $n = 3$, $l_1 h = 1$ and $l_2 h = 1.1$.

these two figures we observe that for a particular frequency just less than the cut-off frequency there is maximum reflection and maximum transmission of the incident wave of wave number M.

The different curves in figures 7.13 and 7.17 correspond to the different angles of incidence, $\theta = 0,\ \pi/18$ and $\pi/9$, while n is fixed at 3 for all these curves. The figures 7.13 and 7.17, which correspond to the reflection coefficient $|R_1^{(M)}|$and transmission coefficient $|T_1^{(M)}|$, do not show such behaviours since reflection and transmission of waves of wave number M for an obliquely incident wave of wave number M always exist irrespective of what the incident wave angle is. Also it is clear from these two figures that as the angle of incident waves increases, the peak values of reflection coefficient $|R_1^{(M)}|$ decreases while the peak values of transmission coefficient $|T_1^{(M)}|$ increases. The different curves in figures 7.12, 7.14 and 7.16 correspond to different numbers of ripples on the bottom surface, when the angle of incidence is fixed at $\theta = 22^\circ$ for all these curves. The figures 7.12 and 7.16 show the cut-off values with respect to reflection and transmission of waves, respectively, for which energy conversion from mode M to mode m takes place for different values of n. Figure 7.14 shows that as the number of ripples increases, the reflection coefficient $|R_1^{(M)}|$ for waves with wave number M for an obliquely incident wave of wave number M always exists and its peak values increase accordingly. All the above numerical values of the reflection and transmission coefficients have been checked for their correctness from the energy identities as given by Bhattacharjee and Sahoo [7] for finite depth. Computations show that as $D/h^4 \to 0,\ \delta/h \to 0$ and the ripple wave numbers in the patches are same, all the above results tend to those for oblique incidence in two-layer fluid with free surface in an ocean with bottom undulation (Maiti and Mandal [49]).

7.8 Conclusion

The work described in this chapter is the classical problem of oblique water wave scattering by a small bottom undulation in a two-layer fluid flowing in an ocean, where the upper layer

is of finite height and is bounded above by a thin ice-cover modelled as a thin elastic plate, which replaces the free surface. In such a situation propagating waves can exist at two different wave number for any given frequency, the one with smaller wave number corresponds to an ice-surface disturbance and the other to an interfacial wave motion. As in the case of a two-layer fluid of finite depth with free surface, here also for an obliquely incident wave train and for some values of incident angles with ice-cover, two cut-off frequencies are obtained. Using perturbation analysis, the problem is reduced up to first-order to a coupled boundary value problem which is solved by a method based on Green's integral theorem with the introduction of appropriate Green's functions. First-order approximations to the reflection and transmission coefficients are obtained in terms of computable integrals and depicted graphically through a number of figures. When the wave is incident on the ice-cover surface we always find energy transfer to the interface, but for interfacial incident waves there are parameter ranges for which no energy transfer to the ice-cover surface is possible. The main advantage of this method, demonstrated through the example of a patch of sinusoidal ripples having two different wave numbers, is that a very few ripples may be needed to produce a substantial amount of reflected energy. Also it is observed that for small angles of incidence, the reflected energy is more as compared to other angles of incidence (except at $\theta = \pi/4$). The solution developed here is expected to be helpful for a wide class of ice-covered two-layer fluid problems in an ocean with oblique incidence and uneven bottom surface.

Chapter 8

Summary and future work

This chapter is completely devoted to a brief summary of the results highlighting the contributions made by this thesis and also of the techniques used in deriving these. It also provides information for the scope of possible extensions of the present work and future investigations.

8.1 Summary

In this thesis the scattering of a train of small amplitude harmonic surface water waves by a sphere or small undulation in a two-layer fluid has been investigated by using linear water wave theory.

In Chapter 2, using the multipole expansion technique, we solve the solution of radiation and scattering problems concerning a submerged sphere entirely located within one of the layers of a two-layer fluid with both layers being of finite depth. The layers are bounded by upper and lower rigid surfaces, which are approximations of the free surface and the bottom surface, respectively, in a channel. The hydrodynamic forces due to radiation and exciting forces for heave and sway motions are derived and plotted against various values of the wave number.

In Chapter 3, the previous work (Chapter 2) is extended to a problem where the upper fluid is bounded above by a thin ice-cover modelled as a thin elastic plate, which replaces the free surface and the lower fluid is bounded by a bottom surface. The radiated energy by the moving sphere in such type of fluid region is handled in this chapter by the same multipole expansion technique. Earlier, Cadby and Linton [9] solved the three-dimensional water-wave scattering in a two-layer fluid, in which the upper layer had a free surface and the lower layer extended to infinite depth. The results that are obtained in this chapter are reasonable to be compared with the work of Cadby and Linton [9] as both the problems bear similarities to a large extent.

The problem of interaction between surface waves and a pre-existing (fixed) pattern of undulation on an otherwise flat bed has received an increasing amount of attention because such patterns may comprise of shore parallel bars or tidally generated features such as sand

waves, lying transverse to the direction of the wave propagation. Therefore, in the rest of the chapters in this thesis, propagation of water wave over small bottom undulation in a two-layer fluid is carried out through formulating and solving different boundary value problems.

Chapter 4 is concerned with the investigation of the problem of propagation of normally incident internal water waves over small bottom undulation on a channel bed of finite depth by assuming that the upper layer is bounded by a rigid horizontal surface. The first-order corrections of reflection and transmitted coefficients have been evaluated by the use of two methods, *i.e.*, Green's integral theorem technique and Fourier transform technique. To evaluate these coefficients numerically, different shape functions are considered in this chapter and the results are best presented graphically. These particular cases of sinusoidal ripples on the ocean-bed are of considerable significance due to the ability of an undulating bed to reflect incident wave energy which is important in respect of possible ripple growth if the bed is erodable in a channel. For these particular cases we observe that a large amount of reflection of the incident wave energy is produced for Bragg resonance. That means the same conclusion can be drawn even if all the ripples in the patch do not have the same wave number.

Chapter 5 is concerned with the scattering of obliquely incident water waves by small bottom undulation on a channel bed. The work described in this chapter is the extension of the work described in Chapter 4. Green's integral theorem is employed to obtain the complete solution of the mixed boundary value problem from which the reflection and transmission coefficients are determined which involve the shape function $c(x)$. The investigation of the problems discussed in Chapters 4 and 5 has not been taken up by anyone earlier. It is hoped that the results obtained here can be used quantitatively for this kind of problems.

Chapter 6 is concerned with the investigation of the problem of scattering of normal incident water waves by small undulation in a two-layer fluid in an ocean which is covered by a thin elastic ice-cover. In this case, time-harmonic waves of a particular frequency can propagate with two different wave numbers: the waves with the higher wave number propagate at the interface while the waves with lower wave number at the ice-cover. Applying perturbation analysis, which involves a small parameter ε present in the representation of the small undulation of the ocean-bed, we establish the boundary value problems which are satisfied by the velocity potential for the scattering of waves by small undulating topography. The solution is obtained by two different techniques, namely the Green's integral theorem and Fourier transform technique. Using this solution, the reflection and transmission coefficients are obtained which involve the shape function $c(x)$. The particular case of a patch of sinusoidal ripples (having two different wave numbers over two consecutive stretches) on the ocean-bed is of considerable significance due to the ability of an undulating bed to reflect incident wave energy, which is important in respect of both coastal protection, and possible ripple growth if the bed can be eroded. It is observed both analytically and numerically that when there is no ice-cover, *i.e.*, the flexural rigidity equals to zero (or tends to zero numerically), and if

the ripple wave numbers in the patches are same, all the results may be interpreted as those for normal incident wave, which can be derived, by taking the incident angle to be zero in the oblique incidence case in a two-layer fluid with free surface in an ocean with bottom undulation (Maiti and Mandal [49]).

The physical boundary value problem in Chapter 6, is extended to the obliquely incident case in Chapter 7. In this chapter also the same Green's integral theorem technique and Fourier transform technique are used to solve the first-order reflection and transmission coefficients. The main conclusion that can be drawn is that when the wave is incident on the ice-cover surface we always find energy transfer to the interface, but for the interfacial incident waves there are parameter ranges for which no energy transfer to the ice-cover surface is possible. In this case also the solutions for the reflection and transmission coefficients may be interpreted as the results obtained by the Maiti and Mandal [49] in the absence of ice-cover. All the results discussed in Chapters 6 and 7 may be useful in the construction of an effective reflector of the incident wave energy for protecting coastal areas from the rough ocean in the polar regions.

8.2 Future work

We now present some informal observations pertaining to the possible extensions of our results to different problems. We briefly outline some interesting problems which can be taken up in future.

Suppose a horizontal channel of finite length, constant width and constant depth contains an inviscid two-layer fluid flowing under gravity. The fluid is bounded internally by a submerged horizontal cylinder which extends right across the channel, and has its generators normal to its sidewalls. Suppose that the fluid is set in motion by a surface pressure varying across the channel. Then some of the energy is radiated to infinity while some of the energy is trapped in characteristic modes near the cylinder. So in this type of case, it is also necessary to study the behaviour of the physical properties in water waves:

1. The trapped water waves in a two-layer fluid in a channel of finite depth.

2. The trapped water waves in a two-layer fluid in an ice-covered ocean of finite depth.

Again, the problem pertaining to water wave propagation over small bottom undulation may further be extended to one over a porous bed. Moreover, the same scattering problem can be further extended to barrier problem (*i.e.*, instead of bottom undulation we may consider the presence of barrier). Therefore, the possible extensions of this type of problems are:

1. Scattering of surface waves by small deformation in a two-layer fluid of ice-covered ocean with porous bed.

2. Scattering of water waves by a vertical barrier in either layer of the two-layer fluid in the presence of surface tension.

3. Scattering of water waves by a vertical barrier in either layer of the two-layer fluid covered by the ice-cover.

While carrying out our work, we observed that all the problems that we considered could possibly be extended to a fluid having more than two layers. There are practical problems where we may find the fluid consisting of different layers such as rocky layer, porous layer, salty layer, fresh water layer etc. It may be possible to tackle this kind of problems with the help of the knowledge garnered through the work done in this thesis.

Bibliography

[1] Z. An and Z. Ye, *Band gaps and localization of water waves over one-dimensional topographical bottoms*, Appl. Phys. Lett., **84** (2004), pp. 2952–2954.

[2] N. J. Balmforth and R. V. Craster, *Ocean waves and ice-sheets*, J. Fluid Mech., **395** (1999), pp. 89–124.

[3] M. Belzons, E. Guazzelli, and O. Parodi, *Gravity waves on a rough bottom: experimental evidence of one-dimensional localization*, J. Fluid Mech., **186** (1988), pp. 539–558.

[4] L. G. Bennetts, N. R. T. Biggs, and D. Porter, *A multi-mode approximation to wave scattering by ice sheets of varying thickness.*, J. Fluid Mech., **579** (2007), pp. 413–443.

[5] J. C. W. Berkhoff, *Computation of combined refraction-diffraction.*, Proc. 13th Conf. on Coastal Engng., July 1972, Vancouver, Canada, ASCE., **2** (1973), pp. 471–490.

[6] ——, *Mathematical model for simple harmonic linear waves wave diffracation and refraction.*, Delft Hydr. Rep., **W** (1976), pp. 154–IV.

[7] J. Bhattacharjee and T. Sahoo, *Flexural gravity wave problems in two-layer fluids*, Wave Motion, **45** (2008), pp. 133–153.

[8] N. Booij, *A note on the accuracy of the mild-slope equation*, Coastal Engng., **7** (1983), pp. 191–203.

[9] J. R. Cadby and C. M. Linton, *Three-dimensional water-wave scattering in two-layer fluids*, J. Fluid Mech., **423** (2000), pp. 155–173.

[10] A. Chakrabarti, *On the solution of the problem of scattering of surface-water waves by the edge of an ice cover*, Proc. R. Soc. Lond. A, **456** (2000), pp. 1087–1099.

[11] P. G. Chamberlain, *Wave scattering over uneven depth using the mild-slope equation*, Wave Motion, **17** (1993), pp. 267–285.

[12] ——, *Symmetry relations and decomposition for the mild slope equation*, J. Engng. Math., **29** (1995), pp. 121–140.

[13] P. G. Chamberlain and D. Porter, *Decomposition methods for wave scattering by topography with application to ripple beds*, Wave Motion, **22** (1995), pp. 201–214.

[14] ——, *Scattering and near-trapping of water waves by axisymmetric topography*, J. Fluid Mech., **388** (1999), pp. 335–354.

[15] ——, *Wave scattering in a two-layer fluid of varying depth*, J. Fluid Mech., **524** (2005), pp. 207–228.

[16] H. Chung and C. Fox, *Calculation of wave-ice interaction using the weinerhopf technique*, N. Z. J. Math., **31 (1)** (2002), pp. 1–18.

[17] G. J. M. Copeland, *A practical alternative to the "mild-slope" wave equation*, Coastal Engng., **9** (1985), pp. 125–149.

[18] D. Das and B. N. Mandal, *A note on solution of the dispersion equation for small-amplitude internal waves*, Arch. Mech., **57** (2005), pp. 493–501.

[19] ——, *Wave scattering by a horizontal circular cylinder in a two-layer fluid with an ice-cover*, International Journal of Engineering Science, **45** (2007), pp. 842–872.

[20] ——, *Water wave radiation by a sphere submerged in water with an ice-cover*, Arch. Appl. Mech., **78** (2008), pp. 649–661.

[21] A. G. Davies, *The reflection of wave energy by undulations of the sea bed*, Dyn. Atms. Oceans, **6** (1982), pp. 207–232.

[22] A. G. Davies and A. D. Heathershaw, *Surface-wave propagation over sinusoidallly varying topography*, J. Fluid Mech., **144** (1984), pp. 419–443.

[23] P. Devillard, F. Dun-lop, and B. Souillard, *Localization of gravity waves on a channel with a random bottom*, J. Fluid Mech., **186** (1988), pp. 521–538.

[24] C. Eckart, *The propagation of gravity waves from deep to shallow water*, In Gravity Waves: (Proc. NBS Semicentennial Symp. on Gravity Waves, NBS, June 15-18, 1951), Washington: National Bureau of Standards, (1951), pp. 165–175.

[25] D. V. Evans, *Mechanisms of the generation of edge waves over a sloping beach*, J. Fluid Mech., **186** (1988), pp. 379–391.

[26] D. V. Evans and C. M. Linton, *Wave scattering by narrow cracks in ice-sheets floating on water of finite depth*, J. Fluid Mech., **278** (1994), pp. 229–249.

[27] D. V. Evans and R. Porter, *Wave scattering by narrow cracks in ice-sheets floating on water of finite depth*, J. Fluid Mech., **484** (2003), pp. 143–165.

[28] C. Fox and V. A. Squire, *On the oblique reflection and transmission of ocean waves at shore fast sea ice*, Phil. Trans. R. Soc. Lond. A, **347** (1994), pp. 185–218.

[29] R. Gayen, B. N. Mandal, and A. Chakrabarti, *Water-wave scattering by an ice-strip*, Journal of Engineering Mathematics, **53** (2005), pp. 21–37.

[30] M. A. Gourgi and S. E. Kassem, *Basic singularities in the theory of internal waves*, Quart. J. Mech. Appl. Math., **31** (1978), pp. 31–48.

[31] E. Guazzelli, E. Guyon, and B. Souillard, *On the localization of shallow water waves by a random bottom*, J. Phys. Lett., **44** (1983), pp. 837–841.

[32] E. Guazzelli, V. Rey, and M. Belzons, *Higher-order bragg reflection of gravity surface waves by periodic beds*, J. Fluid Mech., **245** (1992), pp. 301–317.

[33] T. H. Havelock, *Waves due to a floating sphere making periodic heaving oscillations*, Proc. R. Soc. Lond. A, **231** (1955), pp. 1–7.

[34] E. R. Johnson, *The low-frequency scattering of kelvin waves by stepped topography*, J. Fluid Mech., **215** (1990), pp. 23–44.

[35] M. Kashiwagi, I. Ten, and M. Yasunaga, *Hydrodynamics of a body floating in a two-layer fluid of finite depth. part 2. diffraction problem and wave-induced motions*, J. Mar. Sci. Technol., **11** (2006), pp. 150–164.

[36] S. E. Kassem, *Multipole expansions for two superposed fluids, each of finite depth*, Math. Proc. Camb. Phil. Soc., **91** (1982), pp. 323–329.

[37] ——, *Wave source potentials for two superposed fluids, each of finite depth*, Math. Proc. Camb. Phil. Soc., **100** (1986), pp. 595–599.

[38] S. M. Killen and R. S. Johnson, *Propagation of axi-symmetric nonlinear shallow water waves over slowly varying depth*, Mathematics and Computers in Simulation, **55** (2001), pp. 463–472.

[39] J. T. Kirby, *A note on linear surface wave-current interaction over slowly varying topography*, J. Geophysical Res., **89** (1984), pp. 745–747.

[40] ——, *A general wave equation for waves over rippled beds*, J. Fluid Mech., **162** (1986), pp. 171–186.

[41] ——, *On the gradual reflection of weakly nonlinear stokes waves in regions with varying topography*, J. Fluid Mech., **162** (1986), pp. 187–209.

[42] H. Lamb, *Hydrodynamics*, 6th ed. Cambridge University Press, Cambridge, 1932.

[43] C. M. Linton, *Radiation and diffraction of water waves by a submerged sphere in finite depth*, Ocean Engng., **18** (1991), pp. 61–74.

[44] C. M. Linton and J. R. Cadby, *Scattering of oblique waves in a two-layer fluid*, J. Fluid Mech., **461** (2002), pp. 343–364.

[45] C. M. Linton and H. Chung, *Reflection and transmission at the ocean/sea-ice boundary*, Wave Motion, **38** (2003), pp. 43–52.

[46] C. M. Linton and D. V. Evans, *The radiation and scattering of surface waves by a vertial circular cylinder in a channel*, Phil. Trans. R. Soc. Lond. A, **338** (1992), pp. 325–357.

[47] C. M. Linton and M. McIver, *The interaction of waves with horizontal cylinders in two-layer fluids*, J. Fluid Mech., **304** (1995), pp. 213–229.

[48] P. A. Madsen and J. Larsen, *An efficient finite-difference approach to the mild-slope equation*, Coastal Engng., **11** (1987), pp. 329–351.

[49] P. Maiti and B. N. Mandal, *Scattering of oblique waves by bottom undulations in a two-layer fluid*, J. Appl. Math. and Computing, **22** (2006), pp. 21–39.

[50] B. N. Mandal and U. Basu, *Oblique interface-wave diffraction by a small bottom deformation in two superposed fluids*, Arch. Mech., **19(2)** (1996), pp. 363–370.

[51] B. N. Mandal and U. Basu, *Wave diffraction by a small elevation of the bottom of an ocean with an ice-cover*, Archive of Applied Mechanics, **73** (2004), pp. 812–822.

[52] S. C. Martha and S. N. Bora, *Water wave diffraction by a small deformation of the ocean bottom for oblique incidence*, Acta Mechanica, **185(3-4)** (2006), pp. 165–177.

[53] ——, *Oblique surface wave propagation over a small undulation on the bottom of an ocean*, Geophysical and Astrophysical Fluid Dynamics, **101(2)** (2007), pp. 65–80.

[54] C. C. Mei, *Resonant reflection of surface water waves by periodic sandbars*, J. Fluid Mech., **152** (1985), pp. 315–335.

[55] C. C. Mei and J. L. Black, *Scattering of surface waves by rectangular obstacles in waters of finite depth*, J. Fluid Mech., **38 (3)** (1969), pp. 499–511.

[56] J. W. Miles, *Surface-wave scattering matrix for a shelf*, J. Fluid Mech., **28** (1967), pp. 755–767.

[57] J. W. Miles, *Oblique surface wave diffraction by a cylindrical obstacle*, J. Atmos. Oceans, **6** (1981), pp. 121–123.

[58] J. W. Miles, *Variational approximations for gravity waves in water of variable depth*, J. Fluid Mech., **232** (1991), pp. 681–688.

[59] J. W. Miles and P. G. Chamberlain, *Topographical scattering of gravity waves*, J. Fluid Mech., **361** (1998), pp. 175–188.

[60] T. J. O'Hare and A. G. Davies, *A new model for surface wave propagation over undulating topography*, Coastal Engng., **18** (1992), pp. 251–266.

[61] ——, *A comparison of two models for surface-wave propagation over rapidly varying topography*, Appl. Ocean Res., **15** (1993), pp. 1–11.

[62] D. Porter and R. Porter, *Approximations to wave scattering by an ice sheet of variable thickness over undulating topography*, J. Fluid Mech., **509** (2004), pp. 145–179.

[63] R. Porter and D. Porter, *Interaction of water waves with three-dimensional periodic topography,*, J. Fluid Mech., **434** (2001), pp. 301–335.

[64] ——, *Scattered and free waves over periodic beds*, J. Fluid Mech., **483** (2003), pp. 129–163.

[65] P. F. Rhodes-Robinson, *On the forced surface waves due to a vertical wave-maker in the presence of surface tension*, Proc. Camb. Phil. Soc., **70** (1971), pp. 323–337.

[66] R. Smith and T. Sprinks, *Scattering of surface waves by a conical island*, J. Fluid Mech., **72(2)** (1975), pp. 373–384.

[67] V. A. Squire, *Of ocean waves and sea-ice revisited*, Cold Regions Sci. Tech., **49** (2007), pp. 110–133.

[68] V. A. Squire and T. D. Williams, *Wave propagation across sea-ice thickness changes*, Ocean Modelling, **21** (2008), pp. 1–11.

[69] M. A. Srokosz, *The submerged sphere as an absorber of wave power*, J. Fluid Mech., **95** (1979), pp. 717–741.

[70] D. J. Staziker, D. Porter, and D. S. G. Stirling, *The scattering of surface waves by local bed elevations*, Applied Ocean Research, **18** (1996)), pp. 283–291.

[71] I. V. Sturova, *Problems of radiation and diffraction for a circular cylinder in a stratified fluid*, Fluid Dynamics, **34** (1999), pp. 521–533.

[72] I. Ten and M. Kashiwagi, *Hydrodynamics of a body floating in a two-layer fluid of finite depth. part 1. radiation problem*, J. Mar. Sci. Technol., **9** (2004), pp. 127–141.

[73] R. C. Thorne, *Multipole expansions in the theory of surface waves*, Proc. Camb. Phil. Soc., **49** (1953), pp. 707–716.

[74] G. L. Vaughan and V. A. Squire, *Ocean wave scattering by natural sea ice transects*, J. Geophys. Res., **113 C10022** (2008), p. doi:10.1029/2007JC004278.

[75] S. Wang, *Motions of a spherical submarine in waves*, Ocean Eng., **13** (1986), pp. 249–271.

[76] J. V. Wehausen and E. V. Laitone, *Surface waves*, Handbuch Der Physik, Springer Verlag, Berlin, 1960.

Appendix A

Roots of the dispersion equation with rigid boundary

For two-dimensional and time-harmonic motion, the progressive wave solutions which satisfy Laplace's equation and the rigid boundary conditions (two-dimensional) are given below:

$$\psi(x,y) = -\frac{\cosh k(h+y)}{\sinh kh}\, \mathrm{e}^{\mathrm{i}kx}, \quad \text{in} \quad -h < y < 0, \tag{A.1}$$

$$\phi(x,y) = \frac{\cosh k(H-y)}{\sinh kH}\, \mathrm{e}^{\mathrm{i}kx}, \quad \text{in} \quad 0 < y < H, \tag{A.2}$$

with k satisfying the dispersion relation $\Delta(k) = 0$ where

$$\Delta(k) = \frac{K}{1-\rho}(\cosh kH \sinh kh + \rho \sinh kH \cosh kh) - k \sinh kh \sinh kH. \tag{A.3}$$

It is well known that the above equation has real roots $\pm k_0$ ($K_0 > 0$) and countably infinite number of imaginary roots $\pm \mathrm{i}k_m$ ($m = 1, 2, \cdots$). The positive real root k_0 corresponds to the progressive interface waves with wave number k_0, while the purely imaginary roots correspond to evanescent modes.

Let μ be expressed as $\mu = p/q$ where p and q are integers prime to each other but $p = q$ when $\mu = 1$. The above dispersion equation (A.3) can be written as:

$$Kh \coth \mu z - z + \rho(Kh \coth z + z) = 0. \tag{A.4}$$

If m is a multiple of $p+q$, *i.e.*, when $m = n(p+q)$, say, then it is easy to see (graphically also) that $k_{nq} < k_{n(p+q)} < nq\pi$ ($n = 1, 2, \cdots$) and as n becomes large, $k_{n(p+q)} \to nq\pi$ for any p. The detail discussion had carried out in the works of [65], [18].

The fact that (A.3) has no other roots except $\pm k_0$ and $\pm \mathrm{i}k_m$ ($m = 1, 2, \cdots$), can be proved by employing the Rouche's theorem of complex variable theory.
Let us define

$$F(z) = Kh \coth \mu z - z, \tag{A.5}$$

$$G(z) = \rho(Kh \coth z + z), \tag{A.6}$$

where z is complex ($z = kh$). We consider the contour C of the square with vertices $(\pm(nq + \varepsilon)\pi, \pm(nq + \varepsilon)\pi)$ in the complex z-plane where n is a large integer and $\varepsilon(> 0)$ is sufficiently small. The contour C is chosen in such a way that it does not pass through any of the zeros of the function $F(z)$. The equation $F(z) = 0$ has two real roots and $2n(p + q)$ purely imaginary roots inside C. Therefore total number of roots of $F(z) = 0$ inside C is $2 + 2n(p + q)$.

Now on the upper side of the square C, $z = x+\mathrm{i}(nq+\varepsilon)\pi$, where $-(nq+\varepsilon)\pi \leq x \leq (nq+\varepsilon)\pi$. Then on this side,

$$\left|\frac{F(z)}{G(z)}\right| = \left|\frac{Kh\coth[x + \mathrm{i}(nq + \varepsilon)\pi] - [x + \mathrm{i}(nq + \varepsilon)\pi]}{\rho\{Kh\coth[x + \mathrm{i}(nq + \varepsilon)\pi] + [x + \mathrm{i}(nq + \varepsilon)\pi]\}}\right| \tag{A.7}$$

$$= \left|\left(\frac{Kh\coth[x + \mathrm{i}(nq + \varepsilon)\pi]}{n[\frac{x}{n} + \mathrm{i}(q + \frac{\varepsilon}{n})\pi]} - 1\right) \div \rho\left(\frac{Kh\coth[x + \mathrm{i}(nq + \varepsilon)\pi]}{n[\frac{x}{n} + \mathrm{i}(q + \frac{\varepsilon}{n})\pi]} + 1\right)\right|. \tag{A.8}$$

Thus as n is large, the value of $|F(z)/G(z)|$ on the upper side of C becomes $(1/\rho) > 1$. Hence $|F(z)| > |G(z)|$ on the upper side of C. Similarly we can prove that $|F(z)| > |G(z)|$ on the other sides of the contour C. Therefore $|F(z) > G(z)|$ on the contour C.

Therefore by Rouche's theorem we find that $F(z)$ and $F(z) + G(z)$ have the same number of zeros inside C. This shows that the dispersion equation (A.3) has two real roots and an infinite number of purely imaginary roots and no other roots.

Appendix B

Derivation of bottom boundary condition

The bottom of an ocean with small undulation is described by $y = H + \varepsilon c(x)$ where $c(x)$ is a function with compact support and describes the bottom undulation, H denotes the uniform finite depth of ocean far to either side of the undulation of the bottom so that $c(x) \to 0$ as $|x| \to \infty$ and the non-dimensional number $\varepsilon(\ll 1)$ a measure of smallness of the undulation. The condition on the bottom of ocean-bed is given by

$$\frac{\partial \phi}{\partial n} = 0 \quad \text{on} \quad y = H + \varepsilon c(x), \tag{B.1}$$

where $\partial/\partial n$ denotes the normal derivative at a point (x, y) on the bottom. Now,

$$\tan\theta = \frac{\mathrm{d}y}{\mathrm{d}x} = \varepsilon c'(x), \tag{B.2}$$

$$\cos\theta = \frac{1}{[1+\varepsilon^2 c'^2(x)]^{1/2}}, \tag{B.3}$$

$$\sin\theta = \frac{\varepsilon c'(x)}{[1+\varepsilon^2 c'^2(x)]^{1/2}}, \tag{B.4}$$

$$\begin{aligned}
\frac{\partial \phi}{\partial n} &= \frac{\partial \phi}{\partial x}\cos(x,n) + \frac{\partial \phi}{\partial y}\cos(y,n) \\
&= \frac{\partial \phi}{\partial x}\cos(\frac{\pi}{2}+\theta) + \frac{\partial \phi}{\partial y}\cos\theta \\
&= \frac{\partial \phi}{\partial x}(-\sin\theta) + \frac{\partial \phi}{\partial y}\cos\theta \\
&= -\frac{\partial \phi}{\partial x}\varepsilon c'(x)\left[1 - \frac{1}{2}\varepsilon^2 c'^2(x) + \cdots\right] + \frac{\partial \phi}{\partial y}\left[1 - \frac{1}{2}\varepsilon^2 c'^2(x) + \cdots\right] \\
&= -\varepsilon c'(x)\frac{\partial \phi}{\partial x} + \frac{\partial \phi}{\partial y} + \mathrm{O}(\varepsilon^2) \quad \text{on} \quad y = H + \varepsilon c(x) \\
&= \frac{\partial \phi}{\partial y} - \varepsilon \frac{\partial}{\partial x}\left\{c(x)\frac{\partial \phi}{\partial x}\right\} + \mathrm{O}(\varepsilon^2) = 0 \quad \text{on} \quad y = H \text{ (by the help of Taylor's expansion)},
\end{aligned} \tag{B.5}$$

which is the expanded form of bottom condition on the ocean bed.

List of published and communicated papers

Based on the work in this thesis, the following published and communicated papers have resulted.

1. S. Mohapatra and S.N. Bora, "Water wave interaction with a sphere in a two-layer fluid flowing through a channel of finite depth", *Archive of Applied Mechanics*, **79**, (2009), 725–740, (DOI: 10.1007/s00419-008-0248-z).
2. S. Mohapatra and S.N. Bora, "Propagation of oblique waves over small bottom undulation in an ice-covered two-layer fluid", *Geophysical & Astrophysical Fluid Dynamics*, **103(5)**, (2009), 347–374, (DOI: 10.1080/03091920903071077).
3. S. Mohapatra and S.N. Bora, "Scattering of internal waves in a two-layer fluid flowing through a channel with small undulations", *Ocean Dynamics*, **59(4)**, (2009), 615–625, (DOI: 10.1007/s10236-009-0214-5).
4. S. Mohapatra and S.N. Bora, "Reflection and transmission of water waves in a two-layer fluid flowing through a channel with undulating bed", *Communicated*.
5. S. Mohapatra and S.N. Bora, "Scattering of oblique water waves in a two-layer fluid flowing through a channel with bottom deformation", *Communicated*.
6. S. Mohapatra and S.N. Bora, "Scattering of oblique waves by an uneven ocean-bed in a two-layer fluid with ice-cover", *Communicated*.
7. S. Mohapatra and S.N. Bora, "Propagation of two-dimensional internal waves over small bottom undulation in a two-layer fluid with an ice-cover", *Communicated*.
8. S. Mohapatra and S.N. Bora, "Radiation of water waves by a submerged sphere in an ice-covered two-layer fluid of finite depth", *Communicated*.